UNIVERSITY OF THE WITWATERSRAND, JOHANNESBURG
FACULTY OF ENGINEERING
DEPARTMENT OF CIVIL ENGINEERING

AN EXPERIMENTAL AND THEORETICAL INVESTIGATION OF THE STRUCTURAL BEHAVIOUR OF CROSS-BRACING IN TRANSMISSION LINE STEEL TOWERS

Roberto Hector Behncke

A thesis submitted to the Faculty of Engineering, University of the Witwatersrand, Johannesburg, in fulfilment of the requirements for the degree of Doctor of Philosophy

Johannesburg, 1992

I declare that this thesis is my own original unaided work, except where specific acknowledgment is made by name or in the form of a numbered reference. It has been submitted for the Degree of Doctor of Philosophy in the University of the Witwatersrand, Johannesburg. It has not been submitted before for any degree or examination in any other University.

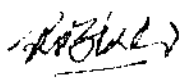

Roberto Hector Behncke
Johannesburg, January 1992

ABSTRACT

This thesis presents the results of theoretical and experimental investigations into the behaviour and ultimate load capacity of latticed tower panels with cross-bracing diagonals made of equal-leg, hot-rolled steel angles under the effects of in-plane loads

Loading tests to collapse are carried out on cross-bracings in reduced-scale two-dimensional frames of various arrangements. The Southwell-plot of deflection measurements immediately prior to first yield of the diagonals is used to define equivalent end eccentricities and effective length factors, which therefore account for geometric and material imperfections of the test specimens.

A proposal for new design formulae for calculating the resistance of struts is presented. The new design equations are based on the secant formula and are calibrated against the experimental results.

A computer model is developed based on flexibility equations which do not require an iterative analysis procedure. The non-linear effects are given through the inclusion of Berry stability functions. The effects of eccentric forces and nodal restraints are simulated at all joints in which diagonals and main chords are connected. An additional model is formulated using a mainframe finite-element code, demonstrating that it is now possible to perform non-linear analyses of complex frames including asymmetric members.

Experimental results from this and other investigations are compared with ultimate load predictions based on the new design equations and the computer models, and also usual buckling curves for design of steel transmission towers. In all cases the proposed models give acceptable predictions of the behaviour and ultimate capacity of the bracings.

In particular, failure loads calculated with the new design equations show improvements with respect to predictions based on current design buckling curves. These equations, therefore, can be used for design of steel latticed tower structures with angle members.

I dedicate this thesis
to Pauline and young Reinet.

ACKNOWLEDGEMENTS

The theoretical and experimental investigations presented in this thesis were carried out under the supervision of Professor A. R. Kemp, Dean, Faculty of Engineering, University of the Witwatersrand, Johannesburg. I wish to express my gratitude to Professor Kemp for his constant personal and academic support.

I also wish to thank:

The University of the Witwatersrand, the CSIR's Fund for Research and Development, the South African Institute of Steel Construction and Eskom, for their financial support;

Powerlines (Pty) Ltd, Transdeco (Pty) Ltd, Genrec Structural Steel (Pty) and Eskom for their donation of test materials;

Messrs D. H. Cretchley, C. P Nisbet, A. C. Britten, G. M. Ferrero, A. Manferdini and Professor R.V. Milford;

The staff of the Civil Engineering Heavy Structures Laboratory at Wits University, for their assistance during the test programme;

Alistair and Glynis Clacherty, for their invaluable editing and proofreading of this thesis;

My family and friends for their encouragement and support, and my wife Pauline and our daughter Reinet for their love and patience.

CONTENTS

CHAPTER 2

THE EXPERIMENTAL INVESTIGATION: METHODS AND PROCEDURES

CHAPTER 3

THE EXPERIMENTAL INVESTIGATION: ANALYSIS AND DISCUSSION OF TEST RESULTS

LIST OF FIGURES

LIST OF TABLES

LIST OF SYMBOLS

The commonly used symbols and notations are given below. Other symbols used in the text are explained when they first occur.

A	Nominal cross-sectional area
a_0	Initial amplitude or initial deformation
B,b	Nominal width of steel angle
B_1-B_4	Berry stability functions
C_x, C_y	Cross-over joint forces
C_c	Elastic limit given as a function of yield stress
e_x, e_y	Eccentricity about x- or y-axis
E	Modulus of elasticity
f_E	Euler critical stress
f_{max}	Maximum stress at the extreme fibre
f_n	Nominal or average stress
f_{ult}	Nominal stress at failure
f_y	Yield stress of material
G	Section's torsional modulus
h	Distance from neutral axis to the extreme fibre
i,j,k	Generic nodes in a structure
I_x, I_y	Moment of inertia about x- or y-axis
J	St Venant's torsional constant for angle sections
K	Effective length factor
k_0	Factor for imperfections, Perry-Robertson equation
L	Overall length of diagonals
L_g	Length of longest diagonal subspan
L_s	Length of shortest diagonal subspan
L_g/r_v	Slenderness ratio about minor axis
L_s/L_g	Length ratio of diagonals
M_x, M_y	Bending moment about x- or y-axis

M_z	Torsional moment about z-axis
P	Axial force in structure members
P_E	Euler critical load
r_u, r_v	Radius of gyration about u- or v-axis
S, S_{xS}	Non-dimensional spring stiffness
t	Thickness of steel angles
u,v	Principal u- and v-axis
V	Shear force
x,y	Orthogonal x- and y-axis
x_g, x_s	In-plane deflections at nodes g, s
y_g, y_s	Out-of-plane deflections at nodes g, s
y_c	Out-of-plane deflections at cross-over joint, node c

α	Slope of main legs
β	Relative inclination of diagonals
ϵ_i	Strain at location i, where i=1,2,3 ...
ϵ_{max}	Maximum strain at heel of the angles
θ_x, θ_y	Strut end rotations about x- or y-axis
θ_z	Torsional rotation about z-axis

CHAPTER 1

INTRODUCTION

1.1 - Elementary concepts

This investigation examines the deflection and buckling characteristics of cross-bracing used in the lateral panels of self-supporting transmission line towers, shown in Figure 1.01, with particular interest in the effects of eccentricity of load and end restraints on the behaviour and ultimate capacity of the diagonals.

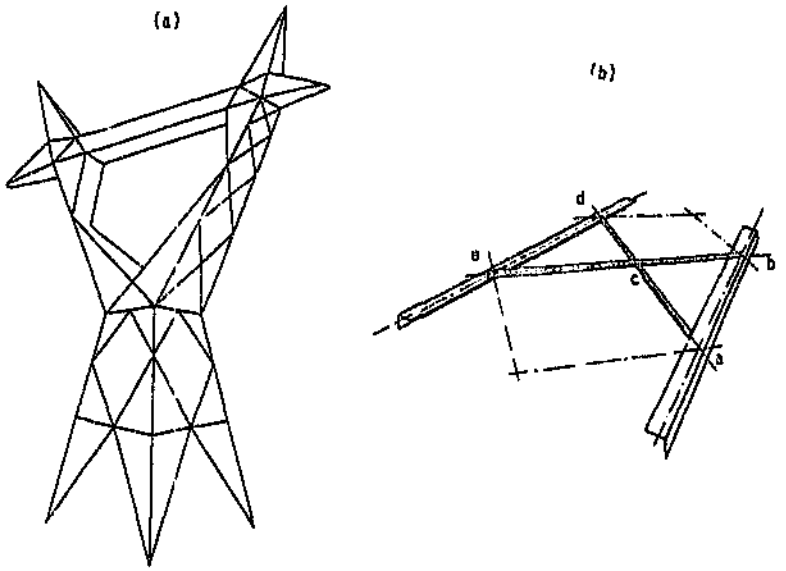

Figure 1.01: (a) A self-supporting transmission line steel tower. Note the lateral panels with cross-bracings. (b) Lateral panel with steel angle crossed diagonals connected back-to-back at the cross-over joint.

Cross-bracing systems comprising ties and struts connected at their cross-over joints act as shear-resisting members, with one diagonal in tension and the other in compression. These lateral, in-plane forces normally arise from the action of external torsional moments produced by unbalanced longitudinal loads, such as stringing and maintenance operations, collapse of an adjacent tower or broken conductors.

As in most tower members, cross-bracing diagonals are made of hot-rolled steel angle sections, which are economic and readily available, easy to manufacture and transport, and adaptable to most structural shapes. However, while the angle members are very convenient structurally, the actual behaviour of the loaded tower is highly complicated and very difficult to reproduce in theoretical models. In particular, the performance of the lateral bracings is significantly influenced by the geometric characteristics of both the tower and the angle sections, and by the connection arrangements. These effects can be summarized as follows:

- The geometric configuration of the structure determines the distribution of forces throughout the bracing.

- The angle section's torsional stiffness and minor axis of inertia bending stiffness are small in comparison to its stiffness about the major axis.

- The steel angles are bolted to other flexible elements of the tower through only one leg, as shown in Figure 1.02. As a result, some degree of eccentric loading is nearly always unavoidable, and the members are consequently subjected to combinations of axial forces and bending moments. This particular condition, typical of most bracing members in

steel transmission towers, may be represented conveniently by a beam-column under biaxial bending.

- The bracing elements in a tower are restrained at the joints against rotation about both orthogonal axes x and y, Figure 1.02, and this has an important effect on the resistance of the members. The degree of end restraint at any particular joint depends upon the number of connecting bolts, the flexural and torsional rigidity and the axial loads of all the adjoining members. This is further complicated by the use of a gusset-plate and packings.

- In the particular case of cross-bracing diagonals, the tie supports the strut at the interconnecting joint, hence reducing the strut's unbraced length and improving its buckling resistance. Experimental results show that the amount of lateral support at the cross-over joint is not constant, but is a function of the increasing forces and lateral deflections in the bracing.

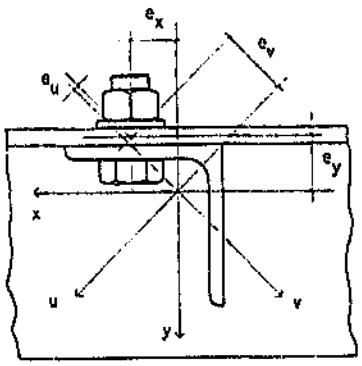

Figure 1.02: Typical transmission tower bolted connection. The framing eccentricity e_y is defined by the distance between the section's orthogoral x-axis and the centre of the main chord's connected leg.

- In addition, it has been observed that the overall stability of the bracing depends upon the ratio of tension to compression force in the diagonals and, finally, that this ratio of bracing forces is influenced by the external loading and boundary conditions, the geometric configuration and the internal structural actions in the towers.

All these combined effects result in the diagonals undergoing significant out-of-plane deflections, twisting and general non-linear behaviour from the onset of loading. Failure of the bracing at medium and even at high values of slenderness ratio is normally initiated by the yielding of the extreme fibres in the compression member, followed by inelastic buckling in the direction of the section's major axis of inertia. At low values of slenderness ratio, however, yield may occur first in the tie, prematurely reducing the load-carrying capacity of the bracing.

These considerations, together with other factors such as rolling and manufacturing tolerances, variations in quality of material, as well as residual stresses, make the response of the whole tower under ultimate loads to be in most cases outside the range of accurate theory.

Significantly, though, framing eccentricities, as well as end and intermediate restraints, are not generally included in analyses of steel towers. In traditional design procedures a tower is assumed to be a latticed system in which individual members behave as though pin-ended, and joints are designed so as to ensure that the centroidal axes of all incoming elements meet at one point. The member axial stresses resulting from a given set of loading conditions are calculated using this simplified model.

Similar limitations exist in definitions of the failure strength specified in design codes, where the ability of angle diagonals to resist compressive loads is treated as a buckling problem, in which empirical effective length factors account for the unknown effects of eccentricity of load and joint restraints.

Experience shows that bolted structures designed on this basis generally provide the required overall load capacity. However, some design problems are still not completely resolved, in spite of many individual and international research initiatives. Test data often indicate that there is considerable disparity between tower member forces calculated in computer analyses and member loads measured during prototype tests [1]. It has been noted that forces on the more heavily loaded elements in a structure, usually legs and main chords, are more accurately computed. However, loads in the majority of structural elements in a tower are relatively light and uncertain. Thus, failures still occur, normally at unexpected locations. This suggests that, to some extent, the complex behaviour of the loaded structure may not be represented effectively by existing models.

As is clear from the discussion above, transmission line tower design has to take account of a multiplicity of factors. In practice, however, designs are based on certain simplifying assumptions, as reported in the following Section.

1.2 - Current design recommendations for tower members under compressive loads

In conventional stress analysis, the transmission line tower is

generally considered as a spatial truss. Solutions of force-displacement linear equations are based on the undeformed geometry of the structure, although some computer programs [2-4] may include in the analysis the additional forces and moments induced in the members by nodal displacements.

Strictly speaking, however, latticed steel towers are spatial frames, in which bracing members behave as beam-columns with elastic restraints. Moreover, most members in a tower are, under some or other load condition, stressed in compression, and must therefore be designed as struts. The exact second-order analysis of such structures may ultimately become hopelessly complex if all the relevant variables are considered, and certainly impractical and expensive for industry design purposes.

Alternatively, simplified methods of structural analysis can be employed which reduce the necessary computations to more reasonable limits. Designers use buckling curves defined by semi-empirical formulae given in tower design manuals. These methods are approximate and are based on past experience and on numerous tests on prototype towers. Recommendations from two of the most commonly used manuals for tower design are examined in the following Sections.

1.2.1 - The ASCE Manual No 52

This guide for design of self-supporting steel towers [5] has been in use by electric power utilities and tower manufacturers since its first publication in 1971. An updated version has been issued in 1989, in which design recommendations for new materials and new tower configurations are included.

In the case of tower members made of hot-rolled steel angles, the ultimate compressive load in the elastic range is determined by the Euler buckling load as follows:

$$\frac{f_{ult}}{f_y} = \frac{1}{\Gamma_k^2} \qquad \text{for } \Gamma_k > \sqrt{2} \qquad \ldots.(1.01)$$

where f_{ult} is the ultimate compressive stress in the strut and f_y is the guaranteed yield stress of material, both in MPa.

In the inelastic range, however, the ultimate load is given by the Column Research Council (now Structural Stability Research Council) [6] equation as follows:

$$\frac{f_{ult}}{f_y} = 1 - \frac{\Gamma_k^2}{4} \qquad \text{for } 0 \leq \Gamma_k \leq \sqrt{2} \qquad \ldots.(1.02)$$

In these equations Γ_k is the relative slenderness ratio, given by the following:

$$\Gamma_k = \frac{kL}{r\pi} \sqrt{(f_y/E)}$$

where:

- k is the effective length factor, and kL/r is the strut's effective slenderness ratio, which is determined by using experimentally-based equations of the type:

$$kL/r = c + d\,(L/r)$$

where coefficients c and d are a function of the end conditions of the tower members and are determined empirically.

- E is the modulus of elasticity of material in MPa.

Thus the stress limit for elastic analysis is given as $\Gamma_k = v2$, which can also be expressed by the following stress ratio:

$$fult = 0.5\ fy$$

In terms of the strut's geometric dimensions, however, the elastic limit is given by:

$$kL/r = C_c,$$

where:

$$C_c = \pi\ v(2E/fy)$$

Local buckling is avoided by limiting the width-to-thickness ratio b/t as follows:

$$(b/t)lim = 210/v(fy)$$

where b and t are as indicated in Figure 1.03.

For cross-bracing systems it is considered that the diagonal in tension gives support at the cross-over joint when the ratio of tension to compression forces in the bracing is equal to or greater than 0.6. The critical slenderness ratio for buckling load is given by the following expressions:

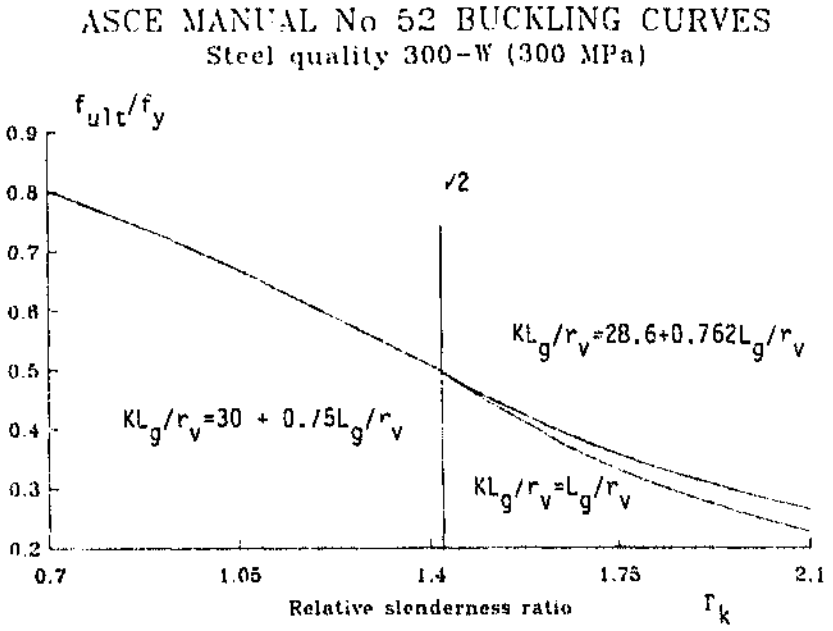

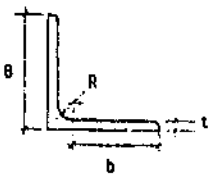

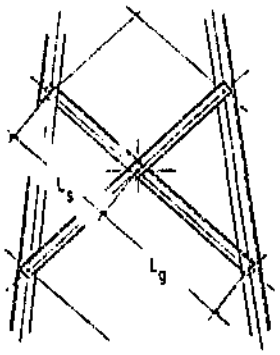

Figure 1.03: ASCE design curves for struts in cross-bracing systems, and details of principal dimensions.

kL_g/r_v, or $k(L_g + 0.5L_s)/r_x$

where r_y and r_x are the radii of gyration about the y and x axes respectively, and L_g and L_s are strut lengths, as shown

in Figure 1.03. ASCE buckling curves for cross-bracing diagonals made of steel angles of quality 300-W are also included in Figure 1.03.

1.2.2 - The ECCS Manual No 39

The ECCS manual [7] was published in 1985, giving buckling curves and recommendations for design of steel sections used in transmission line towers. It includes curves for hot-rolled steel angles as well as cold-formed sections. The buckling resistance of the strut is obtained by solving the following equation:

$$k_0 \frac{f_{ult}}{f_y} = (1 - \Gamma_k^2 \frac{f_{ult}}{f_y})(1 - \frac{f_{ult}}{f_y}) \qquad ....(1.03)$$

in which:

- k_0 is the factor in the Perry-Robertson formula which allows for imperfections, including end eccentricities, and is expressed as:

  $$k_0 = 0.125(\Gamma_k - 0.2)$$

- f_{ult} is the ultimate compressive stress in the strut in MPa.
- f_y is the yield stress of material in MPa.
- Γ_k is the relative slenderness ratio, which in this case is obtained as follows:

  $$\Gamma_k = c + d\Gamma_0$$

$$r_0 = \frac{L}{r\pi} \sqrt{(f_y/E)}$$

where E is the modulus of elasticity of material in MPa. Note that the relative slenderness ratio r_0 is obtained without considering the effect of end conditions, thus assuming initially that the buckling lengths are the centre-to-centre distances between bolts located at the intersections of member design lines. The ratio r_0 is then modified for different end conditions by introducing the coefficients c and d which are also, in this case, determined empirically. The limit against local and torsional buckling is calculated from:

$$(b/t)_{lim} = 0.567 \sqrt{(E/f_y)}$$

The dimensions b and t are shown in Figure 1.04, together with the ECCS buckling curves for cross-bracing diagonals made of steel 300-W.

The design recommendations outlined above have, for the most part, proved adequate and reliable. For example, generally satisfactory results obtained from the use of the ASCE Manual No 52 [5] for design of latticed steel towers of lines up to 500 kV have been reported by Finzi [8]. However, limitations have been identified in existing design procedures, as the following Section shows.

1.2.3 - Limitations of the design recommendations

The sizes of new towers have been increasing as a function of

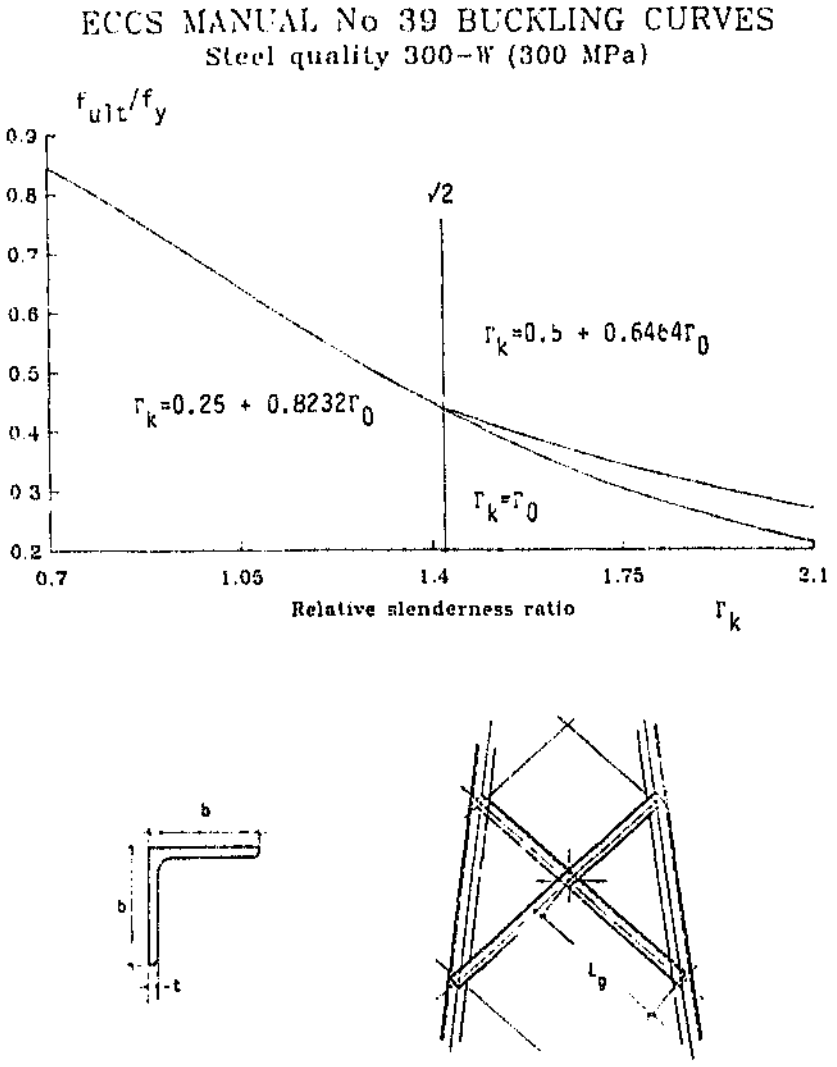

Figure 1.04: ECCS design curves for struts in cross-bracing

greater electric power demands. This has resulted in taller structures, which suffer larger deformations induced by their heavier loads. At the same time, the internal in-plane forces and moments as well as the nodal distortions and restraining actions have also increased with increasing size of towers.

Design curves currently in use, based on an empirical interpretation of test results, may not give correct results in these larger structures, especially at extreme ranges of slenderness ratio, resulting in premature failures.

Tests conducted in South Africa on a 765 kV, 40 metre high rigid suspension tower, for example, resulted in several failures of main legs at less than the specified design loads [9]. These failures were apparently triggered off by premature instability of the adjoining lateral cross-bracings. Yet, no indication existed in the elastic analysis, nor in the dimensioning of members, after allowances for safety, of the possibility of such failures. The detailing and the erection procedures were also found to be faultless.

Other interesting examples of unexpected tower failures have been reported by Short [10]. He observed that most premature prototype failures are due to design simplifications, which may result in incorrect detailing of tower members. Some of the limitations are:

- Insufficient knowledge of the actual restraint provided by nodal points and intermediate supports.

- Excessive concentration of stress in holes of tension members.

- Redundant or supporting members which are nominally unstressed. However, secondary effects in the structure, such as bending due to out-of-plane eccentricities, may induce high forces in these members, resulting in their own failure and subsequent collapse of the supported legs.

Experimental results from tests performed on reduced two-dimensional frames with cross-bracing systems [11] also show differences in the ultimate capacity of the diagonals with respect to the predicted failure loads. It has been found that the calculated results are conservative at high values of slenderness ratio, with the diagonals failing at higher loads than expected. This implies an inefficient use of the angle section's total load capacity per unit weight of steel.

At low values of slenderness ratio on the other hand, design curves give optimistic failure loads, resulting in the diagonals failing at lower loads than expected. This latter anomaly has more serious implications and may be the origin of severe structural damage, since cross-bracings with short unbraced diagonals are located in the top bays of the lateral panels, where axial forces are higher, with no significant nodal distortions and lateral displacements. The axial stress components and the effect of eccentricity of load are predominant in this region, resulting in either torsional buckling failure by twisting of the cross-section, local buckling failure even at safe width-to-thickness ratios b/t, or premature yielding of the tension member at the cross-over joint, which typically occurs prior to buckling in cross-bracings with short diagonals.

Finally, while design buckling curves make allowance for various end conditions of the members, including eccentricity of load and increased end restraints produced by the use of more connecting bolts, they do not consider other effects, such as additional restraint from bracings in adjacent bays, different size and slope of the main legs, as well as relative inclination of the bracings. It is later demonstrated in this thesis that

some of these factors have considerable influence in the performance of the diagonals.

1.3 - Review of previous investigations concerning the behaviour and resistance of typical tower members

Due to uncertainties and simplifications in the design process, most tower models of important transmission systems are tested to destruction prior to commencing production. These full-scale, proof tests are traditionally performed to confirm the ability of the complete towers to withstand the design loads, and also to assess the maximum resistance of the structures. Data on the distribution of member forces and connection behaviour are not normally recorded, although information obtained from prototype tests has been used to improve loading specifications and structural design techniques.

Consistent research on full-scale steel towers has not been common in the past, perhaps due to the limitations of conventional tower testing stations, the difficulties, cost and time involved in tower research, and also the ever-changing requirements of different transmission systems in terms of tower models, loads and dimensions. It has thus been difficult to establish accurate relationships between loadings and member strength based on the observed behaviour of these towers.

In response to this lack of research data, the EPRI tower testing station at the Transmission Line Mechanical Research Centre [12-14] has been established, albeit only recently, in order to improve the quantity and quality of prototype test information through acquisition of accurate and reliable membe-

loads and behaviour, evaluation of member strength and analysis of current design techniques.

Before this, however, evaluation of member and tower response to loads was possible only through research on individual angle struts and on bracings in simplified testing frames. Results from some relevant investigations are summarized in the following Sections.

1.3.1 - Single-angle columns

As stated before, the eccentric attachment of steel angles in transmission towers induces additional biaxial moments in the members due to the amplification effect of axial loads. This normally results in yielding of the external fibres in the compression angles prior to elastic buckling. This problem has been studied extensively and both analytical and experimental work has been carried out to determine the behaviour and ultimate capacity of angles in the elastic and inelastic regions, and for various end conditions.

Firstly, the analysis of flexural buckling of individual members is based on Euler's early formulation on concentrically loaded columns. More related to angles, the elastic behaviour of a generic thin-walled, open section member under symmetrical biaxial bending was initially studied by Goodier [15], who developed the basic differential equations of equilibrium for a simply supported member. Timoshenko subsequently arrived at the same expressions [16], after an analysis of pure bending of prismatic elements and pure torsion of members with open cross-sections. These preliminary studies were based on previous

theoretical analyses in connection with the development of new, light weight sections for use in aircraft structures.

The exact solution to Goodier's system of differential equations was given by Culver [17], although approximate procedures had previously been in use for some ideal boundary conditions. Culver's complete solution requires the use of twelve boundary conditions to evaluate as many constants of integration. After calculation of the displacements, the stresses at any section of the column can be evaluated in terms of the different stress components due to axial force, bending and warping.

More recently, Trahair solved Goodier's differential equations for elastic behaviour of an individual member with elastic end restraints [18]. He made use of numerical techniques and also simulated tests on single-angle columns which had originally been performed by Foehl [19]. Trahair's solution introduces restraint coefficients in the boundary conditions, which are defined as the ratios of the actual end restraining moments to the moments required to develop full end fixity

Further research developments include the study of inelastic behaviour of beam-columns with end restraints. This problem has been solved for angle struts through a number of successive theoretical and experimental investigations performed by Trahair, Usami and Galambos [20-23]. These authors have conducted extensive research in which forty six eccentrically loaded single-angle columns with slenderness ratios between 60 and 200 were tested to failure under three different end conditions. The eccentricities were modelled by welding the angle ends to structural tee sections, as shown in Figure 1.05.

The tests included equal-leg and unequal-leg angles, in both

cases made of mild steel and high tensile steel.

In the theoretical model adopted by Usami [22], also shown in Figure 1.05, struts were treated as end-restrained columns under biaxial bending, with particular attention to their inelastic behaviour. The end restraints were modelled after the observed behaviour of the welded tee sections at the end of the angle struts, as described in Reference [20]. The end restraints are represented in the theoretical model by rotational springs, located in directions which are parallel to the two legs of the angle. The most important conclusions of Usami's investigation relate to the ability of the model to predict inelastic failure of eccentrically loaded single-angles with end restraints. The behaviour of the angles can be summarized as follows:

- Typical non-linear deflections and also twisting occurred from the beginning of loading. Displacements at the center

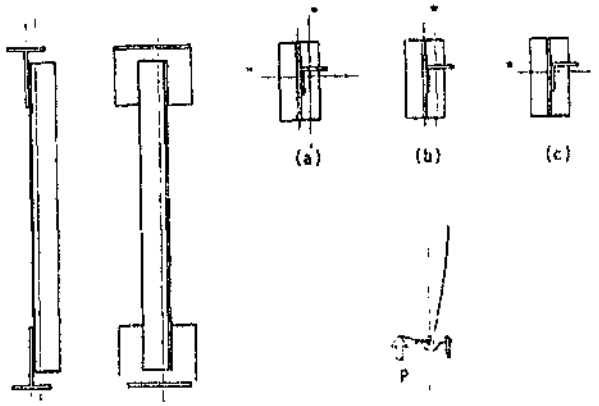

Figure 1.05: Experimental research reported by Usami et al [20-23]. The angle specimens are welded to tee sections, and these are connected to the testing machine. The planes of load are indicated with a star (*) for the three end conditions (a), (b, and (c).

of the column were predominantly perpendicular to the plane of loading, with small displacements in the same plane. The columns buckled inelastically after yielding had taken place at the critical section. Results from tests with unequal-leg angles confirmed that the maximum resistance is obtained when the long leg is perpendicular to the plane of loading. These results were anticipated by Foehl [19].

An experimental investigation was conducted by Kennedy and Madugula [24], in which single and double angle struts with slenderness ratios of up to 90 were tested to failure. The axial loads were applied concentrically, with pinned and fixed end conditions. The test results compare favourably with theoretical predictions for flexural, torsional and local failure modes.

A finite-element analysis was used by Haaijer [25] to model the elastic behaviour of single-angle struts under eccentric loads. It was shown in this investigation that a complex, non-linear model can be used to simulate the behaviour of single struts and, with some limitations, to predict their failure loads. A design criterion is thus recommended, in which effective length factors are used to relate the actual eccentrically loaded angle to an equivalent concentric column.

Results of research in inelastic instability of beam-columns were presented by Lu in 1987 [26]. Studies on equal-leg and unequal-leg angles include the flexural-torsional instability of simply-supported angle columns loaded concentrically, and the flexural-torsional instability analysis of similar columns loaded eccentrically through gusset-plates. Initial deformations and residual stresses were taken into account in this research. However, contrary to previous analyses on unequal-leg angles, it was shown that the long leg outstanding position is not always

the more favourable arrangement. This effect is governed by the slenderness ratio, and it is demonstrated that short struts will give higher ultimate loads with the short leg outstanding instead.

Tests were conducted in Australia on single and double-angle and Tee struts by Kitipornchai and Lee [27,28]. They compared experimental results with theoretical predictions of the elastic and inelastic behaviour of struts. The columns were simply-supported and concentrically loaded. These results compare well with design guides currently in use in Australia and the United States.

Two recent papers by Al-Sayed and Bjorhovde report experimental and theoretical studies on the buckling response of unrestrained, concentrically loaded angle columns [29,30]. Equal and unequal-leg angles were used to establish elastic and inelastic failure characteristics. Careful residual stress measurements were made using the method of sectioning. It was found that the maximum compressive residual stresses occur at the heel and at the toes of the angles, with a maximum value of 22 to 30% of the measured yield stress of the material.

Al-Sayed and Bjorhovde concluded that the flexural-torsional mode of failure is possible in angle members, therefore this should be checked as an additional limit state. The influence of the width-to-thickness ratio b/t was included in the study, but it was acknowledged that further research was required for a more complete assessment of its effect.

Finally, a theoretical analysis was conducted by Lui on unequal-leg angles [31]. His model includes the effects of initial crookedness and twisting, as well as of residual

stresses. Lui proposed an interaction equation for designing unequal-leg angles. It was established, in agreement with Al-Sayed and Bjorhovde, that residual stresses have a deleterious effect on the resistance of struts.

This brief review includes only those studies which are of interest to this research, although there is a considerable amount of literature on the investigation of the behaviour of beam-columns, including single- and compound-angle struts. Comprehensive literature surveys have been published by Chen and Santathadaporn [32] and Madugula and Kennedy [33,34].

It can be concluded that single-angle struts with elastic end restrain s show the following characteristics when subject to biaxial loading:

- General non-linear behaviour from the onset of loading.
- Twisting of the section about its shear centre.
- Considerable deflection in a direction perpendicular to the connected leg.
- Yielding of the external fibres due to bending effect prior to elastic buckling.
- Loading capacity of the strut is significantly affected by the boundary conditions.
- Initial imperfections are negligible in comparison with the effect of eccentricity of axial loads.

1.3.2 - Cross-bracing systems

Unfortunately not much is known about the behaviour of cross bracing systems, since a very limited amount of information exists on experimental results and on analytical predictions of the ultimate resistance of the crossed diagonals under different loadings and end restraint conditions. The few published reports on these problems can be divided into two groups:

- Studies on square or rectangular roof and wall cross-bracing arrangements found in steel buildings, which are subject to lateral wind or crane loads.

- Studies on cross-bracing systems found in lateral panels of communication and transmission line towers under the effect of torsional loads on the tower.

Both cases are examined in the following Sections.

Lateral panels of steel buildings

These are square or rectangular panels, in which the diagonals are divided at the cross-over joint into two equal subspans, Figure 1.06. The slenderness ratios are high, and therefore the effects of the end restraints and eccentricity of loads are neglected: the diagonals are assumed to be pin-ended and concentrically loaded. The horizontal member at the top of the bracing produces an unknown ratio of tension-to-compression force in the diagonal bracing members.

Traditional practice in steel building design considers that lateral loads affecting cross-bracing systems are resisted only by the tension member, or *tie*, thus ignoring the contribution of the compression member, or strut. This assumption implies that the tie does not support the strut against buckling at the cross-over joint, resulting in conservative designs.

In a simple analysis, the tie in the cross-bracing system can be considered as an elastic support to the strut at the interconnecting joint, as indicated in Figure 1.06-a, where β' is the tie's elastic lateral stiffness, which can be calculated from equations of equilibrium of a simply-supported member under tension load, and a transverse force that represents the action of the other diagonal.

The following cases can be identified for a constant compressive load in the strut:

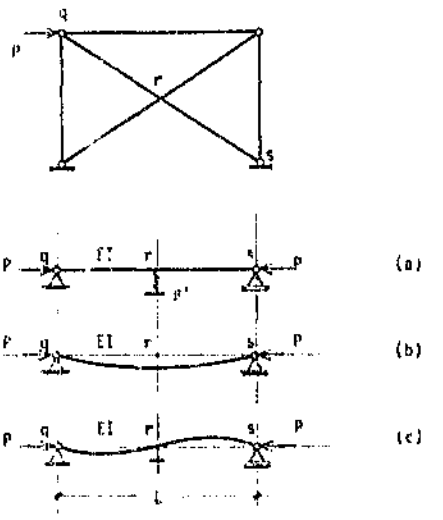

Figure 1.06: Research on cross-bracings of lateral panels in steel buildings [35-46]. (a) Diagonal interaction at cross-over joint, where β' is the tie's lateral restraint coefficient. (b) Case of no restraint: full-wave, first mode of buckling. (c) Case of full restraint: half-wave, second mode of buckling.

- The two diagonals are not interconnected, in which case $\beta'=0$, and no lateral restraint is provided by the tie.

- The diagonals are interconnected, but there is no force in the tie. In this case a partial lateral restraint is given by the tie's flexural stiffness, as follows:

$$\beta' = 48EI/L^3$$

where I is the section's moment of inertia, and E is the modulus of elasticity.

- The diagonals are interconnected, and the force in the tie increases consistently at a rate which can be higher or lower than the force in the strut. The coefficient β' increases with the out-of-plane deflections of the bracing and the force in the tie until it reaches a critical value, after which the tie provides full support at the cross-over joint for additional load.

In the first two cases the effective length factor is k=1, and the critical load is given by the Euler elastic buckling load, with the strut failing in the characteristic half-wave, first mode of buckling, Figure 1.06-b. In the third case, the effective length factor is k=0.5 (for long members in which the effect of eccentric forces can be ignored), and the critical load is, at least theoretically, equal to four times the Euler buckling load. The strut fails in the characteristic full-wave, second mode of buckling, also shown in Figure 1.06-c.

It follows that an increase in the ratio of tension to compression forces in the bracing, which can by simulated by a

reduction of the effective length factor k, will be reflected by an increase of the strut's buckling resistance, thus contributing to the overall load capacity of the frame.

Studies on these effects of diagonal forces at the interconnecting joint have been conducted by Timoshenko [35], De Wolf and Pelliccione [36], Kitipornchai and Finch [37], and more recently a series of investigations have been carried out by Picard [38-43]. Similar studies are also reported by El-Tayem [44] and Stoman [45,46]. The most important conclusions can be summarized as follows:

- The contribution of the compression member to the cross-bracing load capacity cannot be ignored.

- Provided that forces in the tension member are higher than the minimum critical value, a restraint is enforced at the interconnecting joint, allowing the strut to fail in the second mode of buckling.

- The lateral stiffness β' developed by the tie is a function of the flexural rigidity of the tension member and the axial force in the tension member.

- The load capacity of the bracing is significantly influenced by the ratio of tension to compression forces in the diagonals.

Lateral panels of steel transmission towers

Torsional loads in a lattice transmission tower induce shear forces in the transverse and longitudinal panels and, as a result, the internal bracings are loaded in pairs of tension-compression members. This arrangement presents special problems because of the complexity of the interactions between diagonals and main legs, as well as between diagonals themselves. However, very few theoretical models have been developed to describe these bracings, and experimental data are also uncommon.

Lateral panels with crossed diagonals were tested by Carpena [47,48] in an investigation sponsored by ENEL, the Italian Electric Power Authority. Hot-rolled steel angles of various sizes and cold-formed steel members of various shapes were used in the investigation. Test results were compared with buckling curves in the elastic and elastic-plastic regions, in an effort to establish the efficiency of different steel sections.

In this investigation it was shown that the ability of a particular section to carry a compressive load can be expressed as follows:

$$K_E = A/v(I) = v(A)/r$$

i., which:

- A is the area of cross-section,
- I is the moment of inertia about an axis perpendicular to the buckling plane,
- r is the radius of gyration about the minor axis.

The parameter K_E was found to be convenient for comparison of steel sections in the elastic region, since it is proportional to the weight of material required to sustain a given load P on a known member length L. Carpena concluded that a tower using cold-formed steel sections (with higher buckling resistance) requires fewer members than a similar structure made of hot-rolled angles, with additional savings in the number of bolts, cost of manufacturing, and transportation and erection.

A similar investigation on cross-bracing systems was reported by Wood [49], in which a large number of tests were conducted on two-dimensional frames with crossed diagonals connected with 1, 2 and 3 bolts, and with slenderness ratios greater than 120.

It was found that the failure stress in all diagonals was higher than the calculated buckling stress, and that the ratio of failure stress to design stress increases with increasing slenderness ratio. These results thus clearly confirm that traditional design curves are increasingly conservative for longer columns.

Wood's report contain non-dimensional buckling curves, which are based on linear regression analyses of the test results. These curves can be applied to design after including the local values of steel elastic limits and safety factors.

In South Africa, Kemp [50] reveals an early interest in the effects of force distribution in the bracings and eccentricities in the members of shear panels of latticed steel towers. Subsequent investigations by Elmes [51] on a theoretical model, and Behncke [11] on experimental frames, demonstrate the complex and predominantly non-linear behaviour of crossed diagonals.

Elmes' computer analysis of cross-bracing [51] is based on a two-dimensional model in which the member ends are attached to supports with variable rotational fixity, Figure 1.07. This representation of the bracing is consistent with the observed out-of-plane deflections of the diagonals. The eccentricity of loading is modelled by considering an offset equal to the normal framing eccentricity, which is the distance between the plane of contact of two adjoining members and the centroidal axes of the angles.

The effects of various parameters were examined, usually by varying one at a time. It was established that the load-carrying capacity of the bracing is considerably influenced by the following factors:

- Variable end restraint and eccentricity of load.
- Ratio of axial forces in the diagonals.
- Slenderness ratio.

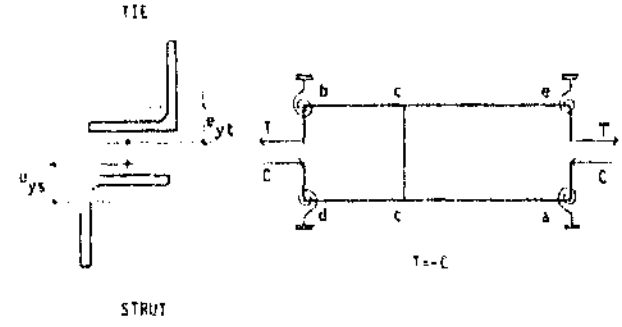

Figure 1.07: Two-dimensional model used by Elmes in his computer analysis of cross-bracing in transmission towers [51]. Node (c) indicates the cross over joint, as in Figure 1.01 (b).

- Size of the angle sections and elastic limit of material.
- Relative inclination between the diagonals and slope of the main legs.

Subsequently, Behncke [11] conducted laboratory tests on equal-leg angle specimens, using frame arrangements as shown in Figure 1.08. Slenderness ratios of 90, 140 and 160 were considered with one and two-bolt end-connections. From evaluation of test results it was possible to identify the factors which influence the resistance of the bracings and, most importantly, these analyses permitted the researcher to isolate and describe typical failure patterns for the bracing. Results from this investigation are examined in more detail in Chapter 2.

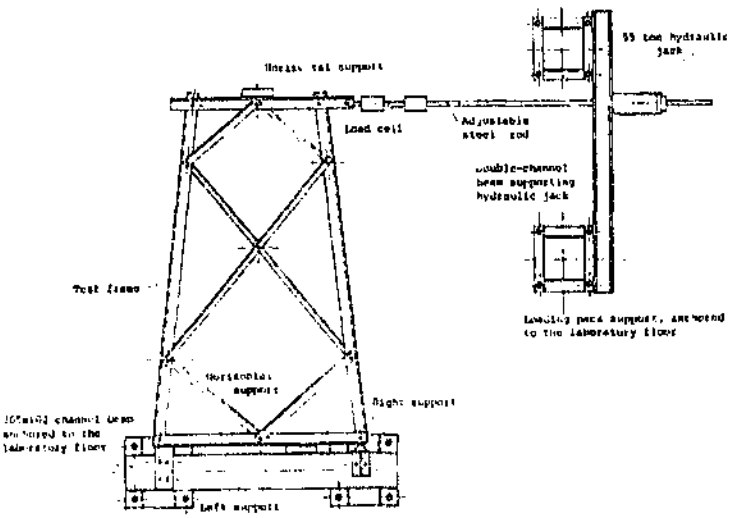

Figure 1.08: Typical model used by Behncke in his experimental analysis of cross-bracing in transmission towers [11]. Note that the transverse beams in the frame imposed full-restraint to the main chord's torsional rotations, also preventing out-of-plane deflections of the outside bracings.

Other important factors in terms of ultimate resistance of tower bracings are initial imperfections, such as residual stresses, and the flexibility of the connections. Some aspects of these problems are reviewed in the following Section.

1.3.3 - Additional effects on column behaviour

Commercially available steel sections generally contain material and geometric imperfections. It is well known that differential cooling during the fabrication process of hot-rolled steel sections, such as angles, induce residual stresses in the cross section. As a consequence, yielding may occur prior to buckling in some parts of the section, resulting in a reduction of stiffness and subsequent loss of strength.

Further, transport of steel columns and also storage and handling operations may induce initial crookedness or out-of-straightness, which results in load-deflection or bending effects due to the axial loads. The resulting additional stresses often cause premature failure of the columns.

These effects are included in the design guidelines given by ASCE [5] (see Equations (1.01) and (1.02) in Section 1.2.1) and ECCS [7] (see Equation (1.03) in Section 1.2.2) for buckling of struts in the elastic and inelastic regions.

Examination of results from previous investigations indicates the following with respect to initial imperfections in steel columns:

- While the detrimental influence of residual stress on

I-sections is well known, its effects on steel angle sections, and particularly small sizes, is not well documented [31].

- The yield stress of the steel has little effect on the magnitude of residual stresses in rolled sections. Rather, the magnitude and distribution of residual stresses depend on the size and type of the cross section (decreasing for smaller sections), and on the cooling conditions [75].

- The combined effect of residual stress and initial crookedness on either straight or deformed columns is not equal to the sum of the separate parts, and this varies with the level of slenderness ratio [75].

- Buckling equations in the inelastic range which are related to the effects of residual stresses, see for example the ASCE's Equation (1.02) in Section 1.2.1, give a close approximation of the values of the secant formula for low and medium values of slenderness ratio [6].

- The effect of eccentric connections, typical of structures with steel angle members, is dominant over small values of initial deformations. Further, an initial bow or curvature can be considered in the limit case as a constant deformation represented by an equivalent eccentricity [34,70].

It is concluded that the effects of these factors (which are predominantly random) on typical angle sections in lateral bracings of steel towers can be included in design equations by means of empirical equivalent eccentricities, assuming that: a) The struts fail when the maximum stress due to the combined effects of axial load and bending reaches the yield point, and b) The material is perfectly elastic up to the yield point [6].

Finally, column behaviour is also influenced by the flexibility of the connections. Unfortunately, not much is known about this problem, largely because of the many variables which influence the joints between two or more members. Two problems are normally related to connections between two or more members in a transmission structure:

The first is the resistance of steel angles subjected to tensile forces. It has been found that the resistance of the connected members is usually less than the nominal tensile strength of the section. This difference can be attributed to the concentration of axial and bearing stresses around the holes. This problem is aggravated by the fact that the edge distances and spacing between bolts are reduced as much as possible during design in order to reduce the size of the joints, and also by the use of gusset-plates at connections with a large number of bolts, due to size and manufacturing restrictions.

The resistance of bolted connections of steel towers has been investigated by Kennedy [52], Marsh [53], Bodegom [54] and Wilhoite [55]. Most design guides recommend reductions of the net area of angles which are connected through only one leg.

The second problem is connection flexibility. Connections are modelled as either perfectly frictionless and pinned, or perfectly rigid and fixed. In reality, actual bolted connection flexibility lies anywhere between these two ideal, extreme cases. Furthermore, this effect has considerable influence in the behaviour and resistance of members in steel frames. At the same time, the modelling of connection behaviour is usually complex, since the moment-rotational response of the connections is non-linear, and depends on various factors.

The influence of connections between diagonal bracing and main legs in transmission line towers has been investigated experimentally by Loria [56]. It was found that connection behaviour is influenced by the number and diameter of the connecting bolts and also by the movement of bolts in their holes. Further variation in connection behaviour and resistance of the bracing is introduced by the use of a gusset-plate, as well as by the thickness and steel quality of the plate.

Kemp and Behncke [57] have simulated special boundary conditions in their analyses of two-dimensional frames with cross-bracing diagonals. These will be examined in more detail in Chapter 4. Further reading on the influence of connection behaviour on the stability of general steel structures can be found in a recent work published by Chen [58].

1.4 - Conclusions

As shown in the above review, current design procedures for members in steel transmission towers have certain limitations. It emerges that the approximate, semi-empirical solutions given in tower design manuals for the assessment of failure loads of cross-bracing diagonals do not always provide adequate, consistent descriptions of the observed behaviour of the bracing.

It is also apparent from the evaluation of previous investigations on individual members, as well as bracings in two-dimensional frames and bolted connections commonly found in steel towers, that some of the non-linear effects which

influence frame resistance are very difficult to simulate in analytical models. Even the most sophisticated computer programs currently in use for non-linear structural analysis of steel frames present problems for modelling the particular characteristics of end restraint, eccentricity and cross-over behaviour of non-symmetric members such as steel angles.

Consequently, there is a need to develop more sensitive experimental and computer models for analyzing these frames, and particularly cross-bracing diagonals in transmission towers. New proposals are required which allow for the inclusion of the important variables of end eccentricities and elastic restraints from the main legs, and also the effects of the relative inclination of diagonals, the relative size of legs and bracings, and the slope of main legs.

1.5 - Thesis: outline of contents

This thesis, therefore, presents the results of experimental and theoretical investigations into the behaviour and ultimate load capacity of plane frames with cross-bracing diagonals made of equal-leg steel angles under the effects of in-plane loads. It also proposes new solutions for calculating the buckling resistance of struts. Special attention is paid to the influence of both frame and member sections' geometric characteristics, boundary conditions and structural actions on the elastic behaviour of the bracing.

Chapters 2 and 3 deal with an extensive experimental research programme in which loading tests to collapse were carried out on cross-bracings in reduced-scale plane frames of various

arrangements, in order to obtain reliable results in a controlled environment. The material of the angle diagonals was hot-rolled steel of Grade 300-W, with a guaranteed yield stress of [illegible] MPa [59]. A survey of towers built in South Africa for various wind zone levels was conducted, and the results of the survey were used to establish rational limits in the analyses and to proportion the experimental models according to real dimensions. Special mechanical devices were designed for the simulation of appropriate in-plane and out-of-plane boundary conditions, as explained in Chapter 2.

The experimental results are presented and discussed in Chapter 3, in which the secant formula and the Southwell-plot of deflection measurements immediately prior to first yield are used to assess the end eccentricities and effective lengths leading to the observed failure stresses in the different experimental models.

A proposal for new design formulae for calculating the resistance of struts with the inclusion of the more important parameters is presented in Chapter 4. Results from the laboratory experiments have been used to calibrate new design equations, which consider the effects of the relative positions of bracing and main legs, as well as the direction of the planes containing the end restraints. In particular, empirical equivalent eccentricities are defined for this and subsequent models which account for initial imperfections (e.g. residual stress). Results from other experimental investigations on crossed diagonals are also evaluated using this model.

Chapter 5 is concerned with a non-linear flexibility analysis of the elastic behaviour of two-dimensional framed structures with cross-bracing diagonals. The deflections and moments about the

principal axes u and v at the intermediate nodes in the theoretical model are considered simultaneously, together with the out-of-plane eccentric actions and restraining moments from the main legs about the orthogonal axes x and y, Figure 1.02.

These restraints are represented in the model by the components of the torsional and flexural stiffness of the main legs in the directions of the bracing diagonals. The eccentricities of the axial force P at the end connections are assumed to be the normal framing eccentricity e_y about the x axis, and e_x about the y axis, as indicated in Figure 1.02.

The end-moments and node displacements of individual elements are assumed to be the unknowns, which are solved using rotation compatibility, joint equilibrium and sway equilibrium equations. Special displacement compatibility equations at the cross-over joint are used for the solution of cross-over forces. The torsional rigidity of the diagonals was not considered in this analysis. The model was programmed in FORTRAN 77 for use in either a personal or a main frame computer.

Chapter 6 describes an additional computer model of the cross-bracing system, which was developed using the finite-element code ABAQUS [60]. The ultimate load capacity of some of the experimental frames has been determined with this model, and the results are compared with the above flexibility approach and with the test results.

A general discussion is presented in Chapter 7, including evaluations of all experimental and analytical results. Chapter 7 is also devoted to the author's conclusions and recommendations for further research, followed by a list of appendices and bibliographical references.

In spite of considerable difficulties in terms of both experimental and computer modelling, this thesis succeeds in improving the understanding of some particular structural problems which are produced, inter alia, by complex non-linear behaviour. The proposed computer models for analysis of cross-bracing systems, although simple in principle and conception, are not appropriate for use in practical design work. However, their application has opened the way to simple, more precise design equations. Results from these analyses are in good agreement with experimental evidence.

1.6 - Research publications

Preliminary findings and some of the final conclusions of this investigation have been included in technical publications by Beuncke and Kemp [57,73,74].

CHAPTER 2

THE EXPERIMENTAL INVESTIGATION: METHODS AND PROCEDURES

2.1 - Introduction

In this Chapter an experimental research programme is presented, in which steel angle crossed diagonals used in transmission towers are examined. This investigation is based on similar studies reported by Wood [49], summarizing CIGRE experimental results [63], and Behncke [11].

In the CIGRE project [49,63] numerous tests were conducted on typical tower panels with cross-bracings. These tests were performed at conventional tower testing stations, and the full-scale frames, shown in Figure 2.01-a, were designed within the range of sizes frequently found in real towers of various voltages. The slopes of legs and diagonals indicated in Figure 2.01-a were constant for all the test alternatives, and the variables were the slenderness ratio of the bracing, defined by Lg in Figure 2.01-a, the size and steel quality of specimens, the size of main legs, and the number and diameter of connecting bolts.

From the instrumentation and locations of strain sensors indicated in Figure 2.01-b, it can be assumed that only the applied loads and the axial forces in the diagonals were recorded. Furthermore, the experimental results were not correlated with a theoretical model other than the Euler buckling equation (thus implicitly assuming elastic behaviour of

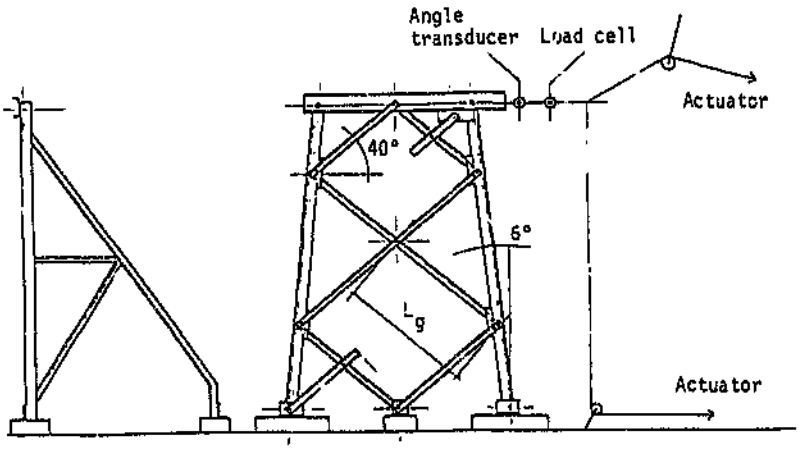

Figure 2.01-a: Typical experimental cross-bracing model, as reported by Wood [49] and CIGRE [63]. Note that the outside bracings and the main chords were connected to transversal beams. The compression members in the outside panels of bracing were reinforced against buckling at midspan by redundant bracings.

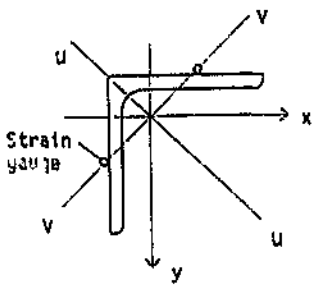

Figure 2.01-b: Strain gauges in the frames above were located on the v-v plane as shown here, on both central diagonals, thus only allowing for calculation of axial forces in the bracings.

the diagonals), and no quantitative evaluations were given on the relative or combined influences of the important factors such as the lengths of struts, connection arrangements, intermediate supports and main leg restraints.

Nevertheless, the buckling curves obtained from regression analysis of these experimental results given in [49] can be used for design, within the same range of slenderness ratios as those used in the experimental procedures.

Behncke [11], on the other hand, conducted tests on similar but reduced-scale frames, as shown in Figure 1.08, under laboratory conditions. Deflections and strains were measured on both the tie and the strut, at midspan and also at the cross-over joints. Based on the analysis of these results, the behaviour of typical cross-bracing systems was described as follows:

- The struts did not reach their elastic buckling load. In all tests, including values of slenderness ratio as high as 160, yield of the extreme fibres due to bending and axial compressive force occurred prior to collapse, thus reflecting inelastic instability.

- For slenderness ratios of 140 and 160 the values of maximum strain in the tie was always lower than those in the strut for similar axial loads. The tie, however, also yielded prior to failure at a slenderness ratio of 90 due to the increasing effect of axial force, indicating that some transfer of load between the diagonals took place after the strut had lost its load-carrying capacity.

- Lateral displacements of both bracings occurred symmetrically at low load levels in a direction

perpendicular to the plane of the frame. However, the out-of-plane stiffness of the diagonal in tension increased with higher loads and larger lateral deflections until a node was enforced at the cross-over joint. As conditions approached failure, there was a change to anti-symmetrical deflections in the struc, while simultaneously large deflections developed in the subspan in which instability was dominant, about the minor axis of inertia of the section. This deformation history, shown in Figure 2.02, generally followed a similar pattern in all the tests at increasing loads.

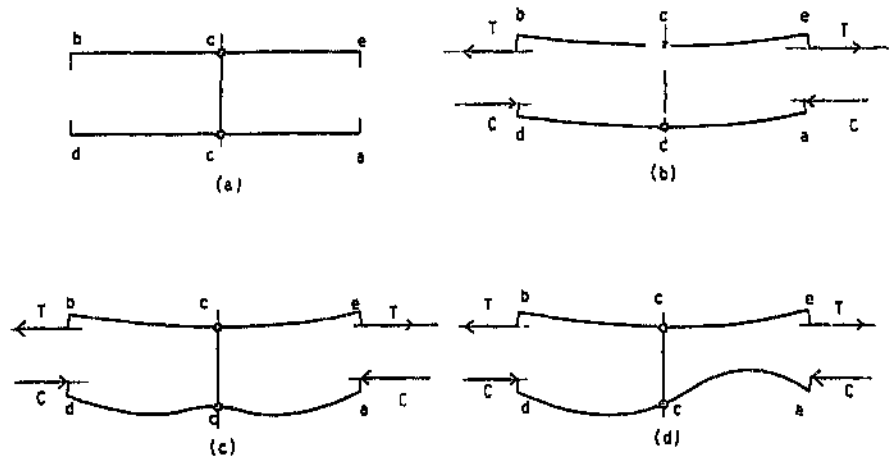

Figure 2.02: Cross-bracing deformation history reported by Behncke [11], see also Figure 1.01-b. a) Unloaded frame: no deflections. b) Low loads: the tie and strut deflect in the same out-of-plane direction. c) Close to failure: the tie gives support at the cross-over joint c. Deflections at midspan of the strut increase. d) Failure: typical anti-symmetrical cross-bracing failure mode. These results are confirmed in the present investigation.

- Finally, it was confirmed that the effects of eccentricity of load and end restraint were not constant, but changed as a function of the slenderness ratio.

It was also established, for the particular test conditions in the investigation referred to above, that the resistance of the bracings was primarily influenced by the following factors:

- The length ratio $r=L_s/L_g$, defined by the slope of the main legs, α, and by the relative inclination of the diagonals, β, as indicated in Figure 2.03. Diagonals with length ratio $r=1.0$, corresponding to frames with parallel legs, required higher forces to collapse in comparison with bracings with identical slenderness ratio but with length ratio $r<1.0$, corresponding to frames with inclined legs.

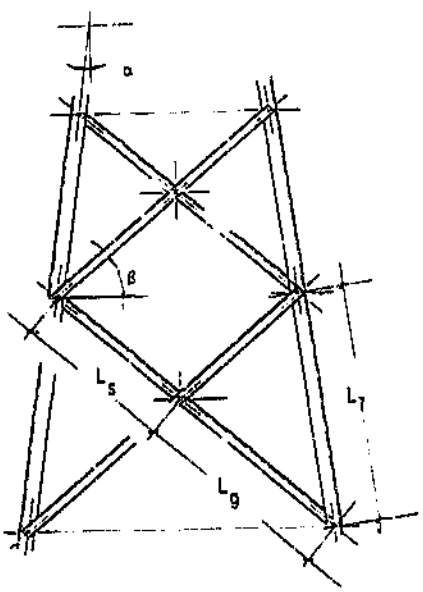

Figure 2.03: Locked-in systems of crossed diagonals.

- The end restraint, which is defined by: (a) the number of bolts in each connection, (b) the flexural and torsional stiffness of the main legs, and (c) the adjacent panels of bracing relative to that of the centre panel of diagonals. It was observed that any increase of end fixity generally resulted in an improvement of the resistance of the bracing.

Experiments on reduced-scale structures or on simplified frames, such as described above, present the problem of an excessive number of influences, which are usually very difficult to identify, control and evaluate. Investigators have to isolate the test specimens from all possible loading and boundary effects, as well as eliminate initial imperfections, in order to assess the material behaviour. Similar problems are encountered when trying to simulate the behaviour of an experimental model, either theoretically or by means of any other method of analytical evaluation.

In the original experimental research conducted by Behncke [11], for example, it was possible to identify the following problems:

- The sizes of the main legs were disproportionately large compared to the sizes of the diagonals.

- The relative inclination of the bracings with respect to the frame's horizontal axis, β=30°, is usually an upper extreme in typical tower panels.

- The frame supports and connecting beams imposed full restraint to torsional rotations of the main legs, see Figure 1.08.

- Tests of diagonals in locked-in frames, as shown in Figure

2.03, gave uncertain results. In particular, the ratio of axial forces in the tie and strut was not constant throughout the experiments, possibly due to movements of the supports.

As a result of these and other imperfections, the observed strength of the bracings was higher than it should have been, leading to optimistic failure predictions in the theoretical model.

Based on these findings, a new experimental programme was established, as described in the following Sections, in order to identify and quantitatively assess the most significant factors influencing the buckling characteristics of cross-bracing diagonals.

2.2 · Description of the experimental research programme

A theoretical non-linear analysis procedure was used in this investigation for modelling two-dimensional frames of various configurations. Several tests on frames with various bracing arrangements were therefore required to provide experimental verification of the analytical results.

In making these tests and the computer results acceptable, the dimensions of the frames had to correspond with the arrangements and relative sizes of diagonals most frequently found in towers of various types. It was therefore necessary to obtain some average values which were common to most towers of any type and voltage, and the range of laboratory experiments were then conducted on a few frames which were representative of the

average panel dimensions. This problem is discussed in the following Section.

2.2.1 - Tower survey

A survey was conducted in which the geometry of various transmission structures built in South Africa was examined, indicating a wide range of extreme values, which made it somewhat difficult to establish basic parameters for reference purposes. The survey included self-supporting towers of the following characteristics.

Voltage	Tower type
132 kV	Suspension Strain, light angle deviation Terminal
275 and 400 kV	Suspension Strain, light angle deviation Strain, heavy angle deviation Terminal

A list of the observed extreme values of various parameters in panels with cross-bracings is included in the table below:

Variable	MIN	MAX
Slenderness ratio L/r (diagonals)	90.0	130.0
Slope of legs α (°)	4.0	8.0
Relative inclination β (°)	30.0	50.0
Ratio of leg/bracing areas	2.4	4.2
Ratio of I/L (leg/bracing)	4.4	34.0

The slenderness ratio of the diagonals was calculated as L_g/r_v, where L_g is the longest unsupported subspan, as indicated in Figure 2.03, and r_v is the radius of gyration

about the minor axis of the angle section.

From the design point of view, the inclinations α and β shown in Figure 2.03 determine the length of the unsupported subspans of diagonals and legs, and also influence the distribution of forces in the members. The slope α of the main legs is a relatively standard parameter, and is proportional to the ratio of height to width of base of the towers, which generally changes very little. The inclination β of the diagonals depends on the position of the bracing in the panel, which is set to improve the compression resistance of the main legs. This requirement varies with the loading conditions, the geometry of the panel and the sizes of the members.

The ratio of areas and the ratio of relative stiffness were used to evaluate the relative size of the diagonals and main legs in the tower panels. The relative stiffness is given by I/L, where I is the moment of inertia about the section's minor axis, and L is the length of bracing L_g, or length of main leg L_l, as shown in Figure 2.03.

With regard to member connections, it was observed that most members in the panels are connected to the legs with two or more bolts, with the exception of suspension towers for lower voltages, which are usually designed with single-bolt connections. However, this is also a function of the sizes of bolts and members, the quality of steel of bolts and angles and, finally, of requirements contained in the design specifications.

The experimental frames were thus designed in accordance with the above typical dimensions of real towers, but, in view of the available space and also the maximum load capacity of the existing equipment and supports in the laboratory, to a reduced

scale.

The direct method of model analysis and the method of dimensional analysis were used to define the relationships between the models and prototype frames. It was found that the most convenient linear scale was approximately 1.8, resulting in the following dimensions for the experimental steel angles and bolts:

Main legs	L70x70x6	through	L90x90x8
Diagonals	L45x45x3		
Bolts	M12		

However, two additional angle sizes were considered, due to the following restrictions:

- Main legs of L70x70x6 accept only one-bolt connections without a gusset-plate. The introduction of a plate is not desirable due to the unknown additional restraint in the joints. Legs of L80x80x6 were thus included as minimum size of main legs for two-bolt connections.

- The width-to-thickness ratio, b/t, of the L45x45x3 diagonals is near the allowable limit for steel of 300-W quality, which may result in local failure of the strut's flanges prior to flexural buckling. Therefore L40x40x3 angles were also included as diagonals.

The size of angles in the outside panels of bracing was L50x50x5 for all tests.

2.2.2 - Characteristics of the experimental frame and bracing arrangements

Numerous tests were conducted on eight principal frame arrangements, such as shown in Figures 2.04-a and 2.04-c, as well as on alternative arrangements, such as locked-in systems, Figure 2.04-b, and diagonals with redundant bracings, as in Figures 2.04-d and 2.04-e.

The experimental frames and diagonals were designed, constructed, assembled and tested in accordance with typical tolerances and recommendations presently in use in South Africa, as contained in Eskom's Code of Practice [64].

The test programme consisted of at least one destruction test for each set of specimens. However, various non-destructive tests were performed in each case, in order to assess and

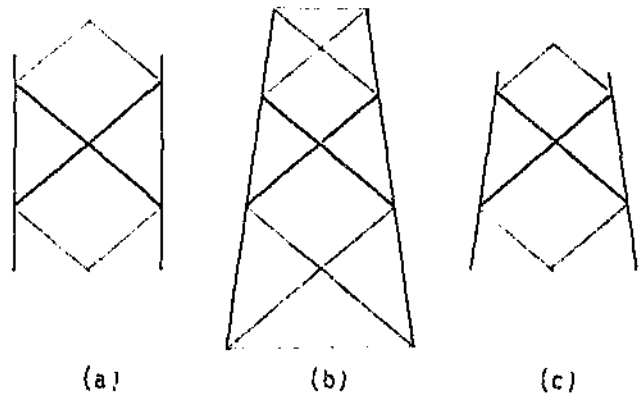

Figure 2.04: Various experimental frame and bracing arrangements in the present investigation. (a) Normal frame, parallel legs. (b) Locked-in system, inclined legs. (c) Normal frame, inclined legs.

confirm the observed behaviour of diagonals and frames, and also for calibration purposes. The main variables for these experiments are listed in Table 2.01, and can be summarized as follows:

- Length of specimens and slenderness ratio (Columns 5-6).
- Relative inclination of diagonals, angle β, and slope of main legs, angle α (Columns 2-3).
- End condition, represented by one or two-bolt connections and by two different leg sizes (Columns 8-9).
- Alternative arrangements of bracing.

The test rigs were specially designed to eliminate as many influences and constraints from the supports as possible, thus simulating conditions existing in continuous panels connected to other parts of the structure, as illustrated in Figure 2.05. This required a particular system of testing equipment, which is examined in the following Sections.

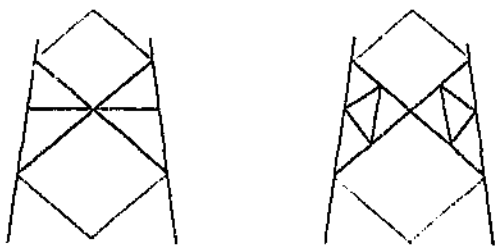

Figure 2.04: (d) and (e) Additional frame arrangements with inclined legs and redundant bracings.

TABLE 2.01

Main characteristics of the test frames and specimens

Test Designation	Frame characteristics			Diagonals L40x40x3			End Conditions	
	α (°)	β (°)	$\frac{L_s}{L_g}$	L_g (mm)	$\frac{L_g}{r_v}$	f_y (MPa)	Leg size (mm)	Bolts M12
1	2	3	4	5	6	7	8	9
102	8	40	0.789	800	100	317	L80x80x6	2
202	0	30	1.000	1000	130	329	L80x80x6	2
302	0	40	1.000	1000	130	333	L80x80x6	2
402	0	50	1.000	1000	130	339	L80x80x6	2
502	8	30	0.850	1000	130	333	L80x80x6	2
602	8	40	0.789	1000	130	325	L80x80x6	2
702	8	50	0.713	1000	130	329	L80x80x6	2
801	8	40	0.789	1250	160	333	L80x80x6	1
802	8	40	0.789	1250	160	321	L80x80x6	2
803	8	40	0.789	1250	160	339	L90x90x8	1
804	8	40	0.789	1250	160	329	L90x90x8	2

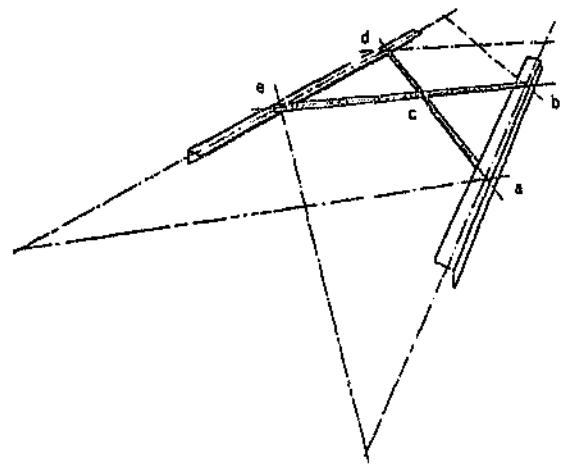

Figure 2.05: The experimental frames were designed to simulate conditions of the bracings and main chords as parts of a larger panel.

2.2.3 - Experimental equipment

The general test setup is shown in . ures 2.06-a, 2.06-b and 2.06-c. Three auxiliary structures were needed to keep the different elements in position and also to comply with the above requirements, as described below:

1- The main supporting structure, which could be adapted to test bracings of any dimensions within the range of sizes considered in this programme. The experimental frames were suspended horizontally from angle beams in the main rig by means of steel rods ended in Cardan's, or universal joints. These bars and joints, which are depicted in Figure 2.07, had the following functions:

   - Restrain out-of-plane frame movements while allowing in-plane displacements with a minimum of friction. To that end, the clamps connecting the bars and the beams were provided with lubricated rollers.

   - Permit free rotations of all nodes at which the frame was connected to the rods, in all directions.

   - Provide for out-of-plane adjustment, in order to control the position of the frame relative to a plane containing the applied and reactive forces.

   Two additional vertical rods with Cardan's joints were used to adjust the out-of-plane deflections of the cross-over points in the panels adjacent to the main diagonals, as indicated in Figures 2.06-a and 2.06-c.

Elevation

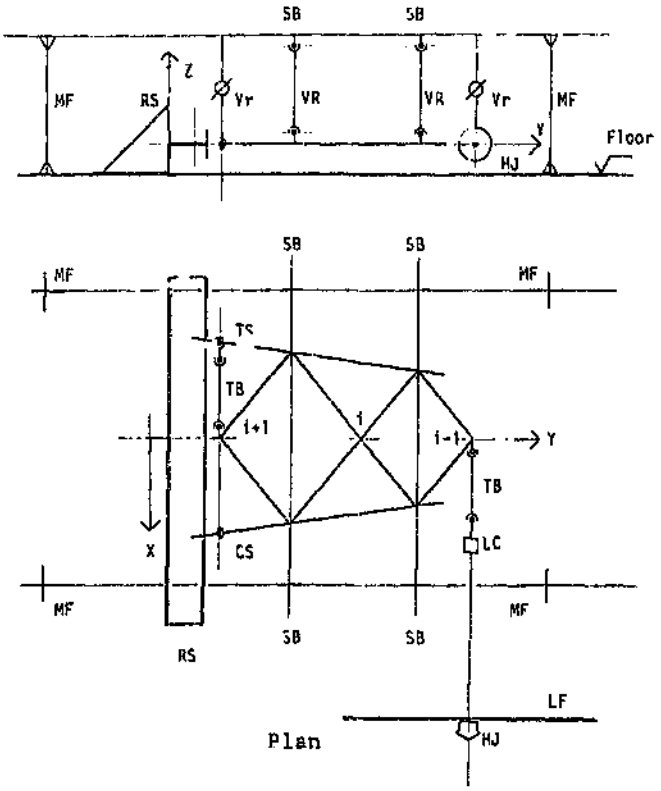

Figure 2.06-a: General test setup in the present investigation.

Notation

MF - Main supporting frame, Figure 2.06-b.
RS - Reaction-support frame, Figure 2.06-d.
LF - Load-pack support frame, Figure 2.11.
SB - Horizontal supporting beam, Figure 2.06-c.
VR - Vertical rods, Figure 2.07.
Vr - Special regulation rods, Figure 2.06-c.
HJ - Hydraulic jack, Figure 2.11.
TS - Tension leg support, Figure 2.10.
TB - Turnbuckle, Figures 2.08-a and 2.08-b.
CS - Compression leg support, Figure 2.09.
LC - Load cell, Figure 2.08-b.

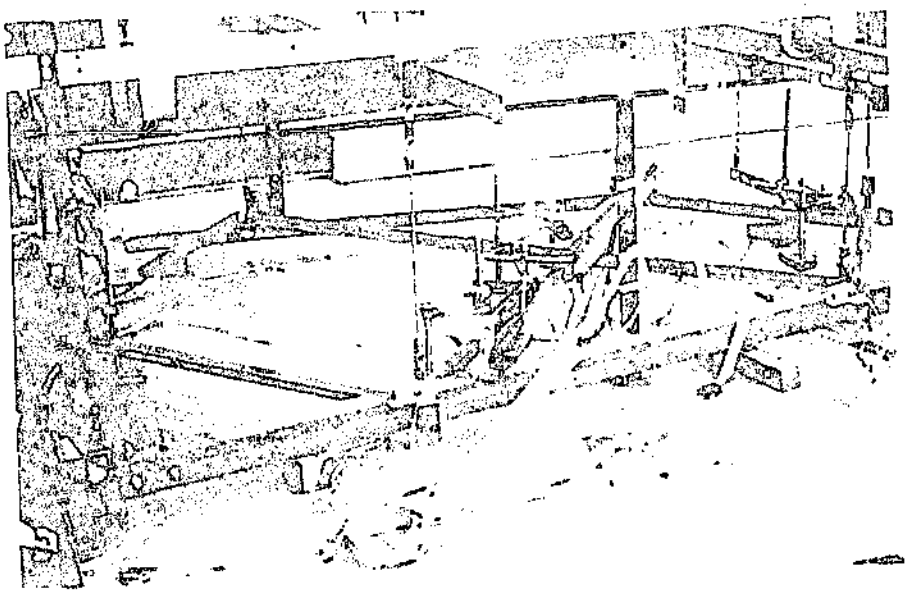

Figure 2.06-b: General view of testing rig assembled on the floor of the laboratory.

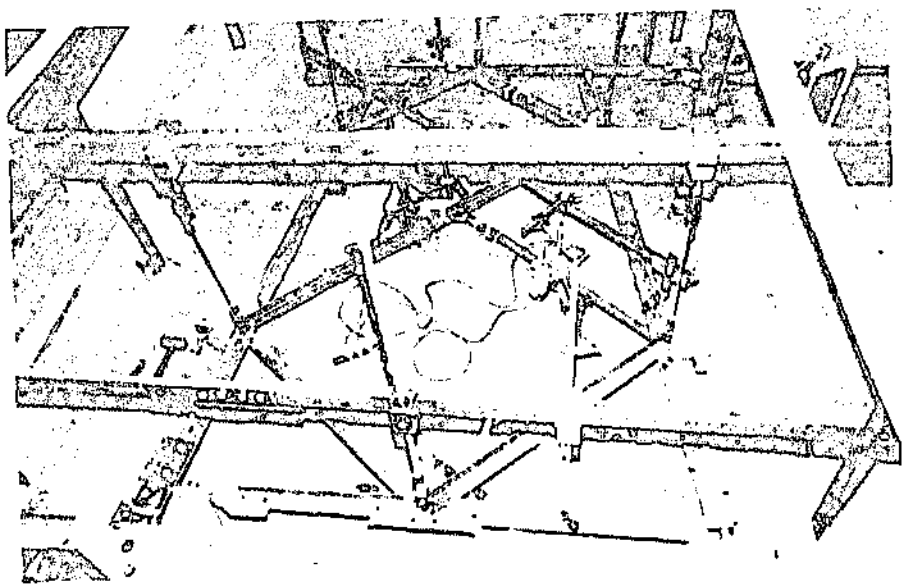

Figure 2.06-c: View of various elements in the main rig, including special regulation rods for adjusting the vertical displacements of the outside bracings.

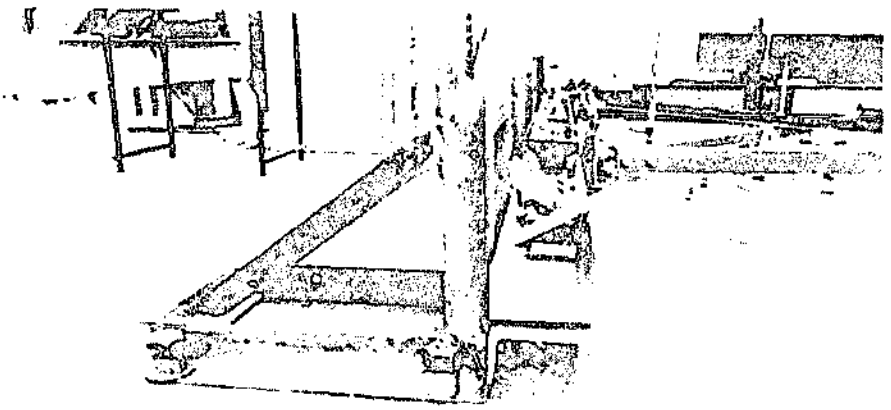

Figure 2.06-d: A view of the reaction-support frame, connected to the foundations.

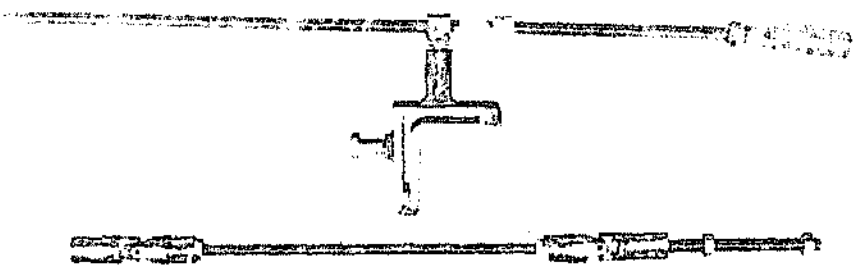

Figure 2.07: Special vertical rods with Cardan's joints.

In typical transmission tower panels, these joints can either be fixed to transverse beams or support , as indicated in Figures 1.08 and 2.01, or be free to displace in the out-of-plane direction, as in the central panel of cross-bracing. As the test frames simulated conditions of similar structures connected to other parts of a tower, as in Figure 2.05, it was felt that these nodes had to displace out of the plane of the frame to some extent.

Although these deformations were not considered as a variable in the present investigation, it is known that the out-of-plane displacements of these joints have an effect on the behaviour of the bracing. Bearing the above considerations in mind, and also to establish a standard procedure, the following empirical criterion was adopted to control these deflections:

- All three cross-over joints, i-1, i and i+1 in Figure 2.06-a, were initially set at the same horizontal level (usually a small deflection was recorded due to the bracing's own weight).

- At each load step, and prior to taking any readings, the out-of-plane displacements at the cross-over joints in the outside panels of bracing were adjusted with respect to the central cross-over as follows:

$$y_{i-1} = y_i . B_{i-1}/B_i$$

$$y_{i+1} = y_i . B_{i+1}/B_i$$

in which:

- y_i indicates the measured out-of-plane deflections at the central cross-over joint at each load interval

- B_{i-1}, B_i and B_{i+1} indicate width of the panel at the respective cross-over joints.

Thus in a frame with parallel legs, for example, out-of-plane displacements were set equal at all three cross-over joints throughout the test.

2- A second structure was designed to carry the reactions from the bracing and main tension and compression leg members to the foundations, as shown in Figure 2.06-d. These supports had the following characteristics:

- The test frame was restrained in the X direction at the lower cross-over point by a turnbuckle and shackles, connected to the reaction framework, see Figures 2.06-a and 2.08-a. The position of the test frame in the X direction was adjusted by acting on the turnbuckle. An identical mechanism was used at the top of the frame to apply the forces, thus ensuring similar boundary conditions, see Figure 2.08-b.

- The compression leg acted on a hemispherical joint and on a double axial ball bearing resting on the supporting structure, as shown in Figure 2.09. This arrangement permitted free rotations but restrained displacements about all three axes X, Y and Z. It was, however, possible to adjust the position of the support in the Y direction, see Figure 2.09.

- The tension leg acted on a similar device, also comprising a hemispherical joint and axial ball bearings, see Figure 2.10. However, its design was more elaborate, due to the difficulty of transmitting a tension force from the main leg, with variable slope, to the restraining frame, through a non-friction joint Free rotations were permitted about all three axes, as well as adjustments in the Y direction.

  Both the tension and compression joints were effectively located at the centre of the hemispheres, and were subsequently assumed theoretically as simply-supported hinges. These joints were designed to carry a maximum axial force of 150 kN.

3- A third structure supported the hydraulic cylinder from which the test forces were applied, and was also anchored to the foundations. The jack was mounted on a double-channel beam which allowed for lateral displacements and adjustment, as indicated in Figure 2.11. A steel rod connected the jack to a load cell and, finally, to the bracing at the top of the frame through a second set of shackles and turnbuckle, as in Figure 2.08-b.

This rather complex test installation was developed through several non-destructive test on various frame arrangements. It eliminated most of the effects induced by the boundary conditions on the test specimens at all load levels, such as out-of-plane frame displacements and, in particular, rotational restraints to the legs, as well as to the nodes connecting the frame and the lateral bracing.

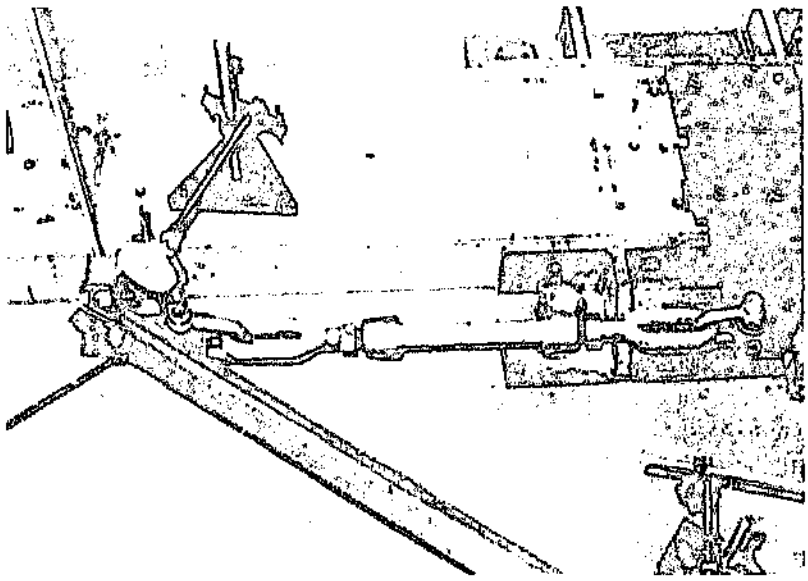

Figure 2.08-a: Turnbuckle and in-plane support of the experimental frame. Also showing the out-of-plane regulation rod at the reaction-level cross-over joint.

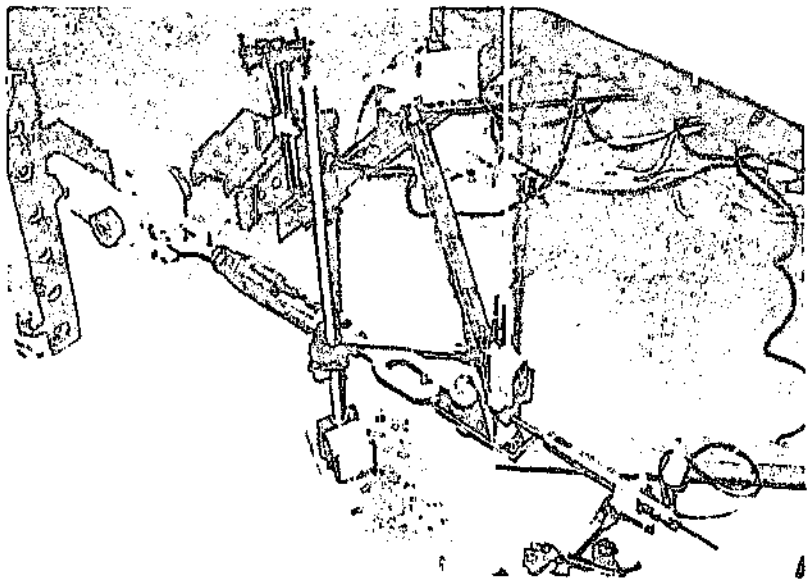

Figure 2.08-b: Turnbuckle, load cell and out-of-plane regulation rod at the load-level cross-over joint.

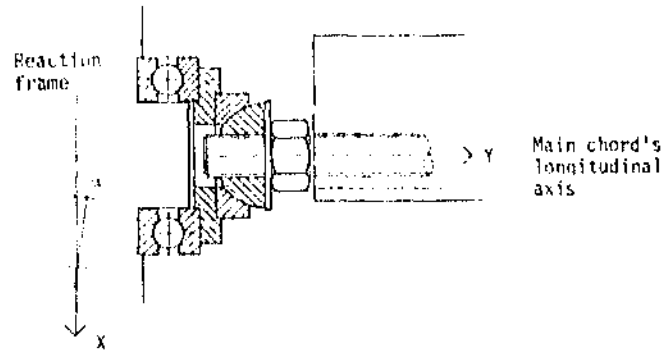

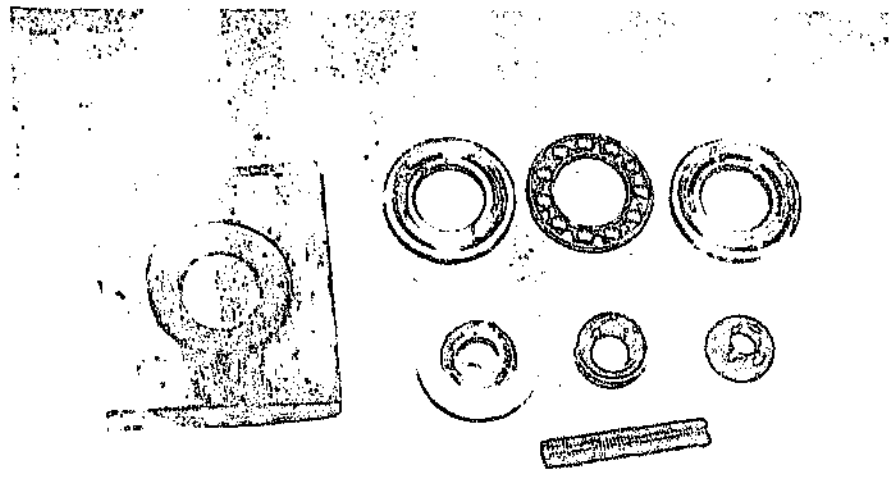

Figure 2.09: Assembly and detail of compression leg support, which was designed to allow for free tor. 'onal rotations of the main chord, as opposed to the fixed support conditions in frames shown in Figures 1.08 and 2.01. The angle ∝ indicates slope of the main chord.

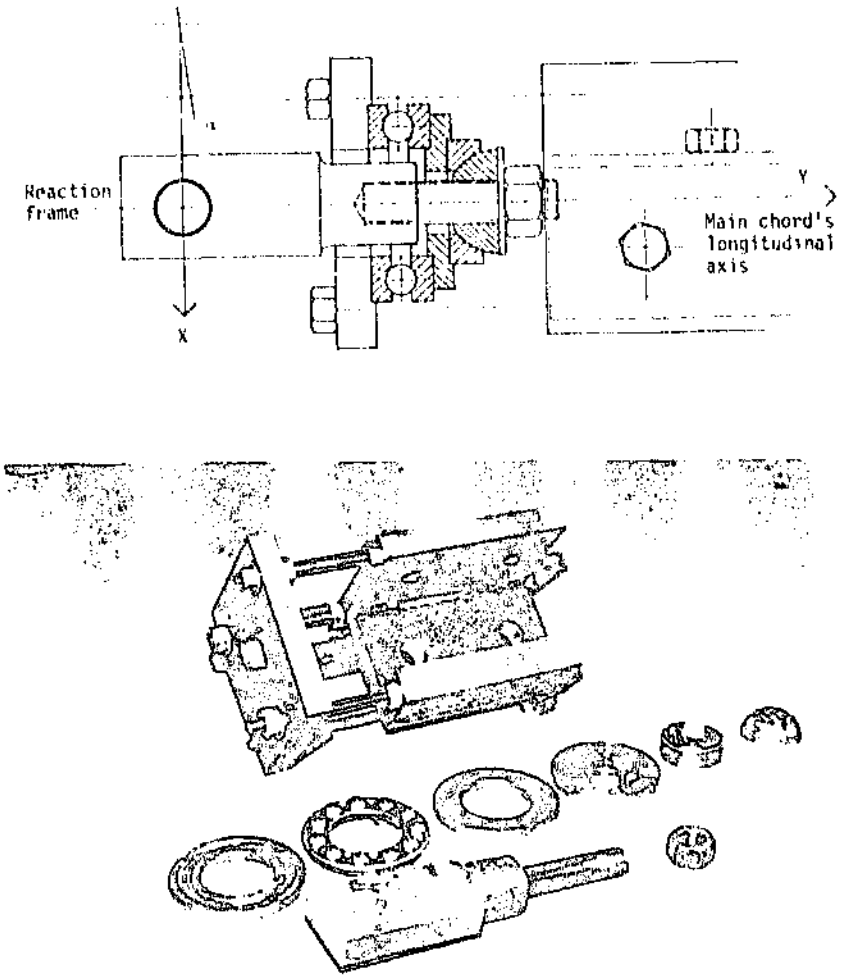

Figure 2.10: Assembly and detail of tension leg support, which was designed to allow for free torsional rotations of the main chord, as opposed to the fixed support conditions in frames shown in Figures 1.08 and 2.01. The angle ∝ indicates slope of the main chord.

The hydraulic system was controlled from a Losenhausen universal testing machine, which allowed for automatic regulation of either constant or variable loading speed during the tests. In addition, loads could be kept constant at any level, for as long as required.

A single-action hydraulic jack was used to apply the loads, with a maximum capacity of 550 kN and a stroke of 152 mm, see Figure 2.11.

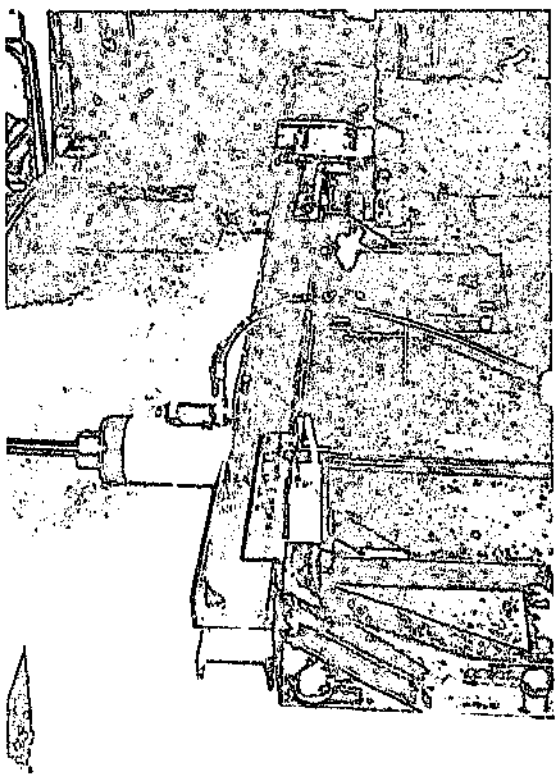

Figure 2.11: Load-pack and load supporting frame, which is connected to the foundations. The hydraulic jack has a capacity of 550 kN, with a maximum stroke of 152 mm. It is operated from a Losenhausen universal testing machine

2.2.4 - Instrumentation and measurements

The frame behaviour at increasing loads was controlled by the following instrumentation:

- Strains were measured at various points on both diagonal specimens by means of electric-wire strain gauges. The strain gauges were located in sets of three, as shown in Figure 2.12. Using these strain readings, it was possible to calculate the axial forces and principal bending moments at each location in the specimens by solving the following matrix equation (see Appendix A):

$$Ek \{\epsilon_i\} = [M] \{F_i\} \qquad ....(2.01)$$

in which:

  - E is the modulus of elasticity of material.
  - k is a strain gauge factor.
  - ϵ_i are the recorded strains.
  - M is a matrix calculated from the known geometric properties of the angle's cross section and the position of the strain gauges, as indicated in Figure 2.12 and also in Appendix A.
  - P_i are the unknown axial forces and bending moments about the principal axes of the angle section.

  Assuming linear strain distribution, it was also possible to estimate the maximum stress at the extreme fibres of the angles.

- Deflections were measured at various points using digital

linear displacement transducers, as indicated in Figure 2.13. The procedure for calculating the deflections of the heels of the angles is given in Appendix B. Locations of particular interest were the central cross-over joint, in the out-of-plane direction; and at midspan on the compression diagonal bracing, in the in- and out-of-plane directions. Additional readings were taken at the top of the frame, in order to evaluate its in-plane translation.

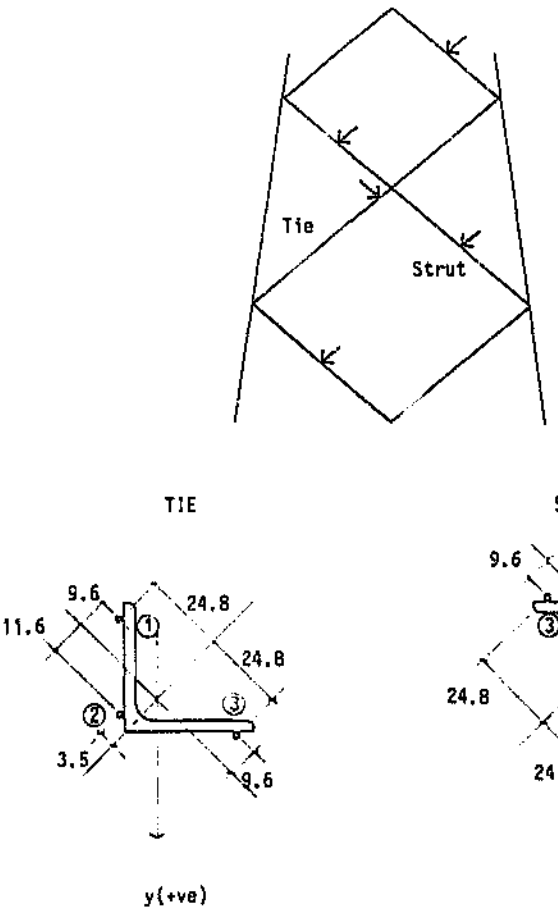

Figure 2.12: Typical location of strain gauge sets on the main diagonals and on the outside bracings. The figure also shows details of the gauge positions (1), (2) and (3) in the tie and strut diagonals.

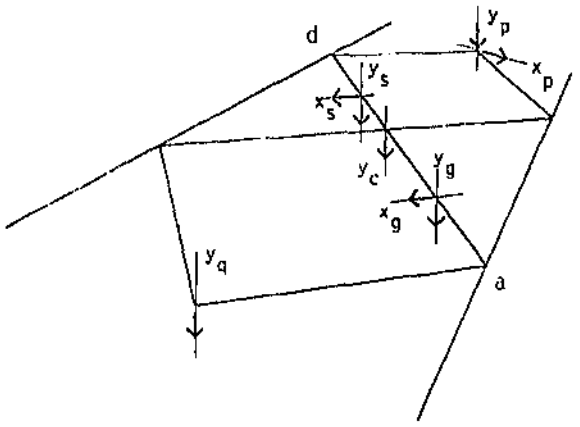

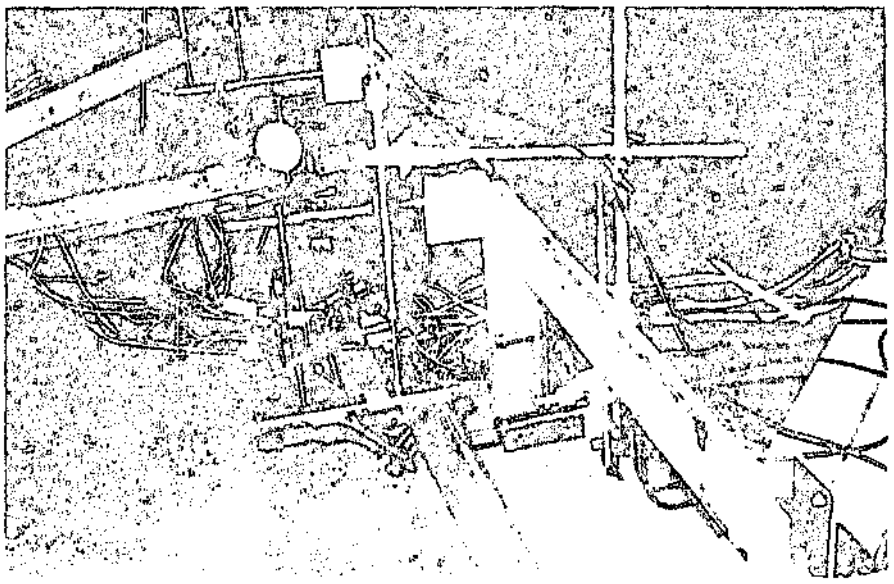

Figure 2.13: Location of displacement transducers in the testing frames. The most important readings were the in- and out-of-plane deformations of the central diagonals. A detail also shows the assembly of the transducers.

- Twelve high-precision digital rotation transducers (also known as inclinometers) were used to monitor rotations of the nodes at which the bracing specimens and the main legs were connected. Of interest were the main legs' torsional and flexural rotations, as well as the flexural rotations of the end of the central panel of bracing. The locations of the angle transducers and typical assemblies are shown in Figure 2.14.

Scanning was performed by a Fluke 2240-B programmable data-logger, and data were recorded on magnetic media by means of a personal computer terminal-emulator routine. A FORTRAN 77 program was then used to read the data and convert the voltage readings into meaningful expressions of force, bending, displacement and rotation. The flowchart depicted in Figure 2.15 summarizes this process.

2.2.5 - Material properties and dimensions of test specimens

The width and thickness of all steel diagonal specimens were measured carefully at various points using a micrometer and vernier, and it was found that the majority of dimensions were within the tolerances recommended by South African Standards for hot-rolled steel angles [59,64]. The cross-sectional properties were then calculated following the procedure and equations given by Madugula and Kennedy [34].

After evaluation of these results, it was determined that the errors introduced by ignoring small dimensional variations would not be larger than the errors introduced by calculating the areas and other properties, neglecting, as usual, the toes and

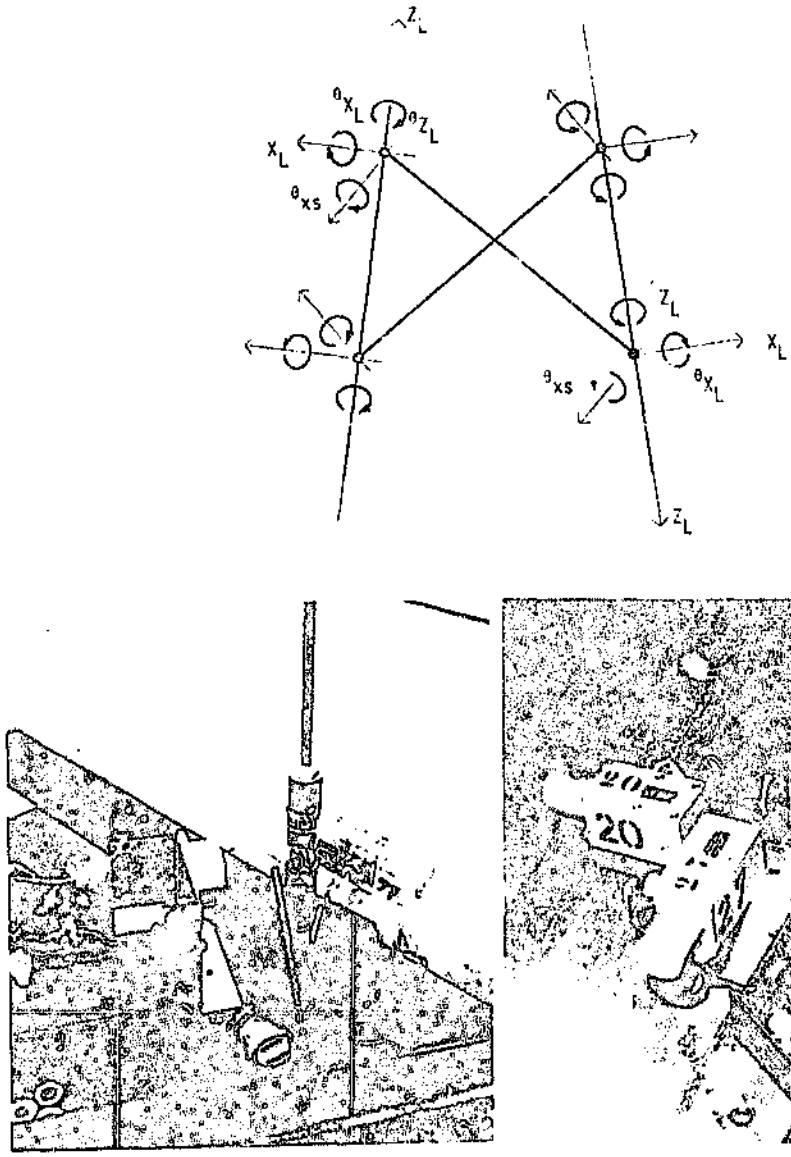

Figure 2.14: Location of angle transducers (inclinometers) at the four important nodes in the testing frames. Readings of interest were the flexural end rotations in the diagonals and the torsional main chord's rotations. A detail also shows the assembly of the inclinometers.

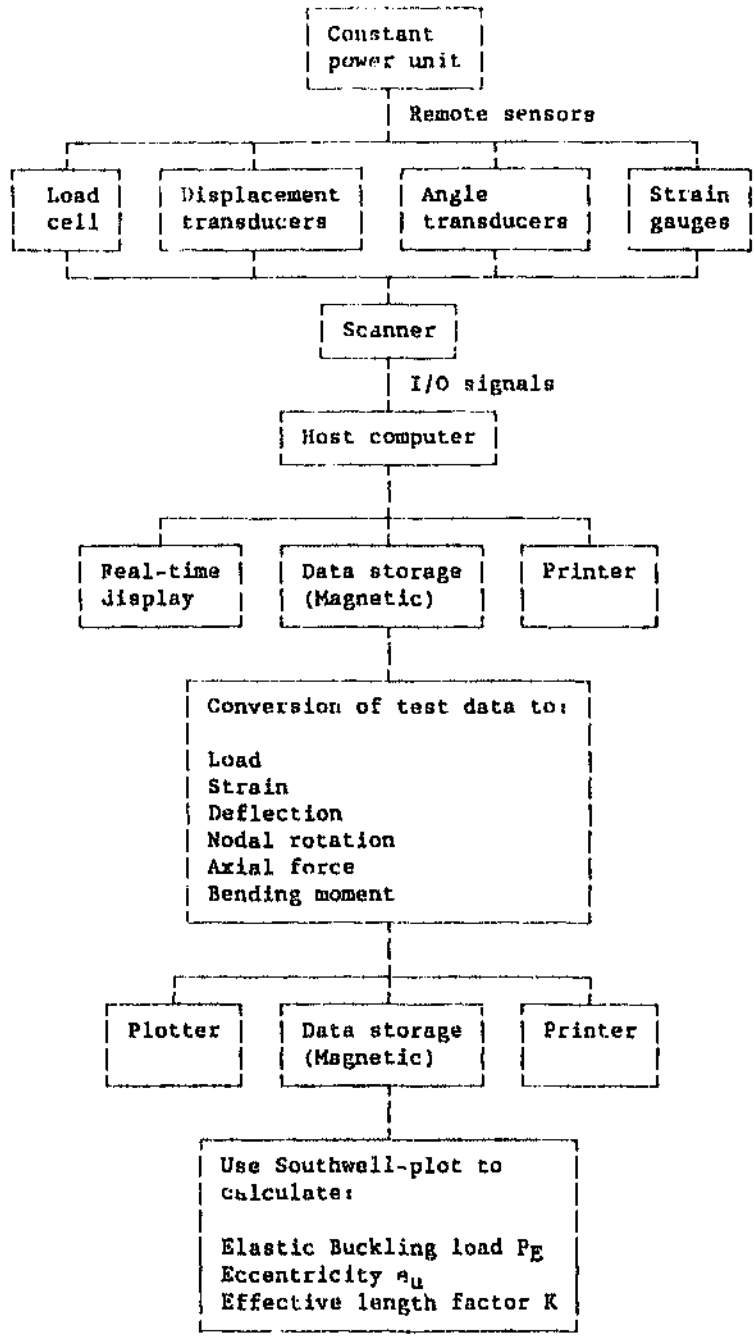

Figure 2.15: Flowchart depicting the recording and processing of test data.

fillet radii of the angles. As a consequence, test results calculations were based on the nominal dimensions of the diagonal specimens as indicated in the South African Steel Manual [59].

Diagonal test specimens were cut from angle steel bars of commercial lengths. Two test coupons were obtained from each bar at two different sections, namely in the middle and near one of the extremes. Tension tests were performed on these samples, as recommended in BS18 [65]. The resulting average tensile yield stresses for diagonal specimens in tests which were conducted to destruction are listed in Column 7 of Table 2.01.

2.2.6 - Test procedure

The test frame was assembled on the floor of the laboratory and, with the help of a crane, lifted into position and suspended from the main supporting structure by means of vertical rods with Cardan's joints, see Figure 2.06-a and 2.06-b.

In a second step, the vertical rods were adjusted until the frame was in a horizontal position, in which the centroidal axes of the legs were coincident with a plane defined by the centre-line of the supports, as indicated in Figure 2.06-a. A spirit-level was used for this operation. The frame was then connected to the horizontal support, Figure 2.08-a, to the tension and compression supports, Figures 2.09 and 2.10, and to the load-pack through the load cell, Figures 2.08-b and 2.11.

Subsequently, the position of the frame was adjusted acting on the turnbuckles, until its longitudinal axis was perpendicular

to a line joining the centroids of both main legs' hemispherical supports. The location of the load-pa k was also adjusted until its centre axis was perpendicular to ae frame's longitudinal axis, as shown in Figure 2.06-a. These stations at the supporting beams were marked in advance for all test alternatives, with the help of a theodolite.

The frame was now in place, ready for testing. The preceding steps were taken consistently to make sure that:

- The frame, the loads and the supports were all in the same horizontal plane. The frame was able to displace laterally, but without possibilities of out-of-plane distortions.

- The loads were initially distributed evenly between the diagonals, thus in principle reducing the possibilities of v riable ratios of tension-to-compression axial forces. This ratio has an effect on the buckling resistance of the struts.

- The axes of the tension and compression main supports were in line with the longitudinal centroidal axes of the main legs, thus excluding the introduction of undesirable bending effects.

The instruments were then installed, connected to the data-logger and, after applying some preload (usually 1-2 kN) to tighten the various shackles and connecting plates, initialized. Loads were applied from the hydraulic jack at approximately constantly increasing rates, and load increments were determined by real-time monitoring of the strain level at the critical section as indicated below:

- Below 1000 micro-strains, load increments of 5 kN.
- Between 1000 and 1300 micro-strains, load increments of 1 kN.
- Over 1300 micro-strains and up to failure, increments of 0.5 kN.

Loads were kept stable at each step for a reasonable time before scanning all instruments.

2.3 - Summary

An experimental frame support system and test procedure have been described in the preceding Sections. These are based on previous experiences on cross-bracing testing reported in [11] and also [49,63].

Particular care was taken during design of the test rig to avoid boundary effects and other distortions. The test specimens were thus isolated, and the various effects which have influence on the buckling strength of the bracing could be examined. The results of these experiments are examined in detail in Chapter 3.

CHAPTER 3

THE EXPERIMENTAL INVESTIGATION: ANALYSIS AND DISCUSSION OF TEST RESULTS

3.1 - Introduction

A considerable amount of information was obtained from different tests on experimental frames with crossed diagonals, as described in Chapter 2. In order to facilitate the analyses, test results have been grouped into seven different cases, each case allowing for one variable parameter, while all others are kept constant. Test results in each case are typical of all the non-destructive and ultimate tests performed for that particular alternative.

Although experimental results of structural members are traditionally represented by means of load-deformation curves, and this is usually very convenient, it was found in this investigation, neglecting a small effect due to residual stress, that strain-deformation curves offered a more consistent basis of comparison between various test alternatives. Two comments are given in order to substantiate this approach:

- The values of yield stress recorded from tension tests of 25 coupons were very uniform, with an average value of 328.4 MPa, a standard deviation of 5.9 MPa and thus a c.o.v. of less than 2%.

- Strains were always recorded [illegible] very near the failure

sections in all the compression diagonals. Therefore the increase of strain at the extreme fibre of the critical sections, and particularly the level of strain at yield, can be expected to be fairly uniform for all the diagonals, irrespective of the levels of axial force in the members.

The strain at the heels of the angles was used as reference, and was calculated by linear extrapolation of strain readings from gauges 1 and 2, as indicated in Figure 2.12 of Chapter 2. In some particular cases, however, load-deflection or other curves were used to enhance the presentation of results. All parameters were plotted until yield occurs at the extreme fibre.

The behaviour of the bracings under different conditions is discussed next, including analyses of the most important parameters, and an assessment of the end eccentricities is introduced in a later Section.

3.2 - Bracing behaviour

A number of test alternatives have been categorized into seven study cases, each addressing the effect of a single variable, as listed below:

- Case I : Variable slenderness ratio L_g/r_v,
- Case II : Variable diagonal inclination β - Parallel legs,
- Case III: Variable diagonal inclination β - Inclined legs,
- Case IV : Variable main leg slope α,
- Case V : Variable end condition,
- Case VI : Variable bracing arrangement, and
- Case VII: Locked-in systems.

3.2.1 - Case I: Variable slenderness ratio

Results from Tests 102, 602 and 802 are examined. The frame alternatives are shown in Figure 3.01, together with the positive directions for displacements and nodal rotations. All conditions, including frame geometry and number of connecting bolts, are the same in all three tests, and the slenderness ratio L_g/r_v is increased from 100 to 130 and 160. Characteristics of the bracing are indicated in Table 3.01, Columns 2 through 9, while failure loads are listed in Column 10.

Figure 3.I.01 (plots showing experimental results have been numbered in accordance with the test cases referred to in this section) shows the main leg's torsional rotations, θ_{zL}, recorded at node a, as indicated in Figure 3.01. It can be seen that the leg rotations for these tests are almost equal at all levels of strain, irrespective of the sizes of the frames.

The main leg's rotations θ_{zL} are also plotted in Figure 3.I.02 against the stress ratio f_n/f_y, where f_n is the nominal axial stress and f_y is the recorded yield stress of material. These curves show that the leg rotations increase with the slenderness ratio for the same level of axial forces in the bracing.

The strut's flexural rotations at the same node a, θ_{xS} in Figure 3.01, are shown in Figure 3.I.03. The effect of increasing the slenderness ratio is reflected by an increase of the strut's end rotations at all levels of load.

Deflections of the bracing are calculated from the test readings of in- and out-of-plane displacements, and also twist of the diagonals, as explained in Appendix B. The curves therefore refer to the absolute deflections of the heels of the angles. At the cross-over joint, however, it is considered that only out-of-plane deflections occur, and without significant twist of the section.

Out-of-plane deflections at the cross-over joint c, Figure 3.01, are shown in Figure 3.I.04. It is clear that these vertical deflections increase with the slenderness ratio L_g/r_v, and this is consistent with the rate of strut's end rotations discussed above.

Figures 3.I.05 through 3.I.07 show vertical and horizontal displacements at midspan g on the strut, and vertical displacements at the cross-over joint c, see Figure 3.01. The plots show that in all cases the horizontal deflections originally occur in the x negative direction, see Figure 3.01. Also, the pattern of vertical displacements at midspan g and cross-over c changes with increasing slenderness ratios as follows. at L/r=100, the cross-over joint always deflects more than at midspan, and the 2 curves never intersect. For slenderness ratio of 160, and particularly for 1-bolt connections, vertical deflections at midspan g can be larger than at the cross-over joint before failure occurs. This point of change in strut out-of-plane displacements occurs earlier at higher slenderness ratios, in coincidence with a higher flexibility in the bracing. Maximum out-of-plane displacements in the tension member, on the other hand, occur always at the cross-over joint c.

Curves of stress components about the minor v-axis at the strut's midspan g from Tests 102 and 802 are shown in Figure 3.I.08. It can be seen that, for the same level of strain, the axial forces account for approximately half of the maximum stress at L/r=100, whereas at L/r=160 the influence of the axial forces is reduced to about 30% of the total stress. This is consistent with the level of strut deformations in each case.

The behaviour of cross-bracing in frames of proportional size at increasing slenderness ratios can be summarized as follows:

- Main-leg torsional rotations increase with higher slenderness ratios. However, the main leg's rotational response is constant at all levels of maximum strain in the struts. The lower level of axial forces at higher slenderness appears to be compensated by a larger bending effect, thus resulting in similar levels of strain in the section at increasing loads.

- Strut-end flexural rotations and bracing out-of-plane deformations increase with higher slenderness ratios.

- The effect of the axial forces on the total maximum stress at the critical section decreases with increasing slenderness ratios. Conversely, the effect of bending through larger deflections increases with the level of slenderness ratio.

- As expected, resistance of the bracing decreases for increasing slenderness ratios, as shown in Column 10 of Table 3.01.

TABLE 3.01

Case I: Variable slenderness ratio

Test Designation	Frame characteristics			Diagonals L40x40x3			End Conditions		Test results
	α (°)	β (°)	$\frac{L_s}{L_g}$	L_g (mm)	$\frac{L_g}{r_v}$	f_y (MPa)	Leg size (mm)	Bolts	$\frac{f_{ult}}{f_y}$
1	2	3	4	5	6	7	8	9	10
102	8	40	0.789	800	100	317	L80x80x6	2	0.491
602	8	40	0.789	1000	130	325	L80x80x6	2	0.431
802	8	40	0.789	1250	160	321	L80x80x6	2	0.336

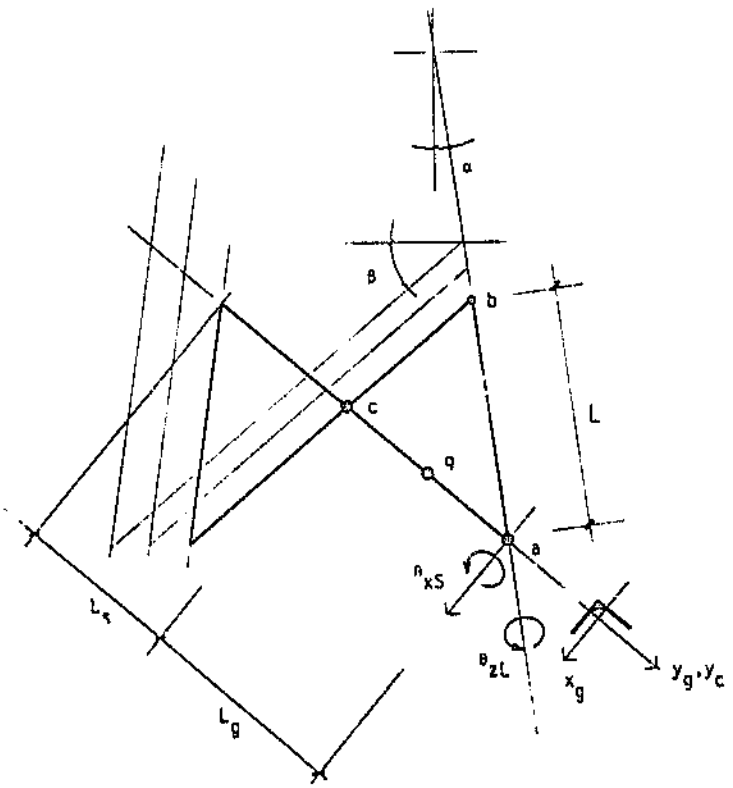

Figure 3.01: Comparison of results from tests on frames with identical conditions and variable slenderness ratios.

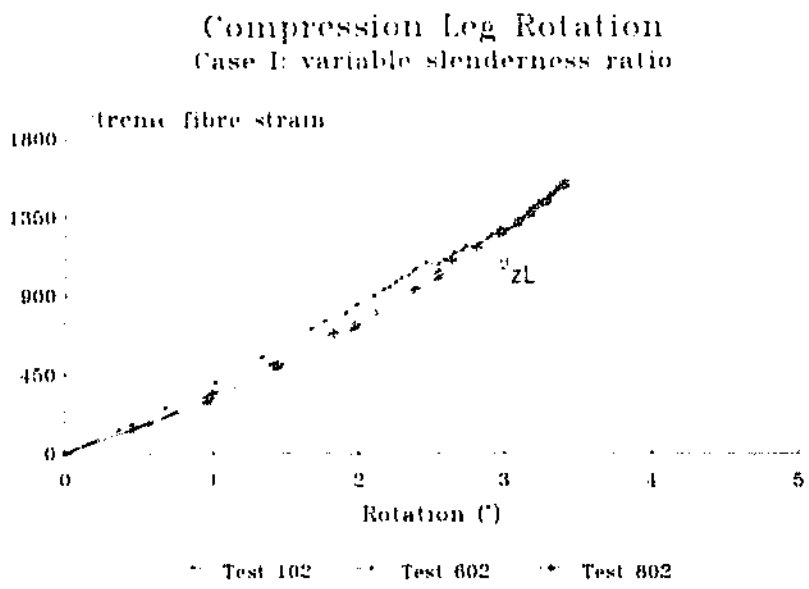

Figure 3.1.01: Main leg's rotational response at node n see Figure 3.01

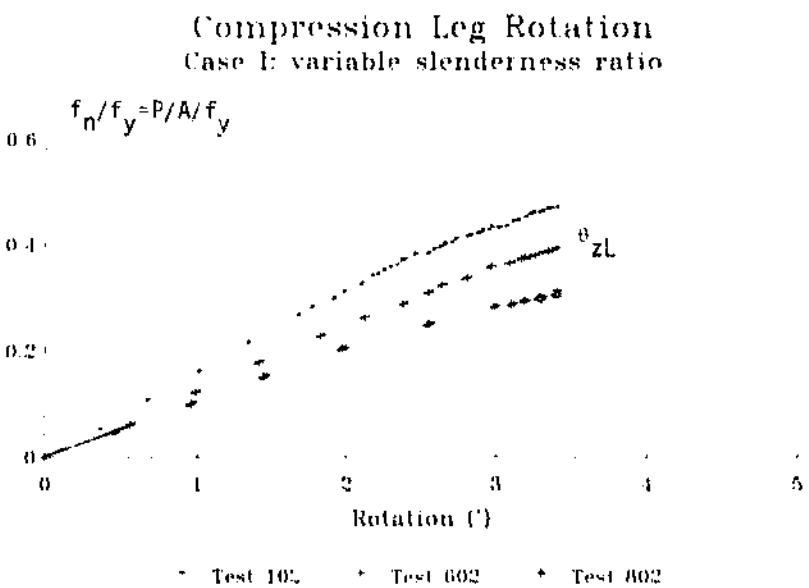

Figure 3.1.02: Main leg's rotational response at node n, see Figure 3.01

Strut Rotation
Case I: variable slenderness ratio

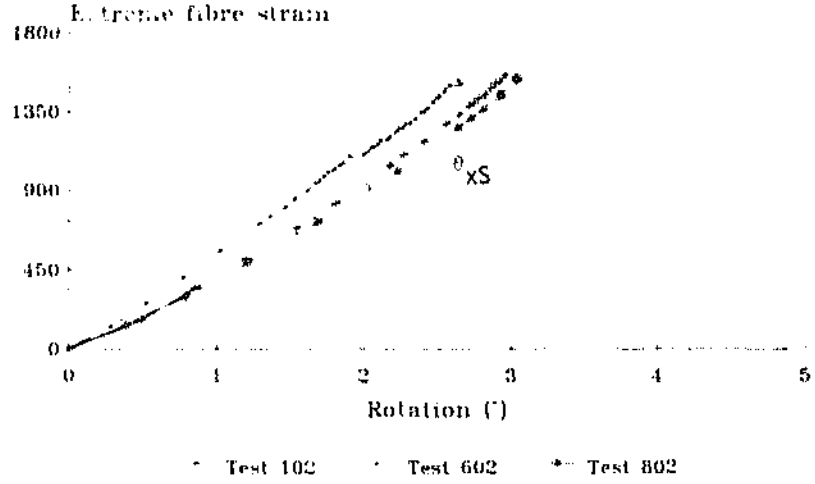

Figure 3.1.03: Strut's rotational response at node a, see Figure 3.01

Cross-over Joint Deflection
Case I: variable slenderness ratio

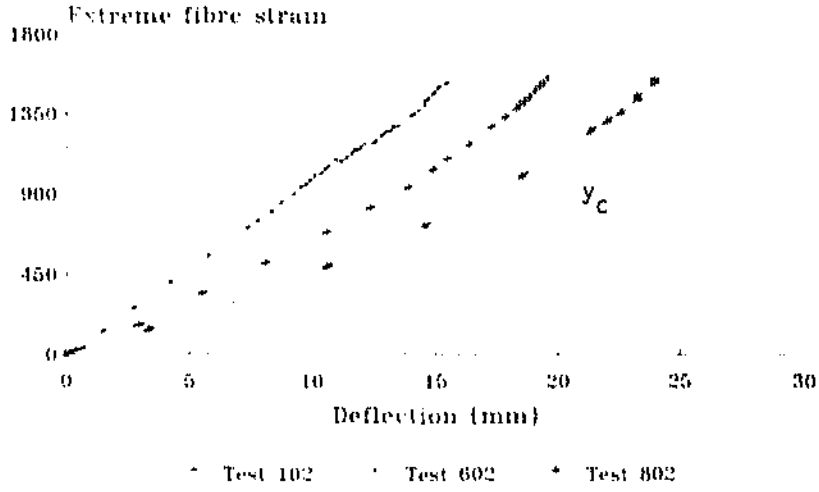

Figure 3.1.04: Bracing out-of-plane deflections at node c, see Figure 3.01

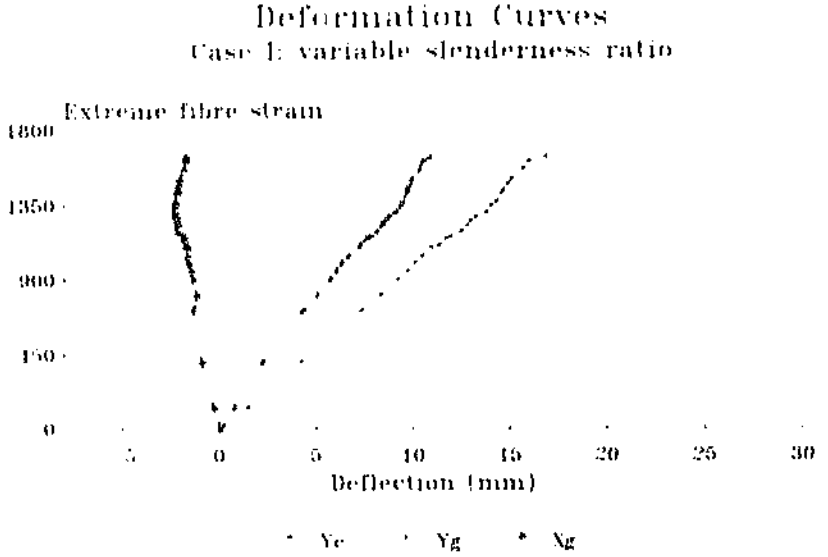

Figure 3.105: Vertical and horizontal strut deflections, see Figure 3.01
Test 102

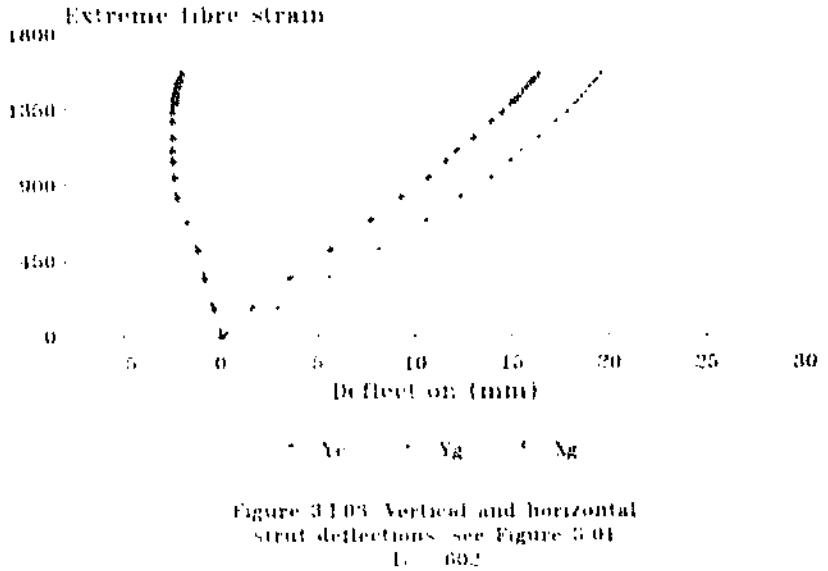

Figure 3.103: Vertical and horizontal strut deflections, see Figure 3.01
Test 602

Deformation Curves
Case I: variable slenderness ratio

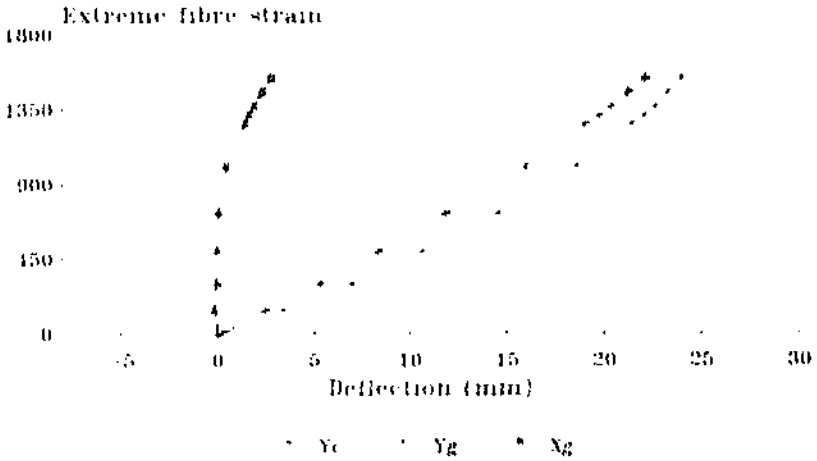

Figure 3.1.07: Vertical and horizontal strut deflections, see Figure 3.01
Test 802

Stress Comparison
Case I: variable slenderness ratio

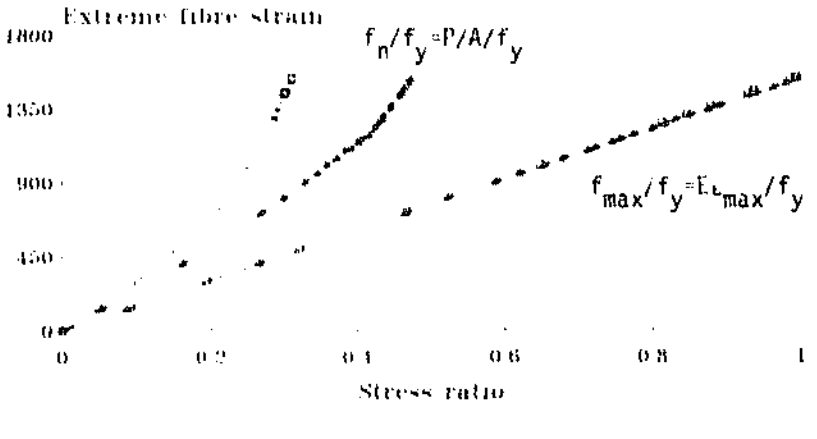

Figure 3.1.08: Nominal and maximum stress ratios for diagonals with slenderness ratios l_g/r_y 100 and 160

In view of the above conclusions it is apparent, for frames of proportional size, identical member sections and fairly similar boundary conditions, that no significant effects are introduced by the torsional stiffness of the main legs. Rather, the bracing appears to be influenced by the legs' flexural stiffness I_x/L, where I_x is the moment of inertia about the main leg's orthogonal axis, and L is the length of main leg between nodes b and a, as indicated in Figure 3.01. This latter effect will be discussed again in the following Sections.

3.2.2 - Case II: Variable diagonal inclination - Parallel legs

Results from Tests 202 through 402 are examined. Frames with parallel legs were tested with variable bracing inclination β, as shown in Figure 3.02. All other parameters, including slenderness ratio and end conditions are constant. Figure 3.02 also shows positive directions for rotations and deflections. Frame and diagonal data are given in Table 3.02, Columns 2 through 9.

In these frames with parallel legs failure occurred at the subspan s, see Figure 3.02. However, to be consistent with analyses of other test cases, nodal rotations and strut deflections corresponding to node s and subspan g will be examined first, and then they will be compared with those rotations and deformations recorded at node d and subspan s respectively.

The main leg's torsional rotations at node a, θ_{zLa} in Figure 3.02, are depicted in Figure 3.II.01. These curves show that leg rotations are larger for frames with increased inclination of

the diagonals, β. Torsional rotations at node d, θz_{Ld} in Figure 3.02, are shown in Figure 3.II.02. It can be seen that, for each test case the legs have rotated, in the positive direction at each node a and d, a similar amount. This clearly shows the uniform behaviour of both main leg supports, shown in Figures 2.09 and 2.10 of Chapter 2.

Similarly, the strut's flexural rotations at nodes a and d, θxS_a and θxS_d in Figure 3.02 and depicted in Figures 3.II.03 and 3.II.04 respectively, also increase with the inclination β, although the main leg rotations at the same nodes are larger.

Figure 3.II.05 shows out-of-plane displacements at the cross-over joint. Deflections increase from β=30° to β=40°, but are very similar between β=40° and β=50°.

Overall strut deformations in both subspans g and s, see Figure 3.02, can be described as follows:

- Test 202, β=30°: Horizontal deflections at midspan g take place initially in the negative x direction, Figures 3.02 and 3.II.06. Vertical deflections at the cross-over joint are always larger than at midspan g, see Figure 3.II.06.

  Combined deflections at both subspans g and s in Figure 3.II.07 show that horizontal and vertical deformations at subspan s (where failure occurred) are larger than at subspan g, and very similar to out-of-plane deflections at the cross-over joint.

- Test 302, β=40°: Figure 3.II.08 shows deflections in subspan g. It appears that an increase of the inclination β of the diagonals causes larger deflections in both the horizontal

and vertical directions, see Figures 3.II.06 and 3.II.08.

Deformations at both subspans g and s are shown in Figure 3.II.09. Note the reduced horizontal deflection at subspan s, while out-of-plane deflections at subspan s and at the cross-over joint are similar. Again, cross-over joint out-of-plane deflections are larger than at subspans g and s.

- Test 402, β=50°: Curves in Figure 3.II.10 confirm that increments of the inclination β of the diagonals induce larger deflections in the x-direction and y-direction at subspan g, see Figure 3.02.

  The combined deflections at subspans g and s in Figure 3.II.11 show also, in this case, that deflections in the x-direction are smaller at subspan s, while there are no changes in the pattern of out-of-plane deflections about the cross-over joint.

Out-of-plane displacements are larger in Tests 302 and 402. Also, the strut vertical deflections at the cross-over joint c are always larger than at subspans g and s, and the curves never intersect. These results, in both the horizontal and vertical directions, were confirmed through second tests in all three cases.

The stress components in the strut at midspan are shown in Figure 3.II.12. It is clear that variations in the inclination of the bracing do not have significant influence on the bending effect, in spite of the observed differences of in-plane and out-of-plane deformations for increasing inclination β.

Table 3.02

II: Variable diagonal inclination

Parallel legs

Test Designation	Frame characteristics			Diagonals L40x40x3			End Conditions		Test results
	α (°)	β (°)	$\frac{L_s}{L_g}$	L_g (mm)	$\frac{L_g}{r_v}$	f_y (MPa)	Leg size (mm)	Bol	$\frac{f_{ult}}{f_y}$
1	2	3	4	5	6	7	8	9	10
202	0	30	1.000	1000	130	329	L80x80x6	2	0.412
302	0	40	1.000	1000	130	333	L80x80x6	2	0.395
402	0	50	1.000	1000	130	339	L80x80x6	2	0.421

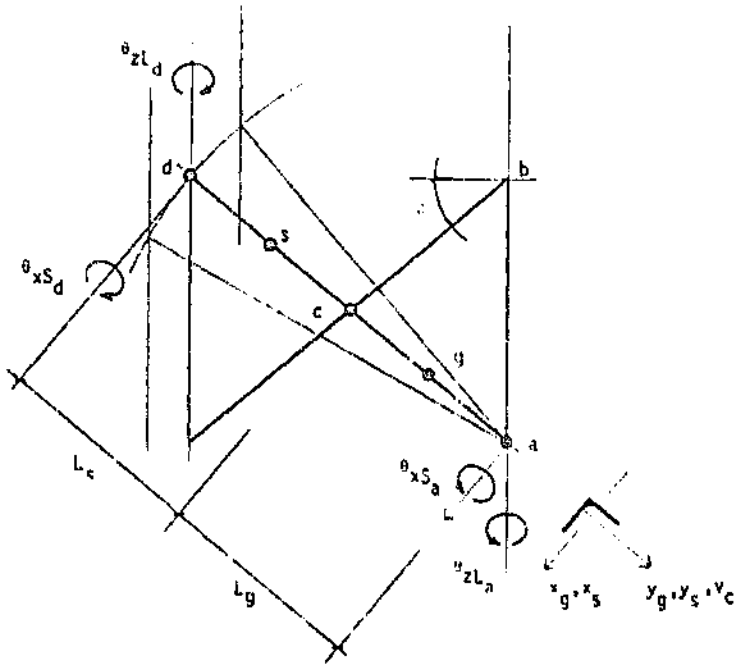

Figure 3.02: Comparison of results from tests on frames with parallel legs, constant slenderness ratios and variable diagonal inclinations.

Compression Leg Rotation
Case II: variable diagonal inclination

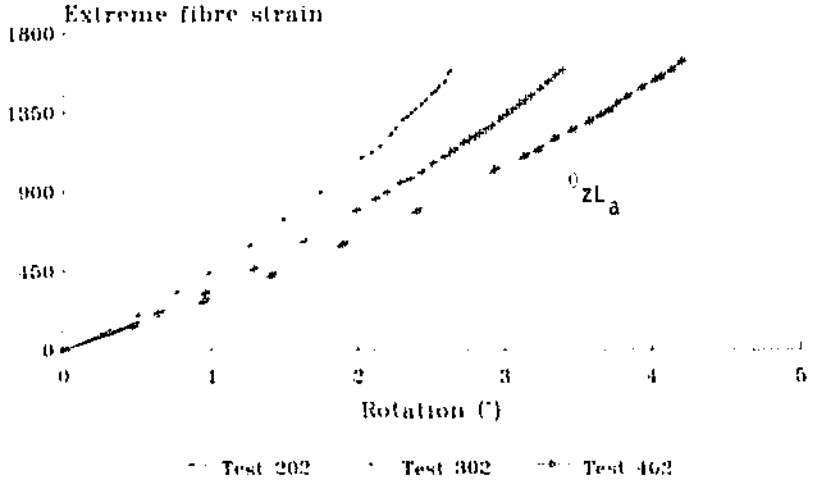

Figure 3.II.01: Main leg's rotational response at node a, see Figure 3.02

Compression Leg Rotation
Case II: variable diagonal inclination

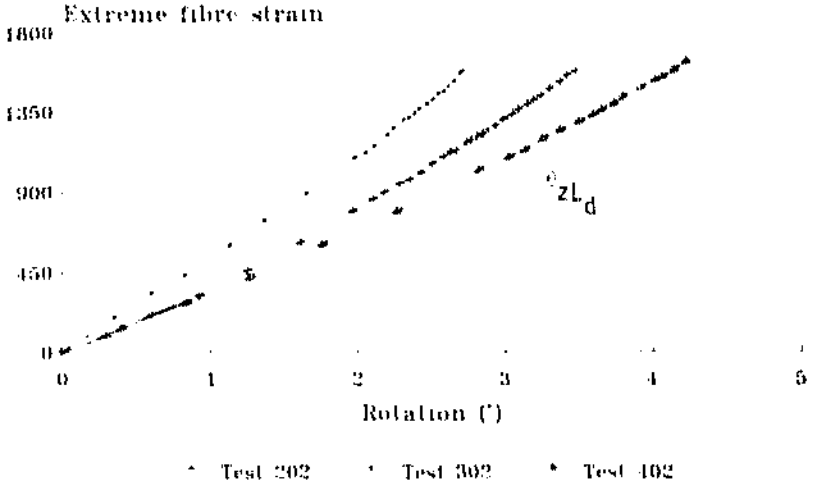

Figure 3.II.02: Main leg's rotational response at node d, see Figure 3.02

Strut Rotation
Case II: variable diagonal inclination

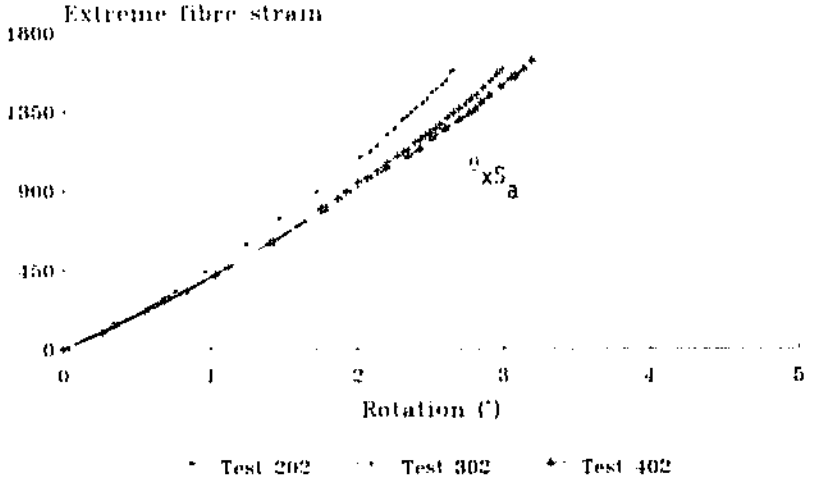

Figure 3.II.03: Strut rotational response at node a, see Figure 3.02

Strut Rotation
Case II: variable diagonal inclination

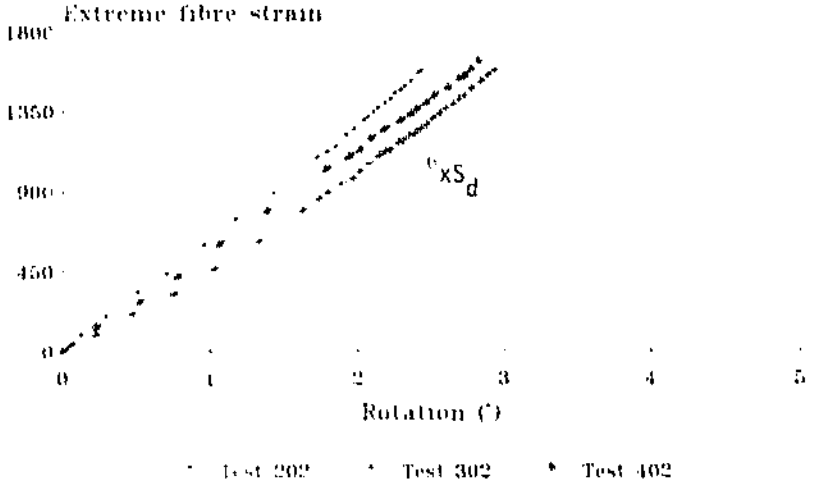

Figure 3.II.04: Strut rotational response at node d, see Figure 3.02

Cross-over Joint Deflection
Case II: variable diagonal inclination

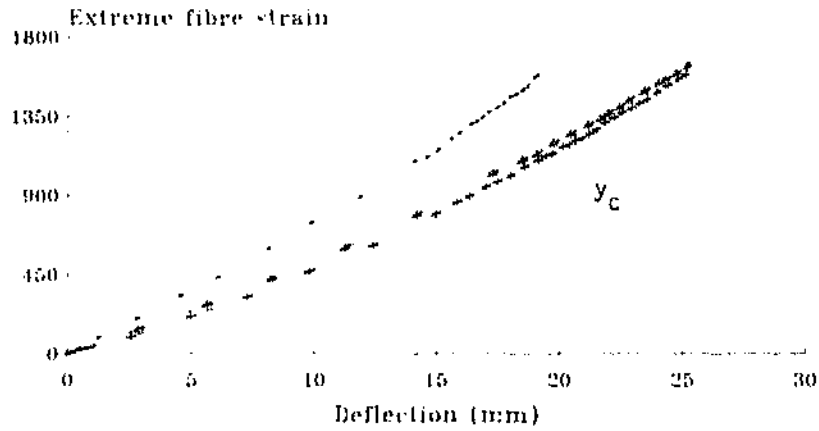

Figure 3.II.05: Bracing's out-of-plane deflections at node c see Figure 3.02

Deformation Curves
Case II: variable diagonal inclination

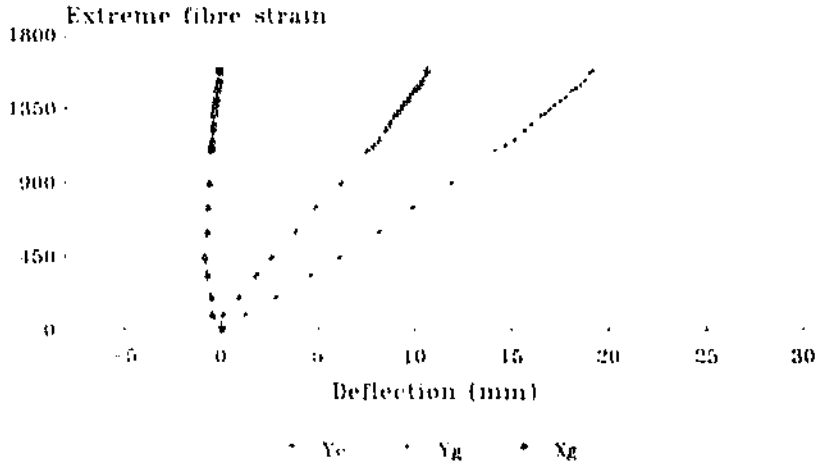

Figure 3.II.06: Vertical and horizontal strut deflections, see Figure 3.02
Test 202 - β=30°

Deformation Curves
Case II: variable diagonal inclination

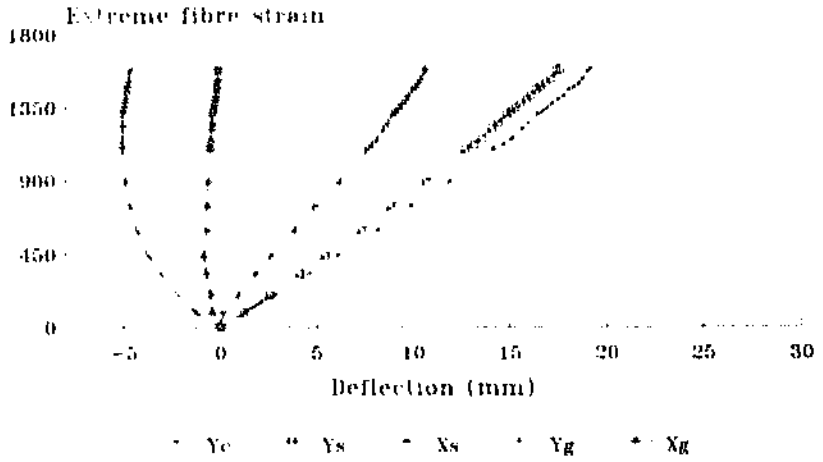

Figure 3.II.07: Vertical and horizontal strut deflections, see Figure 3.02
Test 202 - β=30°

Deformation Curves
Case II: variable diagonal inclination

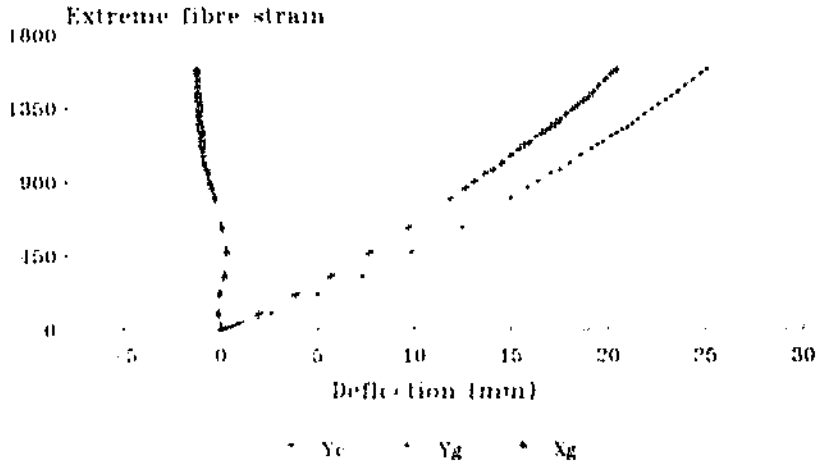

Figure 3.II.08: Vertical and horizontal strut deflections, see Figure 3.02
Test 302 - β=40°

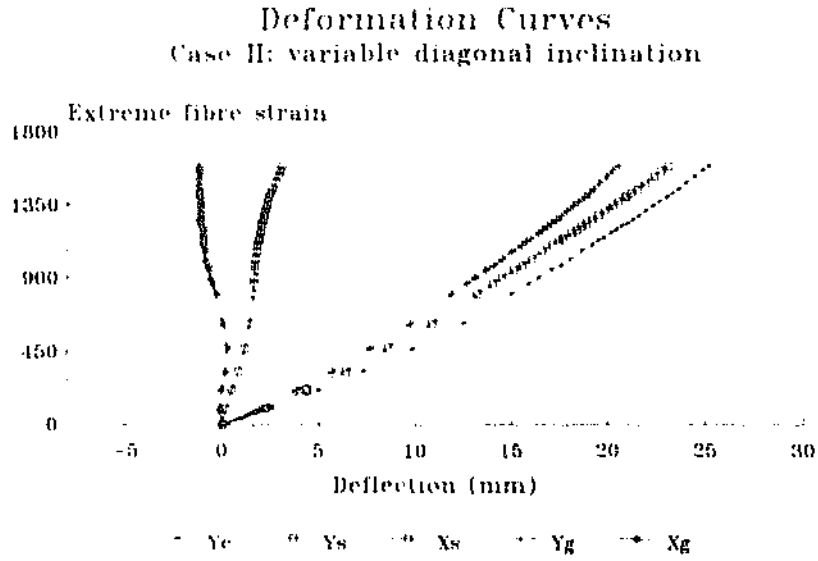

Figure 3.II.09: Vertical and horizontal strut deflections, see Figure 3.02
Test 302 - β=40°

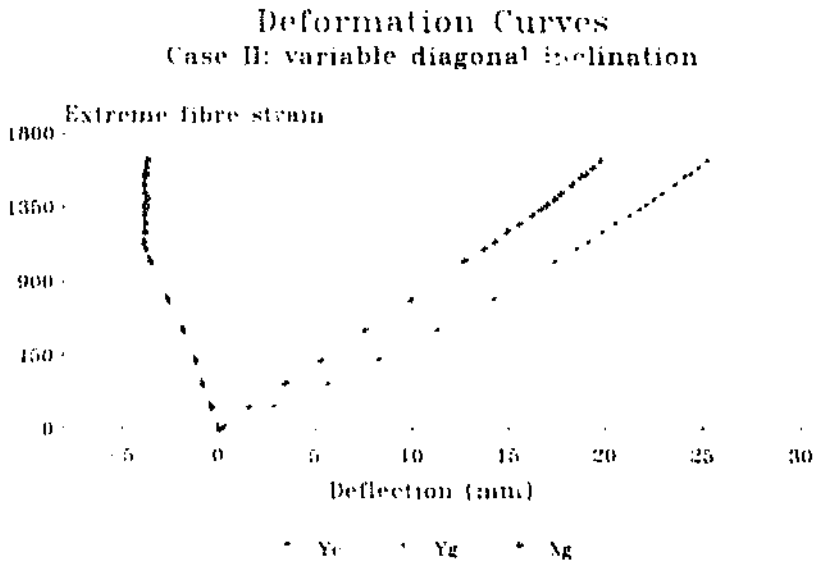

Figure 3.II.10: Vertical and horizontal strut deflections, see Figure 3.02
Test 403 - β=50°

Deformation Curves
Case II: variable diagonal inclination

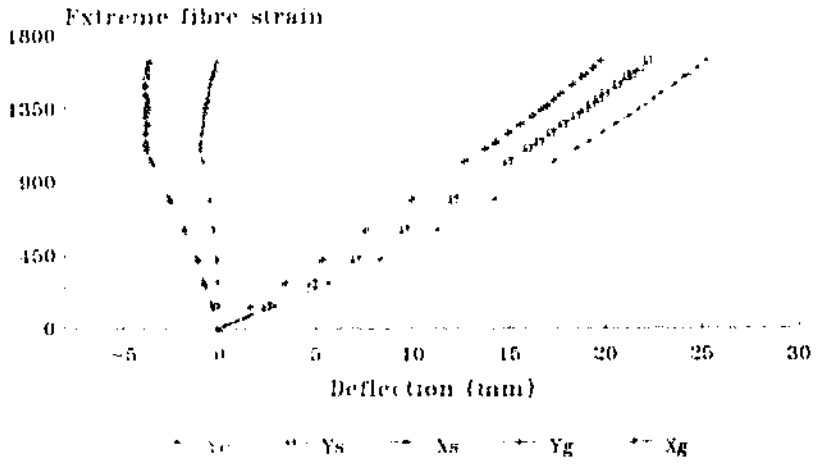

Figure 3.II.11: Vertical and horizontal strut deflections, see figure 3.02
Test 402 - β=60°

Stress Comparison
Case II: variable diagonal inclination

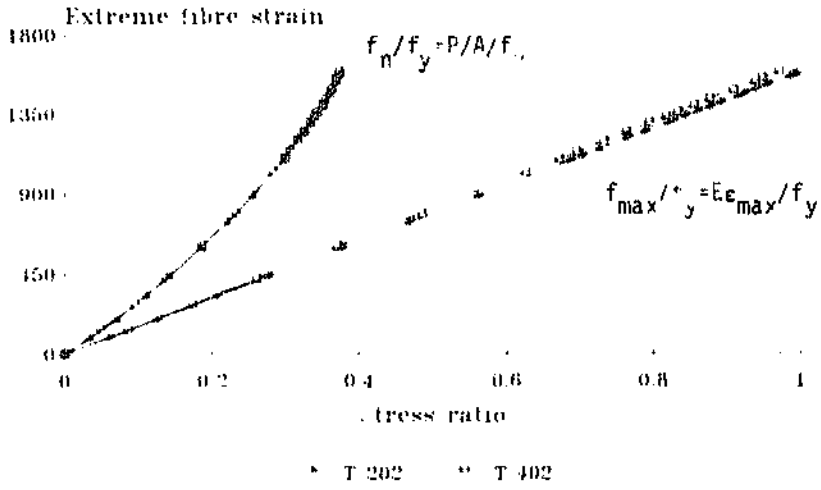

Figure 3.II.12: Nominal and maximum stress ratios at midspan s, Figure 3.02

Once more, the above results suggest that there is no torsional restraint from the supports, since the main leg rotations θ_{zL} are similar at any point on both main legs. However, the fact that failure occurs consistently in subspan s, indicates that there might be other effects, which depend on the distance from the supports to the restraining nodes a and d, see Figure 3.02.

In addition, it was observed in these frames with parallel legs that failure loads were somewhat erratic, and this is in line with previous findings by Behncke [11] and Elmes [51]. It is apparent that the bifurcation between symmetrical and asymmetrical buckling loads in his case with length ratio $L_s/L_g=1$, creates uncertainties over first yield and buckling loads. These effects are also very difficult to reproduce in analytical models.

In conclusion, frames with parallel legs, bracing with different relative inclination and identical slenderness ratio and end conditions, show the following characteristics:

- Torsional rotations of the main leg and the struts' flexural rotations are influenced by the inclination of the diagonals. However, these rotations are very uniform at all four connecting nodes on both legs.

- Overall strut deformations are also affected by changes in the inclination of the diagonals. However, these effects are not proportional to the changes of β, as depicted in Figures 3.II.05 though 3.II.11. In particular, the disparity in horizontal deflections has considerable influence in the bending effect about the minor axis v. It also affects calculations of relative eccentricities using the Southwell-plot. This matter will be addressed again in the

following Sections.

- These variations of bracing behaviour, after all, do not appear to have an important influence on the distribution of stress, as indicated in Figure 3.II.12, nor on the resistance of the members, as shown by the ultimate loads listed in Table 3.02, Column 10.

3.2.3 - Case III: Variable diagonal inclination. Inclined legs

Results from Tests 502 through 702 are examined, where the main parameter is the length ratio $r=L_s/L_g$, defined by the variable inclination of the bracing and constant slope of the main legs, see Figure 3.03. The main frame and other bracing characteristics are constant for all alternatives, as indicated in Table 3.03, Columns 2 through 9.

The main leg rotations at node a, indicated by θ_{zL} in Figure 3.03, are shown in Figure 3.III.01. These rotations increase with the angle of inclination of the diagonals, or with a reduction of the length ratio r, see Table 3.03, Column 4.

The strut's flexural rotations at node a, θ_{xS} in Figure 3.03, are fairly similar for all bracing inclinations β, as shown in Figure 3.III.02, but they are smaller than the leg's rotations. It is also seen that these rotations increase with the length ratio r, or with a reduction of the bracing inclination β.

Out-of-plane deflections at the cross-over joint c, see Figure 3.03, are similar in all three cases, as shown in Figure 3.III.03, but increasing slightly with the bracing

inclination β.

Figures 3.III.04 through 3.III.06 show the bracing deformations at the cross-over joint c and at midspan in the strut g, Figure 3.03. Horizontal midspan displacements initially occur in the x negative direction, increasing with increments of the inclination β. The out-of-plane deflections at the cross-over joint c are similar in all cases, while deflections at midspan g increase more rapidly when the bracing inclination β increases.

The stress ratios are shown in Figure 3.III.07. As in Case II above, no substantial differences due to variations in the length ratio r are observed in the development of nominal and critical stresses. This is also consistent with the very uniform ultimate loads recorded in Table 3.03, Column 10.

Summarizing, the behaviour of these frames with variable length ratio r can be described as follows:

- Leg rotations increase consistently with reductions of the length factor r.

- Strut rotations decrease w' h the factor r, buc w'th a lower dispersion.

- There are variations in the deflection history of the bracing, at both the cross-over joint and at midspan in the strut, but with no significant influence on the ultimate capacity of the bracing, as shown by the stress curves in Figure 3.III.07, and test results listed in Table 3.03, Column 10.

Table 3.03

Case III: Variable diagonal inclination

Inclined legs

Test Designation	Frame characteristics			Diagonals L40x40x3			End Conditions		Test results
	α (°)	β (°)	$\frac{L_s}{L_g}$	L_g (mm)	$\frac{L_g}{r_v}$	f_y (MPa)	Leg size (mm)	Bolts	$\frac{f_{ult}}{f_y}$
1	2	3	4	5	6	7	8	9	10
502	8	30	0.820	1000	130	333	L80x80x6	2	0.437
602	8	40	0.789	1000	130	325	L80x80x6	2	0.431
702	8	50	0.713	1000	130	329	L80x80x6	2	0.430

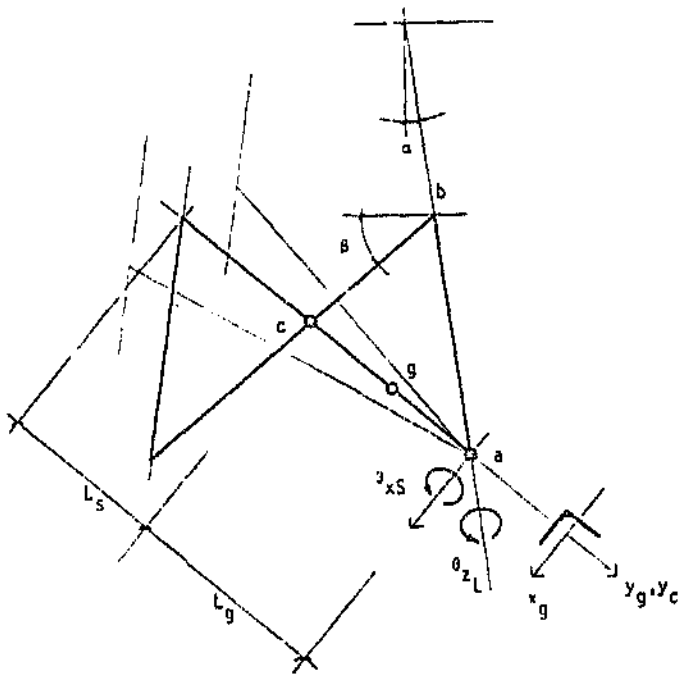

Figure 3.03: Comparison of results from tests on frames with constant slenderness ratios, inclined legs and variable diagonal inclinations.

Compression Leg Rotation
Case III: variable length ratio

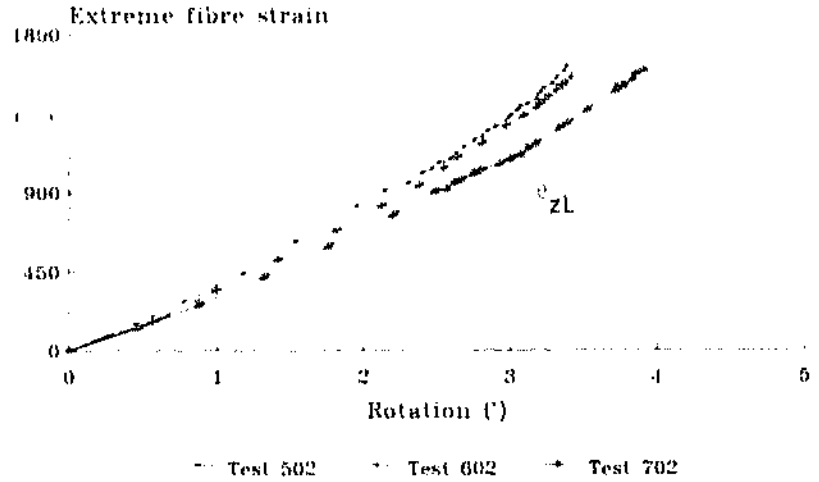

Figure 3.III.01: Main leg's rotational response at node a, see Figure 3.03

Strut Rotation
Case III: variable length ratio

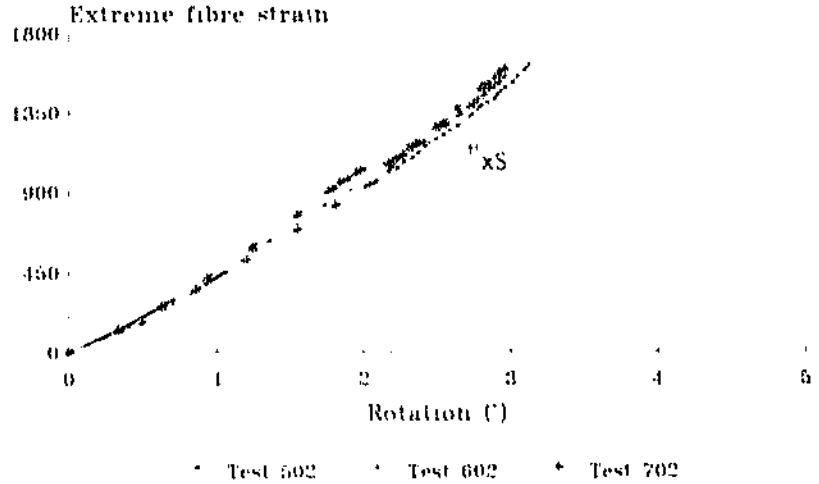

Figure 3.III.02: Strut's rotational response at node a, see Figure 3.03

Cross-over Joint Deflection
Case III: variable length ratio

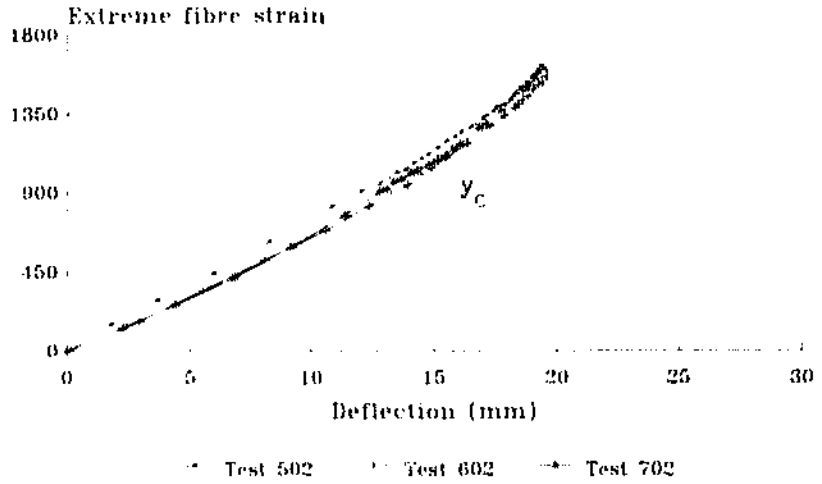

Figure 3.III.03: Bracing's out-of-plane deflections at node c, see Figure 3.03

Deformation Curves
Case III: variable length ratio

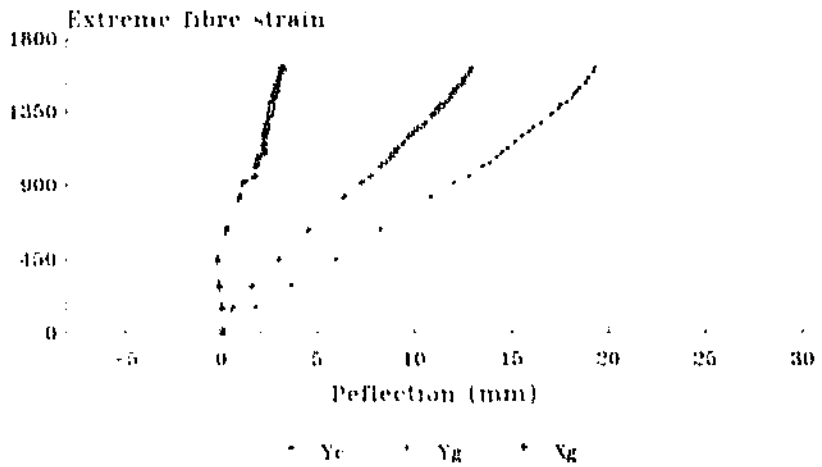

Figure 3.III.04: Vertical and horizontal strut deflections, see Figure 3.03
Test 502 - B=30°

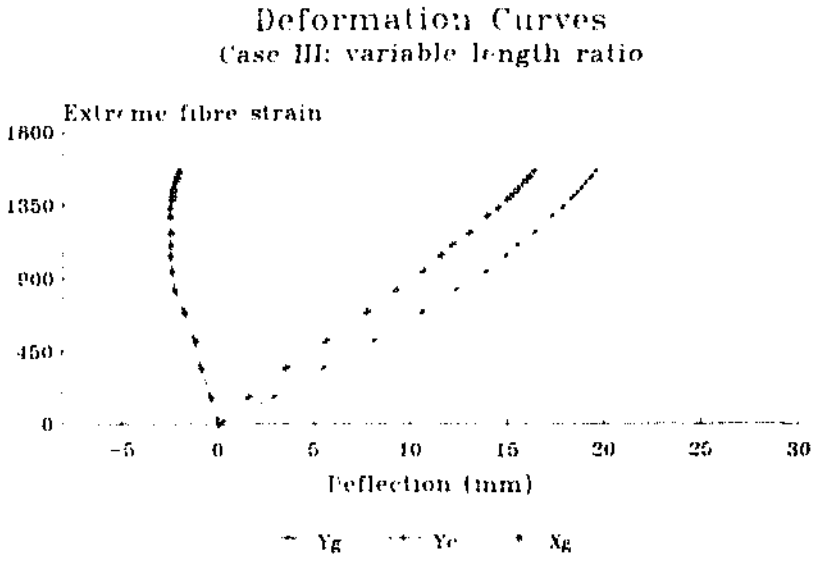

Figure 3.III.05: Vertical and horizontal strut deflections, see Figure 3.03
Test 602 - B=40

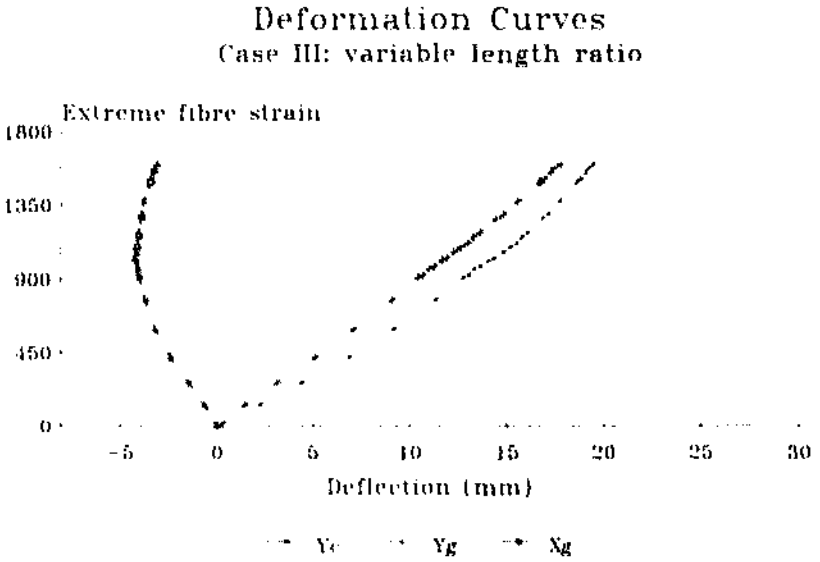

Figure 3.III.06: Vertical and horizontal strut deflections, see Figure 3.03
Test 702 - B=50

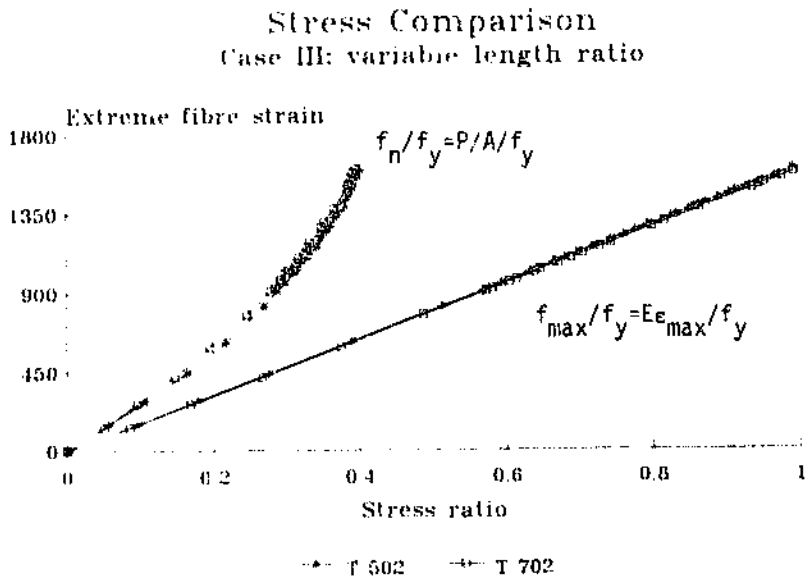

Figure 3.III.07: Nominal, maximum stress ratios at midspan g, see Figure 3.03

3.2.4 - Case IV: Variable main leg inclination - Constant bracing inclination

In Case IV, results from Tests 202 through 702 in Case II and Case III are re-examined, this time comparing the effects of parallel or inclined legs for each bracing inclination β, as depicted in Figure 3.04. Thus for constant slenderness ratio and end connection characteristics, the main variable in each case is the slope of legs α, with variations of length ratio τ. Frame data are listed in Table 3.04, Columns 2 through 9. Only the behaviour at node a and sunspan g are examined, see Figure 3.04.

Main leg rotations at node a, θ_{zL} in Figure 3.04, are indicated in Figures 3.IV.01 through 3.IV.03. In particular,

parallel-leg rotations are smaller than inclined-leg rotations at β=30°, but they increase and are larger at β=50°. Also, all rotations increase slightly with the bracing inclination β.

The strut's flexural rotations at node c, θx_S in Figure 3.04, are fairly constant for all β in frames with inclined legs. The rotations θx_S are again smaller in the frame with parallel legs at β=30°, but larger in the frame with β=50°, as shown in Figures 3.IV.04 through 3.IV.06.

Out-of-plane deflections at the cross-over joint c, Figure 3.04, are the same in both cases for bracing inclination of β=30°, but with larger vertical deflections in frames with parallel legs for β=40° and β=50°, as in Figures 3.IV.07 through 3.IV.09. As the length ratio L_s/L_g decreases (increasing β), a greater difference in behaviour would be expected between frames with parallel and inclined legs. The larger out-of-plane deflections at the cross-over joint are to be expected in parallel-leg cases due to the symmetrical buckling mode of two equal subspans (L_g=L_s) enforced at this node. This also influences the strut flexural rotations θx_S.

Overall bracing deformations at nodes c and g are now discussed, see Figures 3.02 and 3.03. In all cases the behaviour of the parallel-leg bracings at these nodes was very similar to that of inclined-leg frames, as shown in Figures 3.II.06 and 3.III.04 for bracing inclination β=30°, Figures 3.II.08 and 3.III.05 for β=40°, and Figures 3.II.10 and 3.III.06 for β=50°. Both the horizontal and out-of-plane displacement characteristics in each case appear to be a function only of the slenderness ratio L/r.

It is evident, observing the above curves of rotations and nodal deflections, that the restraint provided by the main leg about

its orthogonal axis decreases as the bracing inclination β increases. The response of the bracing to this effect varies with the slope of the legs as follows:

- In the case of parallel legs, this benefit appears to be of similar order to the uncertainties due to double-bolt restraint about the y-axis, and the bifurcation between the symmetrical and asymmetrical failure loads.

- In the case of inclined legs, however, the above effect is offset by the length ratio L_s/L_g. As the bracing inclination β increases, reducing the nodal restraint, the end restraint from the adjacent bay of bracing L_s increases (smaller L_s/L_g), balancing the previous effect.

As a consequence, all these observed differences in bracing behaviour have little or no influence on the development of stress, as shown in curves of Figures 3.II.12 and 3.III.07, or in the ultimate loads, as listed in Table 3.04, Column 10. It can therefore be stated that frames with constant slenderness ratio, similar material properties and similar end conditions, show the following behaviour for variable leg slope α:

- For both cases of parallel and inclined legs, there are variations of leg-torsional and strut-flexural rotations for increasing bracing inclination.

- Out-of-plane deflections at the cross-over joint are fairly constant for inclined-leg frames, but increase with the inclination of the diagonals for parallel-leg frames.

- Horizontal and vertical deflections at midspan g are similar in both cases of parallel- and inclined-leg frames. However,

Table 3.04

Case IV: Variable main-chord inclination
Constant diagonal inclination

Test Designation	Frame characteristics			Diagonals L40x40x3			End Conditions		Test results
	α (°)	β (°)	$\frac{L_s}{L_g}$	L_g (mm)	$\frac{L_g}{r_v}$	f_y (MPa)	Leg size (mm)	Bolts	$\frac{f_{ult}}{f_y}$
1	2	3	4	5	6	7	8	9	10
202	0	30	1.000	1000	130	329	L80x80x6	2	0.412
502	8	30	0.850	1000	130	333	L80x80x6	2	0.437
302	0	40	1.000	1000	130	333	L80x80x6	2	0.395
602	8	40	0.789	1000	130	325	L80x80x6	2	0.431
402	0	50	1.000	1000	130	339	L80x80x6	2	0.421
702	8	50	0.713	1000	130	329	L80x80x6	2	0.430

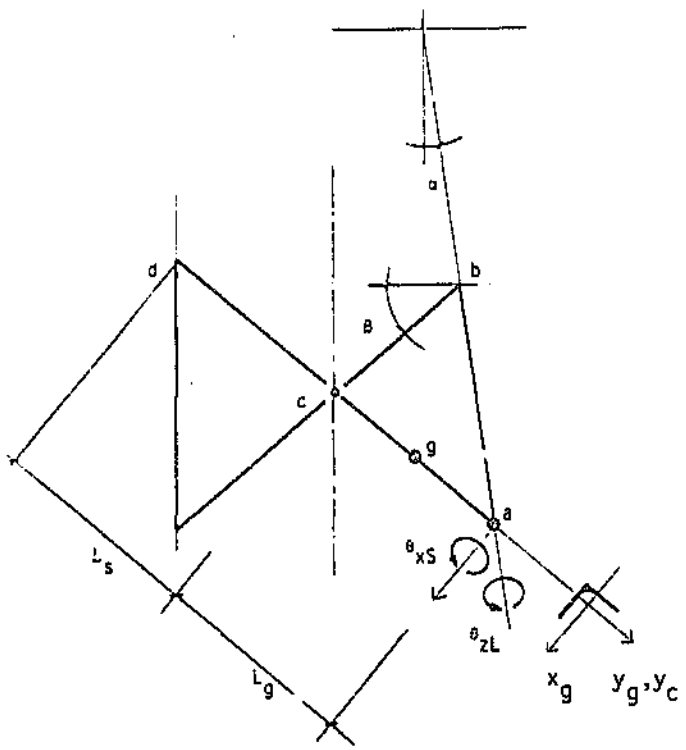

Figure 3.04: Comparison of results from tests on frames with constant slenderness ratios and diagonal inclinations and variable leg slopes.

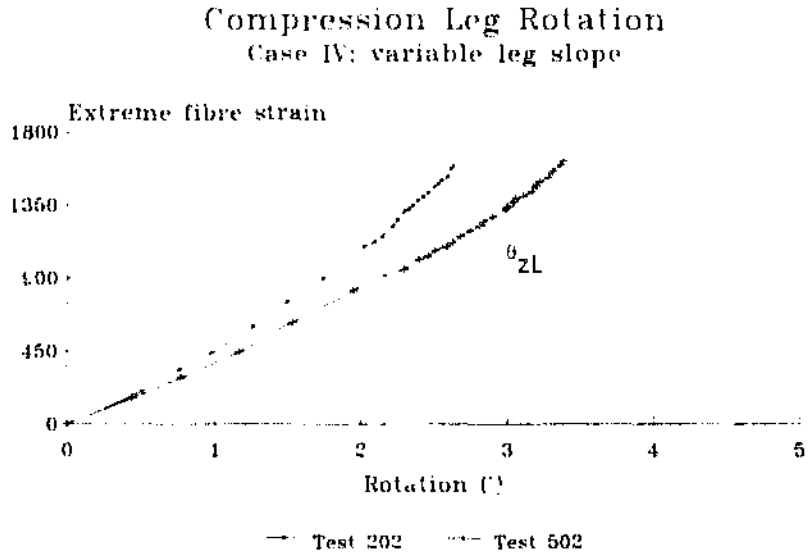

Figure 3.IV.01: Main leg's rotational response at node a, see Figure 3.04
B=30°

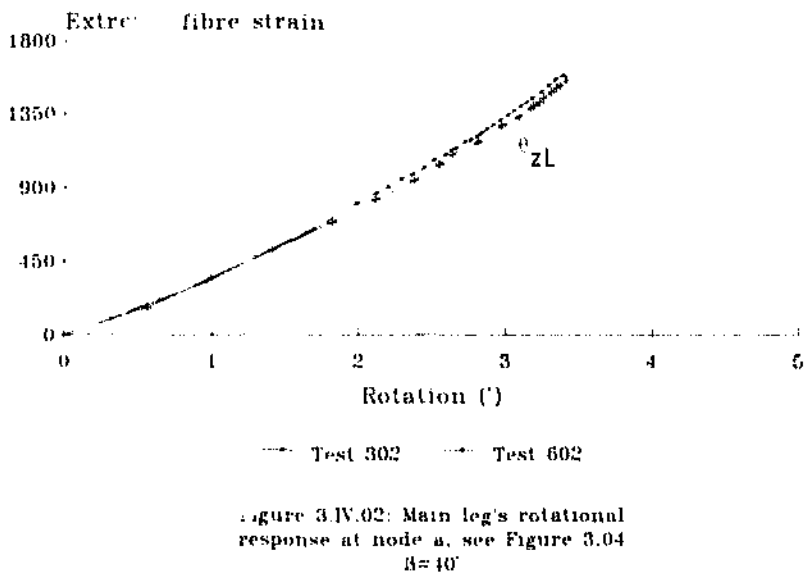

Figure 3.IV.02: Main leg's rotational response at node a, see Figure 3.04
B=40°

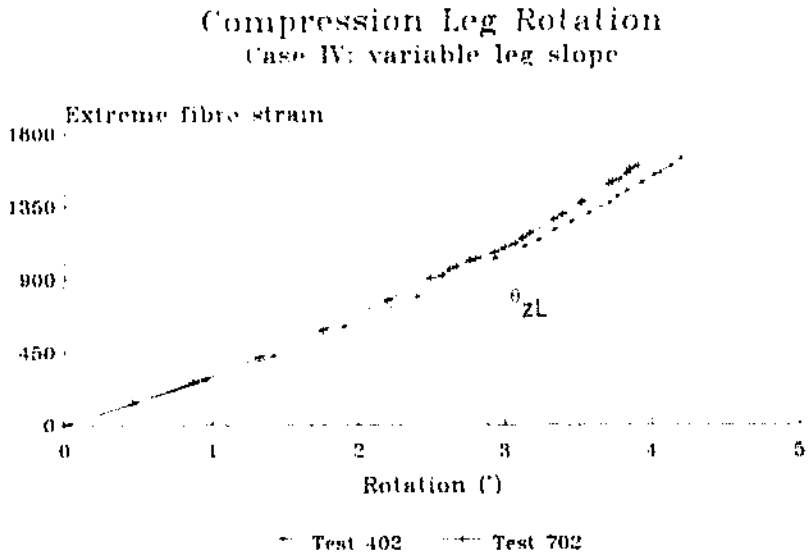

Figure 3.IV.03: Main leg's rotational response at node a, see Figure 3.04
β=50°

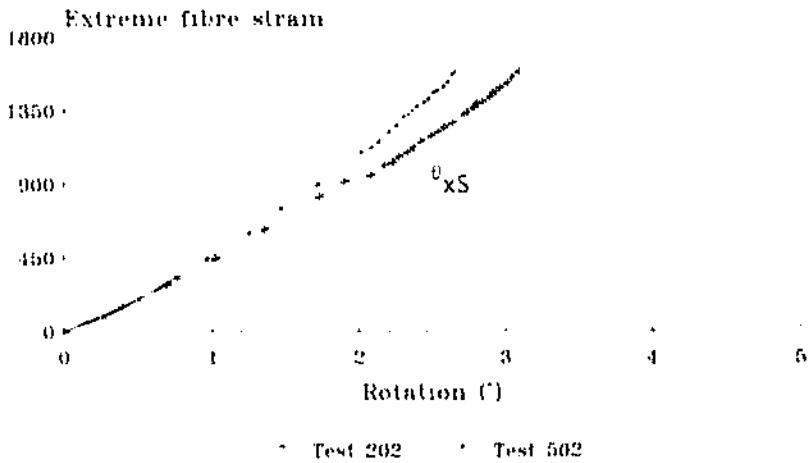

Figure 3.IV.04: Strut's rotational response at node a, see Figure 3.04
β=30°

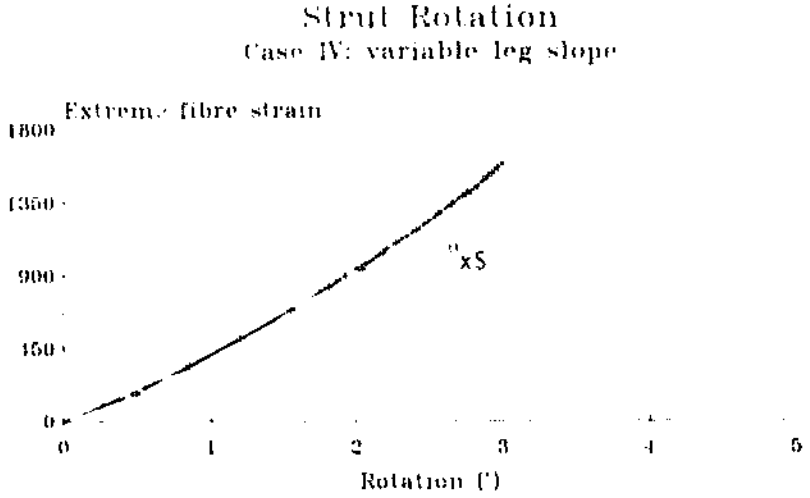

Figure 3.IV.05: Strut's rotational response at node a, see Figure 3.04
β=40°

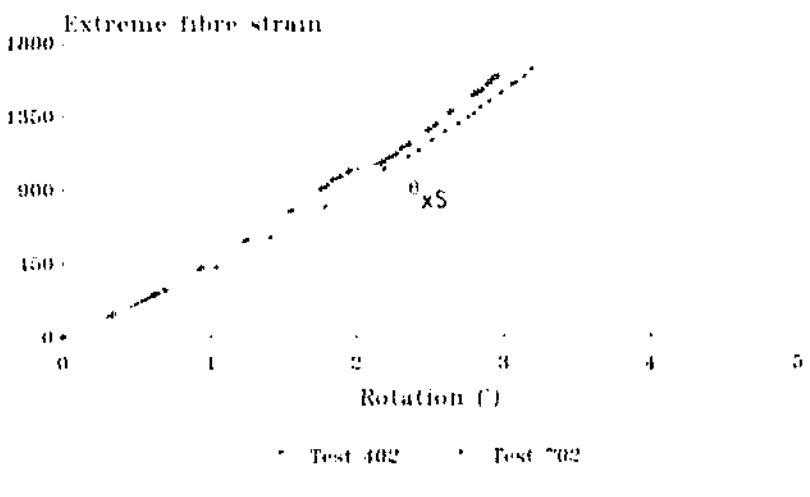

Figure 3.IV.06: Strut's rotational response at node a, see Figure 3.04
β=50°

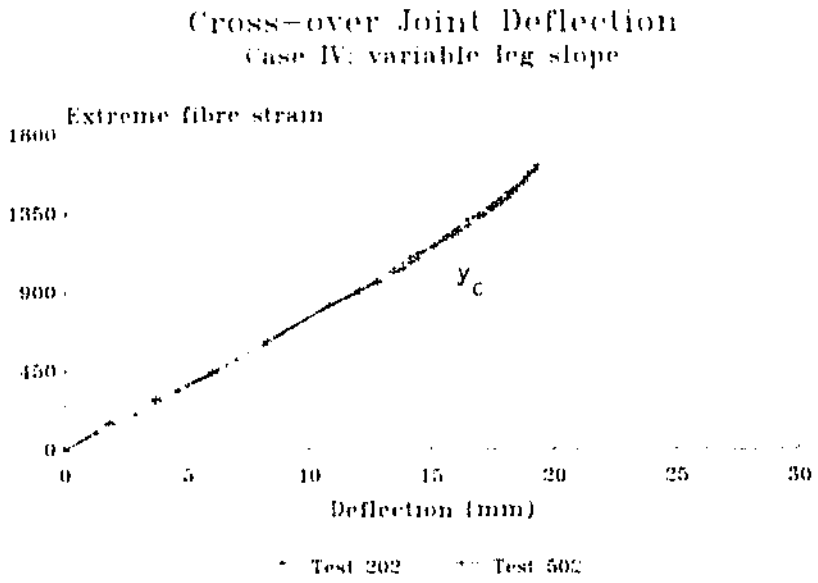

Figure 3.IV.07: Bracing's out-of-plane deflections at node c, see Figure 3.04

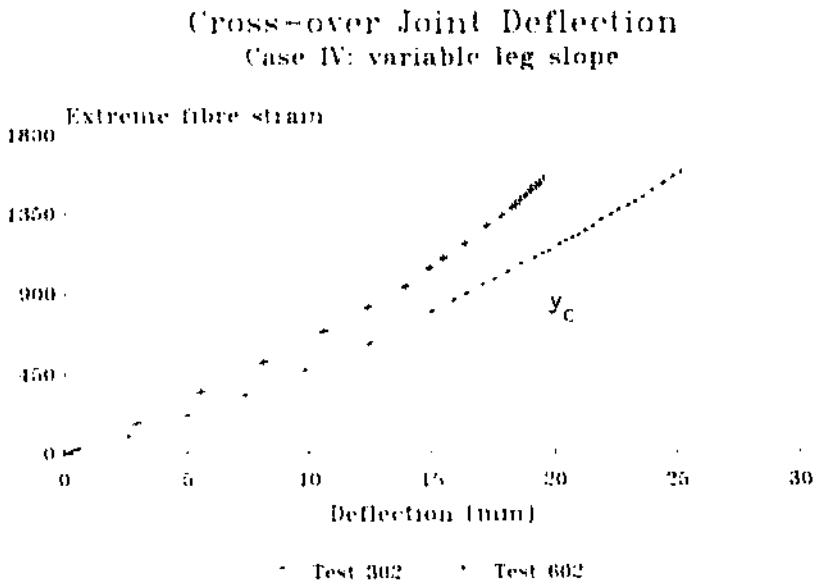

Figure 3.IV.08: Bracing's out-of-plane deflections at node c, see Figure 3.04

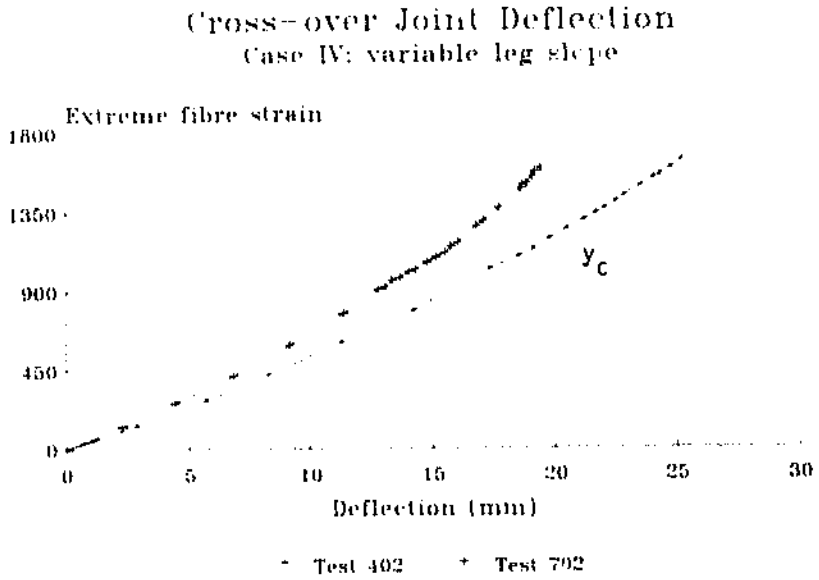

Figure 3.IV.09: Bracing's out-of-plane deflections at node c, see Figure 3.04

failure occurred in the subspan s in the parallel-leg cases, with considerable differences between subspans g and s.

- In all alternatives, however, the development of stress and the resistance of the bracing is fairly constant, suggesting that the ultimate capacity of the struts is a direct function of the slenderness ratio L/r and the end conditions.

3.2.5 - Case V: Variable diagonal end condition

Tests 801 through 804 are examined, with constant slenderness ratio L/r=160 and variable end restraints, see Figure 3.05. The change of end condition is represented by an increase from 1- to 2-bolt end-connections, and from L80x80x6 to L90x90x8 main leg

size. The frame characteristics are listed in Table 3.05, Columns 2 through 9.

The main leg's torsional rotations, θ_{zL} in Figure 3.05, are shown in Figure 3.V.01. It can be seen that all rotations are similar, with no significant dispersion. However, very small reductions of rotation can be noted from 1- to 2-bolt connections for both sizes of legs, and from L90x90x8 to L80x80x6 legs, for 1- and 2-bolt connections. The same applies to the strut's flexural rotations, θ_{xS} in Figure 3.05, shown in Figure 3.V.02.

Out-of-plane displacements at the cross-over joint c, Figure 3.05, are depicted in Figure 3.V.03. These deflections increase with increased end restraint from 2-bolt connections.

The overall deformations displayed in Figures 3.V.04 through 3.V.07 show that the horizontal deflections are initially in the x negative direction, Figure 3.05, increasing in that direction when the restraints are increased. The vertical deflections at the cross-over joint c and at midspan in the strut g increase in the y positive direction, Figure 3.05, when the end restraints are increased. At this level of slenderness ratio, however, the 2 vertical deflection curves always intercept, with larger deflections at midspan g, before failure occurs.

The development of stress is shown in Figure 3.V.07. The influence of variable end conditions is represented by changes in the effect of the nominal stress, which increases for higher end restraints. This is consistent with the pattern of out-of-plane deflections recorded at the cross-over joints.

Summarizing, these test results can be described as follows:

Table 3.05

Case V: Variable diagonal end conditions

Test Designation	Frame characteristics			Diagonals L40x40x3			End Conditions		Test results
	α (°)	β (°)	$\frac{L_s}{L_g}$	L_B (mm)	$\frac{L_g}{r_v}$	f_y (MPa)	Leg size (mm)	Bolts	$\frac{f_{ult}}{f_y}$
1	2	3	4	5	6	7	8	9	10
801	8	40	0.789	1250	160	333	L80x80x6	1	0.288
802	8	40	0.789	1250	160	321	L80x80x6	2	0.336
803	8	40	0.789	1250	160	339	L90x90x8	1	0.324
804	8	40	0.789	1250	160	329	L90x90x8	2	0.364

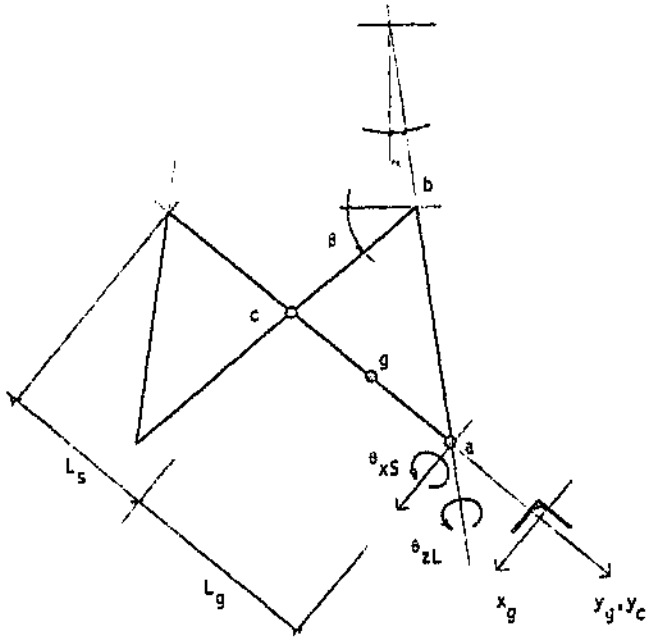

Figure 3.05: Comparison of results from tests on frames with constant slenderness ratios, constant leg and diagonal inclinations and variable end conditions.

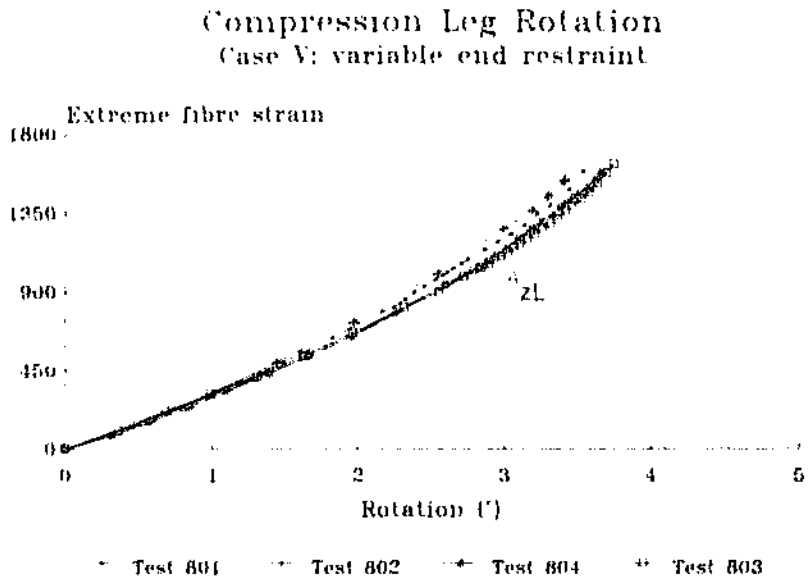

Figure 3.V.01: Main leg's rotational response at node a, see Figure 3.05

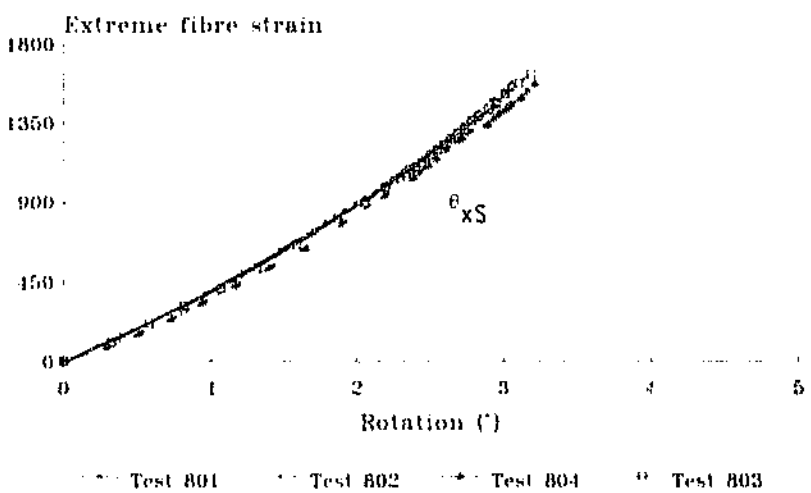

Figure 3.V.02: Strut's rotational response at node a, see Figure 3.05

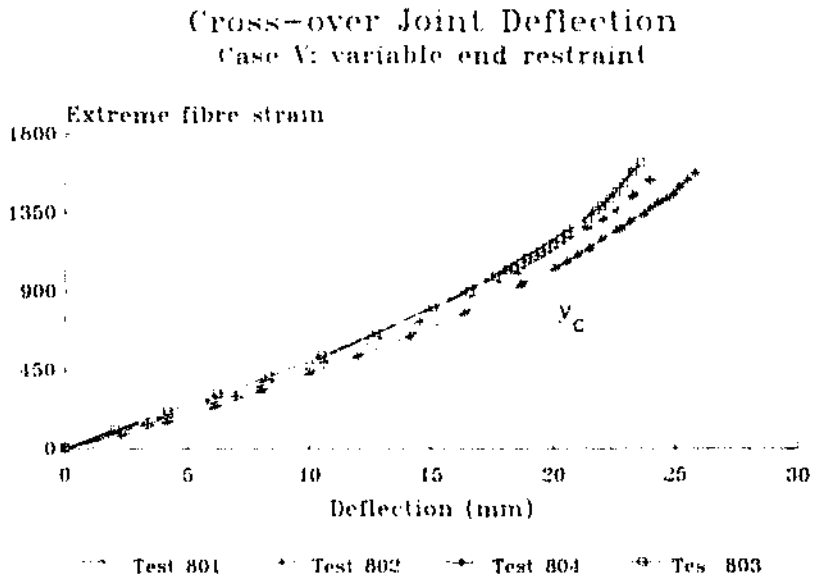

Figure 3 V.03: Bracing's out-of-plane deflections at node c, see Figure 3.05

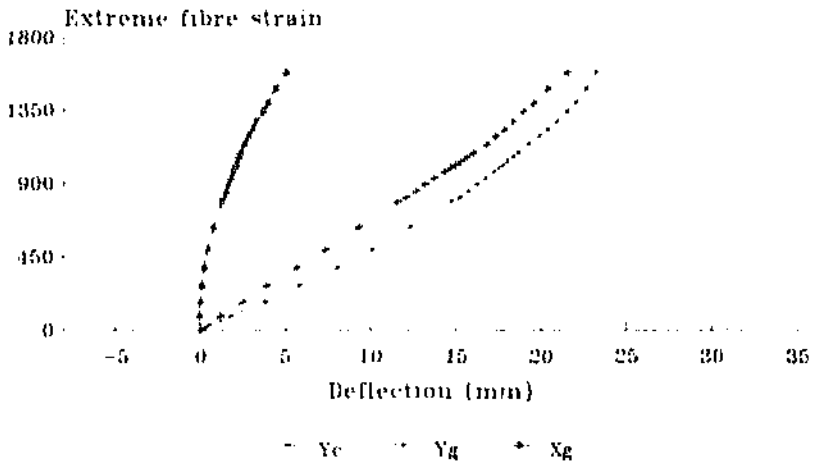

Figure 3.V .04. Vertical and horizontal strut deflections, see Figure 3.05 Test 801

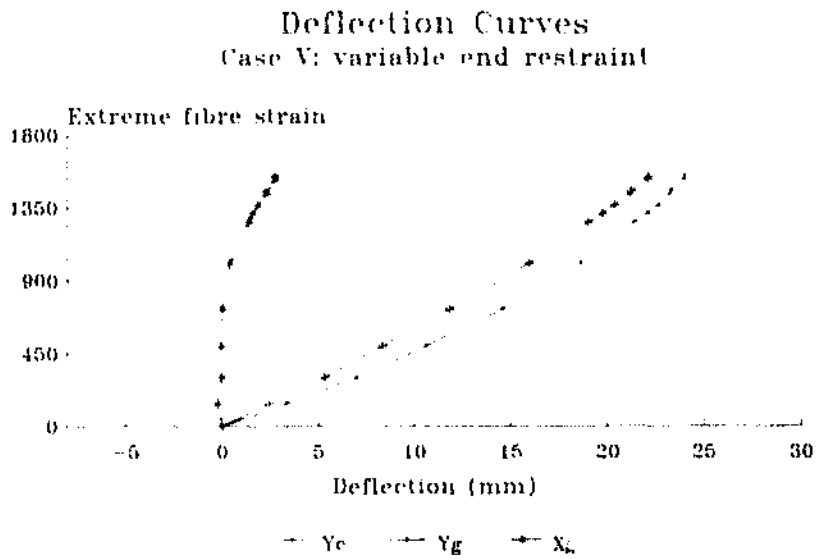

Figure 3.V.05: Vertical and horizontal strut deflections, see Figure 3.05 Test 802

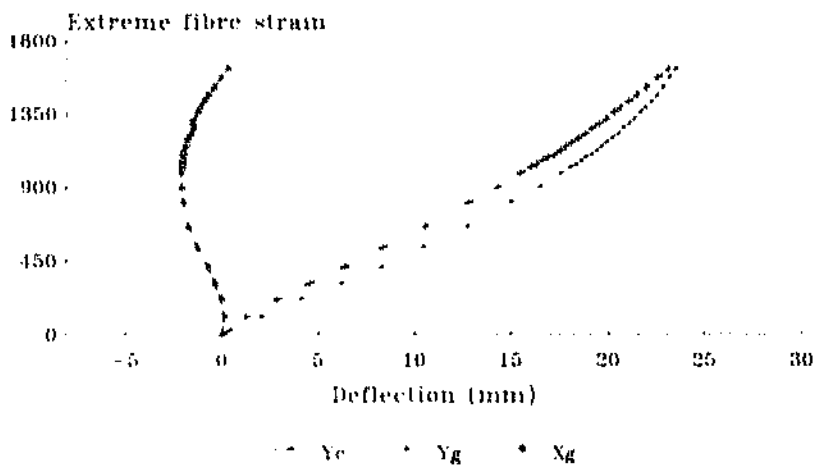

Figure 3.V.06: Vertical and horizontal strut deflections, see Figure 3.05 Test 803

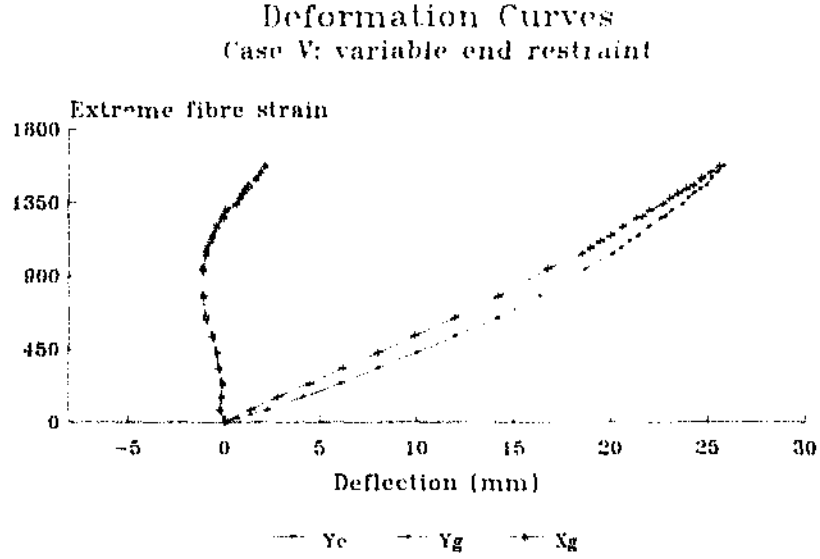

Figure 3.V.07: Vertical and horizontal strut deflections, see Figure 3.05 Test 804

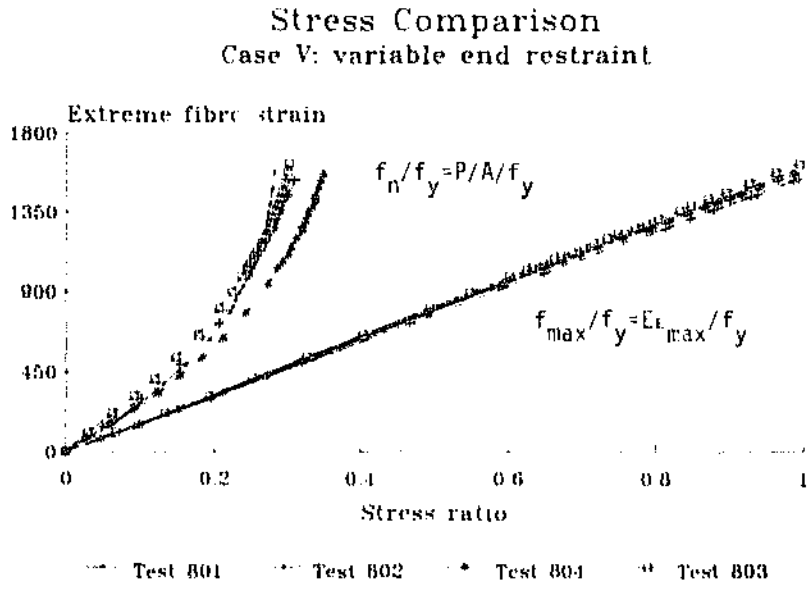

Figure 3.V.08: Nominal and maximum stress ratios at midspan g, Figure 3.05

- Both leg-torsional and strut-flexural rotations are not significantly affected by changes in the end restraints, as seen in the plots at any level of strain in the bracing.

- In-plane and out-of-plane deformations of the bracing are influenced by the increase of end restraint, and midspan deflections are larger than cross-over deflections at increasing loads. It is apparent from these results that higher end restraints increase the load capacity, which, in turn, induces larger deflections.

- Resistance of the diagonals is considerably influenced by the end conditions, as listed in Table 3.05, Column 10. This is in line with previous findings by Elmes [51], Behncke [11], Wood [49], CIGRE [63] and, more generally, Chen [58].

3.2.6 - Case VI: Variable bracing arrangement

The structures described in the previous test cases represent the simplest form of two-dimensional frames with crossed diagonals, as in Figure 3.06-a. In practice, however, different bracing arrangements are used in transmission towers in order to improve the buckling performance of the main legs and also to reduce the size of the bracing.

Thus, extra members are added, connecting the bracing at the cross-over joint with the legs, or connecting the diagonals at midspan with the legs. These are known as redundant bracings, since they act only as supports to the main members, but without carrying significant axial load. Such alternative arrangements,

shown in Figures 3.06-c and 3.06-d, were included in this case and are identified in Table 3.06 and in the plots of this Section as Tests 805 and 806.

One more option was also considered, as shown in Figure 3.06-b. In this case no redundant members were added, but all the diagonals in the frame were connected all-toes-up on one side of the frame, and all-toes-down on the other side. It was anticipated that this arrangement would improve the performance of the bracing, since the bending moments about the longitudinal torsional axis of the main leg at the connections of diagonals with main legs have a subtractive effect. This case is identified in the curves and in Table 3.06 as Test 807.

Tests were conducted on frames 805 through 807, Figures 3.06-b through 3.06-d, and results are compared with the basic case, Test 801 in Figure 3.06-a. Characteristics of the bracings are given in Table 3.06, Columns 2 through 9. In these alternatives the diagonals were connected to the legs with one bolt, and the slenderness ratio of 16[illegible] and all other parameters were the same

Figure 3.VI.01 shows the main leg's torsional rotations θz_L, corresponding to node a, as before. It is seen that these rotations increase for Test 805 with respect to the normal case, but are smaller for Test 806 and also for the case of inverted diagonals, Test 807. Curves of the strut's flexural rotations, Figure 3.VI.02, show similar behaviour, but the minimum corresponds to Test 806.

Out-of-plane deflections are depicted in Figure 3.VI.03. Again, there are noticeable differences with respect to the normal case of Test 801, with increased deflections for Test 805, and reduced deflections for Tests 806 and 807.

Overall bracing deformations are shown in Figures 3.VI.04 through 3.VI.07, with variations of similar order in both the horizontal and vertical directions. The restraint provided by the additional redundancies in Test 806 and the inverted position of the diagonals in Test 807 is reflected in the increasing levels of the nominal stress ratio f_n/f_y, as indicated in Figure 3.VI.08.

In conclusion, the effect of addition of redundant bracings and alternative position of the diagonals can be expressed as follows:

- Both leg-torsional and strut-flexural rotations are influenced by changes in the bracing, but to varying degrees.

- Overall deflections also show the effect of additional bracings, with important reductions in the case of Tests 806 and 807.

- Test results, indicated in Table 3.05, Column 10, show that the resistance of the bracing increases considerably with respect to the normal case, Test 801, due to the redundant bracing in Test 805 and the modified position of the diagonals in Test 807, but only by a smaller amount in Test 806. Nevertheless, the increase in strength in Test 805 for the bracing arrangement depicted in Figure 3.06-c, is not as large as would be expected from a reduction in slenderness ratio corresponding to the orthogonal x-axis, given by r_x.

Frame 805, with extra members connecting the legs with midspan of the diagonals, Figure 3.06-c, shows larger rotations and

deflections than the normal case, Test 801. The ultimate resistance, however, increased by 36%, reflecting, perhaps, some inconsistency. This is possibly due to the fact that the extra bracing, of size L25x25x3, may not have been in proportion to the diagonals of size L40x40x3. This alternative is widely used in transmission towers, and requires extra members, extra holes in the bracing and additional bolts, with an increase in cost.

Frame 806, with a transverse member through the cross-over joint as illustrated in Figure 3.06-d, shows reduced rotations and overall deformations in the bracing, thus indicating a higher degree of restraint. The resistance of the bracing, however, increased only by 3% with respect to the normal case, Test 801. The extra plate at the cross-over joint was 6 mm thick, identical to the thickness of the main leg, as recommended in the design codes. This alternative is also widely used in transmission towers, although it requires a plate, extra members, holes and bolts, also introducing additional costs.

Frame 807, with inverted diagonals, Figure 3.06-b, shows reduced rotations and deflections with respect to the normal case, Test 801, and a more than 12% increase of ultimate resistance. It is important to note that the levels of strain in the tension member are about half of those in the strut for similar axial loads in the diagonals. This also represents a reduction with respect to the levels of strain in the tie of Test 801. This is an interesting option, in which higher resistance is achieved without adding extra bracings, and deserves further attention in the future. The only problem is the addition of holes and bolts, and larger gusset plates for multiple-bolt connections, which may increase the cost of manufacturing.

Table 3.06

Case VI: Variable bracing arrangement

Test Designation	Frame characteristics			Diagonals L40x40x3			End Conditions		Test results
	α (°)	β (°)	$\frac{L_s}{L_g}$	L_g (mm)	$\frac{L_g}{r_v}$	f_y (MPa)	Leg size (mm)	Bolts	$\frac{f_{ult}}{f_y}$
1	2	3	4	5	6	7	8	9	10
801	8	40	0.789	1250	160	333	L80x80x6	1	0.288
805	8	40	0.789	1250	160	332	L80x80x6	1	0.392
806	8	40	0.789	1250	160	332	L80x80x6	1	0.297
807	8	40	0.789	1250	160	329	L80x80x6	1	0.324

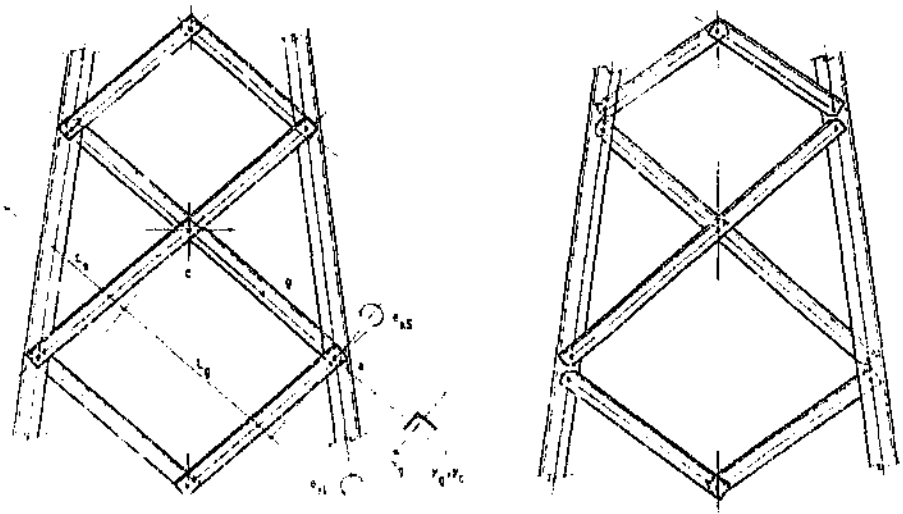

(a) (b)

Figure 3.06: a) Bracing arrangement for Test 801 - Base case.
b) Bracing arrangement for Test 807 - Inverted diagonals in the outside panels.

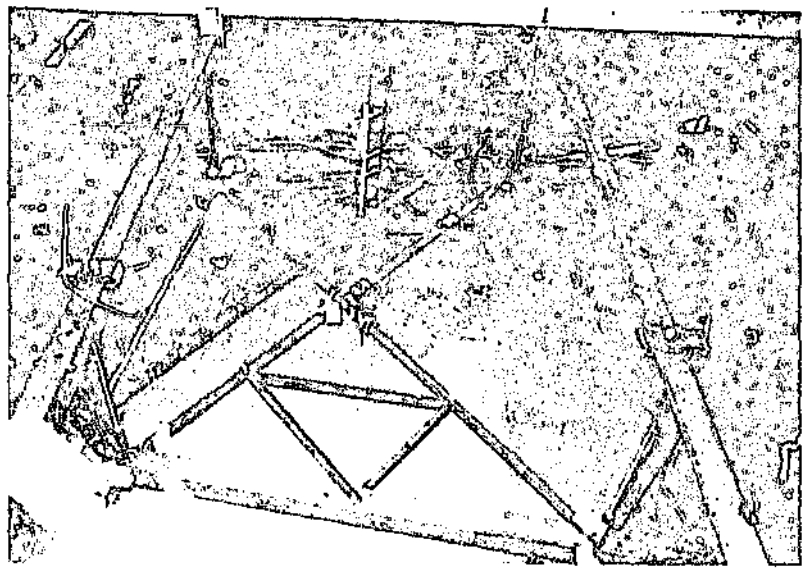

Figure 3.06-c: Bracing arrangement for Test 805.
Redundant bracing.

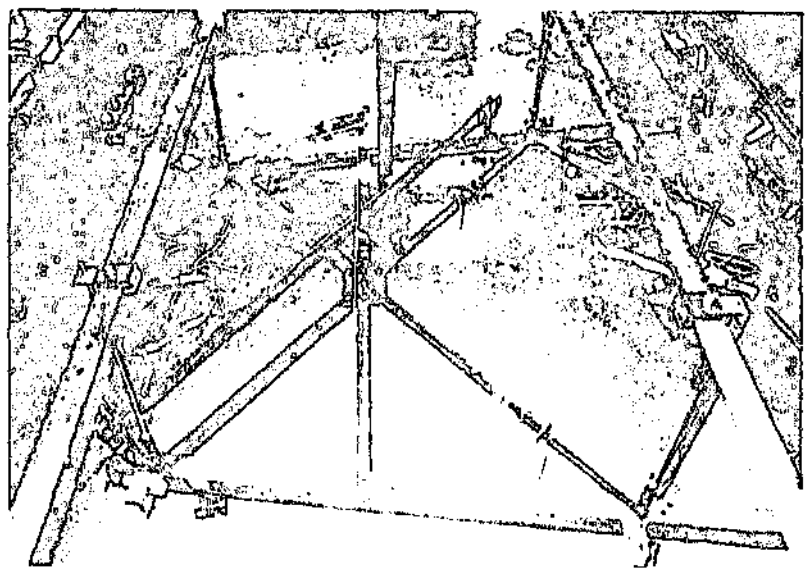

Figure 3.06-d: Bracing arrangement for Test 806.
Redundant bracing.

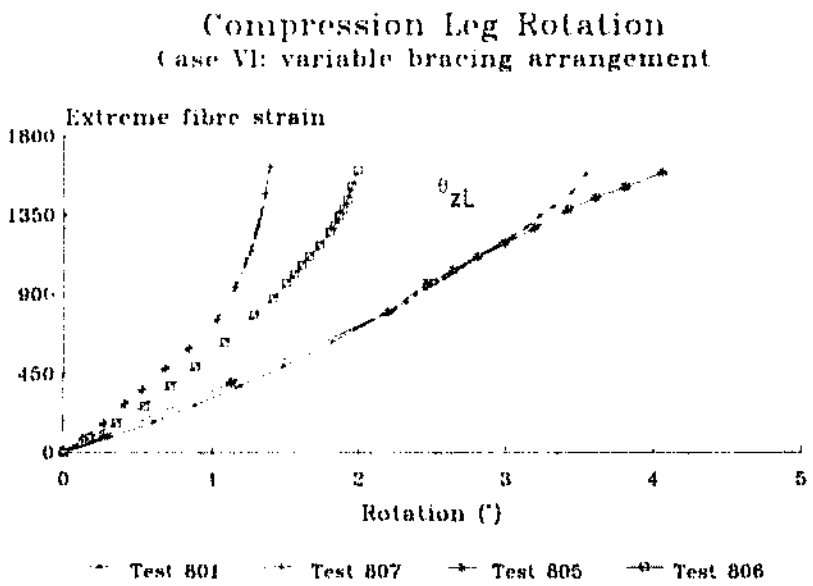

Figure 3.VI.01: Main leg's rotational response at node a, see Figure 3.06-a

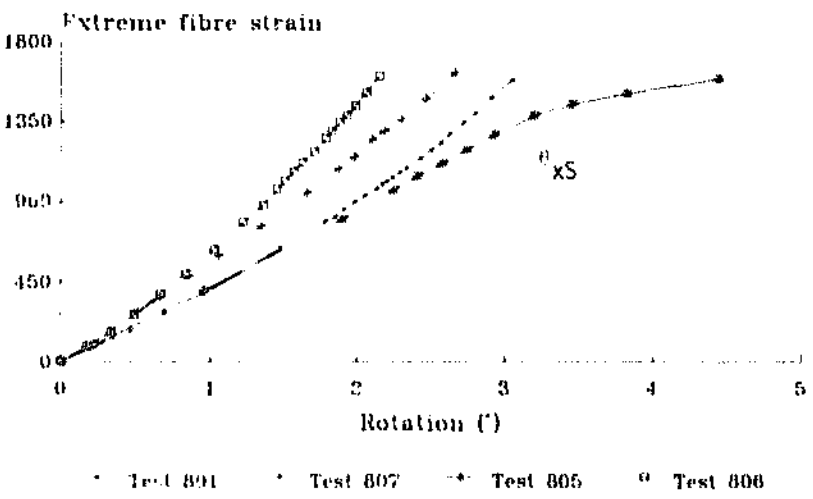

Figure 3.VI.02: Strut's rotations at node a, see Figure 3.06-a

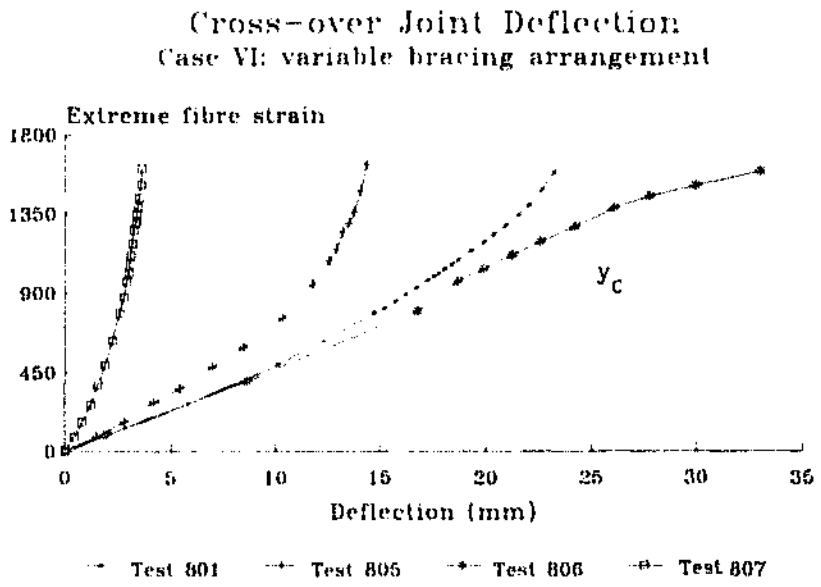

Figure 3.VI.03: Bracing's out-of-plane deflections at node c, see Figure 3.08

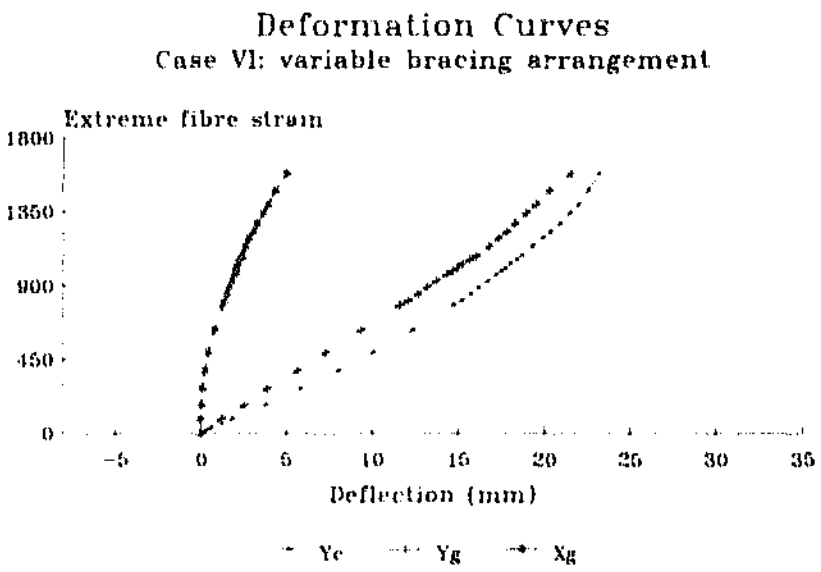

Figure 3.VI.04: Vertical and horizontal strut deflections
Test 801

Deformation Comparison
Case VI variable bracing arrangement

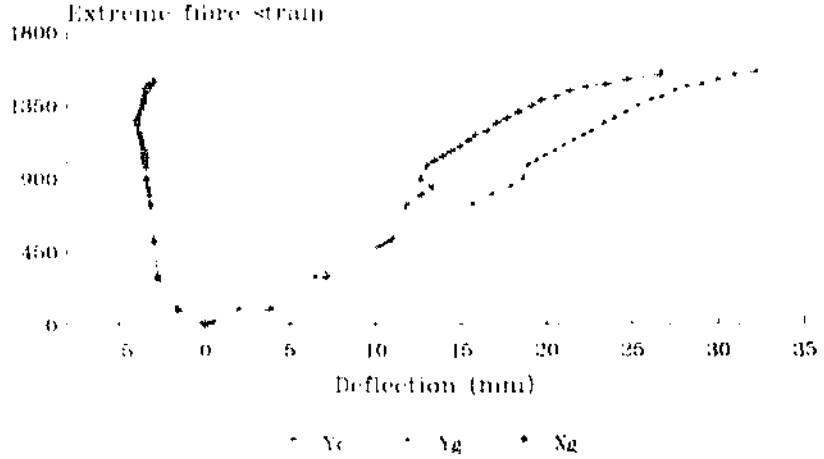

Figure 3.VI.05 Vertical and horizontal strut deflections
Test 805

Deformation Curves
Cas VI variable bracing arrangement

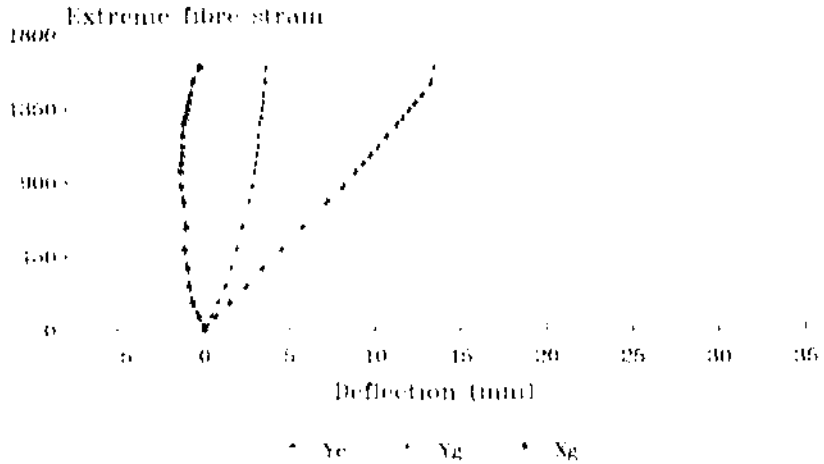

Figure 3.VI.06 Vertical and horizontal strut deflections
Test 806

Deformation Curves
Case VI: variable bracing arrangement

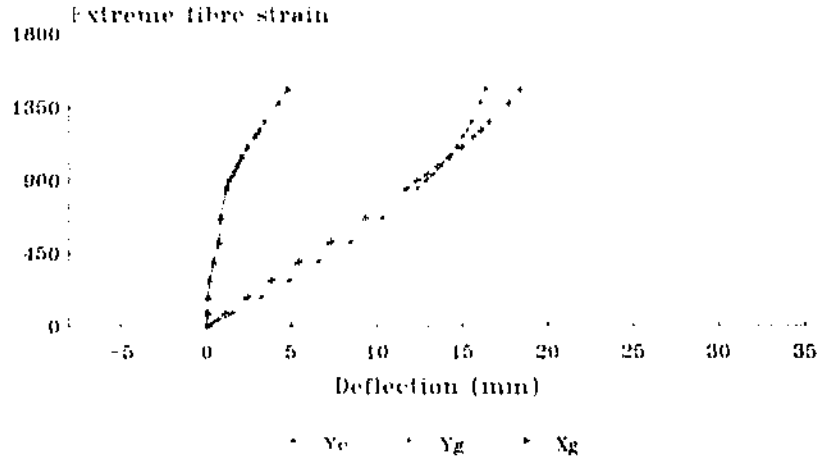

Figure 3.VI.07: Vertical and horizontal strut deflections
Test 807

Stress Comparison
Case VI: variable bracing arrangement

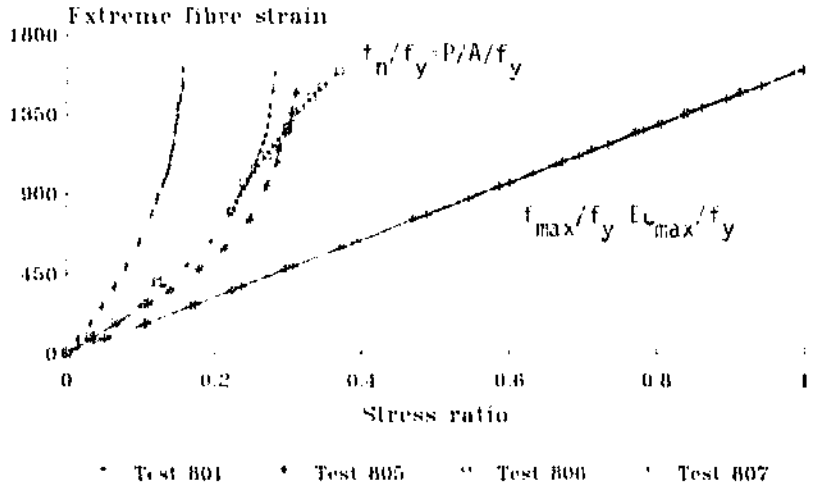

Figure 3.VI.08 Nominal and maximum stress ratios at node g, Figure 3.06 - -

3.2.7 - Case VII: Locked-in systems

Results from Test 612 are examined, corresponding to a frame with locked-in diagonals, as shown in Figure 3.07. All conditions in this alternative, including frame geometry, number of connecting bolts and member sizes, are as in Test 602 of Case III. Therefore results from Tests 602 (normal frame) and 612 (locked-in system) with slenderness ratio of 130 are compared. Characteristics of both frames and diagonals are indicated in Table 3.07, Columns 2 through 9.

Before starting the analysis of results, however, it must be said that these tests on locked-in systems presented special problems from the experimental point of view. Firstly, it was very difficult to restrain the frames in the X direction, see Figure 3.07, while at the same time maintaining the free-rotation properties of the tension- and compression-leg supports. These supports were designed to permit free rotations and also adjustments in all X, Y and Z directions, see Figures 2.09 and 2.10 in Chapter 2 and Figure 3.07 below.

Secondly, as both support nodes m and n in Figure 3.07 kept moving away from each other in the X direction for increasing loads, it was necessary to join them by means of a system of bars and turn-buckle, see details in Figures 3.08 and 3.09. This system was not reliable, and it was thus difficult to adjust the initial position of the frames, and certainly it was impossible to make adjustments during the tests.

Finally, forces in these bigger frames were higher than in the case of normal frames (Test Cases I-VI), and there was some movement of the beam and anchor structures, shown in Figure

2.06-d in Chapter 2, which introduced additional effects and variations in the distribution of forces in the bracing. A typical example, from many trials on several locked-in systems, is shown in Figure 3.VII.01, where the recorded tension and compression forces and the calculated forces in the central panel of bracing are plotted against the applied loads. Nevertheless, Test 612 results are examined next and compared with Test 602.

Figure 3.VII.02 shows the main leg's torsional rotations at node a, θz_L in Figure 3.07. It can be seen that, for identical conditions, these rotations are larger in the case of Test 602. Similar results are observed in Figure 3.VII.03 for the strut's flexural rotations at node a, θx_S in Figure 3.07, and also the out-of-plane deflections y_c at the cross over joint, see Figure 3.VII.04. The nominal stress ratio in Figure 3.VII.05 also shows reductions with respect to Test 602 in Case III.

These variations are explained by the differences in out-of-plane deflections at the outside cross-over joints, i-1 and i+1 in Figure 3.07 (see also Figure 2.06-a in Chapter 2). For tests of normal frames (Case I through Case VI), deflections of the two outside cross-over joints were controlled externally, and were arbitrarily related to deflections in the central cross-over joint, as explained in Chapter 2. The average ratios for frames with inclined legs were as follows, see Figure 3.07:

- $y_{i-1} = 0.80 * y_i$
- $y_{i+1} = 1.30 * y_i$

where y_i, y_{i-1} and y_{i+1} are the out-of-plane deflections at joints i, i-1, and i+1 respectively, as in Figure 3.07.

In the case of locked-in systems, on the other hand, these nodes were free to move, and the recorded deformations from Test 612 are depicted in Figure 3.VII.06. It can be seen that both outside nodes i-1 and i+1 deflected less than the centre cross-over node i, and the recorded average ratios are indicated below:

$$- y_{i-1} = 0.40 * y_i$$
$$- y_{i+1} = 0.70 * y_i$$

The actual ratios of out-of-plane deflections at the outside cross-over joints were thus well below the estimated values for the normal tests (which were based on the geometry of the frames). It is therefore apparent that the lower rate of nodal rotations and midspan deformations in Test 612 with respect to Test 602 are due to the differences noted above for nodes i-1 and i+1, see Figure 3.07. Two important conclusions can be drawn from these results:

- The out-of-plane deflections of the outside bracings relative to the central cross-over joint deflections have significant influence on the behaviour of the bracing and possibly on the failure loads as well.

- The ratio of deformations in the outside and central panels of bracings is a function of the sizes of the members and is thus related to the flexibility and slenderness ratio of the diagonals.

Unfortunately, the results from Test 612, which were typical of all the observed locked-in systems in this investigation, were not conclusive. The distribution of forces in the bracing was erratic, possibly due to movements of the supports, and the

TABLE 3.07

Case VII: Locked-in systems

Test Designation	Frame characteristics			Diagonals L40x40x3			End Conditions		Test results
	α (°)	β (°)	$\frac{L_s}{L_g}$	L_g (mm)	$\frac{L_g}{r_v}$	f_y (MPa)	Leg size (mm)	Bolts	$\frac{f_{ult}}{f_y}$
1	2	3	4	5	6	7	8	9	10
602	8	40	0.789	1000	130	325	L80x80x6	2	0.431
612	8	40	0.789	1000	130	328	L80x80x6	2	0.349

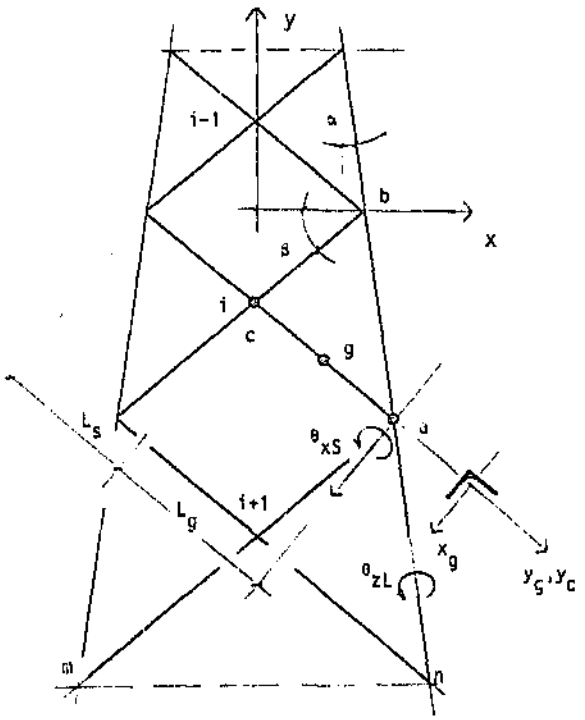

Figure 3.07: Analysis of frames with locked-in systems of crossed diagonals.

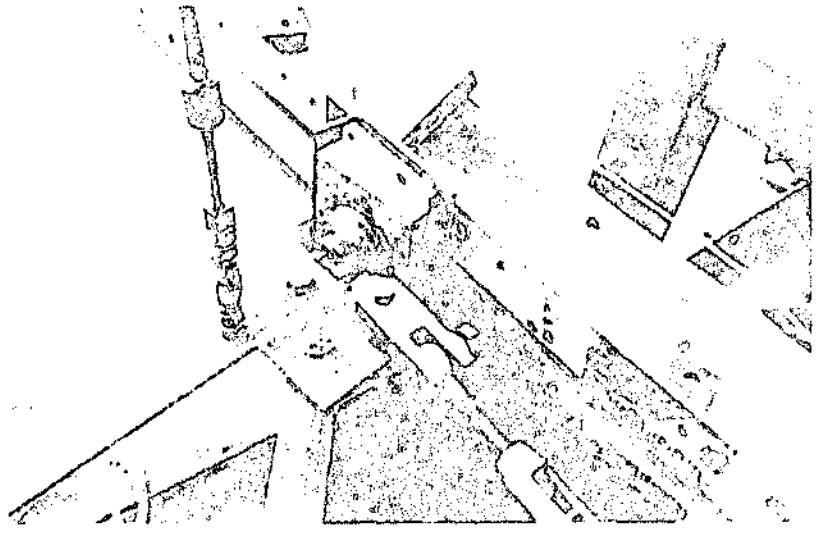

Figure 3.08: Assembly of the compression leg support in frames with locked-in diagonals. A horizontal bar was added to provide restraint in the x-direction, see Figure 3.07.

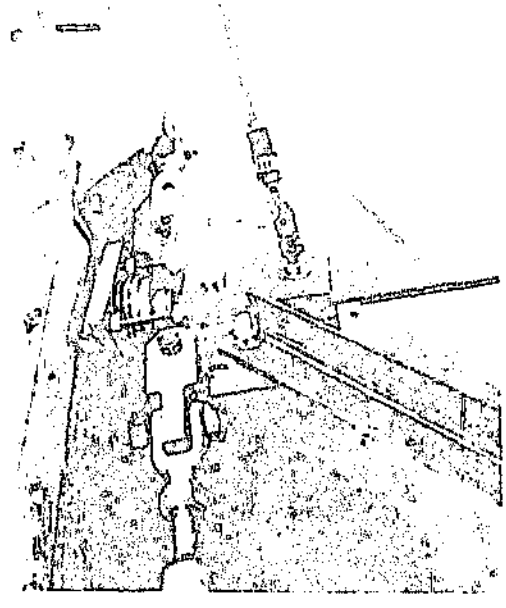

Figure 3.09: Assembly of the tension leg support in frames with locked-in diagonals. Note the adjustable bar joining both main legs, see also Figure 3.07.

Locked-in cross-bracing system
Typical example

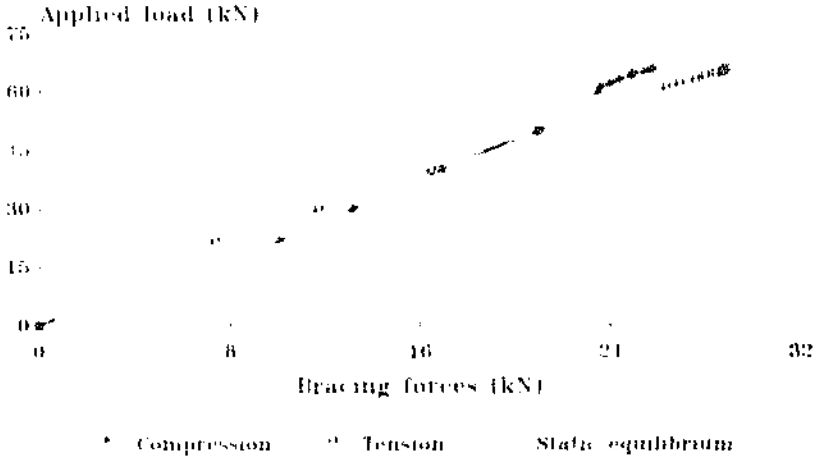

Figure 3.VII.01 Axial forces in the tension and compression diagonals Locked-in systems

Compression Leg Rotation
Case VII: locked-in systems

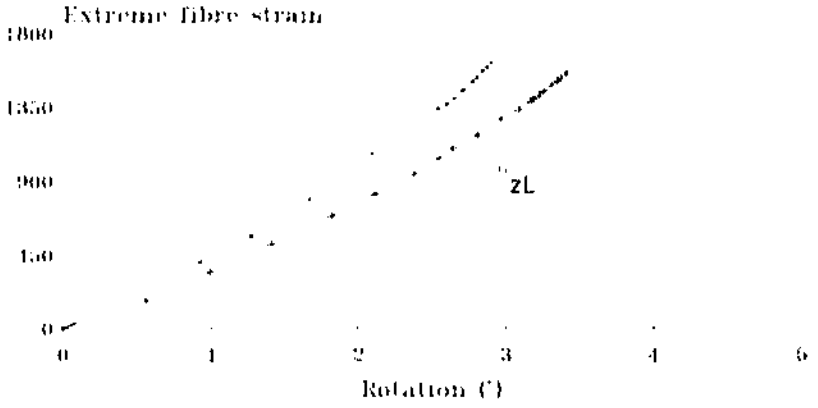

Figure 3.VII.02: Main leg's rotational response at node a, see Figure 3.07 Locked-in systems

Strut Rotation
Case VII: locked-in systems

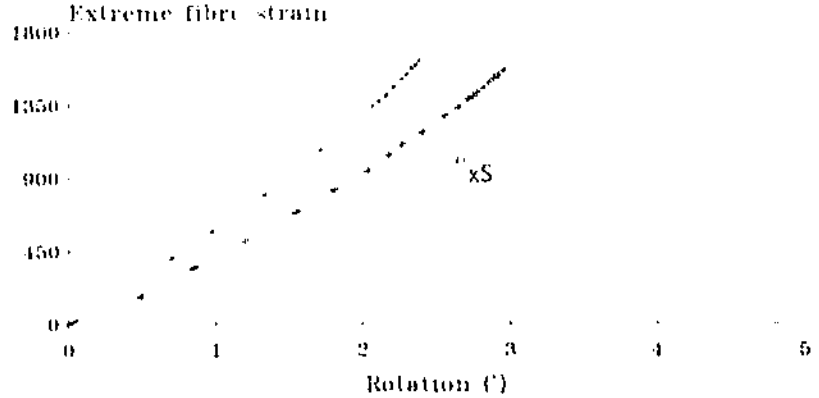

Figure 3.VII.03: Strut's rotational response at node a, see Figure 3.07
Locked-in systems

Cross-over Joint Deflection
Case VII: locked-in systems

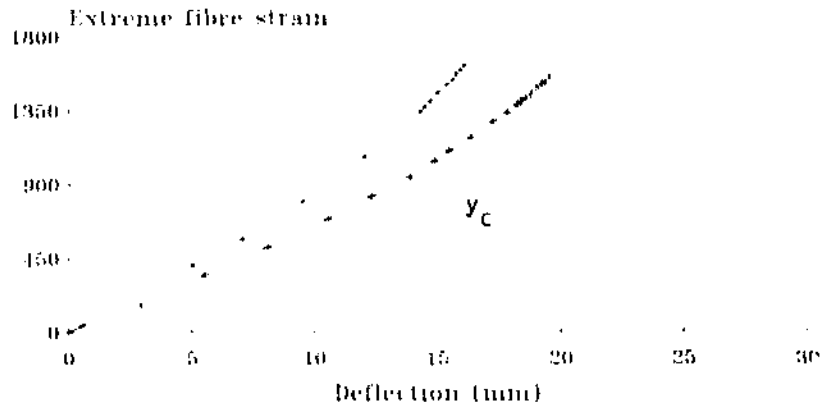

Figure 3.VII.04: Bracing's out-of-plane deflections at node c, see Figure 3.07
Locked-in systems

Stress Comparison
Case VII: locked-in systems

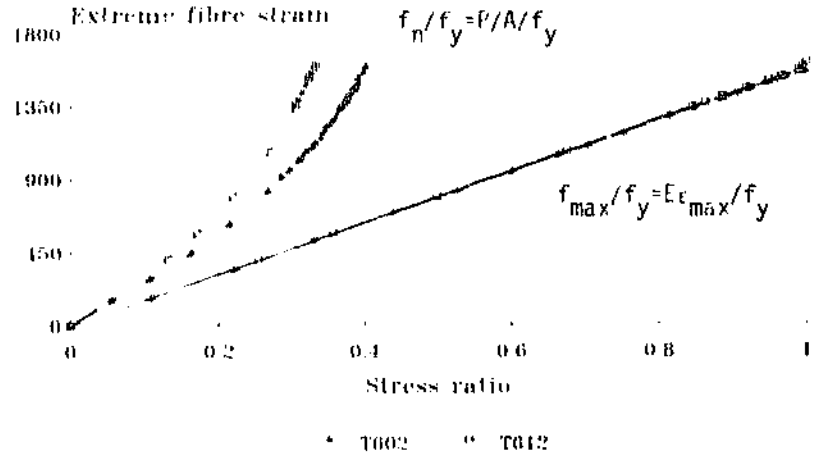

Figure 3.VII.05 Nominal, maximum stress ratios at node g see Figure 3.07 Locked-in systems

Cross-over Joint Deflection
Case VII: locked-in systems

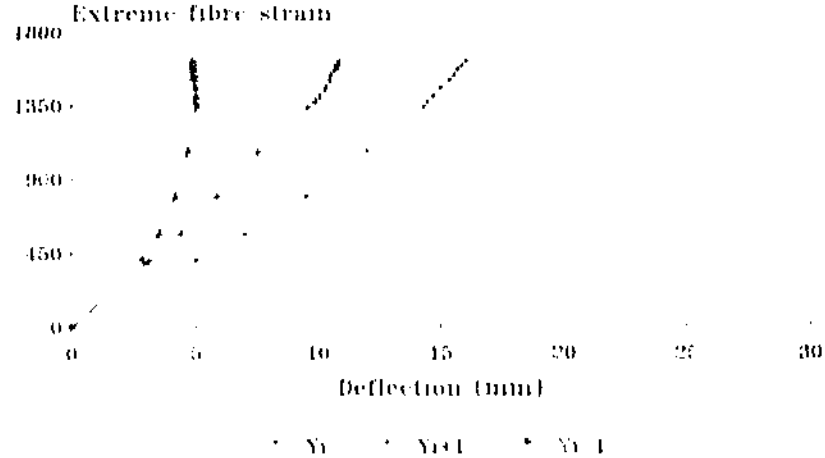

Figure 3.VII.06 Bracing's out-of-plane deflections at cross-over joints Locked-in systems

failure load was far too low, considering the reduction in deflections and rotations with respect to Test 602, see Table 3.07, Column 10. Similar problems with locked-in system have been reported by Behncke [11], who also observed that forces in the bracing were uncertain and thus difficult to predict. In any case, the test arrangement used in this investigation was not the most convenient for testing frames with locked-in diagonals.

After observing the general behaviour of crossed diagonals under different test conditions, a more detailed analysis of some parameters is included in the following Sections.

3.3 - General analysis of deflections

The deflection patterns discussed above for the x- and y-axis in the struts are initially induced by the eccentric forces, as depicted in Figure 3.10-a for the case of 2- or more bolts in the connections. When approaching failure, however, deflections in most cases are predominantly about the weak axis v, which explains why the horizontal displacements are reversed in the x positive direction, as indicated in Figure 3.10-b.

This effect is illustrated in Figure 3.11-a for a frame with slenderness ratio L/r=100, and in Figure 3.11-b for a frame with L/r=160, where fy indicates yielding of the extreme fibre. Observe that, for increasing loads, deflections x_g change direction into the positive x-axis. If x_g and y_g are plotted against each other, a curve similar to Figure 3.10-b is obtained. In the case of frames with partial le[illegible] Figure 3.11-c, this effect is seen in the s[illegible]p[illegible]e Figure 3.02, through deflections x_s and y_s.

Note in Figure 3.10-b that the horizontal deflections in the x-axis negative direction reduce the bending moment about the minor y-axis (and thus the stress on the critical fibre), increasing the buckling resistance of the struts. After first yield occurs, however, out-of-plane deflections increase more rapidly, offsetting that effect.

In the case of parallel-leg frames, Figure 3.11-c, the x-axis deflections at subspans g and s, see Figure 3.02, are different. It is easy to see that the bending effect increases more rapidly at subspan s through a small deflection x_s, while this effect is reduced at subspan g through larger, negative x_g deformations.

This explains why in frames with parallel legs failure occurs at subspan s. However, it also suggests that there are different effective eccentricities about the y-axis, see Figure 3.10-a, at both ends of the strut. It appears that the distance from node a to the right leg support, and the larger distance from node d to the left leg support, see Figure 3.02, have an influence on the 2-bolt end restraint about the y-axis.

Differences in x-axis deflections for 1- and 2-bolt connections for the same leg size can be seen in Figures 3.V.04 and 3.V.05 of Section 3.2.5. It is obvious that the increase of end restraint with two bolts produces larger negative deflections, thus reducing the bending effect and retarding failure.

For 1- and 2-bolt connections and two different leg sizes, Figures 3.V.04 through 3.V.07, the plots show an increase of end restraint about the y-axis for the heavier legs. However, the

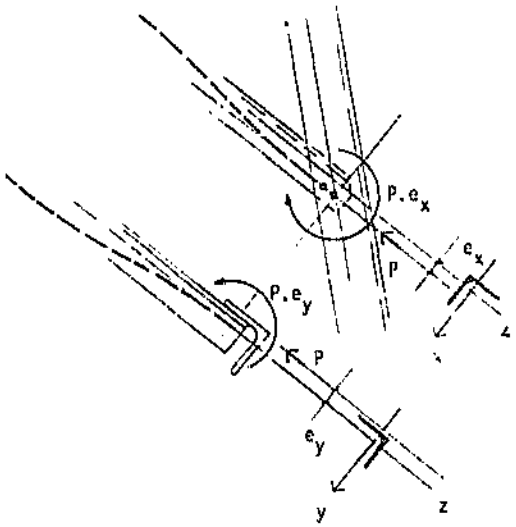

Figure 3.10-a: The bending effect due to the eccentric forces in both planes xz and yz initially induce deflections in the bracings as shown above.

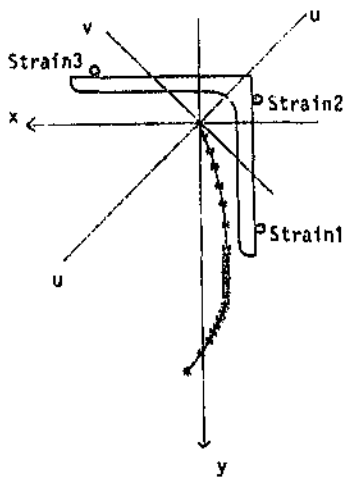

Figure 3.10-b: Typical in-plane and out-of-plane strut deformations at midspan (not to scale). When approaching failure, deflections occur predominantly along the u-axis.

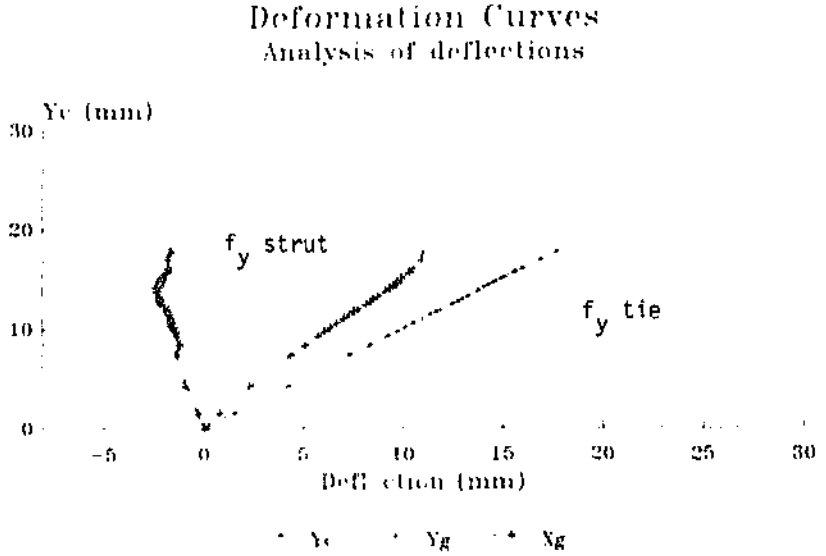

Figure 3.11-a: Vertical and horizontal strut deflections, see Figure 3.01
Test 102

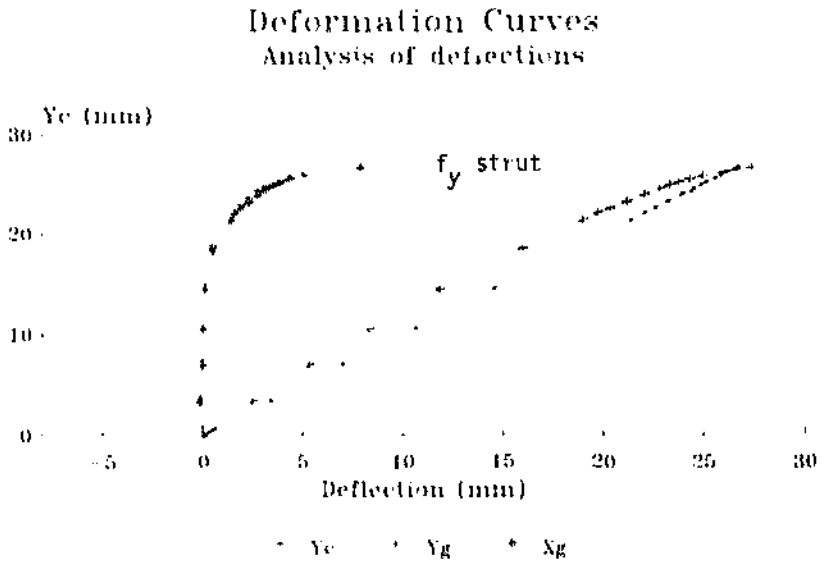

Figure 3.11-b Vertical and horizontal strut deflections, see Figure 3.01
Test 802

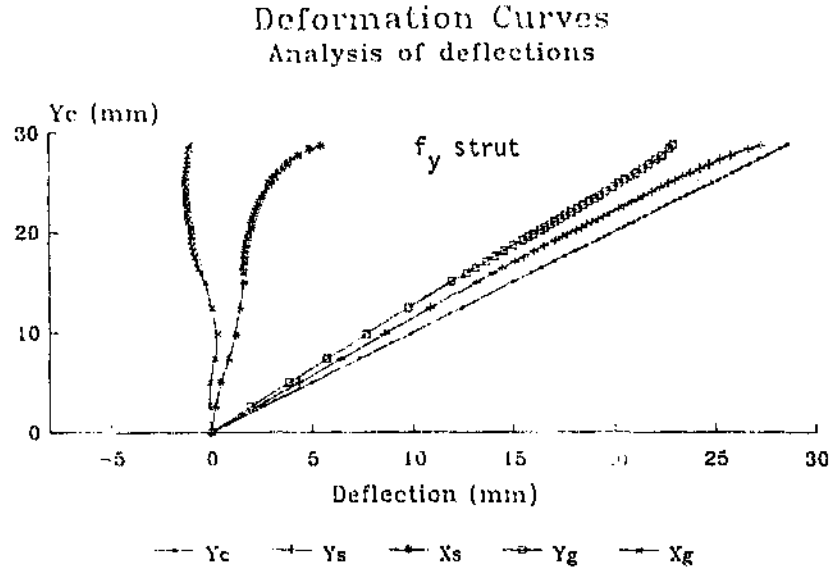

Figure 3.11-c.: Vertical and horizontal strut deflections, see Figure 3.02 Test 302

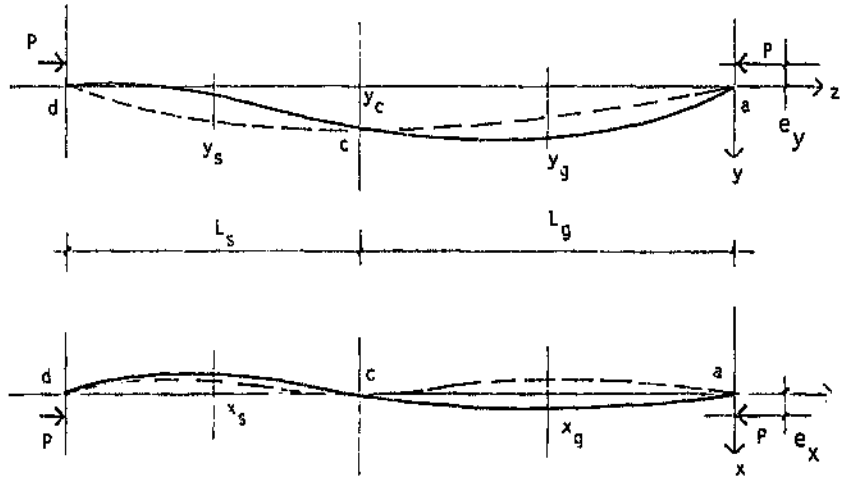

Figure 3.12: Typical strut deformations during tests. Before failure, the diagonals adopt the half-wave, anti-symmetrical curve shown in full line above.

1-bolt connection case is dependent on the torque used for tightening the bolts.

In conclusion, strut deflections vary widely for different test alternatives. In-plane deflections change as a function of the end restraint, and appear to have considerable influence on the resistance of the struts. The proximity of the main leg supports also has an effect on the amount of end restraint about the y-axis. A typical bracing deformation history is shown in Figure 3.12.

3.4 - General analysis of nodal rotations

The rotation measurements at the strut's connecting nodes a and d, Figure 3.13, are examined in more detail in this Section.

Considering the torsional and flexural rotations for 2-bolt connections at nodes a or d in Figure 3.13, where positive directions for nodal rotations are indicated, the following compatibility relationship can be written:

$$\theta_{xS} = \theta_{xS1} + \theta_{xS2} = \theta_{zL}\sin\Phi - \theta_{xL}\cos\Phi + \theta_{xS2} \qquad \ldots (3.01)$$

in which θ_{xS}, θ_{zL} and θ_{xL} are the recorded rotations, as indicated in Figure 3.13, θ_{xS1} is the strut's end connection flexural rotation (or actual node rotation about the strut's x-axis), and θ_{xS2} is an additional strut-end rotation due to flexibility of the connection.

To establish a basic pattern of behaviour, nodal rotations at nodes a and d from Tests 202, 302 and 402 with parallel main

leg are examined. Figures 3.14-a and 3.14-b show the recorded rotations at nodes a and d of Test 202, with bracing inclination β=30°. Note that torsional rotations θ_{zL} are almost equal on both legs (indicating the lack of torsional restraint at the nodes), while the strut's end rotations are reduced at node d, and the main leg's flexural rotations θ_{xL} at nodes a and d are very small and slightly different.

Figures 3.14-c and 3.14-d show the components of flexural rotations at both strut ends a and d respectively, calculated with Equation (3.01). It can be seen that the total recorded strut-end rotations θ_{xS} are larger at node a, while the node rotations θ_{xS1} are approximately the same at both nodes a and d (which is consistent with the symmetry of the bracing and the behaviour of the main legs). These results suggest that the difference in recorded rotations is due to the additional rotations θ_{xS2} from the flexibility of the connections.

Results at nodes a and d for Test 302 with bracing inclination β=40° are depicted in Figures 3.15-a and 3.15-b. Again, the leg's torsional rotations at nodes a and d are very similar, while the main leg's flexural rotations are very small, see Figure 3.13. Results about the strut's x-axis show that the node rotations θ_{xS1} are almost equal at nodes a and d, while the additional rotations θ_{xS2} are larger at node a, thus inducing at that node larger strut-end rotations θ_{xS}, see Figures 3.15-c and 3.15-d.

Similar results were recorded for Test 402 with bracing inclination β=50°, as depicted in Figures 3.16-a through 3.16-d. In conclusion, strut-end rotations in frames with parallel legs show the following characteristics:

- The leg's torsional rotations θ_{zL} are always very similar on both sides of the frame, irrespective of the bracing inclination β. This indicates lack of torsional restraint from the supports, and probably therefore implies lack of torsional restraint by the main leg on the strut. It is to be noted, however, that this is a conservative condition, as some restraint may occur in actual tower arrangements.

- The nodal rotations θ_{xS1} about the strut's x-axis are similar at both ends of the diagonals, irrespective of the bracing inclination β.

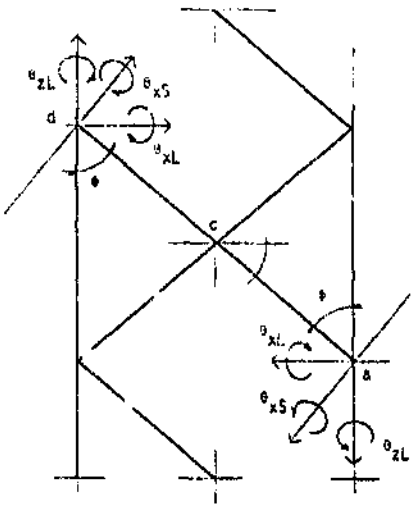

Figure 3.13: Positive directions of recorded nodal rotations at joints a and d.

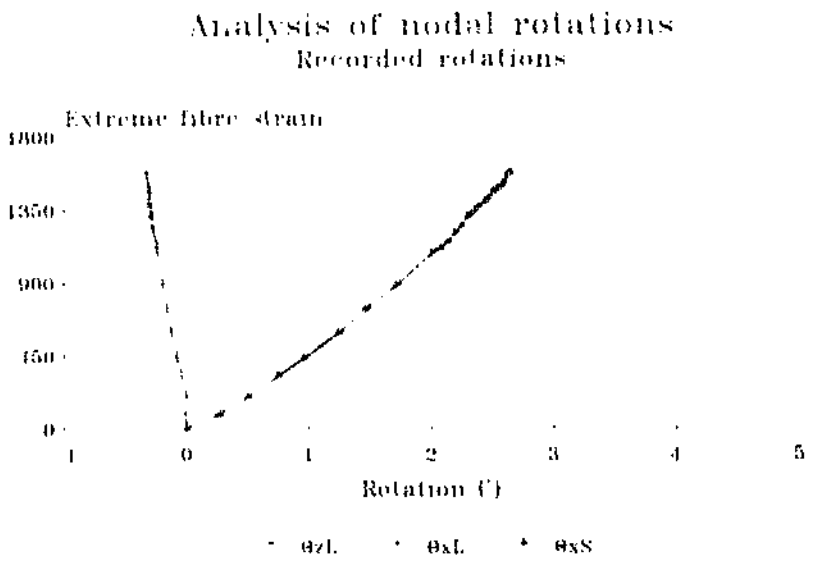

Figure 3.14 - a Recorded rotations at node a, see Figure 3.13
Test 202

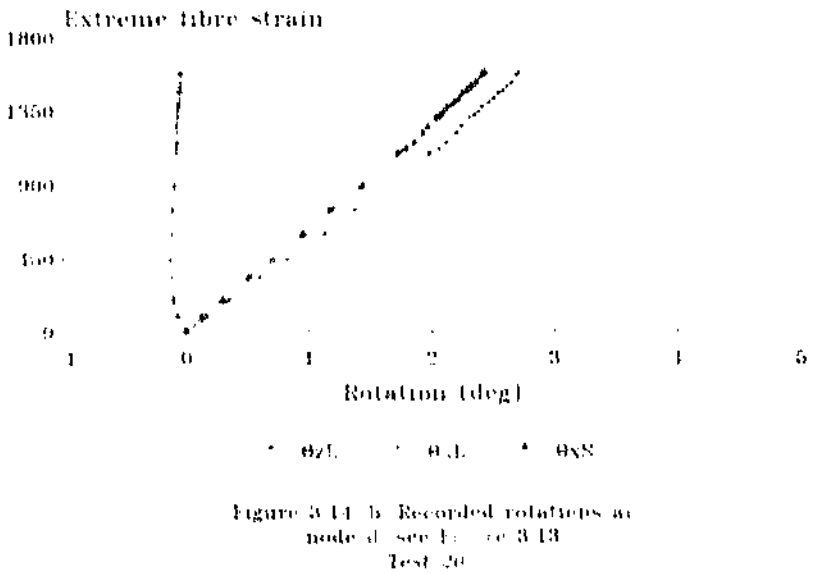

Figure 3.14 - b Recorded rotations at node d, see Figure 3.13
Test 20

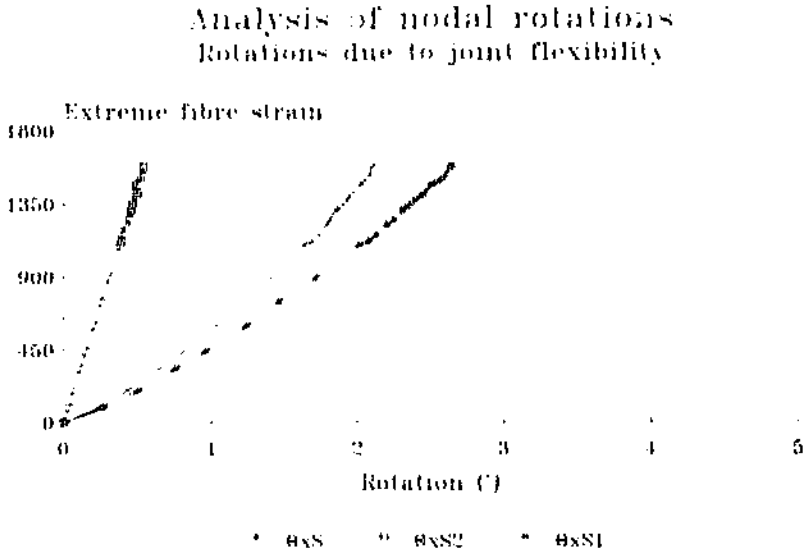

Figure 3.14 - c: Strut-end rotations at node a, see Figure 3.13
Test 202

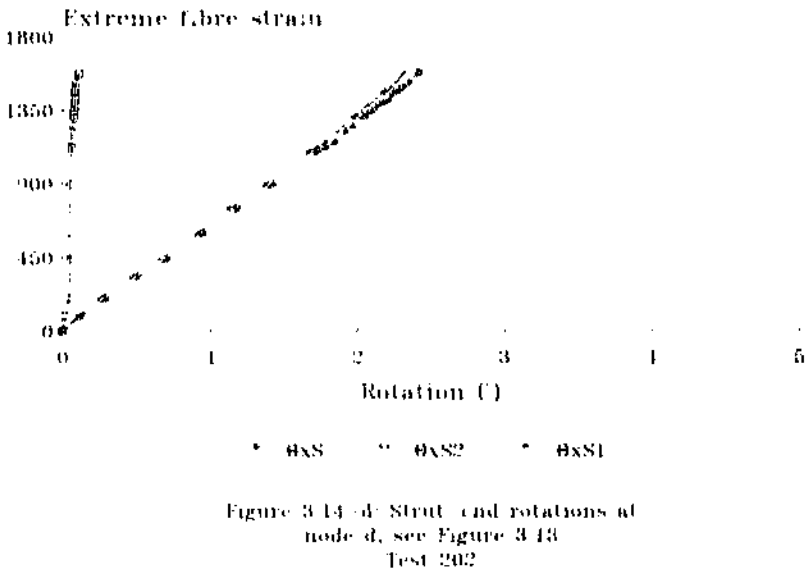

Figure 3.14 - d: Strut-end rotations at node d, see Figure 3.13
Test 202

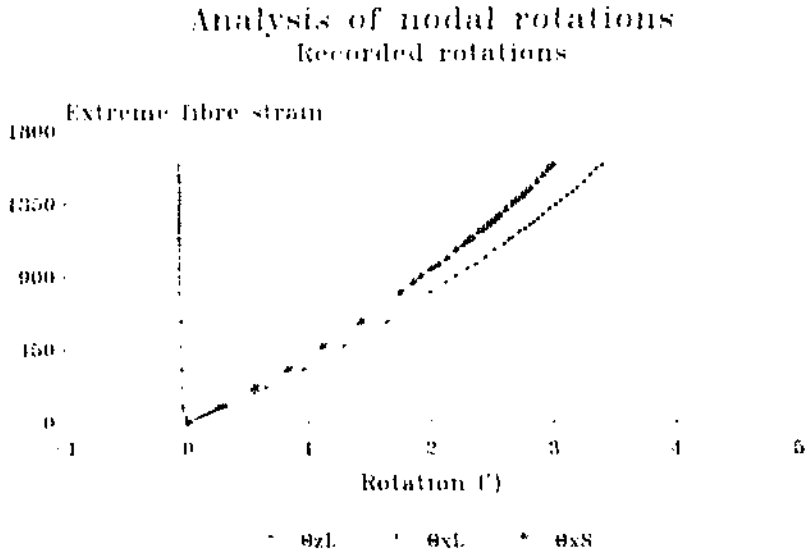

Figure 3.15-a: Recorded rotations at node a, see Figure 3.13
Test 302

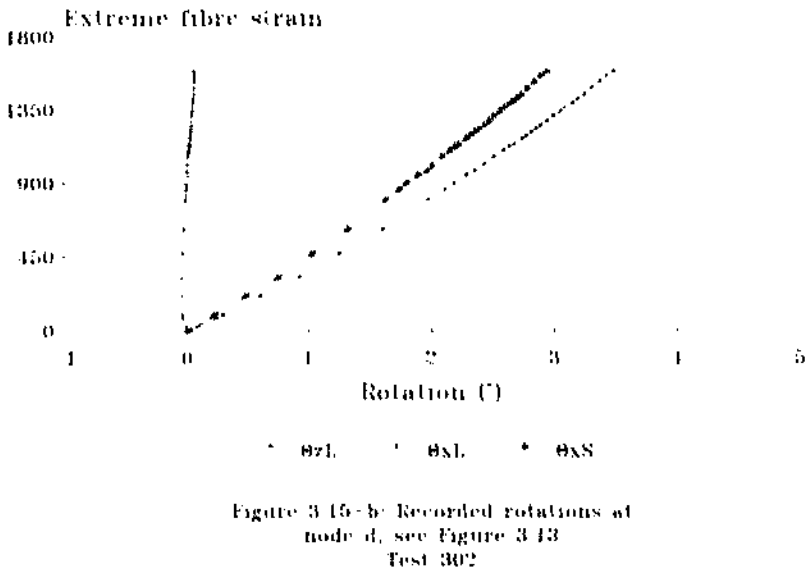

Figure 3.15-b: Recorded rotations at node d, see Figure 3.13
Test 302

Analysis of nodal rotations
Rotations due to joint flexibility

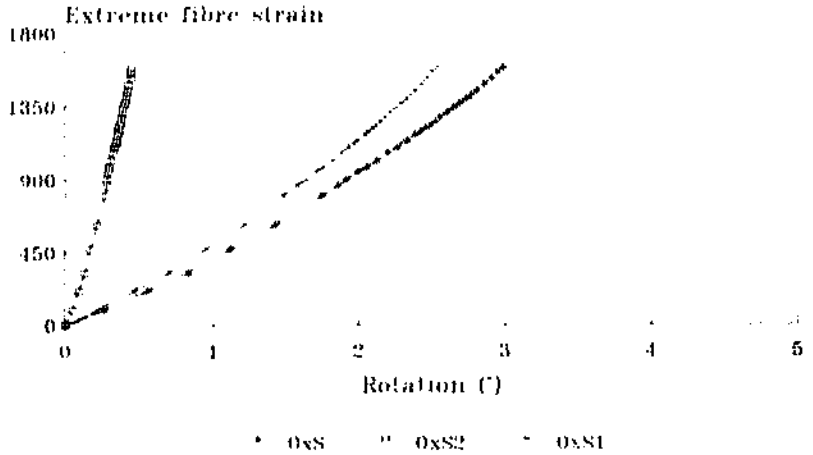

Figure 3.15-c Strut-end rotations at
node a, see Figure 3.13
Test 302

Analysis of nodal rotations
Rotations due to joint flexibility

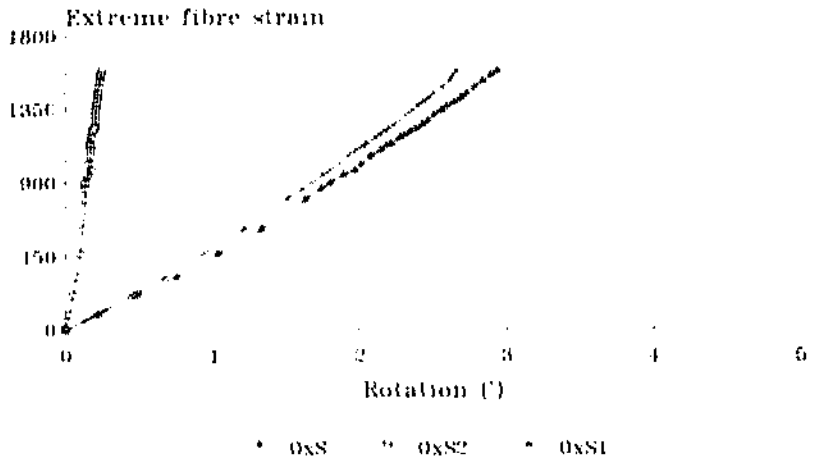

Figure 3.15-d Strut-end rotations at
node d, see Figure 3.13
Test 302

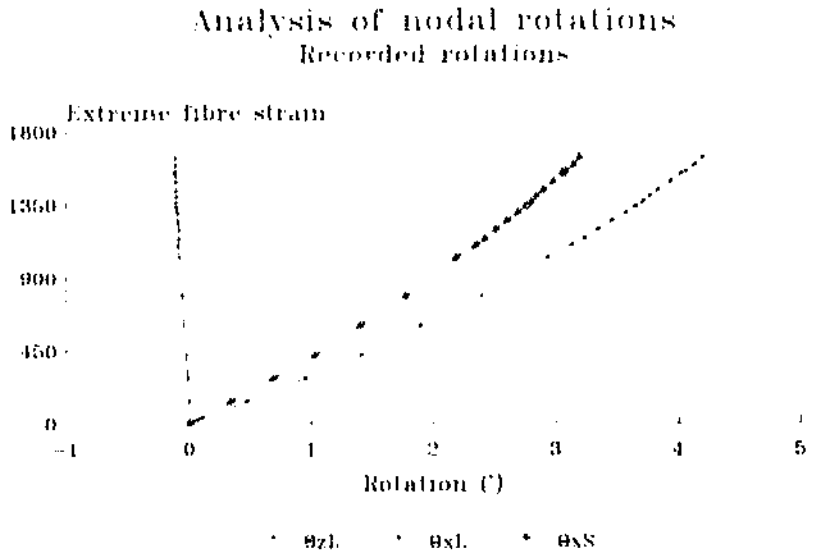

Figure 3.16-a: Recorded rotations at node a, see Figure 3.13
Test 402

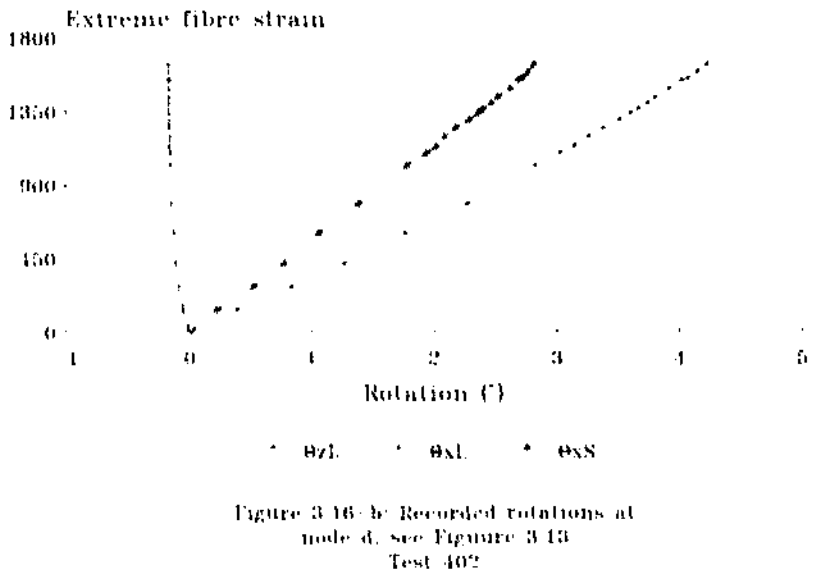

Figure 3.16-b: Recorded rotations at node d, see Figure 3.13
Test 402

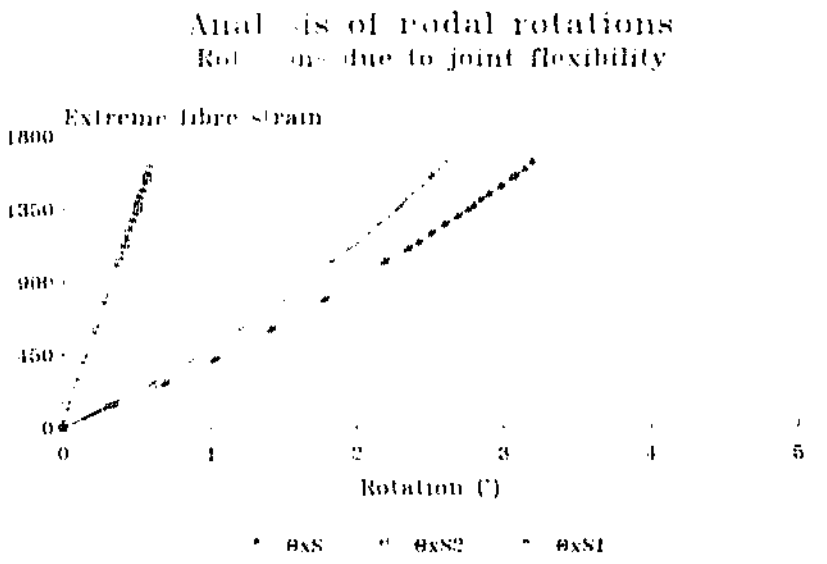

Figure 3.16-c: Strut-end rotations at node a, see Figure 3.15
Test 402

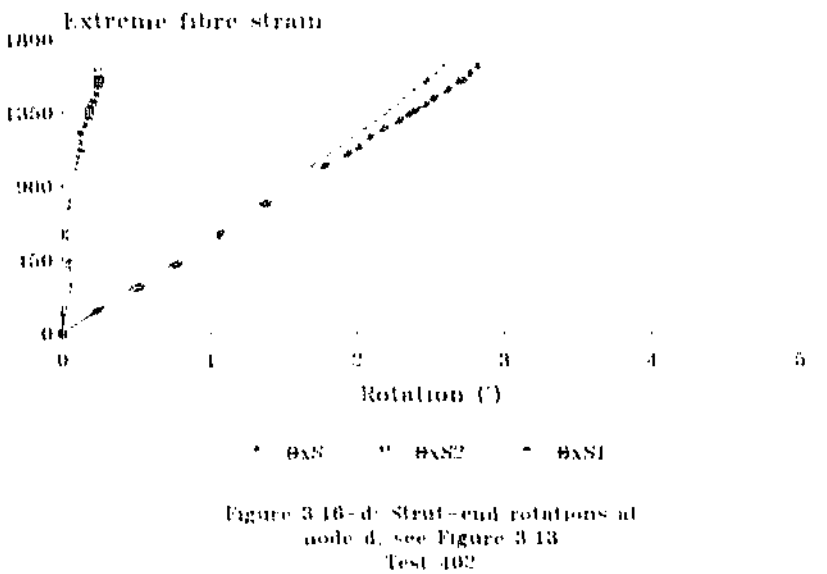

Figure 3.16-d: Strut-end rotations at node d, see Figure 3.13
Test 402

Analysis of nodal rotations
Rotations due to joint flexibility

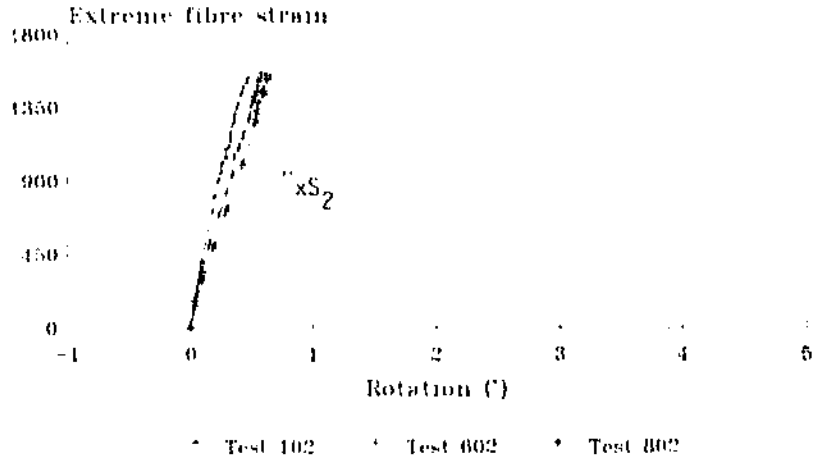

Figure 3.17: Additional rotations at node a due to joint flexibility Increased slenderness ratio

Analysis of nodal rotations
Rotations due to joint flexibility

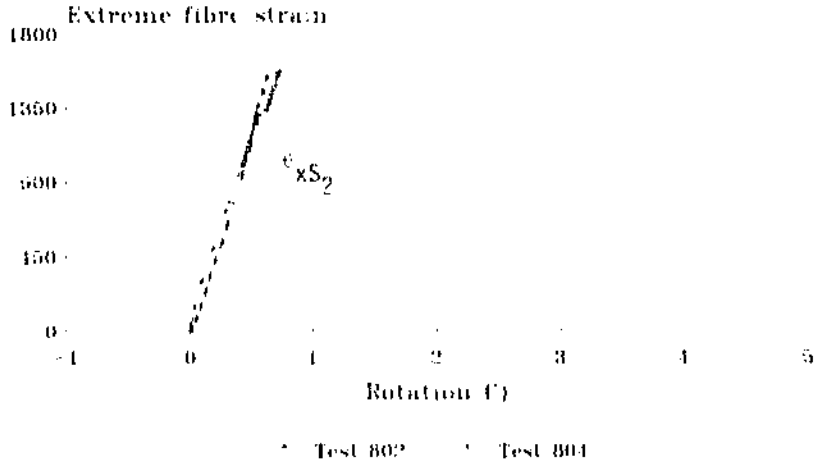

Figure 3.18: Additional rotations at node a due to joint flexibility Increased main leg size

- The additional rotations θ_{xS2} due to flexibility and the recorded strut rotations θ_{xS} are larger at the lower node a. These appear to be related to the leg's flexural rotations θ_{xL} and, finally, the latter could be influenced by the distance from the connection to the nearest leg support, see Figure 3.13. However, these results are uncertain for Tests 302 and 402 with inclination β=40° and 50° respectively. This deserves further attention in future research.

For Tests 102, 602 and 802, with inclined legs, increasing slenderness ratios, but otherwise identical conditions, Figure 3.17 shows that the additional rotations θ_{xS} at node a due to joint flexibility (plotted against strain, i.e. curvature) increase slightly with L/r. This is consistent with the measured torsional and flexural rotations shown in strain-deflection Figures 3.1.01 and 3.1.03 of Section 3.2.1.

Similarly, the additional rotations due to joint flexibility at node a for Tests 802 and 804 with different main leg sizes are shown in Figure 3.18. Note that the deformations of the joint plotted against strain are larger for the heavier angle.

The above review shows that the observed end rotations about the strut's x-axis are larger than the actual node rotations about the same axis. This is apparently due to flexibility of the connection, or, perhaps more specifically, these additional strut-end rotations are due to elastic deformations of the main leg's connected flange or leg. The equality of main leg's torsional rotations [illegible] both ends of the diagonals seems to support this explanation.

The observed differences in main leg's flexural rotations are

too small and uncertain, and thus it is not possible to draw conclusions from this parameter. Finally, as only the effect of in-plane bracing has been considered, it is most likely that a complete three-dimensional connection (as in actual tower construction) will introduce further changes to the behaviour of the joints.

3.5 - Additional comments on test results

While most of the parameters changed consistently in response to increasing loads as described in Section 3.2, there were some exceptions, as indicated below.

- Usual displacement curves at the critical section of the strut in Figure 3.19 can be compared with the strain curves of Figure 3.20-a, typical of tests with L/r of 130 and 160. It is clear that the vertical and horizontal movements of the strut at midspan are consistent with the development of tension and compression strains in the section. Furthermore, it is also apparent, when yield occurs first at section 2 of the angles, that all other parts of the section are well below the yield strain.

  At lower levels of slenderness ratio, however, this is not the case, as depicted in Figure 3.20-b for L/r=100. Maximum strains and hence first yield are recorded at the horizontal toe of the angles, even when the deformation history is very similar to that shown in Figure 3.19 . This is not necessarily inconsistent, and is related to the in-plane and out-of-plane deflection patterns at midspan in the strut, as shown in Figures 3.11-a and 3.11-b for Tests 102 and 802

respectively. This behaviour has been observed by Behncke [11] in previous research.

- Stress ratios for both tension and compression diagonals from Tests 102 and 602 are shown in Figure 3.21, where f_n/f_y refers to the ratio of nominal axial to yield stress, f_{max}/f_y refers to the ratio of maximum extreme fibre to yield stress, and T and C indicate tension and compression members, respectively. Stress was recorded at the cross-over joint c in the tie, and at midspan g in the strut, Figure 3.01.

The stress curves for Test 602 show that yield occurred first at midspan in the strut, while maximum stresses in the tie are about 25% lower at the same level of axial load. The same occurs at any level of slenderness ratio above 130.

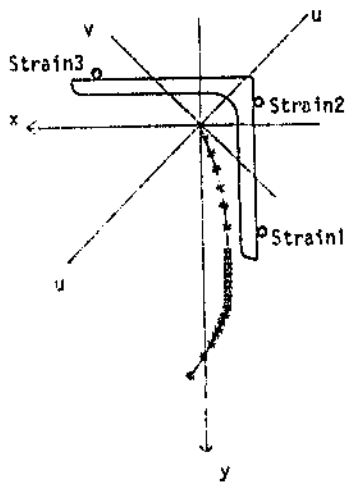

Figure 3.19: Typical in-plane and out-of-plane strut deformations at midspan (not to scale).

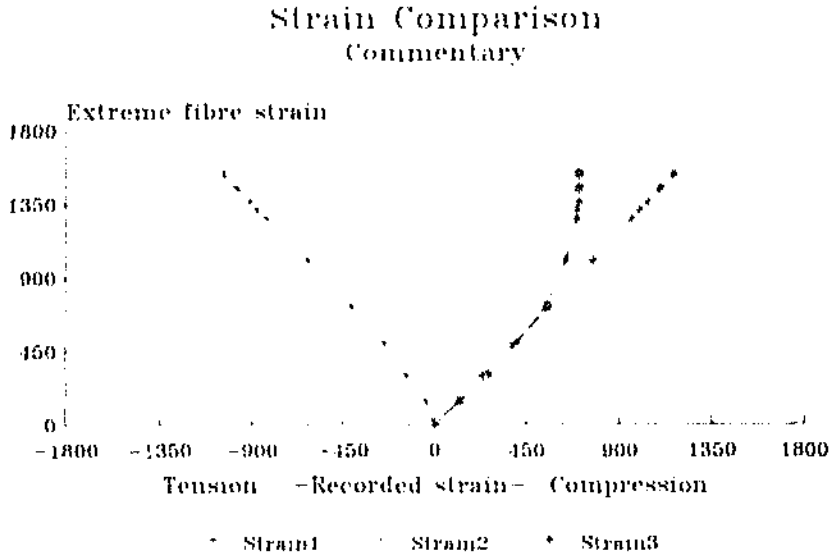

Figure 3.20-a: Typical strain readings
at the strut's critical section
Test 802 with L/r=160

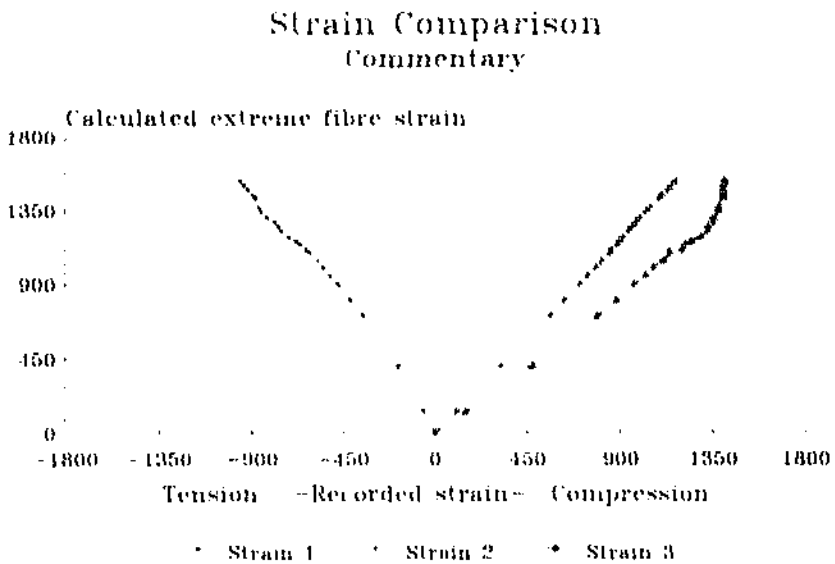

Figure 3.20-b: Strain readings at the
strut's critical section
Test 102 with L/r=100

Extreme Fibre Stress
Commentary

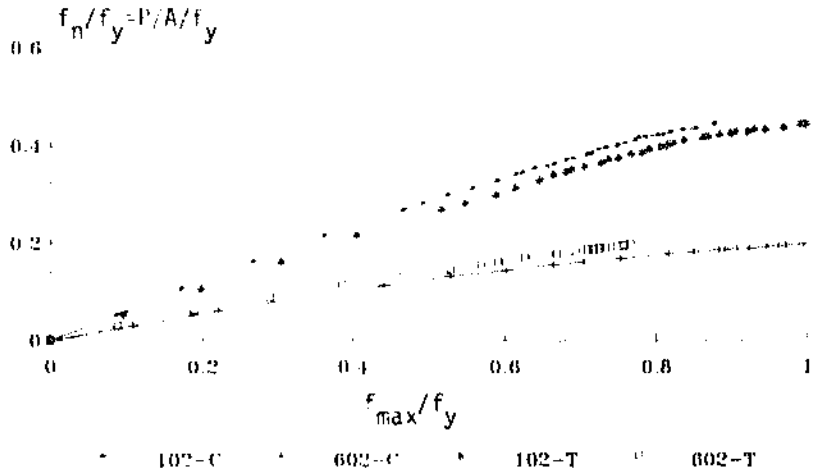

Figure 3.21: Stress ratio at the extreme fibre of the diagonals for Tes 102 and 602

Force Distribution
Commentary

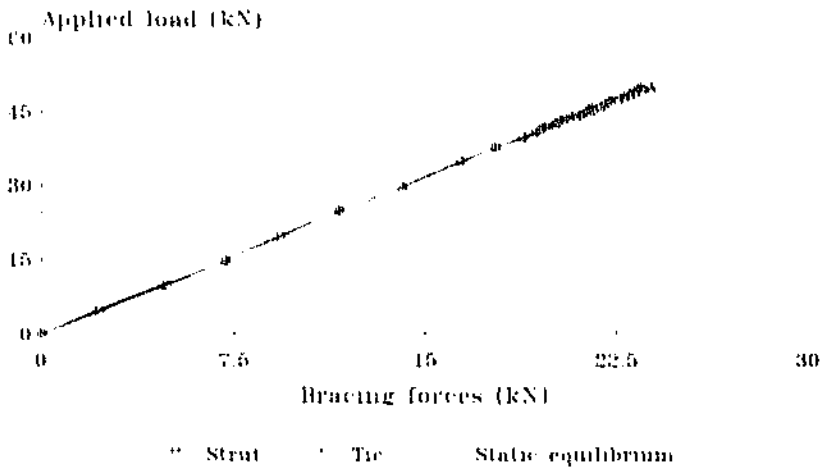

Figure 3.22: Recorded axial forces in the tension and compression diagonals Typical example

In Test 102 with L/r=100, however, yield occurred first in the tie at the cross-over joint, while maximum stress in the strut is about 15% lower at the same level of axial force in the diagonals. This bracing behaviour at low values of slenderness ratio has been anticipated by Elmes [51] and confirmed by Behncke [11] in previous investigations.

- Finally, a typical distribution of forces in the bracing is plotted against the applied loads in Figure 3.22. The observed forces are clearly equal in both the tension and compression members throughout the loading history. A third curve shows the diagonal forces as calculated from static equilibrium, assuming that they are equal and with opposite sign. The calculated forces are higher than the observed forces. This effect has been discussed by Wood [49,63] who defined a correction factor of approximately 0.945 in relation to these forces. The present results are in agreement with that figure.

3.6 - Assessment of end eccentricities

One of the main objectives of the present investigation is the evaluation of the effects of eccentricity of axial forces and end rotational restraints on the behaviour of crossed diagonals of two-dimensional frames with different bracing arrangements.

Measurements of strain and deformations immediately prior to first yield obtained from the test results described in the previous Sections can be used, together with the Southwell-plot procedure, to determine the Euler buckling load. With the Euler

load an effective length factor can be calculated and, finally, the equivalent eccentricities for each test alternative can be obtained with the secant formula. The bases for this procedure are outlined in Appendices C and D.

The Southwell-plot expression is given by Equation (C.01) of Appendix C as indicated below:

$$\frac{u}{P} = \frac{a_0}{P_E} + \frac{u}{P_E} \qquad \ldots.(C.01)$$

in which P is the recorded axial force in the bracing, and

- u is the recorded deflection in the strut at midspan, see Figure C.02-b.
- a_0 is the initial amplitude, given by the intercept or initial ordinate in the Southwell-plot of Figure C.01.
- P_E is the Euler load, given by the inverse of the slope in the Southwell-plot of Figure C.01.

However, it was found during this investigation that the deflection readings were not accurate enough to be used with the Southwell-plot procedure. Although considerable care was taken to install the deflection transducers, as explained in Appendix B (see also Figure 2.13 of Chapter 2), and to calculate the displacements of the heels of the angles, some differences were detected for various test alternatives. It is possible that frame movements, and also movements and distortions of the instruments' supports, were responsible for this problem.

It was therefore necessary to express the Southwell-plot in a different format. Recalling Equation (C.03) from Appendix C, we can write the following:

$$\frac{Mv_{max}}{P} = a_0 + \frac{Mv_{max}}{P_E} \qquad \ldots\ (C.03)$$

This is a modified expression of the Southwell-plot, in which:

- a_0 is the initial amplitude, or initial eccentricity, given by the initial ordinate in the plot.
- Mv_{max} is the bending moment about the minor axis of the section, and is obtained from strain readings.
- P is the recorded axial force, and is also obtained from strain readings.
- P_E is the Euler load, calculated as the inverse of the slope in the plot.

Results from this analysis for the tests in the present investigation are summarized in Table 3.08, in which:

- f_E/F_y is the ratio of Euler to yield stress.
- K is the effective length factor, obtained from the Euler elastic buckling load as follows:

$$KL_g = \pi\sqrt{(EI_v/P_E)} \qquad \ldots.(3.02)$$

where E is the modulus of elasticity, I_v is the moment of inertia about the minor v-axis, and L_g is the unsupported length of the strut.

- a_1/r_v is the relative equivalent eccentricity obtained from the Southwell-plot's initial ordinate.
- e_u/r_v is the relative equivalent eccentricity obtained from the secant formula at the moment of first yield. See Appendix D for details on this approach.

Table 3.07

Relative end eccentricities and effective length factor

Test Designation	Modified Southwell-plot results			
	$\frac{f_E}{f_y}$	K	$\frac{a_1}{r_v}$	$\frac{e_u}{r_v}$
1	2	3	4	5
102	---	---	---	---
202	0.636	0.798	0.354	0.312
302	0.526	0.874	0.287	0.252
402	0.639	0.786	0.326	0.281
502	0.631	0.798	0.258	0.219
602	0.659	0.790	0.307	0.270
702	0.590	0.830	0.261	0.221
801	0.329	0.853	0.163	0.135
802	0.522	0.710	0.429	0.374
803	0.424	0.745	0.276	0.235
804	0.460	0.747	0.250	0.207
805	0.439	---	0.083	0.070
806	0.348	0.830	0.219	0.181
807	0.373	0.793	0.132	0.107

Examining Table 3.08, the following conclusions can be drawn:

- Test 102 with slenderness ratio of 100 gave inconclusive or erroneous answers because of premature yielding of the diagonal in tension, therefore these results are not included in Table 3.08.

- The values for Tests 202 through 702 with constant slenderness ratio seem to be reasonably correlated, particularly regarding the effective length factor K in Column 3 and the relative eccentricity in Column 5.

- The values for Tests 602 and 802 for increasing slenderness ratio are also well correlated. A reduction in the Euler load is consistent with an increase of the slenderness ratio.

- The same can be said for Test 801 in relation to Tests 802 and 803. The increase of Euler load and eccentricity are consistent, as is the reduction of the factor K for higher restraints. Test 804, however, is not correlated to Test [illegible].

- The effective length K for Test 805 is not considered, since the strut's length Lg is undefined, see Figure 3.06-c.

3.7 - Summary

An extensive test programme on two-dimensional frames with steel-angle crossed diagonals has been presented in the previous Sections. The strain-deflection curves for the various test alternatives clearly show the primarily non-linear behaviour of the diagonals at increasing loads. In general, the following conclusions can be drawn from the above test results:

- As expected, nodal rotations and overall deformations in the bracings increase for higher slenderness ratios. Larger out-of-plane deformations increase the bending effect, thus reducing the resistance of the members.

- Frames with parallel legs permitted the study of diagonals in conditions of symmetry for increasing inclination of the bracing. It is confirmed that there is little or no torsional restraint from the main legs. The in-plane and out-of-plane deflections, as well as the nodal rotations, are influenced by the inclination of the bracing β. However, these effects seem to be offset by the possibility of buckling on either side of the cross-over joint, which is

reflected by slightly erratic first-yield and failure loads.

- Frames with inclined legs and bracing of constant slenderness ratio and variable bracing inclination β were used to analyze the effect of the length ratio L_s/L_g. Reductions of this ratio through larger inclinations β induce larger nodal rotations and midspan deformations, indicating a reduced nodal restraint. At the same time, however, smaller L_s/L_g increase the restraint from the shorter panel of bracing, thus counterbalancing the above effect. As a result, failure loads are very uniform for all these alternatives.

- The behaviour of the bracing is influenced by variations of the leg slope α, but to a lesser extent. A larger leg slope induces more out-of-plane deflections. However, nodal rotations are also dependent on the length ratio L_s/L_g. Failure loads are not increased significantly by the leg slope α.

- The resistance of the struts increases with higher end restraints. An increase from one to more bolts in the connections produces variations of in-plane deflections, and this has a retarding effect on the onset of yielding. An increase of the size of the main leg improves the restraining moments at the connections through larger flexural stiffness in the main leg.

- Any addition of redundant bracing to the system of crossed diagonals improves its buckling resistance. The additional members in the frames reduce the nodal rotations and midspan deformations, but to varying degrees. The proposed alternative of inverted diagonals offers a moderate increase

of resistance, with some additional cost of manufacturing. It is suggested that further research be conducted on this type of bracing.

- Locked-in system present special problems for experimental investigations. Nodal rotations and bracing deformations are smaller than in the normal case, but the distribution of forces in the bracing is erratic, and consequently the test results are inconclusive.

- Premature yielding of the tension member is common at low values of slenderness ratio. In addition, failure of the strut may be caused by a more complex combination of effects, other than pure flexural buckling. Significantly, no allowances are included in design procedures to consider these important effects.

- The Southwell-plot procedure and the secant formula proved to be valuable tools for analysis of Euler loads and end eccentricities from experimental results. A modified Southwell-plot was used, based on strain rather than on deflection readings, which yielded more reliable results.

  As indicated in Chapter 1, it is difficult to separate the effects of initial imperfections and end eccentricities on the behaviour of these small angle sections. Theoretical models for design of cross-bracing presented in the following Chapters include equivalent eccentricities based on the test results, which therefore account for these unknown factors (residual stress, initial curvature).

Summing up, the ultimate resistance of the bracing appears to be a direct function of the slenderness ratio, defined by

L_g/r_v, and the end conditions of the bracing, defined by the number of connecting bolts and the sizes of the main legs. These results have been anticipated by Behncke [11], Elmes [51] and Wood [49]. Additional variations in the capacity of the diagonals are introduced by the use of alternative bracing, and from those, the option of inverted diagonals is simpler than the use of redundant bracings.

Finally, a comparison is given in Column 4 of Table 3.09 below of the observed ratio of failure load, P_{ult}, to load at first yield, P_1, where P_y is the axial load required to fully yield the cross section. It can be seen that the failure-first yield load ratio was only slightly greater than 1.0 and in all the tests did not exceed 1.105.

An alternative theoretical model is presented in Chapter 4, which is based on the test results discussed in the previous Sections.

Table 3.09: Ratio of failure to yield load

Test Designation	Test Results		
	First yield	Failure	Load ratio
	$\frac{P_1}{P_y}$	$\frac{P_{ult}}{P_y}$	$\frac{P_{ult}}{P_1}$
1	2	3	4
102	0.474	0.491	1.035
202	0.374	0.412	1.103
302	0.358	0.395	1.103
402	0.387	0.421	1.089
502	0.412	0.437	1.060
602	0.397	0.431	1.086
702	0.396	0.430	1.086
801	0.286	0.288	1.007
802	0.318	0.336	1.056
803	0.317	0.324	1.024
804	0.344	0.364	1.056

CHAPTER 4

A PROPOSAL FOR NEW CROSS-BRACING DESIGN EQUATIONS

4.1 - Introduction

Results from laboratory tests on two-dimensional frames with crossed diagonals typical of steel transmission towers have been examined in Chapter 3. It is evident that the behaviour of cross-bracing comprising steel angle struts and ties connected at their cross-over joints in these latticed structures is subject to some uncertainty.

The analysis of experimental results confirms that the buckling resistance of the bracings is significantly affected by the end eccentricities and end rotational restraints of the bolted connections, as well as by the stiffnesses of main legs and bracings. It is also observed that the relative influence of these effects varies with the slenderness ratio of the diagonals.

The inclination of the bracings relative to the main legs, which defines the length factor $r=L_s/L_g$, has an important influence on the general behaviour of the diagonals at increasing loads. However, it is concluded, from monitoring of this parameter during tests on diagonals where slenderness ratios and support conditions were held constant, that it has little effect on the buckling capacity of bracings.

Clearly, therefore, new cross-bracing design equations which

include the various influences on the behaviour of the diagonals are required. This Chapter makes a proposal for such equations, which are subsequently checked against the present experimental results, and also against tests conducted on cross-bracing systems reported by Behncke [11] and Wood [49,63]. Results from some of the usual buckling curves for design of steel transmission towers are also included.

4.2 - Design equations

Experimental results on typical transmission tower cross-bracing such as reported in Chapter 3, and also from previous investigations by Wood [49], CIGRE [63] and Behncke [11], show that the tension member provides adequate lateral restraint to the out-of-plane deflections of the cross-over joint, and that it is not subject to premature yielding. This has been confirmed in theoretical analyses by Elmes [51] and Picard [38].

Based on the above evidence, and confining the analyses to cases within the practical range of member sizes in transmission towers (usually with slenderness ratios higher than 100), the simplified model shown in Figure 4.01 can be used for assessing the influences of the end restraint on the diagonals and the relative inclination of the main legs and diagonals, given by the ratio $r=L_s/L_g$.

Rotation compatibility equations at the cross-over node c in Figure 4.01 can be written considering appropriate boundary conditions and also flexibility relationships between the end rotations and end moments in the struts of lengths L_s and L_g. Adopting the notation and sign convention given in

Appendix D, the rotations at nodes d, c and a on both subspans in Figure 4.01 can be written, following Equations (D.02) in Appendix D, as indicated below:

$$\theta_{dc} = \frac{Mv_{dc}L_s}{3EI_v} B_1 - \frac{Mv_{cd}L_s}{6EI_v} B_2$$

at the left node d, and ....(4.01)

$$\theta_{cd} = \frac{-Mv_{dc}L_s}{6EI_v} B_2 + \frac{Mv_{cd}L_s}{3EI_v} B_1$$

at the right node c, of the member dc of length L_s. Similarly, we can write:

$$\theta_{ca} = \frac{Mv_{ca}L_g}{3EI_v} B_3 - \frac{Mv_{ac}L_g}{6EI_v} B_4$$

at the left node c, and ....(4.02)

$$\theta_{ac} = \frac{-Mv_{ca}L_g}{6EI_v} B_4 + \frac{Mv_{ac}L_g}{3EI_v} B_3$$

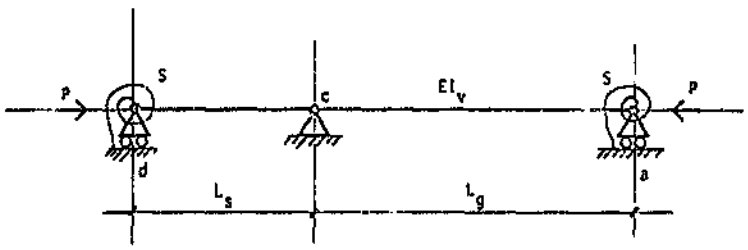

Figure 4.01: Model of strut in cross-bracing. S is the spring stiffness at ends, and is expressed as the ratio of moment to unit rotation of the bolted connection and adjacent main leg

at the right node a of the member ca of length L_g in Figure 4.01. The factors B_1 through B_4, as explained in Appendix D, are the Berry stability functions for adjusting the flexibility matrix to allow for axial load in the spans of lengths L_s and L_g, and EI_v is the flexural rigidity with respect to the minor axis of the section. The following assumptions are now made about the terms in these equations

- At node d: $\theta_{dc} = -M_{dc}/S$

- At node c: $M_{cd} = -M_{ca}$
  $\theta_{cd} = \theta_{ca}$ ....(4.03)

- At node a: $\theta_{ac} = -(M_{ac} + M')/S$

in which

- S is an unknown rotational restraint coefficient, and
- M' is an arbitrary moment due to eccentricity of axial load at node a.

These equations can now be solved for the condition of rotation compatibility ($\theta_{cd} = \theta_{ca}$) at node c in Figure 4.01. Substituting Equations (4.01) and (4.02) into Equations (4.03), solving for M_{dc}, $M_{cd}=-M_{ca}$ and M_{ac}, and substituting these moments into the expressions of rotations at node c (these are all routine deductions and thus are not included), it is possible to establish the following criterion for infinite rotations $\theta_{cd}=\theta_{ca}$, representing the elastic buckling load which is independent of M':

$$[12B_{3g} + S(4B_{3g}^2 - B_{4g}^2)][3 + 3B_{1s}] + [12B_{1s} + S(4B_{1s}^2 - B_{2s}^2)][3 + 3B_{2s}] = 0.0$$

in which the above terms are given as follows:

$$B_{1s} = B_1 L_s / EI_v,$$
$$B_{2s} = B_2 L_s / EI_v$$
$$B_{3g} = B_3 L_g / EI_v$$
$$B_{4g} = B_4 L_g / EI_v$$

The elastic buckling load P_E which satisfies the above equation can be used to calculate an effective length factor K, corresponding to the longer unsupported subspan L_g of the compression bracing. Recalling the Euler buckling equation, we can write the following:

$$KL_g = \pi\sqrt{(EI_v/P_E)} \qquad \ldots.(4.04)$$

where I_v is the inertia of the strut about its minor v-axis. The results of this analysis are given in Figure 4.02, in which the factor K is plotted as a function of the length ratio L_s/L_g, and a non-dimensional spring stiffness S_{xS} given by the following expression:

$$S_{xS} = S/[EI_v/(L_s+L_g)]$$

where S is the spring stiffness of the end restraints at nodes d and a included in the preceding analysis, see Figure 4.01.

Unfortunately, a rigorous determination of S_{xS} is not possible due to the unknown flexibility in the bolted connections between the bracing and main legs. From the analysis above, however, and neglecting torsional restraint from the main legs, a parametric study indicates, in agreement with the observed behaviour of the bracings described in Chapter 3, that S_{xS} should be proportional to the following expression:

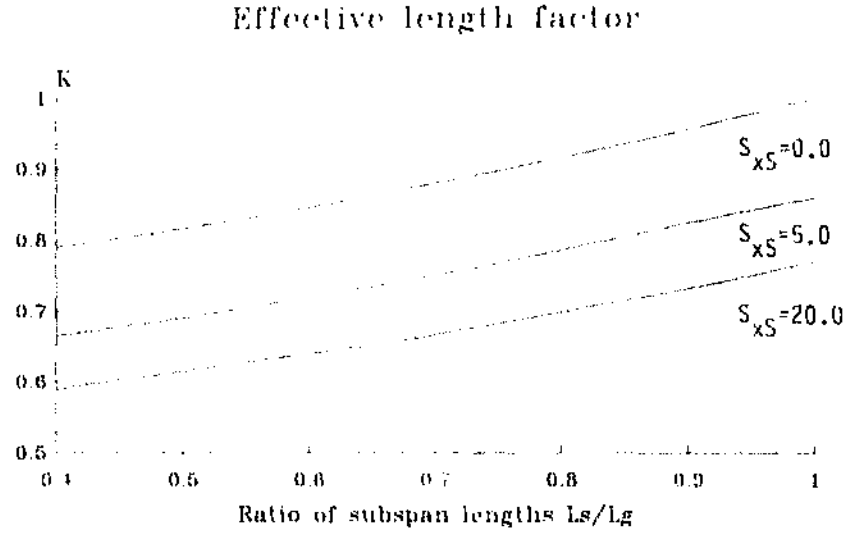

Figure 4.02: Calculated effective length factor for different end conditions

$$I_{xL}/(I_{vS}\sin\beta)$$

in which

- I_{vS} is the strut's moment of inertia about its minor v-axis,
- I_{xL} is the main legs' moment of inertia about its orthogonal x- or y-axis, and
- β is the inclination of the bracing relative to the frame horizontal axis, thus indicating the direction of the plane containing the restraint.

Considering these experimental results together with the analysis of test results using the Southwell-plot at loads close to first yield, as indicated in Table 3.08, the following empirical relation for the relative spring S_{xS} can be written:

$$S_{xS} = x_b \, Ix_L/(Iv_S \sin\beta) \qquad ...(4.05)$$

where x_b is a factor dependent on the restraint provided by the connecting bolts, and is expressed for different end conditions as follows:

- 1-bolt end connection: $x_b = 0.06$
- 2-bolt end connection: $x_b = 0.20$

The increased restraint with more than one bolt in the connections is consistent with a greater utilization of flexural stiffness of the main leg about both orthogonal x- and y-axis.

The effective length factor K given in Figure 4.02 may be represented with reasonable accuracy using an expression incorporating the end restraint coefficient S_{xS}, given by Equation (4.05), as indicated below:

$$K = (0.6+0.4\tau)(1+0.25S_{xS})/(1+0.33S_{xS}) \qquad ...(4.06)$$

in which τ is the length ratio L_b/L_g.

In this way, an effective length factor has been determined, which includes the effects of the relative positions and sizes of diagonals and main legs, the end conditions of the diagonals and, finally, the direction of the plane containing the main restraints.

Consider now a hypothetical pin-ended element a-c of length L_g in Figure 4.01, subjected to an eccentric compressive load P with an equal effective eccentricity e_u at both ends. The maximum bending moment at the centre of this strut is given for all P by the secant formula, as indicated below:

$$M_{vmax} = Pe_u\sec(w) \qquad \ldots(4.07)$$

where $w = 0.5\,m\sqrt{(P/P_E)}$, and P_E is the Euler elastic load. If the axial eccentric force P is progressively increased until the maximum stress in the extreme fibre of the element a-c in Figure 4.01 is equal to the yield stress f_y, we can write the following:

$$\frac{f_{ult}}{f_y}\left[\frac{e_u h \sec(w)}{r_v^2} + 1\right] - 1 = 0 \qquad \ldots(4.08)$$

in which

- f_y is the yield stress of material,
- f_{ult} is the average axial stress in the strut at yield of the extreme fibre,
- e_u is the effective end eccentricity,
- h is the distance of the extreme fibre from the minor v-axis,
- $w = 0.5m\sqrt{(f_y/f_E)}\sqrt{(f_{ult}/f_y)}$,
- f_E is the Euler stress, given by $\pi^2E/(KL_g/r_v)^2$, and
- r_v is the radius of gyration about the minor axis.

This approach, therefore, can be used to evaluate the axial forces P which will induce yield of the extreme fibre in the element a-c of length L_g in Figure 4.01. It now remains to evaluate the effective end eccentricity e_u.

Eccentricities at end connections also have a significant influence on the resistance of the bracing, particularly at

lower slenderness ratios. The effective end eccentricities e_u calculated for the tests in the present investigation using the Southwell-plot of deflection measurements prior to first yield, are listed in Table 3.08. On the basis of these results, a mean relative eccentricity $e_u/r_v=0.25$ can be used as an appropriate approximation.

It is concluded, therefore, for values of slenderness ratios in the range 90 to 160 in towers represented by the test conditions described in Chapter 2 and also in previous research by Behncke [11], where it has been consistently observed that yielding of the extreme fibre occurs just prior to buckling, that the secant-yield expression of Equation (4.08) may be used to predict the strength of cross-bracing.

For design purposes the spring coefficient S_{xS} and the effective length factor K may be obtained from Equations (4.05) and (4.06) respectively, and the ultimate buckling resistance may be obtained by solving Equation (4.08) in terms of the stress ratio fult/fy, for a relative eccentricity $e_u/r_v=0.25$.

Indicative values of K, Equation (4.0b), are given in Table 4.01 for given values of the bracing inclination β, leg slope α and the ratio of inertia I_{xL}/I_{vS}, Equation (4.05), and also considering the coefficients x_b given in Equation (4.05) for 1- and 2-bolt connections. Note that Table 4.01 is based on x_b in Equation (4.05) of 0.20 representing 2-bolt connection. For single-bolt details the effective value of I_{xL} should be reduced to 30% of its actual value, represented by $x_b=0.30*0.20=0.06$.

Indicative values of the ultimate stress ratios f_{ult}/f_y, Equation (4.08), are listed in Table 4.02 for given values of the effective slenderness ratio KL_E/r_v and yield stress f_y. This latter table incorporates conservative values of $h/r_v=2.20$ for angle sections and $e_u/r_v=0.25$ in Equation (4.08). Figure 4.03 illustrates the stress curves of Table 4.02.

Table 4.01: Effective length factor K for 2-bolt end connections. (Reduce I_{xL} to 30% of its value for 1-bolt connections)

α	β	I_{xL}/I_{vS}									
		5	10	15	20	25	30	35	40	45	50
0	25	0.894	0.852	0.830	0.816	0.807	0.800	0.795	0.791	0.788	0.785
0	30	0.904	0.862	0.839	0.824	0.814	0.806	0.801	0.796	0.793	0.789
0	35	0.911	0.870	0.847	0.831	0.820	0.812	0.806	0.801	0.797	0.793
0	40	0.918	0.877	0.853	0.837	0.826	0.817	0.810	0.805	0.801	0.797
0	45	0.923	0.883	0.859	0.842	0.830	0.821	0.814	0.809	0.804	0.800
0	50	0.927	0.888	0.863	0.847	0.834	0.825	0.818	0.812	0.807	0.803
0	55	0.930	0.892	0.867	0.850	0.838	0.829	0.821	0.815	0.810	0.806
0	60	0.933	0.895	0.871	0.854	0.841	0.831	0.824	0.817	0.812	0.808
0	65	0.935	0.898	0.873	0.856	0.844	0.834	0.826	0.820	0.814	0.810
5	25	0.866	0.825	0.804	0.791	0.782	0.775	0.770	0.766	0.763	0.760
5	30	0.869	0.829	0.807	0.792	0.783	0.775	0.770	0.766	0.762	0.759
5	35	0.869	0.830	0.807	0.793	0.782	0.775	0.769	0.764	0.760	0.757
5	40	0.868	0.829	0.806	0.791	0.780	0.772	0.766	0.761	0.757	0.753
5	45	0.863	0.826	0.803	0.788	0.777	0.769	0.762	0.757	0.752	0.749
5	50	0.857	0.821	0.798	0.783	0.771	0.763	0.756	0.751	0.746	0.743
5	55	0.848	0.813	0.790	0.775	0.764	0.755	0.748	0.743	0.738	0.734
5	60	0.835	0.801	0.779	0.764	0.752	0.744	0.737	0.731	0.727	0.723
5	65	0.817	0.784	0.763	0.748	0.737	0.728	0.722	0.716	0.711	0.707
10	25	0.839	0.800	0.780	0.767	0.758	0.752	0.747	0.743	0.740	0.737
10	30	0.837	0.798	0.777	0.763	0.754	0.747	0.742	0.737	0.734	0.731
10	35	0.831	0.794	0.772	0.758	0.748	0.741	0.735	0.730	0.727	0.724
10	40	0.823	0.787	0.765	0.751	0.740	0.733	0.727	0.722	0.718	0.715
10	45	0.812	0.777	0.756	0.741	0.731	0.723	0.717	0.712	0.708	0.704
10	50	0.798	0.764	0.743	0.729	0.719	0.711	0.704	0.699	0.695	0.692
10	55	0.781	0.748	0.728	0.714	0.703	0.695	0.689	0.684	0.680	0.676
10	60	0.758	0.728	0.708	0.694	0.684	0.676	0.670	0.664	0.660	0.657
10	65	0.730	0.701	0.682	0.668	0.658	0.651	0.645	0.640	0.636	0.632

Bracing ultimate capacity stress ratio

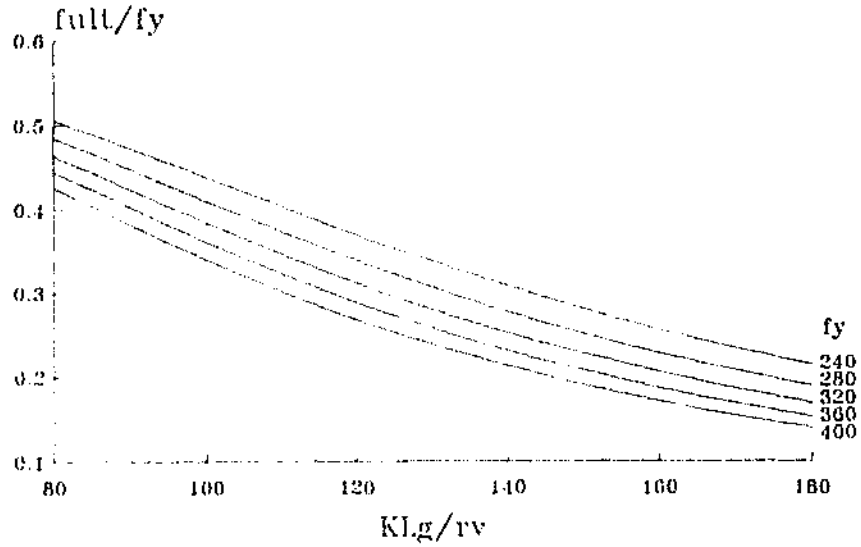

Figure 4.03: Calculated failure loads, see Equation (4.08)

Table 4.02: Bracing ultimate capacity, expressed as stress ratio f_{ult}/f_y - f_y in (MPa)

$\frac{KL_g}{r_v}$	$\frac{f_{ult}}{f_y}$					$\frac{KL_g}{r_v}$	$\frac{f_{ult}}{f_y}$				
	f_y=240	f_y=280	f_y=320	f_y=360	f_y=400		f_y=240	f_y=280	f_y=320	f_y=360	f_y=400
80	0.506	0.485	0.464	0.445	0.426	130	0.337	0.306	0.280	0.258	0.238
82	0.500	0.478	0.456	0.436	0.417	132	0.331	0.300	0.274	0.252	0.233
84	0.493	0.470	0.448	0.428	0.408	134	0.325	0.294	0.268	0.246	0.228
86	0.486	0.463	0.440	0.419	0.399	136	0.319	0.288	0.263	0.241	0.222
88	0.480	0.455	0.432	0.410	0.390	138	0.313	0.283	0.258	0.236	0.218
90	0.473	0.446	0.424	0.402	0.382	140	0.308	0.277	0.252	0.231	0.213
92	0.466	0.440	0.415	0.394	0.373	142	0.302	0.272	0.247	0.226	0.208
94	0.459	0.432	0.408	0.385	0.364	144	0.296	0.266	0.242	0.241	0.203
96	0.452	0.423	0.400	0.377	0.356	146	0.291	0.261	0.237	0.216	0.199
98	0.445	0.417	0.392	0.369	0.348	148	0.286	0.256	0.232	0.212	0.195
100	0.438	0.410	0.384	0.361	0.340	150	0.280	0.251	0.227	0.207	0.190
102	0.431	0.402	0.376	0.353	0.332	152	0.275	0.246	0.223	0.203	0.186
104	0.424	0.395	0.369	0.345	0.324	154	0.270	0.242	0.218	0.199	0.182
106	0.417	0.388	0.361	0.338	0.316	156	0.265	0.237	0.214	0.195	0.178
108	0.410	0.380	0.354	0.330	0.309	158	0.260	0.232	0.210	0.191	0.175
110	0.403	0.373	0.346	0.323	0.302	160	0.256	0.228	0.206	0.187	0.171
112	0.396	0.366	0.339	0.316	0.295	162	0.251	0.224	0.201	0.183	0.168
114	0.389	0.359	0.332	0.309	0.288	164	0.247	0.220	0.198	0.179	0.164
116	0.382	0.352	0.325	0.302	0.281	166	0.242	0.215	0.194	0.176	0.161
118	0.376	0.345	0.318	0.295	0.274	168	0.238	0.211	0.190	0.172	0.158
120	0.369	0.338	0.312	0.288	0.268	170	0.234	0.208	0.186	0.169	0.154
122	0.362	0.332	0.305	0.282	0.262	172	0.230	0.204	0.183	0.166	0.151
124	0.356	0.325	0.298	0.276	0.256	174	0.226	0.200	0.179	0.162	0.148
126	0.350	0.319	0.292	0.270	0.250	176	0.222	0.196	0.176	0.159	0.145
128	0.343	0.312	0.286	0.264	0.244	178	0.218	0.193	0.172	0.156	0.142
						180	0.214	0.189	0.169	0.153	0.140

4.3 - Comparison of theoretical and experimental results. General discussion

The design equations developed in the previous Sections incorporate most of the important variables which influence cross-bracing behaviour and ultimate resistance of the diagonals, as identified in Chapter 3. In particular, the effective length factor K is developed as a function of the strut's end conditions, both in terms of number of connecting bolts and the sizes of the bracing and main legs. Further, the inclination β of the bracing and the lengths of the strut at either side of the cross-over node (given by the ratio $\tau=L_s/L_g$) are also included in the coefficient K.

The solution for failure stress includes the strut's material properties, the cross-section geometric characteristics, and the Euler elastic load, therefore incorporating the influence of the slenderness ratio L/r.

In the analysis that follows, various test alternatives from three experimental investigations are examined using the design curves for steel angles given in Section 4.2 above. In addition, comparisons with results from the following methods of transmission tower design are included:

- The buckling curves for steel angles given in the ASCE Manual No 52 [5].
- The buckling curves for steel angles given in the ECCS Manual No 39 [7].
- The design curves for steel angles given in Wood's report on CIGRE cross-bracing tests [49,63].

4.3.1 - Present investigation

A description of the frames, main legs and test specimens for this series of tests is given in Tables 4.03-a and 4.03-b. Note that some additional tests on L45x45x3 specimens with M16 bolts, which were not used in the analyses in Chapter 3, are now incorporated for evaluation of analytical models.

A comparison is given in Table 4.03-c of the stresses fult/fy obtained from the tests (Column 8) and also calculated from design curves in ASCE (Column 3), ECCS (Column 5) and CIGRE (Column 7), where fult is the failure stress, fy is the recorded stress of material (Column 7 of Table 4.03-b), and fg is the Euler stress. The effective slenderness ratio r_k is obtained by modifying the relative slenderness ratio r_0 in Table 4.03-b (Column 8) by an effective length coefficient K. This coefficient is obtained empirically as indicated in the references above.

Results in Table 4.03-c show that the design curves in ASCE and ECCS give optimistic predictions of failure loads at low values of slenderness ratio (Tests 102 and 312), resulting in the diagonals failing at lower loads than expected. Curves given by Wood from CIGRE tests are not applicable for slenderness ratios below 120.

At medium range of slenderness (Tests 202-702), on the other hand, the ASCE and ECCS design curves appear to provide reasonable assessments of the failure loads, whereas the CIGRE results are optimistic in all cases. It is clear in Table 4.03-c that variations of main leg and bracing inclination, given by

Table 4.03 a Test frame characteristics

Test Designation	Frame			Main chords			
	α (°)	β (°)	L_s/L_g	Size (mm)	I_{xL} ($10^6 mm^4$)	z_b	Φ_b
1	2	3	4	5	6	7	8
102	8	40	0.789	L80x80x6	0.5582	2	M12
202	8	30	1.000	L80x80x6	0.5582	2	M12
302	8	40	1.000	L80x80x6	0.5582	2	M12
312	8	40	1.000	L80x80x6	0.5582	2	M16
402	8	50	1.000	L80x80x6	0.5582	2	M12
502	8	30	0.850	L80x80x6	0.5582	2	M12
602	8	40	0.789	L80x80x6	0.5582	2	M12
702	8	50	0.713	L80x80x6	0.5582	2	M12
801	8	40	0.789	L80x80x6	0.5582	1	M12
811	8	40	0.789	L80x80x6	0.5582	1	M16
802	8	40	0.789	L80x80x6	0.5582	2	M12
812	8	40	0.789	L80x80x6	0.5582	2	M16
803	8	40	0.789	L90x90x8	1.0440	1	M12
804	8	40	0.789	L90x90x8	1.0440	2	M12

Table 4.03-b: Test specimen characteristics

Test Designation	Diagonals						
	Size (mm)	I_{vS} ($10^6 mm^4$)	r_v (mm)	L_g (mm)	L_g/r_v	f_y (MPa)	r_0
1	2	3	4	5	6	7	8
102	L40x40x3	0.0144	7.820	800	102.3	317.0	1.274
202	L40x40x3	0.0144	7.820	1000	127.9	329.0	1.623
302	L40x40x3	0.0144	7.820	1000	127.9	333.0	1.633
312	L45x45x3	0.0207	8.810	1000	114.0	335.0	1.460
402	L40x40x3	0.0144	7.820	1000	127.9	339.0	1.646
502	L40x40x3	0.0144	7.820	1000	127.9	333.0	1.633
602	L40x40x3	0.0144	7.820	1000	127.9	325.0	1.613
702	L40x40x3	0.0144	7.820	1000	127.9	329.0	1.623
801	L40x40x3	0.0144	7.820	1250	159.8	333.0	2.040
811	L45x45x3	0.0207	8.810	1250	142.0	335.0	1.818
802	L40x40x3	0.0144	7.820	1250	159.8	321.0	2.003
812	L45x45x3	0.0207	8.810	1250	142.0	360.0	1.865
803	L40x40x3	0.0144	7.820	1250	159.8	339.0	2.058
804	L40x40x3	0.0144	7.820	1250	159.8	329.0	2.028

the length ratio L_s/L_g, are not taken into account in these procedures.

At higher values of slenderness (Tests 801-804) the ASCE and ECCS predictions are conservative, with the diagonals failing at higher loads than expected. The CIGRE results in these tests provide close predictions in all cases. While the calculated failure loads reflect the effect of change from 1- to 2-bolt end connections, they do not consider the effect of increasing the size of the main legs. Results of Test 801 and 803, and Test 802 and 804, with two different sizes of main legs, clearly illustrate this effect.

A comparison between the predicted values of fult/fy obtained from Equation (4.08) in Section 4.2 and the observed test results is given in Table 4.03-d, Columns 5-6. The calculated values for the end restraint coefficient SxS, the effective length factor K and the effective slenderness ratio KL_g/r_v are also included in Table 4.03-d, Columns 2-4.

As seen in Table 4.03-d, the formulae proposed for calculating the ultimate resistance of the struts allow for all the important parameters. The theoretical failure loads obtained in this way are slightly conservative, but compare favourably with the test results at all levels of slenderness, and also show improvements with respect to predictions based on the ASCE, ECCS and CIGRE design curves.

It is important to note that this model was developed for the test conditions described in Chapter 2, in which special supports were designed to eliminate out-of-plane displacements and restrictions to torsional rotations of the main legs.

Comparison of results

Table 403-c: Current design equations

Test Designation	Design Codes						Test results
	ASCE [5]		ECCS [7]		CIGRE [63]		
	r_k	$\frac{f_{ult}}{f_y}$	r_k	$\frac{f_{ult}}{f_y}$	f_E (MPa)	$\frac{f_{ult}}{f_y}$	$\frac{f_{ult}}{f_y}$
1	2	3	4	5	6	7	8
102	1.332	0.556	1.301	0.507	---	---	0 491
202	1.604	0.389	1.552	0.373	124.3	0.483	0.412
302	1.613	0.384	1.558	0.371	124.3	0.479	0.395
312	1.482	0.455	1.446	0.424	---	---	0.399
402	1.627	0.378	1.567	0.367	124.3	0.472	0.421
502	1.613	0.384	1.558	0.371	124.3	0.479	0.437
602	1.594	0.394	1.545	0.376	124.3	0.488	0.431
702	1.604	0.389	1.552	0.373	124.3	0.483	0.430
801	2.046	0.239	2.046	0.223	79.7	0.292	0.288
811	1.823	0.301	1.823	0.277	100.8	0.355	0.371
802	1.890	0.280	1.799	0.285	79.7	0.354	0.336
812	1.821	0.302	1.722	0.309	100.8	0.387	0.396
803	2.064	0.235	2.064	0.219	79.7	0.287	0.324
804	1.913	0.273	1.814	0.280	79.7	0.348	0.364

Table 403-d: Proposed solution

Test Designation	Proposed solution				Test results
	s_{xs}	K	$\frac{Kl_g}{r_v}$	$\frac{f_{ult}}{f_y}$	$\frac{f_{ult}}{f_y}$
1	2	3	4	5	6
102	12.061	0.730	75.5	0.500	0.491
202	15.506	0.797	102.0	0.371	0.412
302	12.061	0.806	103.1	0.365	0.395
312	8.390	0.822	93.7	0.399	0.399
402	10.121	0.813	104.0	0.358	0.421
502	15.506	0.749	95.8	0.393	0.437
602	12.061	0.738	94.4	0.405	0.431
702	10.121	0.720	92.1	0.410	0.430
801	3.618	0.795	127.0	0.267	0.288
811	2.517	0.815	105.7	0.316	0.371
802	12.061	0.738	118.0	0.318	0.336
812	8.390	0.753	106.9	0.334	0.396
803	6.767	0.762	121.8	0.294	0.324
804	22.558	0.720	115.0	0.324	0.364

4.3.2 - Tests on cross-bracing reported by Behnc · [11]

A desc ription of the frames, main legs and spec imens for this series of tests with slenderness ratios of 90, 140 and 160 is given in Tables 4.04-a and 4.04-b. The experiments were performed on a more rudimentary test rig, shown in Figure 1.08 of Chapter 1, in which the frame supports were fixed and the main legs were bolted to transverse beams, therefore introducing considerable restraint to the nodal tations. The central panel of diagonals was inclined in all tests at 50°, and the main leg's slope in the inclined legs case was 6.5°.

It is now evident that the le·s and transverse beams (L100x100x8 steel angles) and the outside panels of bracing (L65x65x5 s'eel angles) were too heavy relative to the main diagonals (L40x40x3 steel angles). However, these tests confirmed the complex, non-linear behaviour of the bracing which had been anticipated by Elmes in his theoretical analysis [51], and also demonstrated the strut's mechanism of failure.

The lure loads calculated with the ASCE [5], ECCS [7] and C GFE [63] design curves are compared in Table 4.04-c with the te t results [11] given in Column 8. At high slenderness ratios and 1-bolt connections (Tests 0121-0421) the ASCE and ECCS results are again conservative, while the CIGRE curves provide reasonable predictions of failure loads. Frames in Tests 1351 and 1451, also for 1-bolt connections, had main legs of L70x70x6 angles. Further, while in Test 1351 the outside bracings were L65x65x5 angles, in Test 1451 they were L40x40x3 angles.

The test results in Column 8 of Table 4.04-c show the effects of

Experimental results reported by Behncke [11]

Table 404-a: Test frame characteristics

Test Designation	Frame			Main chords			
	α (°)	β (°)	l_g/l_g	Size (mm)	$I_x.E6$ (mm^4)	z_h	Φ_h
1	2	3	4	5	6	7	8
0121	6.5	50	0.760	L100x100x8	1.4480	1	M12
0221	6.5	50	0.760	L100x100x8	1.4480	1	M12
0321	6.5	50	0.760	L100x100x8	1.4480	1	M12
0421	6.5	50	0.760	L100x100x8	1.4480	1	M12
0522	6.5	50	0.760	L100x100x8	1.4480	2	M12
0611	0.0	50	1.000	L100x100x8	1.4480	1	M12
0712	0.0	50	1.000	L100x100x8	1.4480		M12
0842	0.0	50	1.000	L100x100x8	1.4480	2	M12
0931	6.5	50	0.760	L100x100x8	1.4480	1	M12
1032	6.5	50	0.760	L100x100x8	1.4480	2	M12
1112	0.0	50	1.000	L100x100x8	1.4480	2	M12
1351	6.5	50	0.760	L70x70x6	0.3688	1	M12
1451	6.5	50	0.760	L70x70x6	0.3688	1	M12

Table 404-b: Test specimen characteristics

Test Designation	Diagonals						
	Size (mm)	$I_x.E6$ (mm^4)	r_v (mm)	L_g (mm)	L_g/r_v	f_y (MPa)	r_0
1	2	3	4	5	6	7	8
0121	L40x40x3	0.0144	7.820	1250	159.8	350.0	2.092
0221	L40x40x3	0.0144	7.820	1250	159.8	350.0	2.092
0321	L40x40x3	0.0144	7.820	1250	159.8	357.0	2.112
0421	L40x40x3	0.0144	7.820	1250	159.8	357.0	2.112
0522	L40x40x3	0.0144	7.820	1250	159.8	353.0	2.101
0611	L40x40x3	0.0144	7.820	1100	140.7	353.0	1.849
0712	L40x40x3	0.0144	7.820	1100	140.7	353.0	1.849
0842	L40x40x3	0.0144	7.820	700	89.5	360.0	1.183
0931	L40x40x3	0.0144	7.820	1100	140.7	357.0	1.860
1032	L40x40x3	0.0144	7.820	1100	140.7	353.0	1.849
1112	L40x40x3	0.0144	7.820	1100	140.7	353.0	1.849
1351	L40x40x3	0.0144	7.820	1250	159.8	350.0	2.092
1451	L40x40x3	0.0144	7.820	1250	159.8	375.0	2.165

these changes of leg and auxiliary bracing sizes. Note that the ASCE and ECCS failure loads are closer to the experimental results in Tests 1351 and 1451, while the CIGRE curves are slightly conservative. Result of Test 0522 with 2-bolt connections is not consistent with any of the model predictions.

At slenderness ratios of 140 with one- and 2-bolt connections (Tests 0611, 0712, 0931, 1112), the ASCE and ECCS results are still conservative, while the CIGRE results are correct in all cases. The result of Test 1032 with 2-bolt connections is not consistent with any of the model predictions.

Test 0842 was a special case, with parallel legs and a slenderness ratio of 90. During the experiment, yield occurred in the tie and then in the strut prior to failure. However, the experimental result was too high in comparison with similar frames with inclined legs. This case illustrates once again the apparent additional strength of frames with parallel legs due to the bifurcation of buckling modes.

Test results are compared in Table 4.04-d with the proposed model, see Columns 5-6. Predictions for tests with L/r=160 and 1-bolt connections are correct, although the model does not recognize the difference in size of the bracings in the outside panels, Tests 1351 and 1451. Predictions for tests with L/r=140 are conservative, but seem to be correct for Test 0842 with L/r=90.

The observed differences of failure loads in these tests are due to the different conditions of the frames. As stated above, the model has been calibrated for tests in frames with no support restrictions. By contrast, the experiments reported by Behncke [11] were carried out in frames with full fixity in both

Comparison of results

Table 404-c: Current design equations

Test Designation	Design Codes						Test results
	ASCE [5]		ECCS [7]		CIGRE [63]		
	Γ_k	$\frac{f_{ult}}{f_y}$	Γ_k	$\frac{f_{ult}}{f_y}$	f_g (MPa)	$\frac{f_{ult}}{f_y}$	$\frac{f_{ult}}{f_y}$
1	2	3	4	5	6	7	8
0121	2.097	0.227	2.097	0.213	79.7	0.279	0.280
0221	2.097	0.227	2.097	0.213	79.7	0.279	0.296
0321	2.118	0.223	2.118	0.209	79.7	0.275	0.304
0421	2.118	0.223	2.118	0.209	79.7	0.275	0.306
0522	1.982	0.255	1.861	0.267	79.7	0.331	0.43
0611	1.854	0.291	1.854	0.269	102.7	0.345	0.343
0712	1.790	0.312	1.698	0.317	102.7	0.398	0.420
0842	1.292	0.582	1.230	0.555	---	---	0.587
0931	1.864	0.288	1.864	0.266	102.3	0.341	0.374
1032	1.790	0.312	1.698	0.317	102.3	0.398	0.520
1112	1.790	0.312	1.698	0.317	102.3	0.398	0.429
1351	2.097	0.227	2.097	0.213	79.7	0.279	0.257
1451	2.170	0.212	2.170	0.199	79.7	0.264	0.218

Table 404-d: Proposed solution

Test Designation	Proposed solution				Test results
	S_{xs}	K	$\frac{KL_g}{r_v}$	$\frac{f_{ult}}{f_y}$	$\frac{f_{ult}}{f_y}$
1	2	3	4	5	6
0121	7.876	0.746	119.2	0.298	0.280
0221	7.876	0.746	119.2	0.298	0.296
0321	7.876	0.746	119.2	0.294	0.304
0421	7.876	0.746	119.2	0.294	0.306
0522	26.253	0.703	113.1	0.316	0.430
0611	7.876	0.825	126.1	0.306	0.343
0712	26.253	0.783	110.1	0.327	0.420
0842	26.253	0.703	70.0	0.530	0.587
0931	7.876	0.746	104.9	0.344	0.374
1032	26.253	0.708	99.5	0.365	0.520
1112	26.253	0.703	110.1	0.327	0.429
1351	2.066	0.817	130.5	0.264	0.257
1451	2.066	0.817	130.5	0.251	0.218

supports. The support restraint appears to be particularly significant in enhancing the strength of the specimen with two bolts. The torsional restraint is less significant because the torsional stiffness of the main leg is so low. These results therefore highlight the effects of boundary conditions on the resistance of cross-bracing.

4.3.3 - CIGRE tests on cross-bracing reported by Wood [63,49]

These experiments were performed on full-scale frames, as indicated in Figure 2.01-a of Chapter 2, thus representing conditions similar to those found in real transmission towers. Data on the legs and bracings are given in Tables 4.05-a and 4.05-b. Note that the legs had a slope of 6", while the diagonals were inclined at 40", thus giving in all cases a constant length ratio Ls/Lg. Various sizes of main legs and diagonals were used, with 1- and 2-bolt connections. Slenderness ratios varied for the examined cases between 140 and 160.

It should be noted that the main legs in Figure 2.01-a were fully restricted at the supports against torsional and flexural rotations, and were joined by a transverse beam. Furthermore, the compression members in both outside panels of bracing were supported at midspan by redundant elements, thus reducing their in-plane buckling length. The effect of these additional bracings on the nodal rotations and therefore on the behaviour and resistance of the main diagonals is unknown.

Failure loads are compared in Table 4.05-c. The CIGRE predictions are not included in the discussion, since the CIGRE design curves are based empirically on these test results, and

Experimental results reported by Wood [49] and CIGRE [63]

Table 405-a: Test frame characteristics

Test Designation	Frame			Main chords			
	α (°)	β (°)	L_g/L_g	Size (mm)	$I_x.E6$ (mm^4)	z_b	Φ_b
1	2	3	4	5	6	7	8
005	6	40	0.838	L70x70x7	0.4320	1	M16
006	6	40	0.838	L70x70x7	0.4320	1	M16
031	6	40	0.838	L70x70x7	0.4320	1	M16
032	6	40	0.838	L70x70x7	0.4320	1	M16
014	6	40	0.838	L70x70x7	0.4320	2	M16
015	6	40	0.838	L70x70x7	0.4320	2	M16
038	6	40	0.838	L70x70x7	0.4320	2	M16
039	6	40	0.838	L70x70x7	0.4320	2	M16
040	6	40	0.838	L70x70x7	0.4320	2	M16
041	6	40	0.838	L70x70x7	0.4320	2	M16
092	6	40	0.838	L115x115x10	2.7890	2	M20
093	6	40	0.838	L115x115x10	2.7898	2	M20
108	6	40	0.838	L110x110x12	2.8400	2	M20
109	6	40	0.838	L110x110x12	2.8400	2	M20
148	6	40	0.838	L130x130x12	4.6700	2	M24
149	6	40	0.838	L130x130x12	4.6700	2	M24

Table 405-b: Test specimen characteristics

Test Designation	Diagonals						
	Size (mm)	$I_x.E6$ (mm^4)	r_v (mm)	L_g (mm)	L_g/r_v	f_y (MPa)	r_0
1	2	3	4	5	6	7	8
005	L45x45x5	0.0326	8.707	1380	158.5	343.3	2.055
006	L45x45x5	0.0326	8.707	1380	158.5	392.3	2.196
031	L50x50x5	0.0454	9.736	1559	160.1	323.6	2.015
032	L50x50x5	0.0454	9.736	1559	160.1	326.6	2.024
014	L45x45x5	0.0326	8.707	1380	158.5	364.8	2.118
015	L45x45x5	0.0326	8.707	1380	158.5	348.1	2.069
038	L50x50x5	0.0454	9.736	1559	160.1	375.6	2.174
039	L50x50x5	0.0454	9.736	1559	160.1	400.1	2.240
040	L50x50x5	0.0454	9.736	1380	141.7	356.9	1.873
041	L50x50x5	0.0454	9.736	1380	141.7	372.6	1.914
092	L64x64x5	0.0920	12.50	1750	140.0	274.2	1.622
093	L64x64x5	0.0920	12.50	1750	140.0	308.5	1.720
108	L70x70x5	0.1300	13.78	2120	153.8	307.4	1.887
109	L70x70x5	0.1300	13.78	2120	153.8	294.2	1.846
148	L90x90x6	0.3330	17.85	2735	153.2	290.2	1.851
149	L90x90x6	0.3330	17.85	2735	153.2	298.2	1.851

by definition should therefore correlate accurately. Tests with 1-bolt connections are examined first (Tests 005, 006, 031, 032). The ECCS and ASCE curves give conservative predictions of failure loads, but the ECCS results are more conservative. Both procedures identify the differences of slenderness ratio and size of diagonals in these tests.

The above experiments are repeated for 2-bolt connections (Tests 014, 015, 038, 039). The ASCE and ECCS curves are conservative, but this time the ASCE predictions are more conservative. Note that in both 1- and 2-bolt cases with the same size of main legs, the calculated failure loads are closer to the test values in the case of heavier diagonals.

Tests 040, 041, 092 and 093 have reduced slenderness ratios for two different ratios of diagonal/main leg sizes. Both ECCS and ASCE curves are optimistic in the case of light members, and the diagonals resist less than expected. In Tests 092 and 093 the members in the frames are heavier, and the ASCE and ECCS give very conservative results.

Tests 108, 109, 148 and 149 have the same slenderness ratio, with two ratios of diagonal/main leg sizes. Both the ASCE and ECCS curves give similar results, but are conservative in all cases.

Results from the model proposed in this Chapter are presented in Table 4.05-d. The restraint coefficients $S_x S$, which in this case are not influenced by changes in the bracing inclination β, are smaller than in the previous cases, thus suggesting a greater relative flexibility of the bracings. The effective length factors ω, which in this case are not influenced by changes in the length ratio L_s/L_g, are as a rule higher than

Comparison of results.

Table 405-c: Current design equations

Test Designation	Design Codes						Test results
	ASCE [5]		ECCS [7]		CIGRE [63]		
	r_y	$\frac{f_{ult}}{f_y}$	r_k	$\frac{f_{ult}}{f_y}$	f_E (MPa)	$\frac{f_{ult}}{f_y}$	$\frac{f_{ult}}{f_y}$
1	2	3	4	5	6	7	8
005	2.060	0.236	2.060	0.220	80.9	0.288	0.288
006	2.202	0.206	2.202	0.194	80.9	0.257	0.273
031	2.020	0.245	2.020	0.229	79.3	0.298	0.288
032	2.029	0.243	2.029	0.227	79.3	0.295	0.270
014	2.001	0.250	1.872	0.264	80.9	0.327	0.325
015	1.955	0.262	1.841	0.272	80.9	0.338	0.345
038	2.054	0.238	1.909	0.255	79.3	0.315	0.260
039	2.113	0.224	1.952	0.244	79.3	0.302	0.270
040	1.810	0.305	1.714	0.311	101.3	0.391	0.295
041	1.849	0.293	1.740	0.303	101.3	0.379	0.263
092	1.571	0.405	1.551	0.374	103.7	0.484	0.500
093	1.667	0.360	1.615	0.347	103.7	0.443	0.503
108	1.793	0.311	1.722	0.308	85.9	0.387	0.318
109	1.754	0.325	1.696	0.317	85.9	0.399	0.393
148	1.760	0.323	1.699	0.316	86.6	0.397	0.438
149	1.760	0.323	1.699	0.316	86.6	0.397	0.412

Table 405-d: Proposed solution

Test Designation	Proposed solution				Test results
	S_{xS}	K	$\frac{KL_E}{r_v}$	$\frac{f_{ult}}{f_y}$	$\frac{f_{ult}}{f_y}$
1	2	3	4	5	6
005	1.237	0.869	137.8	0.245	0.288
006	1.237	0.869	137.8	0.221	0.273
031	0.888	0.884	141.5	0.245	0.288
032	0.888	0.884	141.5	0.244	0.270
014	4.123	0.805	127.5	0.262	0.325
015	4.123	0.805	127.5	0.271	0.345
038	2.961	0.823	131.8	0.244	0.260
039	2.961	0.823	131.8	0.233	0.270
040	2.961	0.823	116.6	0.301	0.295
041	2.961	0.823	116.6	0.299	0.263
092	9.432	0.764	106.9	0.388	0.500
093	9.432	0.764	106.9	0.365	0.503
108	6.797	0.778	119.7	0.320	0.318
109	6.797	0.778	119.7	0.329	0.393
148	4.364	0.801	122.8	0.317	0.438
149	4.364	0.801	122.8	0.317	0.412

in the previous cases, thus giving lower buckling loads.

The predicted failure loads are conservative in most of the cases and, in further analysis, they are very similar to the ASCE failure loads given in Table 4.05-c, Column 3. It is therefore apparent that the test specimens in the CIGRE experimental programme are affected by the additional restraining conditions in the frames, resulting in higher failure loads, particularly in the 2-bolt tests. The proposed design procedure does not consider these particular conditions, giving as a result lower failure loads.

4.4 - Summary

A simplified, semi-empirical model for the calculation of cross-bracing buckling loads has been presented in the preceding Sections. This model is based on the experimental results reported in Chapter 3, and therefore includes most of the parameters that influence bracing behaviour.

Comparisons of test results with the calculated failure loads show that the proposed method reflects the variations recorded in the tests for various conditions and are, to a small degree, conservative. The calculated loads show improvements with respect to predictions based on usual buckling curves. As an example, Figure 4.04 shows curves calculated with buckling equations from ASCE [5] and the proposed model in this Chapter, for a typical combination of strut and main leg sizes in lateral panels of steel transmission towers.

It can be seen, for the usual range of slenderness ratios in

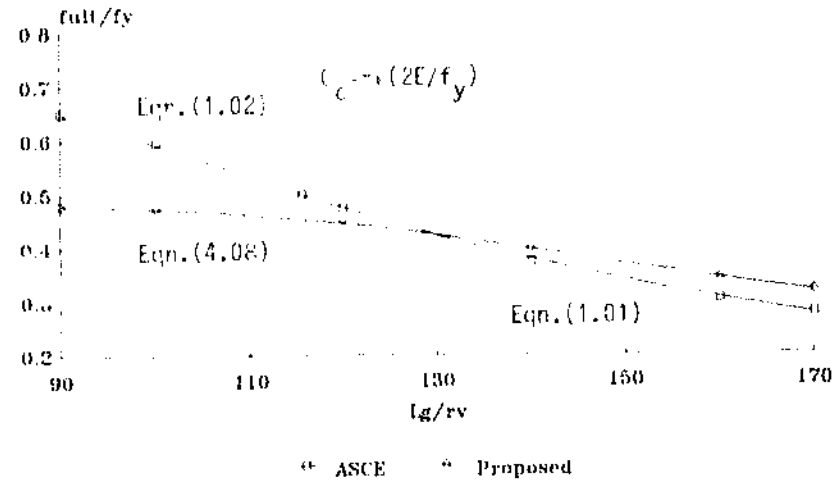

Figure 4.04: Design curves for struts in cross-bracing systems (2-bolts)

these structures, that results from the proposed design equations are less conservative at higher slenderness ratios, while the strength of the bracing is reduced at lower values of slenderness. These predictions are in line with experimental results.

When the conditions of tests are very different from those in the present investigation, however, the calculated results are considerably more conservative, and of the same order as those obtained with the ASCE and ECCS design curves.

A more complex non-linear computer analysis is introduced in the following Chapter, in which the conditions of the bracings and the bolted connections are modelled based on flexibility equations.

CHAPTER 5

A COMPUTER MODEL FOR NON-LINEAR ANALYSIS OF TWO-DIMENSIONAL FRAMES

5.1 - Introduction

The exact analysis of two-dimensional frames composed of open-section main legs and bracings is extremely complicated and difficult to comprehend, because of a multiplicity of interrelated factors. The bracing diagonals are subjected primarily to in-plane forces and moments induced by the actions of external loads on the structure. They also sustain out-of-plane end moments caused by eccentricities of their connections to adjoining members.

These and other effects have been modelled with some difficulty for single beam-columns after selection of the appropriate boundary conditions, and also assuming that the elements' geometric and material characteristics are perfectly known. As seen in the review of related investigations presented in Chapter 1, differential equations of the deflected axis of the columns, in equilibrium with the external forces, can be written even for the most complicated case of biaxial bending, and this analysis can also be extended to consider inelastic behaviour of the angle struts.

Most of these particular conditions, however, cannot be formulated appropriately for members with asymmetric cross-sections which form part of larger planar frames, as in

the case of tower panels with cross-bracings. The major problem is the difficulties in defining proper values of equivalent end eccentricities and end restraints, as well as the direction of the planes containing these restraints, while at the same time considering the beam-column's behaviour at midspan about the section's principal axes. Similar problems are encountered when trying to analyze the interactions between the tie and strut diagonals at the cross-over joint.

A typical example of such a problem is given in a publication by Kemp et al [68], in which diagonal struts of plane frames were modelled using the finite-element program ADINA [69]. Although a fairly sophisticated program, ADINA allowed only for symmetric beam elements in non-linear structural analysis. Therefore the bracing was represented by one strut formed by various non-linear beam elements in which only the weakest axis of the angle bracing was modelled. The torsional and other restraints relating to the boundary conditions were represented in simplistic terms by considering an effective eccentricity applied to the angle strut relative to the design axis.

It was found that the ADINA finite-element package could be used for modelling the non-linear behaviour and predict the failure loads of struts in cross-bracing systems, but noting, however, that the diagonals were analyzed as single members, with simulation of the boundary conditions at the cross-over joint and at the ends of the strut, for which some preliminary manipulation was required.

A more complete design facility was not available in any design package at the time of commencing the present investigation. Consequently, a non-linear flexibility model was developed, incorporating most of the important effects typical of angle

struts in transmission tower panels. This model is described in the following Sections, and comparisons of results are also presented of test results and predictions of failure loads from the proposed computer model.

5.2 - A program for non-linear flexibility analysis of plane frames

Two-dimensional panels with steel angle cross-bracings such as outlined in Figure 1.01 for transmission towers show sharply non-linear behaviour under loads, and this may be attributed to three causes, namely material, geometric and boundary non-linearity.

For the purposes of the study of diagonal cross-bracings undertaken in this investigation, however, only the second effect is examined. Angle members are therefore analyzed within the elastic range, and any influences from the boundary conditions are assumed to be linear.

Solution techniques of structural problems are normally based on two methods: the displacement or the force methods of matrix analysis. In the former method the unknown displacements for each degree of freedom are obtained from solution of the following set of simultaneous linear equations:

$$\{F\} = [K]\ \{u\}$$

where

- F are the nodal forces,

- K are the coefficients of the structure stiffness matrix, and
- u are the nodal displacements.

Commonly, in a non-linear analysis the external loads are increased in various steps, at each of which the structure stiffness is updated in order to account for axial force in the elements and the deflected geometry of the frame. After each load iteration it is necessary to solve the equilibrium equations until convergence of the axial forces in the members is reached. This may be a lengthy process, involving large amounts of computer time and memory capacity.

The traditional force or flexibility matrix analysis of statically indeterminate structures, on the other hand, presents the problem of identifying the redundancies, which are considered as unknowns. This process is relatively simple when applied to the solution of frames with a small degree of static indeterminacy. For larger and more complex frames, however, the selection of redundancies becomes rather difficult, uncertain and time consuming, although Robinson's Rank Technique [61] allows for automatic identification of the degree of indeterminacy and subsequent selection of redundancies.

Consequently, a new method and a computer program described by Kemp [66] for non-linear flexibility analysis of two-dimensional frames are adapted for the structural arrangements in this investigation, as discussed below.

Kemp's method is based on a mixed flexibility approach, in which the member end moments and relative nodal displacements about the section's principal axes are adopted as unknowns, without making any reference to static indeterminacy or redundancies. A

similar technique has been proposed previously by Bleich [67], in which the end moments are **a priori** selected as unknowns.

Figure 5.01-a shows the two-dimensional frame with steel angle legs and diagonals simulated in the computer analysis. The structure is assumed to be supported at the four nodes a, b, d and e, where no out-of-plane deflections are permitted, but where these nodes are free to rotate in any direction.

The axial loads in the members are calculated from linear equations of equilibrium of the structure under external loads, with the inclusion of additional factors as follows:

$$P = P_q K_q$$

in which:

- P is the axial force in each diagonal.
- P_q is the nominal load on the bracing, calculated from static equilibrium.
- K_q is a factor defined as indicated below:

$$K_q = K_1 K_2 K_3$$

where

- K_1 identifies tension or compression member.
- K_2 gives the ratio of tension to compression forces in the bracing, and it is assumed initially that the tension and compression forces in the diagonals are equal.
- K_3 is a load-increment factor.

The stability conditions and the non-linear behaviour of the members are formulated through the inclusion of the Berry functions B_1 and B_2 in the flexibility matrices. The details of this approach are given in Appendix D.

The members in the bracing system are each divided into two or more equal subspans, and four unknowns are considered at the intermediate nodes, Figure 5.01-b, as indicated below:

- About the u-axis: d_u and M_u
- About the v-axis: d_v and M_v

where d indicates nodal displacement and M indicates end bending moment.

Equations are written of moment equilibrium for each element and rotation compatibility at each intermediate node of the frame (i.e. nodes a, c or g in Figure 5.01-a) about the members' principal axes to solve these unknowns. Additional equations are required to describe the conditions at some particular nodes, such as the cross-over joints (i.e. nodes p, c or q in Figure 5.01-a), and also at the points of connection between the bracings and the main legs of the frame (i.e. nodes a, b, i or e in Figure 5.01-a). These latter connections require further analysis, in which the effects of eccentric loading and end connections to the main legs are considered about appropriate axes.

The following assumptions are also made:

- The diagonals and the main legs are equal-leg, hot-rolled steel angles with constant cross-section, and they are connected together in the frame as indicated in Figure 5.01-a,

- No gusset-plates are used at the connections between bracing and legs,

- The tie and strut diagonals have equal geometric and material properties, without initial imperfections,

- Only out-of-plane deflections at intermediate nodes are considered. Frame lateral translations are not included in the analysis, and

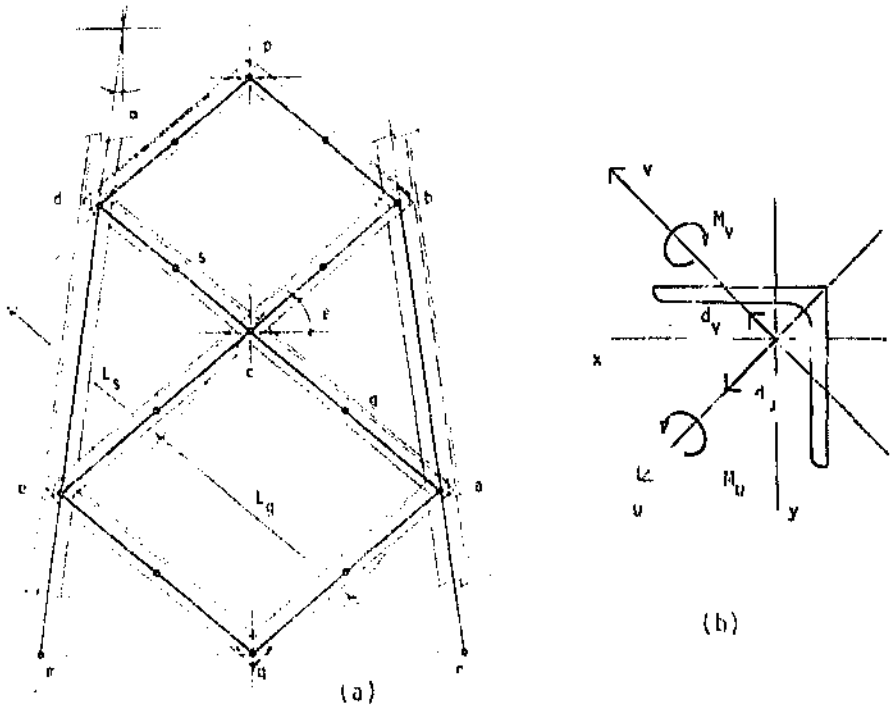

Figure 5.01: a) Two-dimensional frame with crossed diagonals, as simulated in the analytical model. Note that the positions of the main chords and bracings are as in the experimental frames. b) The unknowns at each of the nodes about the principal axes are also indicated.

- Strain distribution is assumed to be linear across the depth of the section.

All nodal relationships form a system of simultaneous equations in which the unknowns are the end moments and nodal deflections about each principal axis, and the coefficients are given as functions of the members' dimensions and the calculated axial forces. Additional unknowns are included to define the forces at the cross-over joints and the rotations of the main legs at the connecting joints.

In a last step the extreme fibre stresses are calculated at the sections of maximum bending moments, and are compared with the yield stress of the material. No iterations are required, except in the last step. If, after considering the maximum specified load, the maximum stress at any section under consideration is not equal to the specified yield stress of material, iteration procedure follows, in which the load-increm factor K_3 is adjusted until the stresses converge on the elastic limit. Normally only two to four extra runs are required.

The most important characteristics of this analytical model are examined in the following Sections and the detailed derivation is given in Appendix D.

5.2.1 - Simulation of end restraint at bolted connections

The analysis of test results in Chapter 4 demonstrates the important influence of end restraints on the ultimate resistance of bracings in planar frames. It is considered that variations

of end restraint are caused by the number of connecting bolts, the relative size of the main legs, and the bracing inclination β (see Figure 5.01-a).

The exact, non-linear modelling of the complete connection behaviour in a multiple-node frame is a near-impossible task, which is aggravated if the connecting members are non-symmetrical sections, as in the case of steel angles. However, examination of frame behaviour and common engineering judgement indicate that some convenient generalizations can be made, as explained below.

A typical connection between an angle diagonal and a main leg is

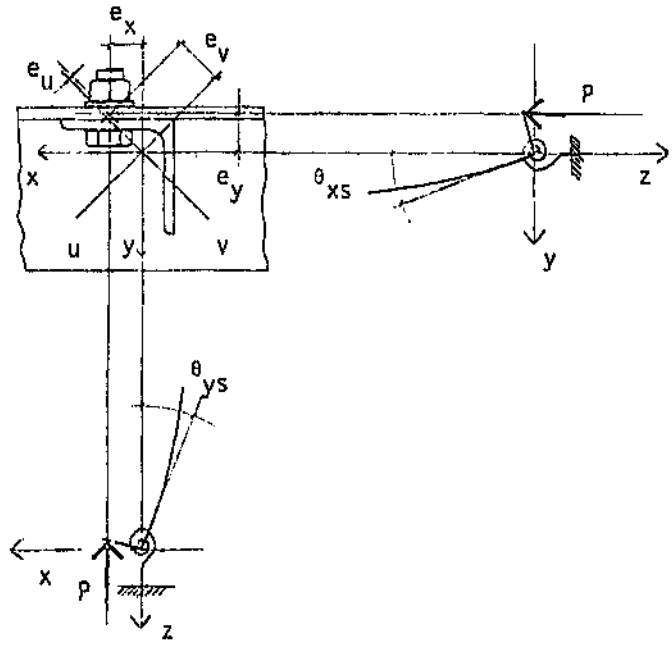

Figure 5.02: Simulation of end restraints at a typical bolted connection between two steel angles. Note the eccentricities about the orthogonal x- and y-axis.

illustrated in Figure 5.02. Forces are transmitted between the main member and only one leg of the strut or tie by the connecting bolts. The applied force P is considerably eccentric to the orthogonal centroidal axis x, but to a varying degree to the y-axis. This is because the e_x eccentricity about the y-axis depends on the relative distance between the backmarks, or design axis where the bolts are located, and the y-axis of the member, Figure 5.02.

Observing the strut-main leg connection in Figure 5.02, the following criterion can be established for defining the restraining action about the x- and y-axis:

About the y-axis. In the case of single-bolt connections, free rotations are permitted at the end of the bracing about the y-axis, and this can be expressed as follows:

$$M_{yL} = 0$$

where M_{yL} represents the main leg's restraining moment about the strut's y-axis. Consequently, there is no restraint at the joint, and the bracing is assumed to behave as pin-ended about the y-axis.

In the case of multiple-bolt connections, on the other hand, only small rotations are possible about the y-axis, which can be approximated by equating the rotations to zero as follows:

$$\theta_{yS} = 0$$

in which θ_{yS} are the strut's end rotations about its y-axis. This case can be represented as a full-restraint, or fixed-end

condition.

About the x-axis. For analysis of single- and multiple-bolt connections about the x-axis, no relative rotations are permitted initially between the main leg and the bracing, also indicating a fully-rigid connection at these joints. During calibration of the computer model, however, it became evident that this solution was not completely correct for the x-axis. A modification was therefore introduced, as explained in Section 5.2.3.

5.2.2 - Conditions at intermediate nodes

Consider any two generic elements ij and jk in a bracing under compressive load P, meeting at the rigid joint j of the diagonal, as shown in Figure 5.03, where there is one unknown end moment and one unknown nodal displacement in the plane uz. The following equations are used to solve the unknowns:

1) One equation of rotation compatibility at the node j, reflecting the equality of rotations at the ends of members ji and jk. This is written as follows:

$$\theta vji = \theta vjk = \theta j$$

These rotations can be expressed in terms of the end moments and relative node displacements, as indicated in Appendix D and, after considering equilibrium of forces at the node j and rearranging terms, we can write:

$$-\frac{Mv_iL_1B_2}{6}+\frac{EI_v}{L_1}u_i+\frac{Mv_j(L_1B_1+L_2B_3)}{3}-EI_vu_j\left(\frac{1}{L_1}+\frac{1}{L_2}\right)$$

$$+\frac{Mv_kL_2B_4}{6}+\frac{EI_v}{L_2}u_k=0 \qquad \ldots(5.01)$$

where B_1-B_4 are the Berry stability functions corresponding to the elements ij and jk about the v-axis, and $Mv_{ji}=-Mv_{jk}=Mv_j$.

2) One equation derived from sway equilibrium conditions of the elements ij and jk. The sway equilibrium equations are written in terms of the end moments and include the effect of the axial force P, as shown in Figure 5.03. Taking moments to the left of the node j, we can write:

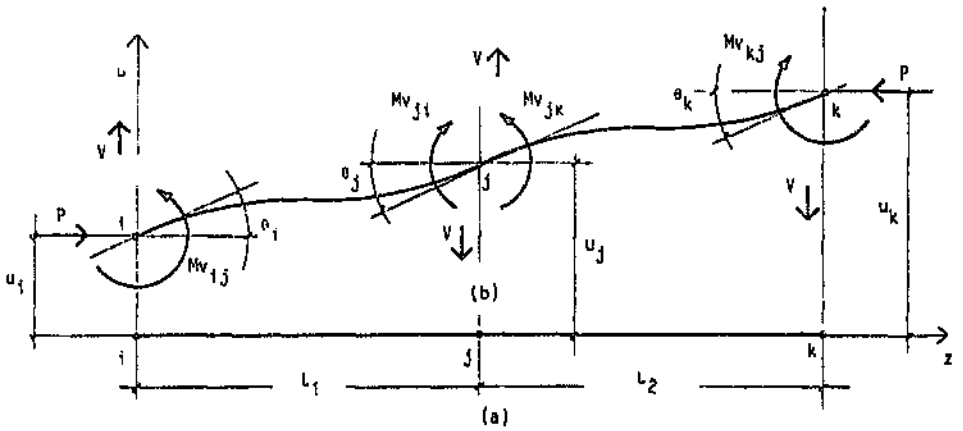

Figure 5.03: Conditions at intermediate nodes in the bracing. a) Undeflected position. b) Considering the general case of compression forces and sway.

$$- Mv_i + Mv_j + VL_1 - P(u_j - u_i) = 0$$

in which V is the shear force and u are unknown nodal deflections in the plane uz. Operating on the above expression:

$$-\frac{Mv_i}{L_1} + \frac{Mv_j}{L_1} + V - \frac{P}{L_1}(u_j - u_i) = 0 \qquad \ldots.(5.02)$$

Similarly, taking moments to the right of node j:

$$-\frac{Mv_k}{L_2} + \frac{Mv_j}{L_2} - V + \frac{P}{L_2}(u_k - u_j) = 0 \qquad \ldots.(5.03)$$

By elimination of the shear force V between Equations (5.02) and (5.03), we finally obtain in terms of the unknown moments M_v and deflections u:

$$-\frac{Mv_i}{L_1} + \frac{P}{L_1}u_i + Mv_j\left(\frac{1}{L_1} + \frac{1}{L_2}\right) - Pu_j\left(\frac{1}{L_1} + \frac{1}{L_2}\right) - \frac{Mv_k}{L_2} + \frac{P}{L_2}u_k = 0 \qquad \ldots(5.04)$$

Thus Equations (5.01) and (5.04) are written as functions of the unknown end moments and joint displacements corresponding to the elements which are directly connected to node j.

A similar pair of equations equivalent to (5.01) and (5.04) can be written for the plane vz at this joint, and also for all other intermediate nodes on both tension and compression members.

5.2.3 - Conditions at joints where diagonals and main legs are interconnected

Consider now a generic segment ij of length L of a diagonal, connected to a main leg at the joint j, as indicated in Figure 5.04-a. By definition, displacements at node j are equal to zero, since it is one of the structure's supports. Thus we can write two equations of displacement compatibility at node j in the direction of the strut's principal axes as follows:

$$u_j = 0$$
$$v_j = 0$$

End rotations about the principal u- and v-axis in the diagonals can be expressed as functions of the unknown end moments, including the effect of the eccentric axial forces at the connections. However, as indicated before, a distinction must be made between single and multiple-bolt connections about the x and y orthogonal axes.

Rotations about the x-axis for single and multiple bolt connections

Figure 5.04-a shows a connection between a diagonal bracing and a main leg at a generic node j. If the connection is initially assumed to be rigid, the condition of equality of rotations, projected on the plane yz in the strut, can be expressed as follows:

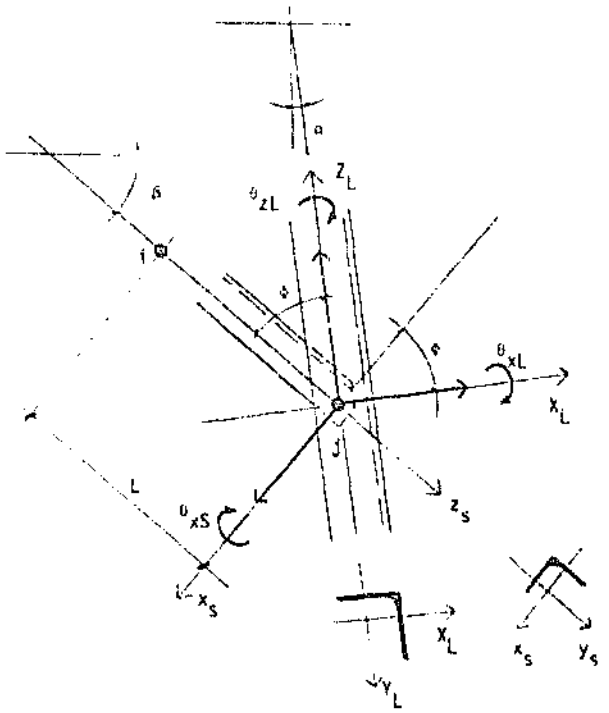

(a)

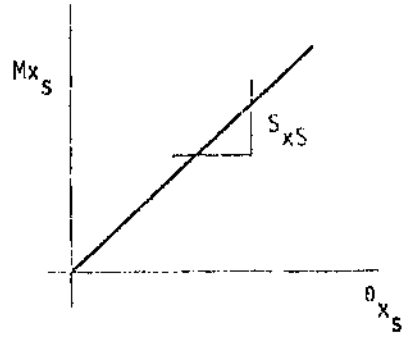

(b)

Figure 5.04: a) Conditions at joints connecting diagonals and main chords. Directions of end moments and end rotations in the bracings are also indicated. b) Note the rotational spring which represents the flexibility of the joint about the x-axis.

$$\theta x_S + \theta x_L \cos\Phi + \theta z_L \sin\Phi = 0$$

in which

- θx_L and θz_L are rotations at the connecting node about the main leg's orthogonal axis x_L and longitudinal axis z_L respectively, and are considered as additional unknowns.

- θx_S is the diagonal's end rotation about its orthogonal x-axis.

- The angle Φ in Figure 5.04-a indicates the relative inclination between the strut and the main leg.

However, this assumption in the model about the x-axis does not provide good correlation with the experimental results. As seen in Chapter 3, there are indications of additional end rotations due to the flexibility of the joint between the bracing and the main leg about the strut's x-axis. A semirigid joint model is therefore adopted, in which the total end rotations can now be expressed as follows:

$$\theta x_S + \frac{M_{xS}}{S_{xS}} + \theta x_L \cos\Phi + \theta z_L \sin\Phi = 0 \qquad \ldots.(5.05)$$

in which M_{xS}/S_{xS} are additional rotations due to the action of a rotational spring S_{xS}. The moment-rotation ratio is assumed to be linear, as indicated in Figure 5.04-b, and the values for S_{xS} are found empirically, as in Chapter 4.

Observing now Figure 5.05, the moments and rotations about the

strut's x-axis at joint j can be written as follows:

$$Mx_S = \frac{1}{\sqrt{2}} (Mu_S + Mv_S)$$

$$\theta x_S = \frac{1}{\sqrt{2}} (\theta u_S + \theta v_S) \qquad \ldots\ldots(5.06)$$

and from Appendix D, rotations θu_S and θv_S in element ji at joint j can be expressed as functions of the end moments and nodal displacements in this element as indicated below:

$$\theta u_S = \frac{Mu_j LB_1}{3EI_u} - \frac{Mu_i LB_2}{6EI_u} + \frac{v_j - v_i}{L}$$

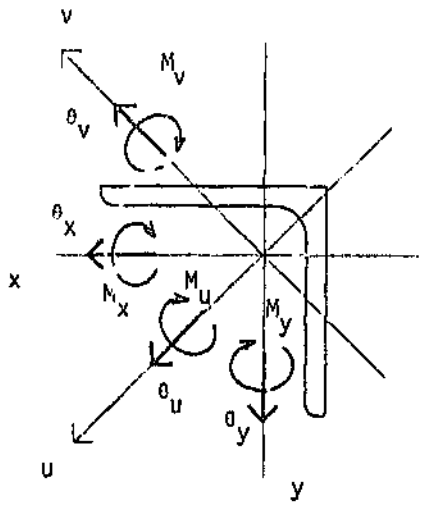

Figure 5.05: Positive directions of end moments and rotations in the bracing.

$$\theta v_S = \frac{Mv_j L B_3}{3EI_v} - \frac{Mv_i L B_4}{6EI_v} + \frac{u_j - u_i}{L} \qquad \ldots.(5.07)$$

where B_1 - B_4 are the Berry functions corresponding to the element ij about the u and v principal axes respectively. The final expression for rotation compatibility at this node in the yz plane are thus obtained by substituting Equations (5.06) and (5.07) in Equation (5.05).

Rotations about the y-axis for single-bolt connections

For 1-bolt end connections in the plane xz, Figure 5.06, it is assumed that there is no restraint in the node, and this condition is expressed as follows:

$$My_S - P\, e_x + My_L = 0$$

in which

- My_S is the strut's end moment at node j about the y-axis.
- P is the axial force.
- e_x is the eccentricity in the plane xz, as in Figure 5.06.
- My_L is the main leg's restraining moment about the strut's y-axis.

By definition, however, the leg restraint My_L is equal to zero, and therefore the above expression can be written, after Figure 5.05, as indicated below:

$$M_{yS} = \frac{1}{\sqrt{2}} \cdot (Mu_j - Mv_j) = P\ e_x$$

from which,

$$Mu_j - Mv_j = \sqrt{2}\ P\ e_x$$

It is important to note that this last equation relates the

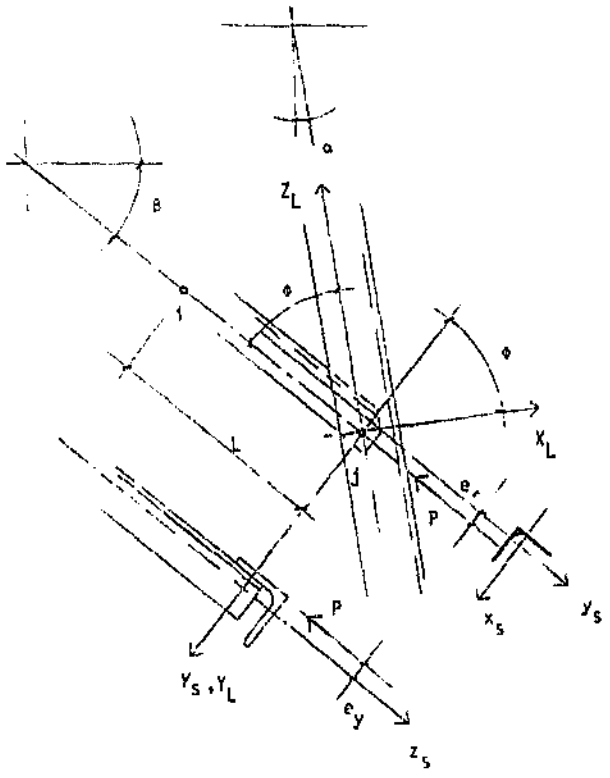

Figure 5.06: Conditions at the connection in Figure 5.04-a. Note the eccentric forces about the orthogonal x- and y-axis.

strut's end moments about the principal u- and v-axis, and the external moment due to eccentricity of the axial load about the orthogonal y-axis.

Rotations about the y-axis for multiple-bolt connections

For two or more bolt end-connections in the plane xz, Figure 5.06, it is assumed that a rigid restraint condition exists in the node, and this can be described as follows:

$$\theta y_S - \theta y_L = 0$$

where θy and θy_L are the angles rotated by the diagonal and the main leg about the y-axis. Observing Figure 5.05, we can write these rotations and end moments as follows:

$$\theta y_S = \frac{1}{\sqrt{2}} (\theta u_j - \theta v_j)$$

$$M_{yS} = \frac{1}{\sqrt{2}} (Mu_j - Mv_j)$$

The end rotations θu_j and θv_j about the principal axes can now be written as a function of the stability factors, as in Equations (5.07). A similar analysis is performed for all the diagonals about both principal axes at their connections with the main legs.

5.2.4 - Main leg unknowns

It is at the bracing-to-main leg connections where some of the most important assumptions are made in this procedure, as explained below:

- The axial loads are applied eccentrically on the diagonals by the main legs, thus inducing bending effects about the local x- and y-axis, see Figures 5.02 and 5.06.

- The eccentricity about the x-axis is defined by the normal framing eccentricity, e_y, while the eccentricity e_x about the y-axis is defined by the distance between the backmark design axis, on which the bolts are located, and the centroidal longitudinal axis, as shown in Figures 5.02 and 5.06.

- The main leg provides flexural restraint through the bolted connection about its x_L and y_L orthogonal axes.

- The main leg's torsional restraint about the z_L axis is defined by the St. Venant's torsional constant of the angle sections, which is calculated as written below:

$$Iz_L = \frac{1}{3} \Sigma(bt^3)$$

where b and t indicate the angle's width and thickness respectively. For equal-leg angles, however, Iz_L can be approximated as indicated by Kennedy in [34]:

$$Iz_L = \frac{1}{3} t^3(2b - t)$$

- As a simplification, the main leg is assumed to be a beam with the sectional and material properties of the actual steel angle section, but no eccentricities are considered about any of its principal, orthogonal or longitudinal axes.

Three additional equations of moment equilibrium are written at the supporting nodes for solving the three possible unknown rotations about the main leg's orthogonal axes, as functions of the eccentric bracing forces, the end moments in the bracing, and the main leg's torsional and orthogonal restraining moments.

Consider the connection between a main leg and two diagonals at a generic node j, as shown in Figure 5.07-a. The moments applied to the node by the incoming elements in the three orthogonal directions are written as indicated below, assuming that the moments in the main leg are zero about the three axes outside of the central panel of bracing:

In the x_L direction - Projecting the end moments on the main leg's x_L axis at node j, see Figure 5.07-a, we can write:

$$Mj_{xL} + (Mj_{xt} - P\, e_{yt})\cos\Phi_2 - (Mj_{xs} - P\, e_{ys})\cos\Phi_1 = 0$$

in which

- subscripts L, t and s refer to the main leg, tie and strut respectively.
- eccentricities e_y are as shown in Figures 5.02 and 5.06.
- Φ_1 and Φ_2 are angles between the bracings and the main

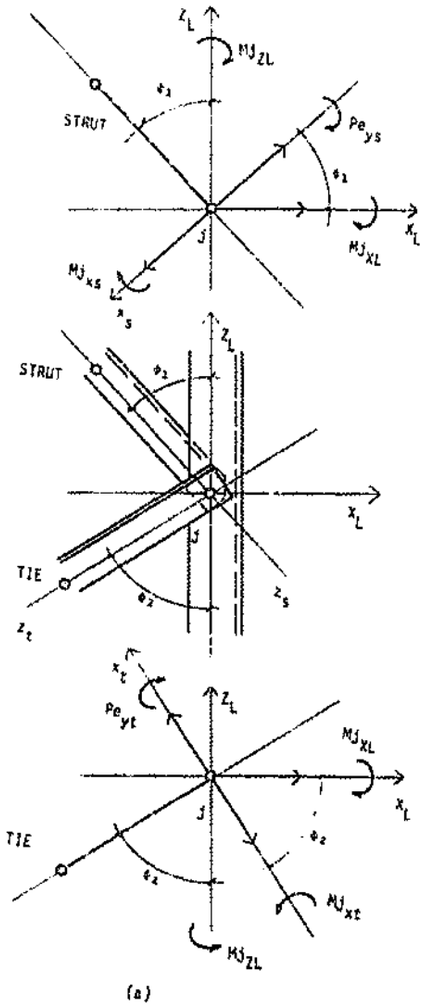

Figure 5.07-a: Main leg rotations. Conditions at the connecting nodes about the x_L- and z_L-axis.

leg, as in Figure 5.07-a.

As seen before, the end moments for the tie and the strut about their orthogonal x-axis can be expressed as functions of the principal moments M_u and M_v as follows:

$$Mj_{xs} = (Mj_{us} + Mj_{vs})/\sqrt{2}$$

$$Mj_{xt} = (Mj_{ut} + Mj_{vt})/\sqrt{2}$$

where moments Mj_u and Mj_v are the unknown end moments at the end of the strut and tie about the principal axes u and v, respectively, as in Figure 5.05. The main leg's restraining moment about its x_L-axis can be written from slope-deflection equations as indicated below:

$$Mj_{xL} = \frac{EIx_L}{L_1} [4\theta j_{xL} + 2\theta i_{xL}]$$

where

- E is the modulus of elasticity.
- Ix_L is the main leg's moment of inertia about its orthogonal x_L-axis.
- L_1 the length of main leg between nodes j and i in t' frame, as shown in Figure 5.07-b.
- θj_{xL} and θi_{xL} are the unknown rotations in the main leg about its x_L-axis at nodes j and i respectively.

In the y_L direction - Projecting all end moments on the main leg's y_L axis at node j, see Figure 5.07-c, we can write:

$$Mj_{yL} - (Mj_{yt} - P\,e_{xt}) + (Mj_{ys} - P\,e_{xs}) = 0$$

in which e_x are eccentricities as indicated in Figures 5.02 and 5.06. As before, the orthogonal end moments in the diagonals can be expressed as functions of the principal end moments as follows:

$$Mj_{yt} = (Mj_{ut} - Mj_{vt})/\sqrt{2}$$

$$Mj_{ys} = (Mj_{us} - Mj_{vs})/\sqrt{2}$$

and the restraint moment from the main leg about its y_L-axis

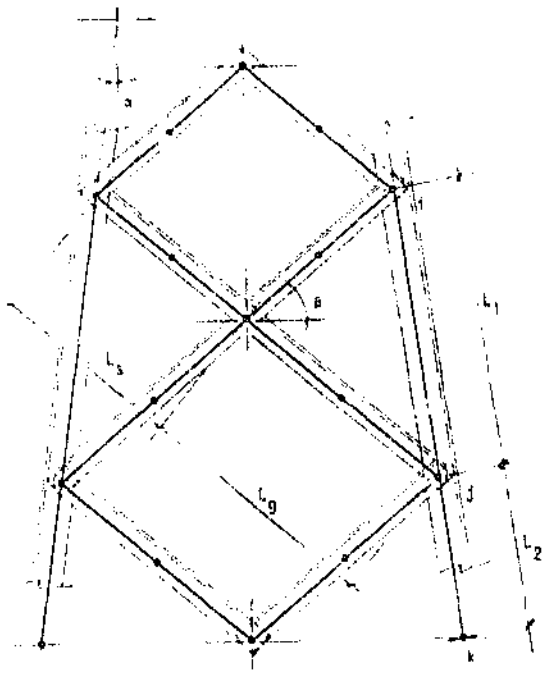

(b)

Figure 5.07-b: Main leg rotations. Detail of main leg lengths L1 and L2.

is given by the following slope-deflection expression:

$$Mj_{yL} = \frac{EIy_L}{L_1} [4\theta j_{yL} + 2\theta i_{yL}]$$

where

- Iy_L is the leg's moment of inertia about its orthogonal y_L-axis.
- E and L_1 are as indicated above for the x_L-axis.
- θj_{yL} and θi_{yL} are the unknown rotations in the main leg about its y_L-axis at nodes j and i respectively.

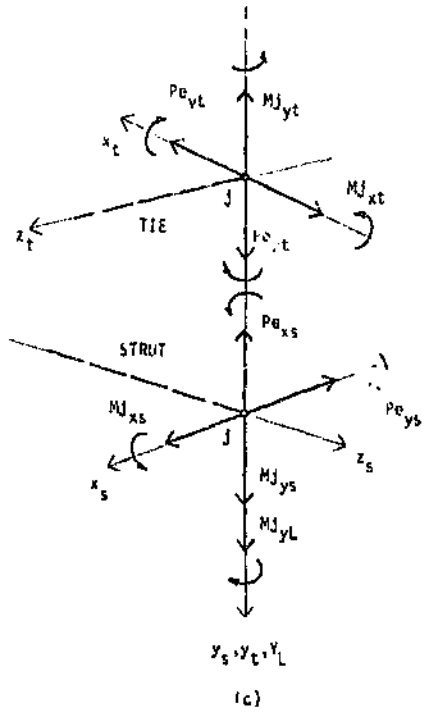

(c)

Figure 5.07-c: Main leg rotations. Conditions at the connecting nodes about the y_L-axis

In the z_L direction - Projecting all end moments on the main leg's longitudinal z_L-axis at node j, see Figure 5.07-a, the following equations can be written:

$$Mj_{zL} - (Mj_{xt} - P\ e_{yt})\sin\Phi_2 - (Mj_{xs} - P\ e_{ys})\sin\Phi_1 = 0$$

where ey, Mj_{xt} and Mj_{xs} are expressed as in the x_L direction, and the main leg restraint in the z_L direction is initially given by the expression of torsion of an element of length L_1 as follows:

$$Mj_{zL} = \frac{GIz_L}{L_1}\ [\theta i_{zL} - \theta j_{zL}]$$

in which G is the section's torsional modulus, Iz_L is the St. Venant's torsional constant as given before, and θj_{zL} and θi_{zL} are the unknown torsional rotations of the main leg at nodes j and i respectively, see Figure 5.07-b.

This approach, therefore, implies that there is no torsional restraint at the supports of the frame, m and n in Figure 5.01. It must be remembered at this point that considerable care was taken in designing and detailing frictionless tension and compression supports for the testing frames, as shown in Figures 2.09 and 2.10 of Chapter 2.

However, an option was included in the program for the simulation of boundary effects about the z_L longitudinal axis, as explained below. Observing Figure 5.07-b, the unknown torsional restraining action of a support at node k can be considered as an additional torsional moment as follows:

$$M'_{jzL} = \frac{GIz_L}{L_2} [\theta j_{zL} - \theta k_{zL}]$$

in which L_2 is now the length of main leg between node j and the support at node k, and θk_{zL} is the unknown rotation of the support k. This rotation can be expressed as a function of the additional torsional moment as indicated below:

$$\theta k_{zL} = \frac{M'_{jzL}}{S_{zL}}$$

where S_{zL} is a linear restraint coefficient representing the stiffness of the supporting joint k, and is determined empirically. Replacing this rotation in the above moment equation:

$$M'_{jzL} = \frac{GIz_L}{L_2} [\theta]_{zL} - \theta k_{zL}] = \frac{GIz_L}{L_2} [\theta]_{zL} - \frac{M'_{jzL}}{S_{zL}}]$$

and substituting, we can finally express the additional torsional moment at end j of element jk as a function of the rotation θjzL, as indicated below:

$$M'_{jzL} = \frac{S_{zL}L_2}{S_{zL}L_2 + GIz_L} \frac{GI_{zL}}{L_2} \theta j_{zL} \qquad \ldots.(5.08)$$

from which the total main leg rotational restraint results:

$$Mj_{zL} = \frac{GIz_L}{L_1} [\theta i_{zL} - \theta j_{zL}] + M'_{jzL}$$

When the restraint coefficient S_{zL} is equal to zero, see Equation (5.08), the support acts as pin-ended, as in the initial assumption. When the restraint coefficient tends to infinity, the support acts as fix-ended, and there is an additional torsional restraint in the main leg given by the following expression:

$$M'_{jzL} = \frac{GI_{zL}}{L_2} \theta j_{zL}$$

As can be seen in the above cases describing the main leg's behaviour, the unknown end moments about the principal axes of each diagonal are considered simultaneously with the bending effect induced by the eccentric forces and the main leg's restraining moments, all being projected on the main leg's orthogonal axes. It has been found throughout this investigation that these arrangements, although simplified with respect to the more complex actual conditions, cannot be modelled completely in standard linear or non-linear programs for structural analysis.

5.2.5 - Conditions at cross-over joints

One of the main characteristics of a cross bracing system is that its diagonals are interconnected at the cross-over joint. This is a point of interaction between the members, in which the tie provides lateral support to the strut, allowing, under

particular conditions, for a non-symmetrical mode of buckling. The lateral stiffness in the tie is primarily dependent on its flexural rigidity, as well as the amount of axial force in the member, as explained in [38,43]. Two cases are considered in the present study, as indicated below.

Cross-over joint in the central panel of bracing

Consider a generic central cross-over joint j in the panel of Figure 5.08-a. Three unknowns are introduced in the program for analysis of this joint, namely one vertical force C_y, equal and opposite in both diagonals, and one horizontal force for each diagonal, C_{xs} and C_{xt}. These are the cross-over forces as indicated in Figure 5.08-c.

For the analysis of these forces, consider the members ij and jk of total length L in the plane uz as shown in Figure 5.08-b, supported by the main legs at nodes i and k, where displacements are equal to zero. At the intermediate joint j there is a connection to a second bracing, which is contained in a separate vertical plane. The interactions between the diagonals at joint j induce forces C_y and C_u on both bracings in the vertical and horizontal directions, as indicated in Figure 5.08-c. Taking moments in the plane uz about the node i, we can write the following:

$$Mv_k - Mv_j + V_k L + C_u L_j = 0$$

in which C_u indicates the cross-over force in the node j projected on the uz plane. The shear force V_k can now be

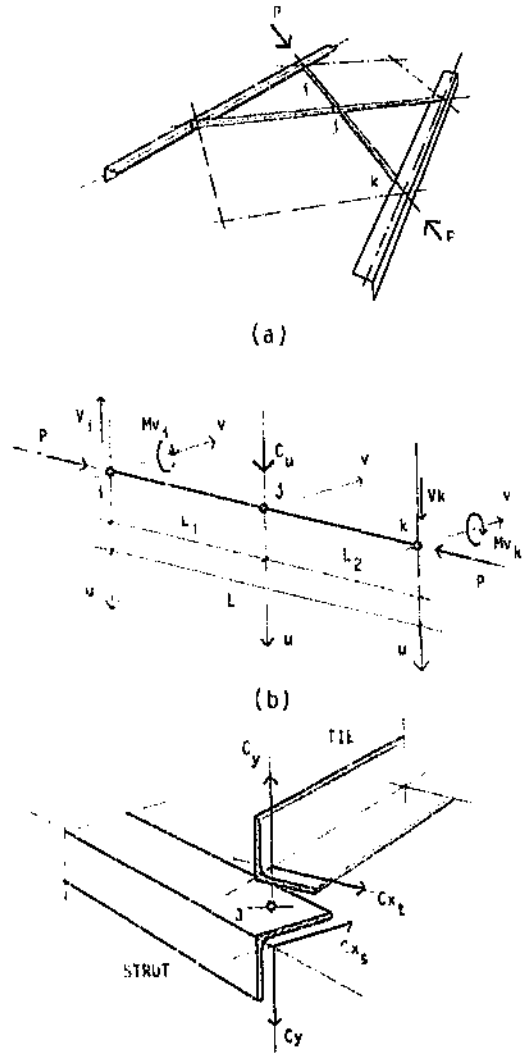

Figure 5.08: Conditions at the cross-over joint in the central panel of bracings.

expressed as a function of the unknown forces and moments as follows:

$$V_k = -\frac{C_u L_1}{L} + \frac{Mv_i - Mv_k}{L} = -\frac{(C_x + C_y)L_1}{L\sqrt{2}} + \frac{Mv_i - Mv_k}{L}$$

Note that the force C_u has been written above as a function of the orthogonal cross-over forces C_y and C_x, see Figure 5.08-c. Similarly, taking moments about node k, we find the following equation:

$$V_i = \frac{C_u L_2}{L} + \frac{Mv_i - Mv_k}{L} = \frac{(C_x + C_y)L_2}{L\sqrt{2}} + \frac{Mv_i - Mv_k}{L}$$

The shear forces in the diagonals are thus expressed as functions of the end moments in the adjacent members and cross-over forces, all of which are unknowns. Equations of sway equilibrium can now be written for both planes uz and vz, for any element in both diagonals, such as ij to the left of the cross-over joint, Figure 5.08-b, as follows:

$$Mv_{ij} - Mv_{ji} - V_i L + P(u_j - u_i) = 0$$

in which V_i is the shear force and is expressed as a function of the cross-over forces C_x and C_y, as in the equations above. Similar equations are developed for all principal planes in both diagonals intercepting at this point.

Two additional compatibility conditions are included at the cross-over joint, as indicated below:

$$y_s = y_t$$

indicating equal out-of-plane deflections in both diagonals, and

$$x_s = x_t = 0$$

indicating a condition of zero relative in-plane displacements of the joint. The subscripts s and t above refer to the strut and the tie respectively.

Cross-over joints in the outside panels of bracing

As explained in Chapters 2 and 3, the out-of-plane displacements of the cross-over joints in the outside panels of bracing, p and q in Figure 5.01, were adjusted during the tests as a function of the out-of-plane deformations in the central cross-over c. These deflections, as well as the particular conditions of these joints, have been simulated in the computer model through the inclusion of moment and sway equilibrium equations at nodes p and q in Figure 5.01 as explained below.

- As in the case of diagonal-main leg connections in the previous Section, consider moment equilibrium about three orthogonal axes at a generic cross-over node j, as indicated in Figure 5.09-a. The moments applied to the node in the three orthogonal directions can be written as follows:

  About the X-axis - Projecting the end moments in the diagonals on the X-axis, see Figure 5.09-a, we have the following:

  $$(M_{jxt} - P\, e_{yt})\sin\beta + (M_{jxs} - P\, e_{ys})\sin\beta = 0$$

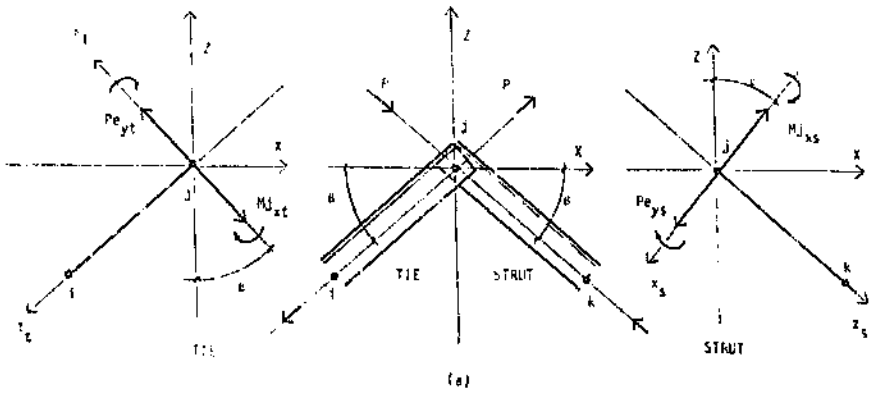

Figure 5.09-a: Conditions at the cross-over joints in the outside panels of bracings, about the X- and Z-axis.

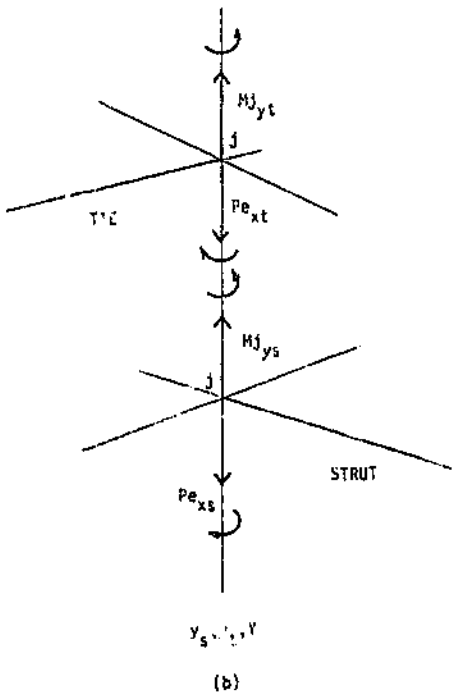

Figure 5.09-b: Conditions at the cross-over joints in the outside panels of bracings, about the Y-axis.

in which

- ey are eccentricities in the diagonals, as in Figure 5.02,
- Mj are end moments in each diagonal at node j about its local x-axis, and
- P is the eccentric axial force in the bracings.

The orthogonal end moments can be expressed in terms of moments about the principal axes, after Figure 5.05, as follows:

$$Mj_{xt} = \frac{1}{\sqrt{2}} (Mj_{ut} + Mj_{vt})$$

$$Mj_{xs} = \frac{1}{\sqrt{2}} (Mj_{us} + Mj_{vs})$$

in which moments Mju and Mjv are unknowns. Operating on the above equilibrium equations, we can finally write:

$$Mjus + Mjvs + Mjut + Mjvt = 2\sqrt{2}\ P\ ey$$

where the eccentricity ey is considered to be equal in both diagonals.

About the Y-axis - Projecting end moments in the diagonals on the Y-axis, see Figure 5.09-b, we have the following expression:

$$(Mjys - P\ e_{xs}) + (Mjyt - P\ e_{xt}) = 0$$

where, after operating as in the case above, we finally obtain:

$$Mj_{us} - Mj_{vs} + Mj_{ut} - Mj_{vt} = 2\sqrt{2}\ P\ e_x$$

About the Z-axis - Projecting end moments in the diagonals on the Z-axis, see Figure 5.09-a, we have the following expression:

$$-(Mjxt - P\ eyt)\cos\beta + (Mjxs - P\ eys)\cos\beta = 0$$

Considering equal eccentricities in both diagonals, the following equation is obtained for the Z-axis:

$$Mjus - Mjvs - Mjut + Mjvt = 0$$

- Consider now sway equilibrium equations in the strut's plane uz, as in Figure 5.09-c. For the element in the strut between nodes j and k, the following relation applies:

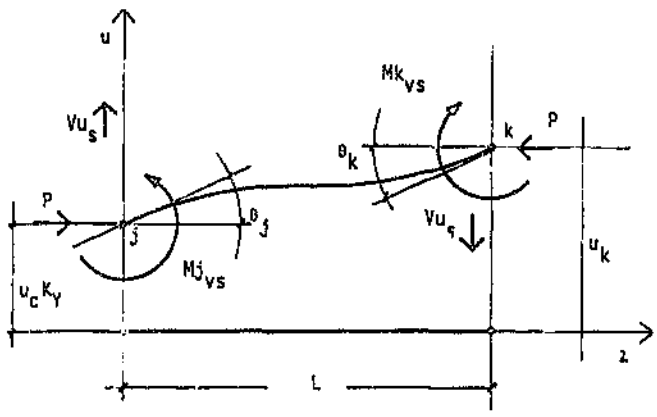

Figure 5.09-c: Conditions at the cross-over joints in the outside panels of bracings, definition of sway conditions.

$$Mj_{vs} - Mk_{vs} - Vu_s L + P(u_k - u_c K_Y) = 0$$

in which:

- u_k are the relative displacements of node k, and u_c are the displacements at the central cross-over joint c, as in Figure 5.01, in the plane uz,
- K_Y is a factor relating displacements at node j to displacements at cross-over node c in the central panel of bracing, see Figure 5.01, in the uz plane. Values of K_Y are as in the laboratory tests for each frame arrangement, as explained in Chapters 2 and 3. Note that u_j is no longer an unknown at this node.

Similar sway equilibrium equations are written about both principal axes in both diagonals, in which the new unknowns are the shear forces V_u and V_v.

- Finally, an additional compatibility equation is included as indicated below:

$$y_{js} = y_{jt}$$

which indicates equality of out-of-plane deflections at node j for both diagonals.

The analysis shown above solves the problem for the outside cross-over joints. The unknowns at these nodes are now the shear forces V_u and V_v, from which the cross-over forces can be calculated.

5.2.6 - Solution of the system of equations

From the analysis of conditions at intermediate nodes, cross-over joints and diagonal-main leg connecting nodes presented in the previous Sections, a system of 'n' simultaneous equations with 'n' unknowns has been formed, where 'n' is obtained as follows:

- Four unknowns at each node of each member, corresponding to one end moment and one end displacement about each of the section's principal axes.

- Three additional unknowns at the central cross-over joint, corresponding to forces in the out-of-plane and in-plane directions for each diagonal. At the outside cross-over joints, the displacements are expressed as functions of the central cross-over displacements, and the four new unknowns are the shear forces in the two principal planes of both the strut and the tie.

- Three additional unknowns at each node connecting diagonals and main legs, corresponding to nodal rotations about three main leg longitudinal and orthogonal axes.

Solution of this system of equations yields the magnitude of the end moments and node displacements for all members in the frame, from which the nodal rotations can be calculated from expressions such as Equations (D.02) or (D.03) in Appendix D. The stresses at critical sections are calculated as indicated in the following Section. This analysis has the following characteristics:

- It is a geometric non-linear, elastic analysis in which no iterations are required because the axial force is known at each load step, and the flexibility conditions of the members are updated at each load level through the Berry stability functions.

- The equations in the computer model have been developed to simulate the general conditions and, in particular, the boundary conditions of the experimental frames with cross-bracings described in Chapter 2.

- Conditions are considered about the principal u and v axes of the diagonals and, simultaneously, the boundary conditions allow for the inclusion of the orthogonal eccentric axial forces and the main leg's flexural and torsional restraining actions.

- Cross-over forces and main leg rotations are calculated through the introduction of additional equations of equilibrium and compatibility at the relevant nodes.

The following step is to calculate the stresses in each member, based on the end moments on each of the planes defined by the principal axes. This is discussed in the following Section.

5.2.7 - Determination of ultimate diagonal strength

The maximum compressive stress f_{max} at the extreme fibre due to the combination of axial loads and bending about the principal axes in Figure 5.10 can be expressed as indicated below:

$$f_{max} = \frac{P}{A} + \frac{Mv\ d_{u1}}{I_v}$$

at the heel of the angle and

$$f_{max} = \frac{P}{A} + \frac{Mv\ d_{u2}}{I_v} + \frac{Mu\ d_v}{I_u}$$

at the toes of the angle section in Figure 5.10, where:

- P is the axial force in the member.
- A is the area of the section.
- d_u and d_v are distances indicated in Figure 5.10.
- M_u and M_v are the calculated end moments about the principal u- and v-axis at each node in the structure.

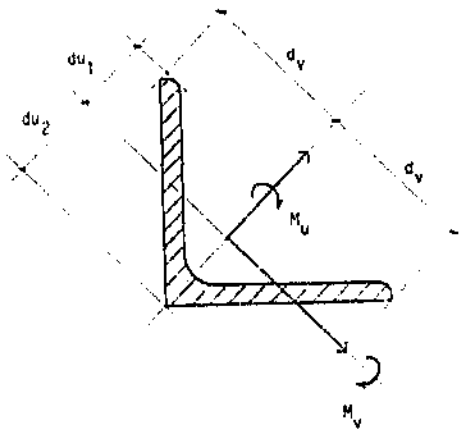

Figure 5.10: Assessment of stress at the critical sections. Geometry of the angle's cross-section.

It has been observed in this and previous investigations [11,23] that failure of steel angle struts occurs almost immediately after first yield has taken place in the extreme fibre of the critical section, see Table 3.09 in Chapter 3. Based on this the following criterion has been adopted in the present theoretical analysis: the ultimate load resisted by the bracing is the load at which yielding of the most highly stressed fibre starts at any intermediate section of any of the strut diagonals in the frame. The general procedure presented in the previous Sections is illustrated in the flowchart depicted in Figure 5.11.

5.3 - Analysis of plane frames: correlation with experimental results

The non-linear computer program described before, which has been called PANEL, is now used to predict the failure loads of the diagonals in the test frames of this and other investigations, as examined in Chapter 4. The input of data is simple and comprises the following:

- The yield stress of material and the maximum load applied to the frame,
- The number of load steps, the magnitude of load increments, and the ratio of axial forces in the bracing,
- The geometric characteristics of all the bracings and the main leg, and the length L_g in the main diagonal,
- The slope of the legs and inclination of the diagonals in all subpanels of bracing,
- The coefficients Ky giving the ratio of out-of-plane displacements between the outside and the central cross-over joints, and

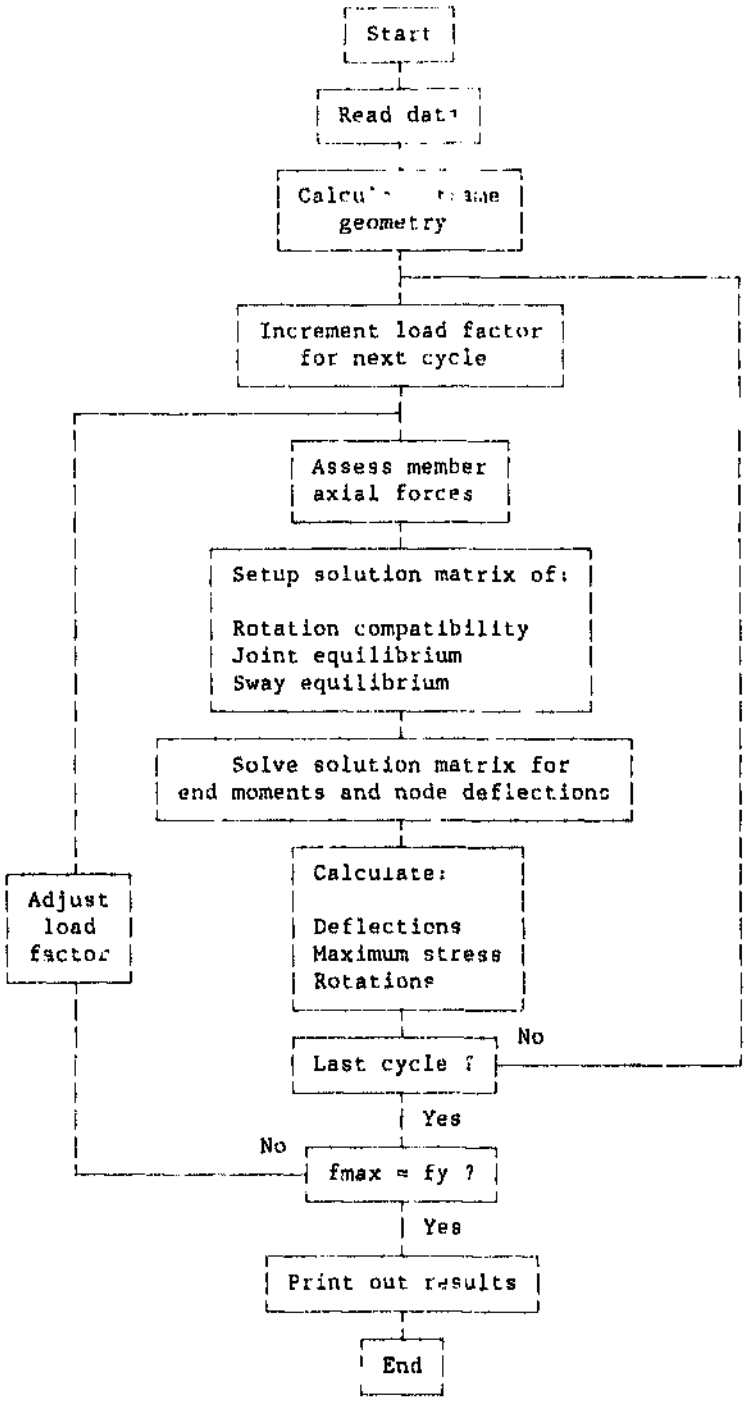

Figure 5.11: Flowchart depicting the general analytical procedure used in the present investigation for the analysis of two dimensional frames with cross-bracings.

- The S_{xS}, S_{yS} and S_{zS} restraint coefficients at the connecting nodes and at the leg supports.

For the analysis of tests with PANEL, the following rules were observed:

- For the tests conducted in this research the coefficients K_y were based on the test measurements. In the cases of other frames with transverse beams, see Figure 1.08, $K_y \approx 0$.

- The coefficient of torsional restraint to the main legs by the supports was kept equal to zero, thus simulating the conditions defined in the design of the same nodes in the experimental frames. The cases of frames with fixed leg supports, as in Figure 1.08, were represented by a very large restraint coefficient.

- The restraint condition at the nodes about the y-axis is included in the program for 1-bolt connections (pinned). For 2-bolt connections a fixed condition was simulated about the same axis by a very large restraint coefficient, S_{yS}.

- The restraint coefficient at the nodes about the x-axis, S_{xS}, was as calculated for the simplified model in Chapter 4 using Equation (4.05). It is noted that the empirical restraint coefficient S_{xS} was developed in each case as a function of the actual observed conditions in the connections, including the effects of relative inclinations, relative sizes of the members and the boundary conditions.

Plots of deflections and nodal rotations are included for some indicative cases, and the comparisons between the theoretical and the experimental results are based on the following

parameters:

- Failure stress ratio fult/fy,
- Mechanism of failure of the struts, as described in Chapter 3,
- In-plane and out-of-plane midspan deflections in the strut and at the cross-over joint,
- Strut end rotations, and
- Main leg torsional rotations.

These are examined in the following Sections for the tests studied in this investigation, and also tests reported by Behncke [11] and Wood [49].

5.3.1 - Present investigation

Data on the frames and diagonal specimens for these tests are given in Tables 4.03-a and 4.03-b of Chapter 4. Results from the analyses with PANEL are given in Table 5.01 below, in which the assumed restraint coefficients for the bracings about the x-axis (from Equation (4.05) in Chapter 2) are given in Column 2, about the y-axis in Column 3, and the torsional restraint coefficients at the main leg supports are given in Column 4, where F and P refer to Fixed (full restraint) and Pinned (no restraint) end conditions respectively. The calculated failure loads are listed in Column 5, which are compared with the test results in Column 6.

The calculated failure load for Test 102 with L/r 100 is conservative, with yield taking place first in the tie at the cross-over joint C, and then in the strut, see Figure 5.12. The

calculated deflections at nodes g and c in Figure 5.12 are shown in Figure 5.13-a, where it can be seen that the predicted out-of-plane deflections are correct at the cross-over (y_c) and larger than in the test at midspan (y_g). The predicted in-plane deflections at midspan (x_g) are smaller than recorded in the tests and in the positive x-direction, while the experimental deflections were generally in the negative x-direction, see Figure 5.12.

The strut's end rotations θ_{xS} computed with PANEL at node a, see Figure 5.12, are smaller than recorded, as indicated in Figure 5.13-b. The computed main leg torsional rotations θ_{zL} at the same node are significantly larger than the experimental records, and this is shown in Figure 5.13-c.

The predicted failure loads at slenderness L/r=130, Tests 202 through 702 in Table 5.01, are, in general, conservative, except for Test 312. These are all good approximations to the actual

Present investigation

Table 5.01: PANEL - Comparison of results

Test Designation	PANEL				Test results
	θ_{xS}	S_{yS}	S_{zL}	$\frac{f_{ult}}{f_y}$	$\frac{f_{ult}}{f_y}$
1	2	3	4	5	6
102	12.061	F	P	0.422	0.491
202	15.506	F	P	0.390	0.412
302	12.061	F	P	0.380	0.395
312	8.390	F	P	0.406	0.399
402	10.121	F	P	0.370	0.421
502	15.506	F	P	0.393	0.437
602	12.061	F	P	0.394	0.431
702	10.121	F	P	0.395	0.430
801	3.618	P	P	0.280	0.288
811	2.517	P	P	0.327	0.371
802	12.061	F	P	0.337	0.336
812	8.390	F	P	0.345	0.396
803	6.787	P	P	0.291	0.324
804	22.558	F	P	0.343	0.364

failure loads. Comparisons of results for Test 302 are examined as an example of typical behaviour for these tests. Deflections at nodes g and c, see Figure 5.12, are shown in Figure 5.14-a. Note that both out-of-plane deflections z_c and y_g are larger in the computer model. In-plane deflections x_g were recorded in the x-negative direction, while PANEL predicts small positive deflections along the same axis.

At node s in the strut, see Figure 5.12, out-of-plane experimental deflections are larger than in the computer model, and in-plane deflections are both in the x-positive direction, but the experimental deformations are larger, see Figure 5.14-b. It is to be noted that experimental failure occurred at subspan

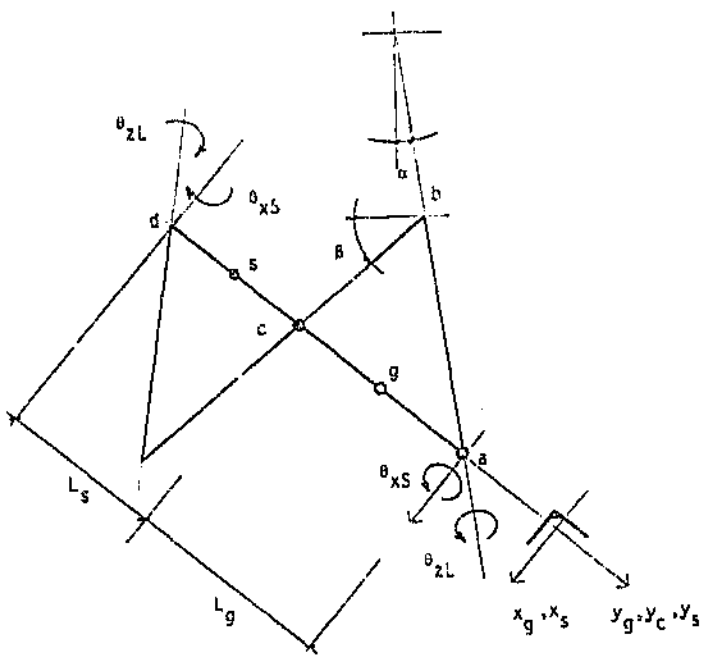

Figure 5.12: Comparison of test results with the model PANEL. The positive directions of deflections and nodal rotations are indicated.

s, Figure 5.12, while PANEL predicts equal strain development and almost simultaneous failure at both spans g and s. Also, y_g and y_s (and x_g and x_s) deflections in the computer model are symmetrical about the cross-over joint c.

Nodes a and d strut rotations (θ_{xS}) are depicted in Figure 5.14-c, where it can be seen that the predicted rotations are very close to the test results and also equal at both nodes. Main leg torsional rotations at the same nodes (θ_{zL}) are shown in Figure 5.14-d, and it is again noted that the computer predictions are larger than the test records, and equal at both nodes. The positive directions for nodal rotations and displacements are indicated in Figure 5.12.

Predictions of failure loads for tests with slenderness ratios of L/r=160, Tests 801 through 804 in Table 5.01, are very reasonable and generally conservative. Failure is in all cases predicted at node g in the strut, see Figure 5.12, which is in agreement with the experimental results.

Comparison of deflections for Test 801 with 1-bolt connections is given in Figure 5.15-a. It can be seen that the computed out-of-plane deflections at nodes c and g are larger than the test records, while in-plane deformations at node g are predicted correctly. For the case of 2-bolt connections, for example Test 804, Figure 5.15-b shows improved predictions of deflections y_c and y_g.

Computed strut end rotations θ_{xS} at node a, Figure 5.12, are given in Figures 5.15-c and 5.15-d for Tests 801 and 804 respectively. It can be seen that they are similar to the experimental results but with the following characteristics: for Test 801 with 1-bolt connections, rotations θ_{xS} are larger

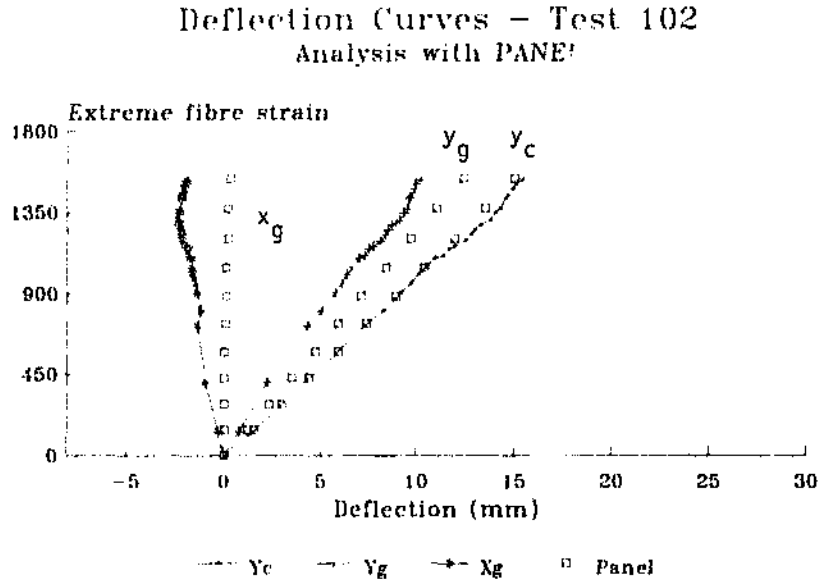

Figure 5.13-a: Vertical and horizontal strut deflections see Figure 5.12

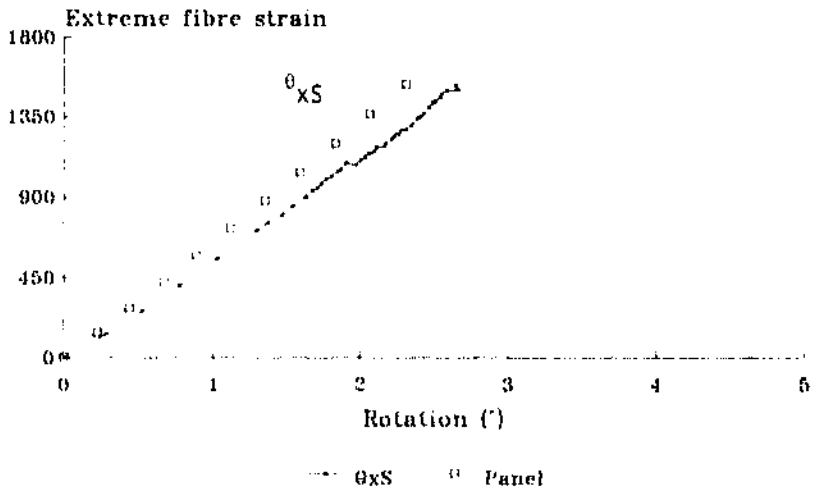

Figure 5.13-b: Strut's rotational response at node a, see Figure 5.12

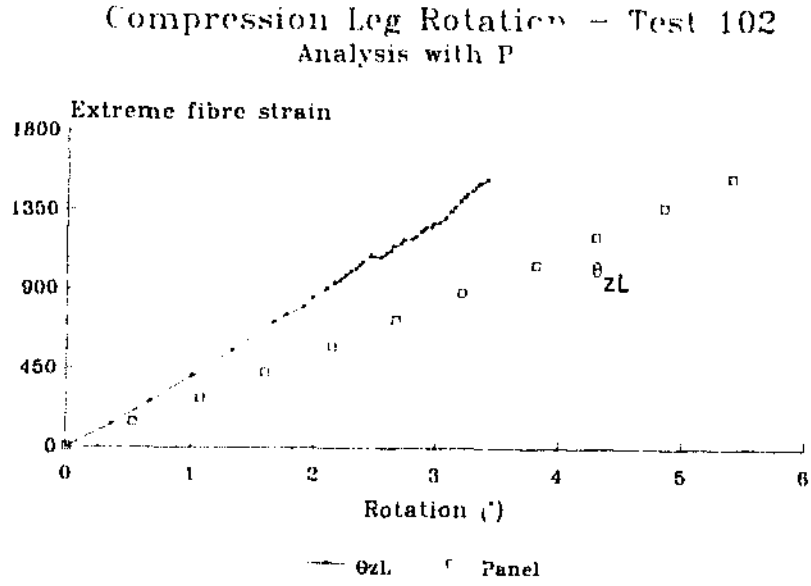

Figure 5.13-c: Main leg's rotational response at node a, see Figure 5.12

than those recorded in the tests. For Test 804 with 2-bolt connections, the same rotations are smaller than the experimental records.

As in the previous cases, predicted main leg torsional rotations θ_{zL} at node a are larger than those recorded in the tests. For Test 801 in Figure 5.15-e, however, these differences are too large and are not at all related to the experimental evidence. This situation improves for Test 804, as shown in Figure 5.15-f, where computed rotations are still larger, but the difference appears to be reasonable.

The results from the computer analyses using PANEL are typical for each level of slenderness ratio and therefore allow for the following conclusions:

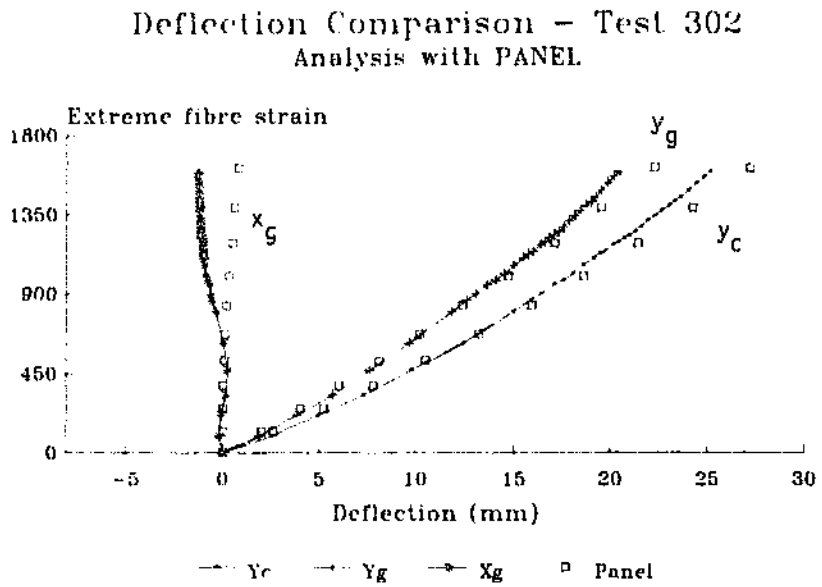

Figure 5.14-a: Vertical and horizontal strut deflections, see Figure 5.12

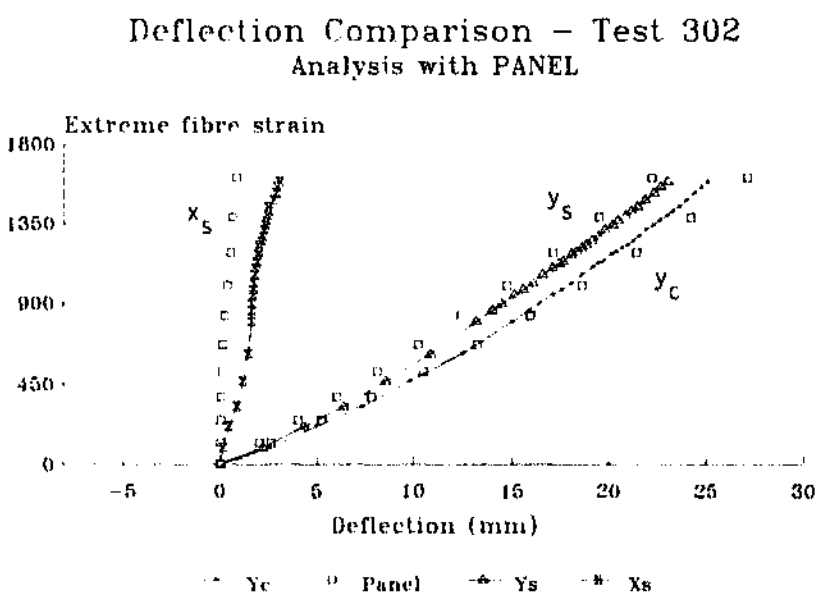

Figure 5.14-b: Vertical and horizontal strut deflections, see Figure 5.12

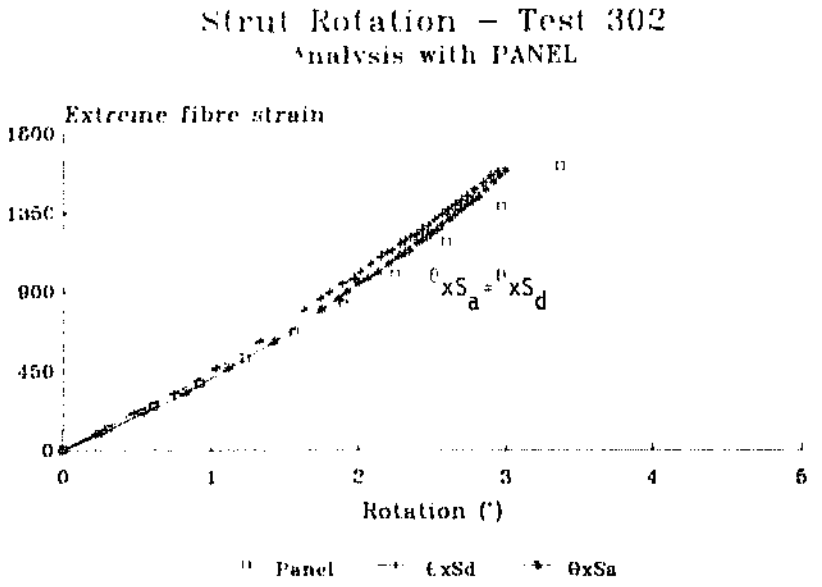

Figure 5.14-c: Strut rotational response at nodes a and d, Figure 5.12

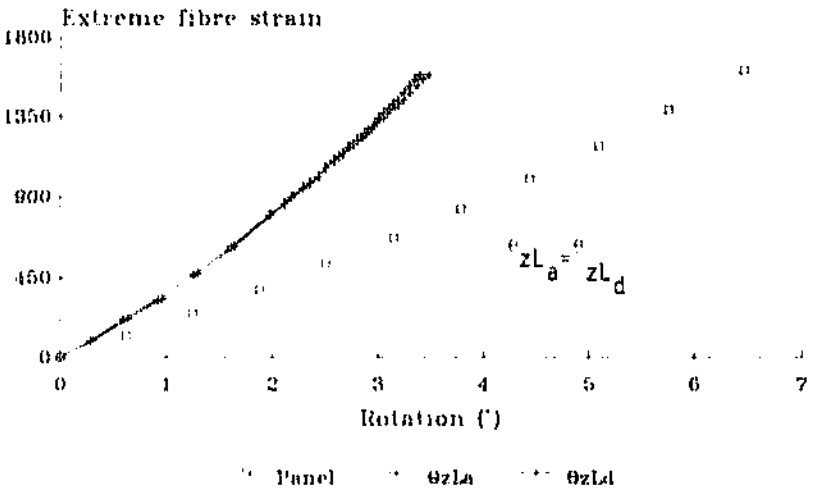

Figure 5.14-d Main leg's rotational response at nodes a and d, Figure 5.12

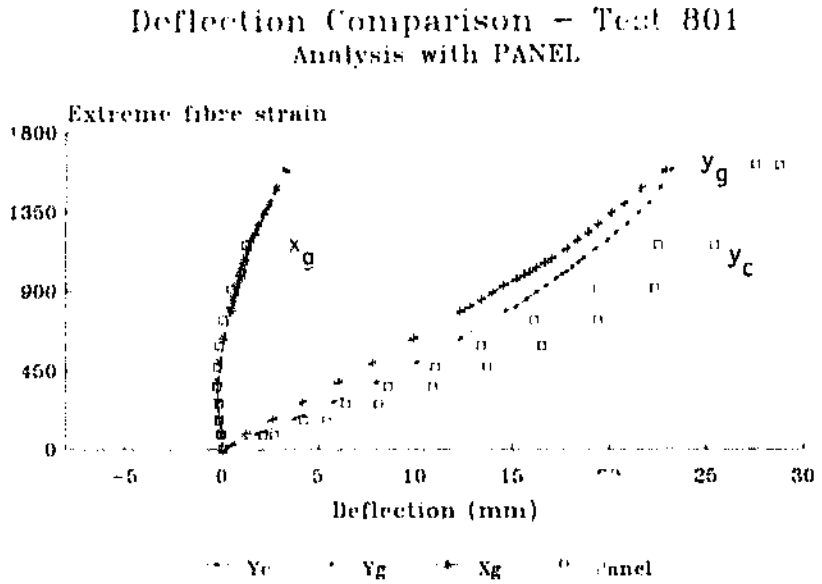

Figure 5.15–a: Vertical and horizontal strut deflections see Figure 5.12

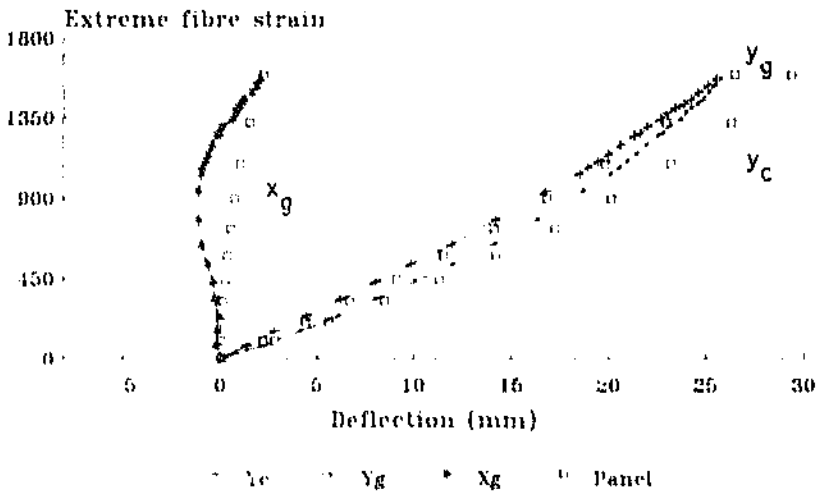

Figure 5.15–b: Vertical and horizontal strut deflections, see Figure 5.12

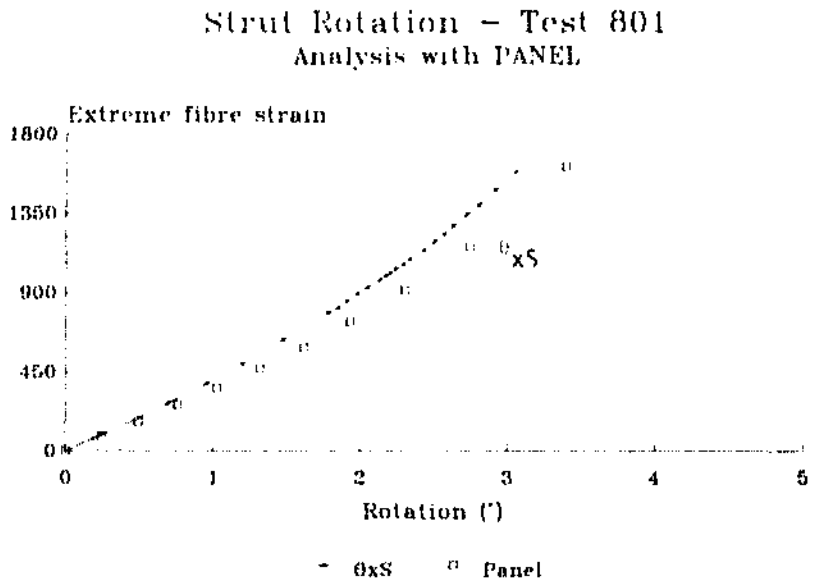

Figure 5.15–c: Strut's rotational responce at node a, see Figure 5.12

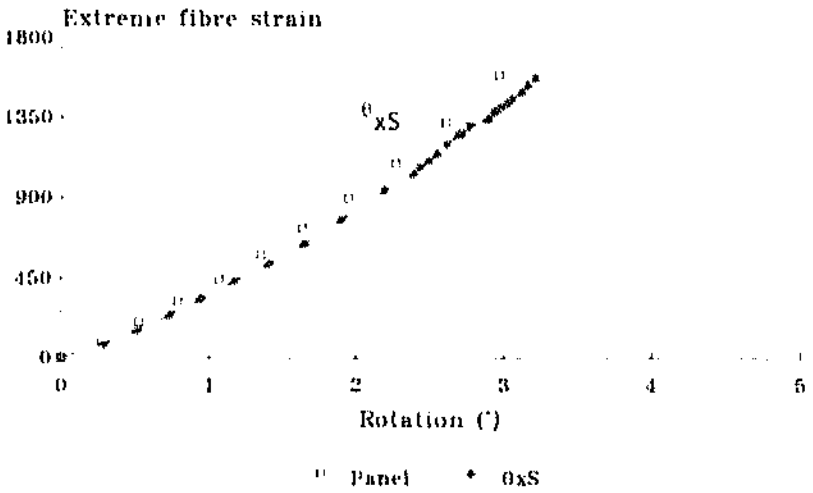

Figure 5.15–d: Strut's rotational response at node a, see Figure 5.12

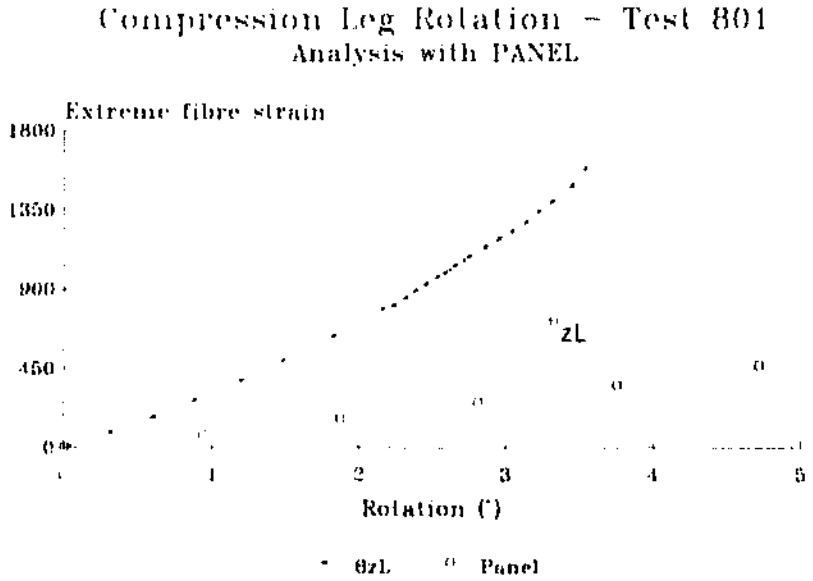

Figure 5.15–e: Main leg's rotational response at node a, see Figure 5.12

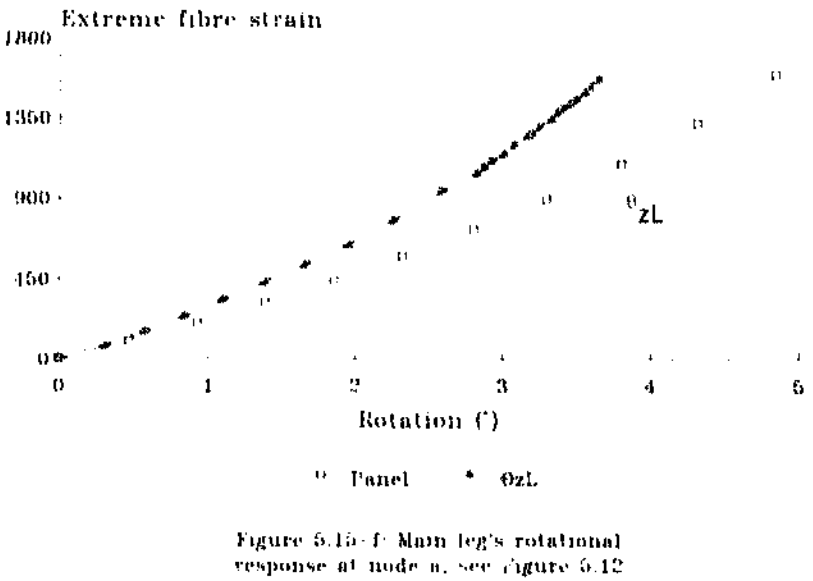

Figure 5.15–f: Main leg's rotational response at node a, see Figure 5.12

- The computed failure loads are generally conservative, but give reasonable predictions of the strength of the bracing at various levels of slenderness ratio and for various bracing arrangements.

- The mechanism of failure in the computer model is in all cases correct, with yielding taking place at the heel of the angle struts, and at the longest unsupported subspan g, see Figure 5.12. In the case of low slenderness ratio, Test 102, yield occurs first in the tie at the cross-over joint, as in the tests.

- Predictions of out-of-plane deflection in the strut at midspan and at the cross-over joint are generally correct for all alternatives, with a lower accuracy for the case of Test 801 with 1-bolt connections. In-plane deflections are correct at higher values of L/r, but with larger differences at lower values of L/r.

- Predictions of strut end rotations are fairly accurate in all cases. By contrast, computed main leg torsional rotations are in all cases larger than the experimental values. In the case of Test 801 these differences are unacceptable. It is apparent that the computer model fails to simulate the torsional behaviour of the main legs, particularly for the case of 1-bolt connections.

In addition, it was observed that the model PANEL is highly sensitive to variations of the following parameters:

- The strut-end spring coefficient S_{xS}, which simulates the flexibility of the bolted connections about the local x-axis.

- The main leg support spring coefficient S_{zL}, which simulates the restrictions to torsional rotation of the main legs.

- The cross-over joint coefficient K_y, which relates the out-of-plane deflections of the outside and central cross-over joints.

The computed results presented above were obtained after innumerable modifications and improvements were introduced to the model PANEL. At each step, extensive calibrations of the model against the experimental results were performed. It is apparent, however, that further modifications are required to simulate the case of 1-bolt connections, and also the torsional rotations of the main legs of the frames. This and other limitations of PANEL will be addressed again at the end of this Chapter.

5.3.2 - Tests reported by Behncke [11]

Data on the frames and diagonal specimens for these tests are given in Tables 4.04-a and 4.04-b of Chapter 4. Results from the analyses with PANEL are given in Table 5.02 below, in which the assumed restraint coefficients for the bracings about the x-axis (from Equation (4.05) in Chapter 2) are given in Column 2, about the y-axis in Column 3, and the torsional restraint coefficients at the main leg supports are given in Column 5, with F and P defined as before. The calculated failure loads are listed in Column 5, which are compared with the test results in Column 6.

These tests were performed on frames such as those shown in Figure 1.08, where two beams were used to connect the two main legs at the top and bottom sections. As a consequence, the outside cross-over joints were fixed against out-of-plane displacements and the two main legs were fixed against torsional rotations. All these conditions were simulated with PANEL.

The calculated failure load for Test 0842 with L/r=90 is correct, with yielding taking place first in the tie at the cross-over joint. This is in agreement with the experimental evidence.

For frames with slenderness of L/r=140, Tests 0611, 0712, 0931 and 1032, the predicted results are conservative for the cases of 1-bolt connections (0611 and 0931), and optimistic for the cases of 2-bolt connections (0712 and 1032). The predicted mechanism of failure for these tests is correct.

In the case of frames with slenderness ratio of L/r=160, Tests

Experimental results reported by Behncke [11]

Table 5.02: PANEL - Comparison of results

Test Designation	PANEL				Test results
	S_{xS}	S_{yS}	S_{zL}	$\frac{f_{ult}}{f_y}$	$\frac{f_{ult}}{f_y}$
1	2	3	4	5	6
0121	7.876	P	F	0.288	0.297
0522	26.253	F	F	0.467	0.435
0611	7.876	P	F	0.304	0.343
0712	26.253	F	F	0.461	0.420
0842	26.253	F	F	0.581	0.587
0931	7.876	P	F	0.335	0.374
1032	26.253	F	F	0.528	0.520
1351	2.066	P	F	0.267	0.257
1451	2.066	P	F	0.264	0.218

0121, 0522, 1351 and 1451, the calculated results are correct for test 0121, but are optimistic in all other cases. This problem is more evident in Test 1451, with main legs of L70x70x6 and all bracings of L40x40x3 angles, and therefore a lower ratio of main leg-to-diagonal sizes.

It can be seen that PANEL (which was calibrated for the case of legs with no torsional restraints and given ratios of out-of-plane cross-over deflections) presents some problems in predicting correct failure loads for these tests. It is to be noted, however, that the test frames depicted in Figure 1.08 were rather rudimentary, and offered poor control over the most important variables.

5.3.3 - CIGRE tests reported by Wood [49,63]

Data on the frames and diagonal specimens for these tests are given in Tables 4.05-a and 4.05-b of Chapter 4. Results from the analyses with PANEL are given in Table 5.03 below, in which the assumed restraint coefficients for the bracings about the x-axis (from Equation (4.05) in Chapter 2) are given in Column 2, about the y-axis in Column 3, and the torsional restraint coefficients at the main leg supports are given in Column 5, with F and P defined as before. The calculated failure loads are listed in Column 5, which are compared with the test results in Column 6.

As in the test cases described in the previous Section, the CIGRE test frames had transverse beams at the top and bottom sections, as can be seen in Figure 2.01, which imposed

restrictions to main leg rotations and out-of-plane cross-over deflections. As all the diagonals were of the same size and had the same cross-sectional properties, the top and bottom struts were reinforced by a redundant member, as shown in Figure 2.01, in order to secure failure of the main compression diagonal.

Finally, it has to be considered that complete data on these tests was not available, except for the basic dimensions of the frames and frame members, the observed yield stress of material and the failure stress for each test case. The reinforcement of the struts in the adjacent panels of bracing was simulated in PANEL by doubling the member's inertia about the minor axis.

Under these conditions, PANEL is not applicable for the case of 1-bolt connections (005-032), see Table 5.03, since the calculated failure loads and the mechanism of failure are not

Experimental results reported by Wood [49] and CIGRE [63]

Table 5.03: PANEL - Comparison of results

Test Designation	PANEL				Test results
	S_{xS}	S_{yS}	S_{zL}	$\frac{f_{ult}}{f_y}$	$\frac{f_{ult}}{f_y}$
1	2	3	4	5	6
005	1.237	P	F	N/A	0.288
006	1.237	P	F	N/A	0.273
031	0.888	P	F	N/A	0.288
032	0.888	P	F	N/A	0.270
014	4.123	F	F	0.311	0.325
015	4.123	F	F	0.319	0.345
038	2.961	F	F	0.301	0.260
039	2.961	F	F	0.289	0.270
040	2.961	F	F	0.355	0.295
041	2.961	F	F	0.348	0.265
092	9.432	F	F	0.428	0.500
093	9.432	F	F	0.416	0.503
108	6.797	F	F	0.390	0.318
109	6.797	F	F	0.399	0.393
148	4.364	F	F	0.399	0.438
149	4.364	F	F	0.399	0.412

related to the known test results and behaviour of the bracings.

For cases with 2-bolt connections, the predicted results are accurate, but not in all cases. For tests 038-041, the calculated results are optimistic, which is again coincident with low values of main leg-to-diagonal size ratios.

For the remaining tests, the calculated failure loads are conservative, but to a varying degree, and apparently depending upon the strength of each set of diagonals, see Tables 4.05-a through 4.05-d.

5.4 - Summary

A computer model for non-linear flexibility analysis of plane frames with crossed diagonals, PANEL, has been developed. Unlike other models which allow only for single-member analysis or behaviour about a single axis, this model includes, simultaneously and for all members, the end effects of eccentric forces and nodal restraint about the orthogonal axes while the resulting system of equations is solved for the bending effect and deflection about the principal axes at all the nodes.

Through the extensive computer analyses and comparisons with experimental data described in the previous Sections, it is clear that PANEL can be used for solution of frames with bracing arrangements and support conditions similar to those presented in this investigation (described in Chapter 2). Of those cases, the 1-bolt connection arrangement needs some improvement.

Some of the differences between the observed experimental

results and the failure loads and bracing behaviour as computed with PANEL which have become apparent through this research can be explained by the following details:

- This and other investigations have been focused on the behaviour of the main diagonals (with measurements of in- and out-of-plane deflections, end rotations, midspan distortions and strain development), and the influence of their eccentric connections with the main legs.

- The diagonals in the adjacent panels of bracing were not investigated. Their deflection, end rotation and strain histories are unknown, as is their influence on the nodal restrictions, and thus on the main strut behaviour and loading capacity. This is shown by Test 307, see Case VI in Chapter 3, where it is seen that inversion of the diagonals in the outside panels of bracing produces an increment in the resistance of the main strut, with significant reductions of midspan displacements and nodal rotations.

  The size of the outside bracings was increased in the present investigation, to secure failure of the main strut. The same effect was obtained in the CIGRE tests [63] by including a redundant member in the outside panels of bracing. Any additional effects on the main diagonals from one or the other solution are not known from analysis of the existing data.

- The diagonal or main leg in-plane rotations at the connecting nodes were not recorded, because the inclinometers (or rotation transducers) are able to read rotations only within a vertical plane (plus or minus a small tolerance). Therefore the models do not include in their solutions the influence of a parameter (i.e. restraint coefficient) describing this

effect. This is clearly shown by the model PANEL's poor predictions for 1-bolt connections. It is clear that a pinned end condition about the y-axis, represented by zero restriction from the main leg as simulated in the model, does not necessarily occur in the tests and may depend on bolt tensioning.

- The main legs were not investigated experimentally and have been assumed in all models as symmetric beams with the orthogonal-flexural and longitudinal-torsional characteristics of the actual angle sections. Further, the main legs were assumed to be connected to the diagonals at their centroidal axes. No eccentricities were considered about any axis of the main legs, and no assumptions were made concerning the main legs' behaviour about their principal axes. This is a significant departure from the actual conditions as illustrated by Figure 5.16, where it can be seen that in fact the connections were effectively eccentric, as in the case of the diagonals.

  Finally, the above concepts are also valid for the longitudinal axis of the main legs, since the tension and compression supports were located at the centre of gravity of the sections, thus along their centroidal longitudinal axis. But in fact the connections to the bracings are all displaced from that axis, see Figure 5.16. These differences may well explain the model's poor predictions of main leg rotation observed in the previous Section.

In view of the above, it was concluded that further development of PANEL will, without additional experimental data, prove inconvenient and ineffective. However, inclusion of some, or all, of these additional conditions may well render the problem

intractable from the theoretical point of view.

In closing this analysis it can be said that the calculated results presented in Tables 5.01 through 5.03, and the predicted behaviour of the bracing shown in the plots above, are the best approximations that can be obtained with PANEL in its present format. As the test programme and test setup were designed to evaluate, without any external influence, the most important parameters which affect cross-bracing behaviour, the model succeeds, under the same conditions, to produce accurate predictions of frame behaviour.

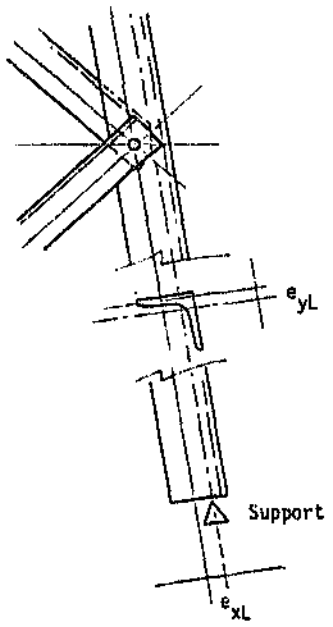

Figure 5.16: Note the position of the main leg support, along the centroidal axis. The connections are effected eccentrically about both orthogonal x- and y-axis.

It remains to conduct similar analyses with an alternative computer model, in order to correlate results and to validate the proposed solution. Therefore, a finite-element model of cross-bracing is introduced in the next Chapter, and comparisons with PANEL are included in the discussions.

CHAPTER 6

AN ALTERNATIVE COMPUTER MODEL USING ABAQUS

6.1 - Introduction

As discussed in the previous Chapter, no suitable computer package was found, at the time of conducting this research, to formulate proper non-linear models for analyses of complex frames composed of non-symmetrical members. This restriction resulted in the development of a non-linear flexibility model for the evaluation of cross-bracing systems in the present investigation. The characteristics and limitations of that model, PANEL, were examined in Chapter 5.

It is only very recently that ABAQUS [60], a general-purpose finite-element code, has incorporated non-symmetrical beam elements for non-linear analysis of structures, thus facilitating the modelling of more complicated frame arrangements, while at the same time reducing the number of simplifying assumptions.

An alternative cross-bracing model is developed in the following Sections using ABAQUS. Comparisons of results are also presented, including test results and predictions of failure loads from the computer model PANEL.

6.2 - Description of the ABAQUS cross-bracing model

The proposed model, shown in Figure 6.01-a, has the following characteristics:

- The structure is a three-dimensional frame, where the elements are rigidly connected to one another. The global system of coordinates is also shown in Figure 6.01-a, where node 1 is adopted as origin of coordinates.

- All main legs, diagonals and bolts in the structure are outlined as two-node beams in space (thus with six degrees of freedom at each node), and are described as general beam sections, with linear elastic section response. No numerical integration across the section is considered. Material properties are given by the Young's modulus E and torsional shear modulus corresponding to steel.

- The main leg members are given as elements with symmetric cross-section, with geometric properties corresponding to the actual steel angle's orthogonal and longitudinal axes. The supports on the main legs, and the nodes connecting with the diagonals, are located at the centre of gravity of these assumed sections, thus without introducing any additional bending or torsional effects. As in the case of the model PANEL, behaviour about the main leg's principal axes is not considered.

- The diagonals' sectional properties are given about their principal axes, therefore including in the analyses their non-symmetric condition. The directions of the principal axes in the space are given by the direction cosines for

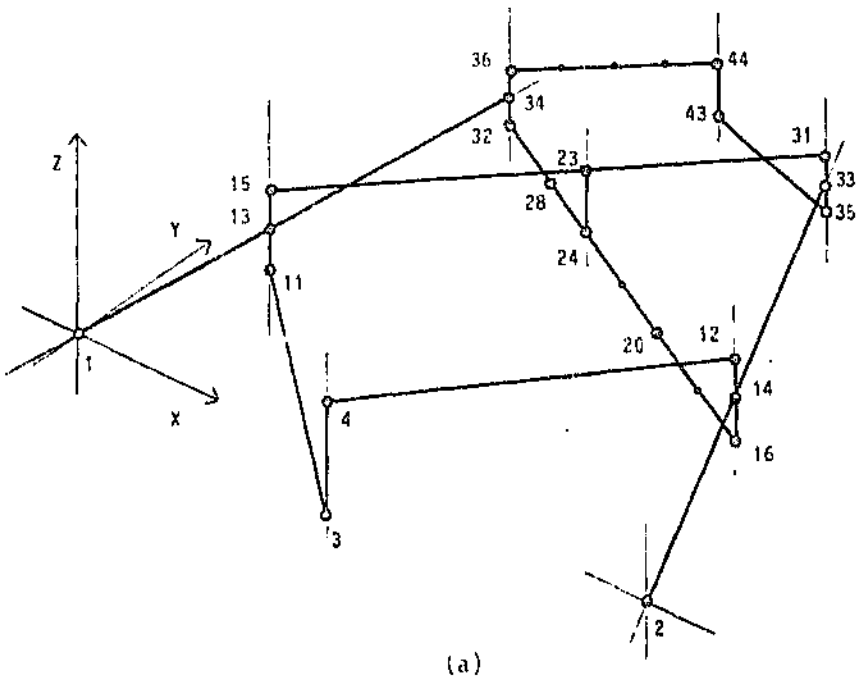

(a)

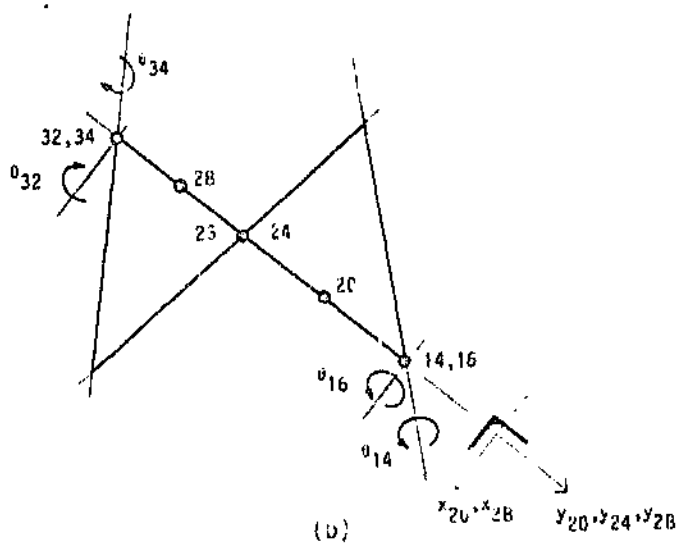

(b)

Figure 6.01: a) . ADUS model for analysis of cross bracings. Only the most important nodes are indicated. b) Note the positive directions of deflection and rotation, about the local axes.

the first local axis, which in this case was selected to be coincident with the minor v-axis (axis 1), as indicated in Figure 6.02. These properties complete the description of the asymmetric steel angles as part of the structure for non-linear analysis with ABAQUS. This is an important improvement with respect to other computer codes.

In addition, each diagonal is divided into four segments or beam elements between each connecting node, see Figure 6.01-a.

- The diagonal members are defined along their centroidal longitudinal axes, which are eccentric with respect to the point of connection with the main legs. The bolts are thus beam elements connecting the main legs and the diagonals, and the eccentricities are the normal framing eccentricities, as illustrated in Figure 6.[illegible]. A very large flexural stiffness is given to the bolt ele[illegible]s, which represents a rigid connection about the strut's x-axis.

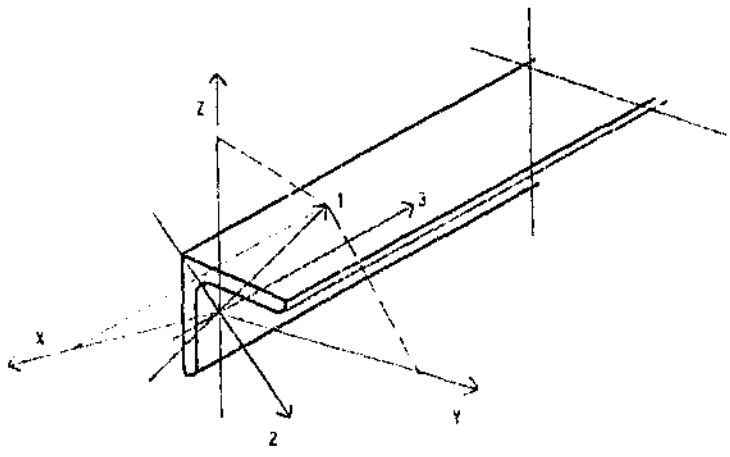

Figure 6.02: Direction cosines for the first axis of a non-symmetric section (directions are indicative). The remaining axes are defined by the right-hand rule.

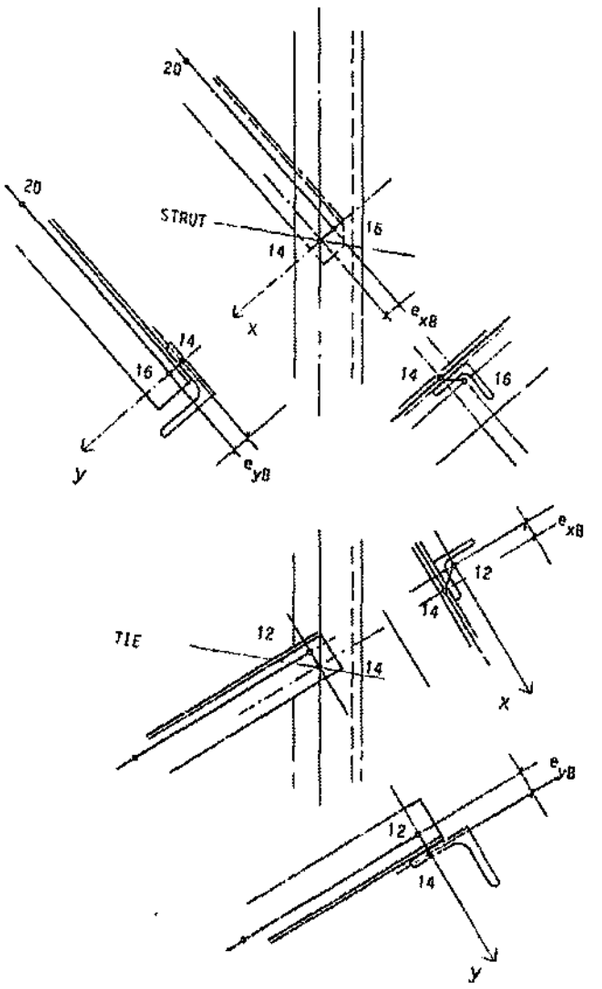

Figure 6.03: Definition of connection eccentricities in the ABAQUS model. Members 14-16 and 14-12 are beam elements representing the bolts in the frame, refer to Figure 6.01-a.

The end condition about the y-axis is solved through the torsional stiffness of the bolt elements as follows: a small J represents single-bolt connections, and a large J represents multiple-bolt connections (the central cross-over joint is always represented as a 1-bolt connection), where J is the section's polar moment of area. These values of the torsional constant J were calibrated using the experimental data.

In this way, this assumed arrangement represents the eccentricity of the connections about both local orthogonal x- and y-axis, and also the end condition about both axes, see Figure 6.03.

- The structure is supported at nodes 1 and 2 in the X-, Y- and Z- directions (fixed displacements) and, initially, there are no rotational restrictions to the main legs at these nodes. Horizontal restraint to the bracing is given at nodes 3 and 4 in the X-direction. Finally, out of plane restraint is given at nodes 13, 14, 33 and 34, thus simulating the actual testing conditions of the frames, see Figure 6.01-a.

The out-of-plane displacements of the cross-over joints in the central and outside panels of bracing are related through a linear multi-point constraint of the form:

$$A_1u_1 + A_2u_2 + \ldots A_nu_n = 0.0$$

in which A_i, u_i are parameters indicating which nodes are constrained about a given degree of freedom (2 in this case), and the magnitude of the constraint. These values are also, in this case, related to the experimental frames.

- The model described above is analyzed as a static load step, subject to geometric non linearity, and 20 iterations are allowed for convergence at each load increment. Output of stress and deflection is averaged at nodes.

- Finally, the loads are applied at nodes 43 and 44, in the X-direction, see Figure 6.01-a. Direct control is used for increment of loading, and 20 increments are selected to model the step.

  The strut's failure is defined by the stress readings at any of the intermediate nodes (i.e. when the calculated stress at the extreme fibre is equal to the yield stress of material for that particular case).

As seen in the description of the ABAQUS cross-bracing model of Figure 6.01-a, considerable care has been taken in order to simulate most of the design conditions of the experimental frames, including the relative positions of the bracings and supports, bolted connections and also strut-end details. Some of the test cases described in Chapters 3 and 4 were analyzed with the above ABAQUS model, and the results are presented for discussion in the following Sections.

6.3 - Analysis of cross-bracing with ABAQUS: correlation with experimental results

6.3.1 - Present investigation

Data on the frames and diagonal specimens for these tests are given in Tables 4.03-a and 4.03-b of Chapter 4. Results from the analyses with ABAQUS are given in Table 6.01 below. The parameters I_{xB} and I_{zB} in Columns 2-3 of Table 6.01 are the second moment of area and the polar moment of area respectively, corresponding to the beam elements simulating the bolts in the structure. These parameters have been established by calibration of the ABAQUS model against the experimental results. Column 4 gives the main leg torsional restraint coefficient S_{zL} at the supports, which is considered in all cases as Pinned. The calculated failure loads are listed in Column 5, which are compared with the test results in Column 6.

It can be seen in Table 6.01 that the predicted failure load for Test 102 with slenderness of L/r=100 is slightly optimistic. However, it was observed that the mechanism of failure is correct, with yielding occurring first in the tie at the cross-over joint (node 23 in Figure 6.01-a), and then in the strut at midspan.

The positive directions for deflections and rotations are indicated in Figure 6.01-b. The deflections in the strut at midspan node 20 and at the cross-over node 24, see Figure 6.01-b, are shown in Figure 6.04-a. It can be seen that the calculated in-plane and out-of-plane deflections are very

Present investigation

Table 6.01: ABAQUS - Comparison of results

Test Designation	ABAQUS Present investigation				Test results
	I_{xB} (mm^4)	I_{zB} (mm^4)	S_{zL}	$\frac{f_{ult}}{f_y}$	$\frac{f_{ult}}{f_y}$
1	2	3	4	5	6
202	1.0E 5	1.0E 3	P	0.517	0.491
302	1.0E 5	1.0E 3	P	0.436	0.395
602	1.0E 5	1.0E 3	P	0.446	0.431
801	1.0E 5	1.0E-2	P	0.274	0.288
802	1.0E 5	1.0E 3	P	0.348	0.336
804	1.0E 5	1.0E 3	P	0.343	0.364

similar to the experimental results.

The strut's end rotations θ_{16} at node 16 in Figure 6.01-b are smaller in the ABAQUS model, see Figure 6.04-b. Also, the main leg's torsional rotations θ_{14} at node 14 are smaller in the computer model, as indicated in Figure 6.04-c.

Similar results are recorded for Test 602 with slenderness of L/r=130 and inclined legs, see Table 6.01 and Figures 6.05-a through 6.05-c.

Prediction of failure load for Test 302, with slenderness ratio of 130 and parallel legs, is also optimistic, with a difference of 10% with respect to the experimental result. Failure in the ABAQUS model, however, occurs at node 28 in the strut, see Figure 6.01-b, and this is in agreement with the observed failure of cross-bracing in frames with parallel legs.

In- and out-of-plane deflections at node 20 and at the cross-over node 24 on the strut, see Figure 6.01-b, are shown in Figure 6.06-a, and in Figure 6.06-b for nodes 24 and 28 in the

strut. Note that in all cases the calculated deflections are very similar to the experimental records.

Experimental and calculated strut-end rotations at nodes 16 and 32 in the model of Figure 6.01-b are shown in Figure 6.06-c. The predictions are all correct. Similar results are obtained for the main legs' torsional rotations at nodes 14 and 34, which are shown in Figure 6.06-d.

In the region of slenderness ratio of 160, Tests 801, 802 and 804 in Table 6.01, the predicted failure loads are generally correct, and the strut's failure is correctly predicted by ABAQUS at the longest unsupported subspan, node 20 in Figure 6.01-b.

The calculated in- and out-of-plane deflections for Test 801 with 1-bolt connections are shown in Figure 6.07-a, where it can be seen that they are very close to the experimental records. The recorded end rotations at node 16 in the strut are larger than the predicted rotations, and the same happens with the main leg's torsional rotations at node 14, see Figures 6.01-b, 6.07-b and 6.07-c. As in the case of the PANEL model for 1-bolt connections, the ABAQUS model predictions of leg rotations are not correct, but in this case the predicted rotations are significantly smaller that the experimental values.

The calculated deflections and rotations at the same nodes for Tests 802 and 804 with 2-bolt connections are shown in Figures 6.08-a through 6.08-c, and Figures 6.09-a through 6.09-c respectively. Note that the predictions of leg rotations improve for the case of 2-bolt connections.

Examination of the above comparisons of results between the

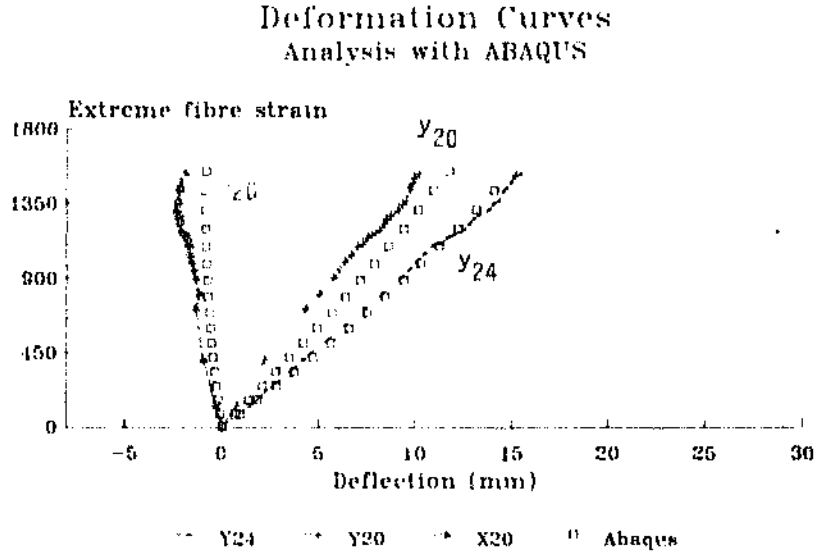

Figure 6.04-a: Vertical and horizontal strut deflections, see Figure 6.01
Test 102

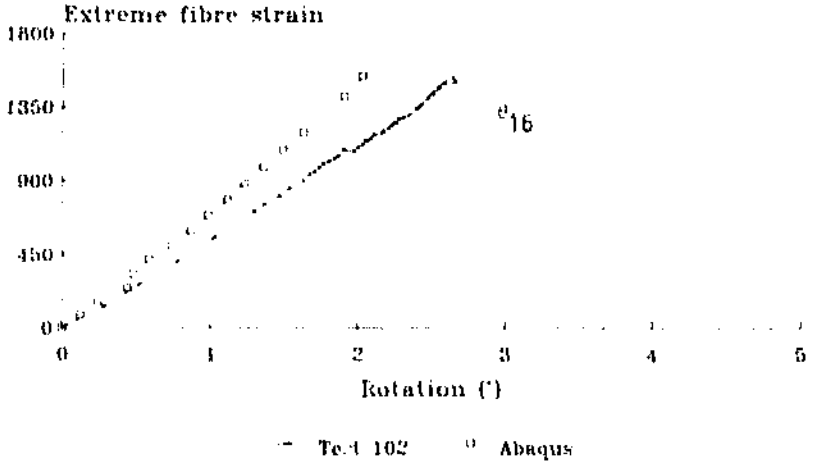

Figure 6.04-b: Strut's rotational response at node 16, see Figure 6.01
Test 102

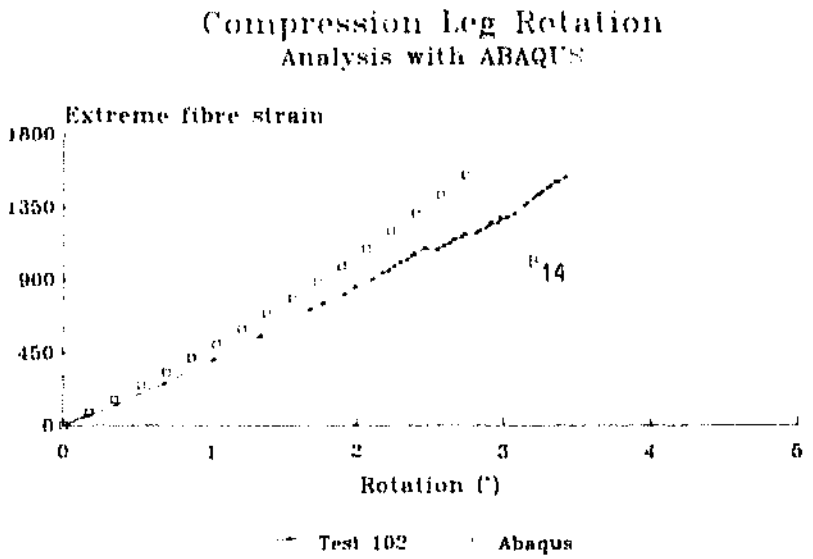

Figure 6.04-c: Main chord's rotational response at node 14, see Figure 6.01
Test 102

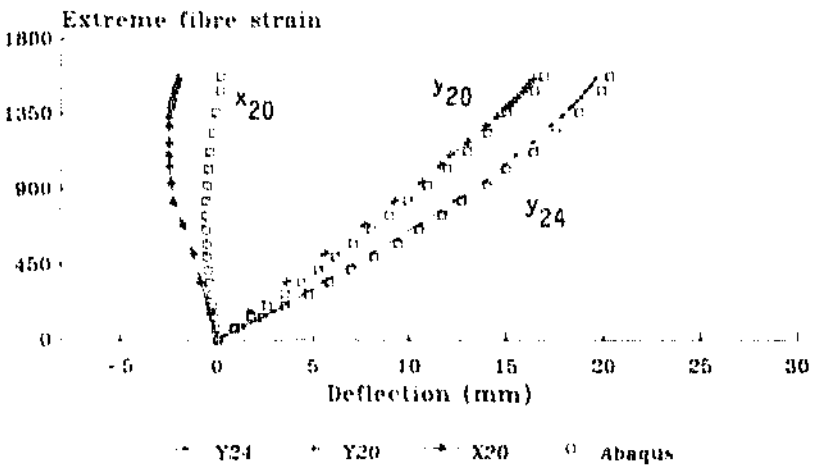

Figure 6.05-a: Vertical and horizontal steel deflections, see Figure 6.01
Test 602

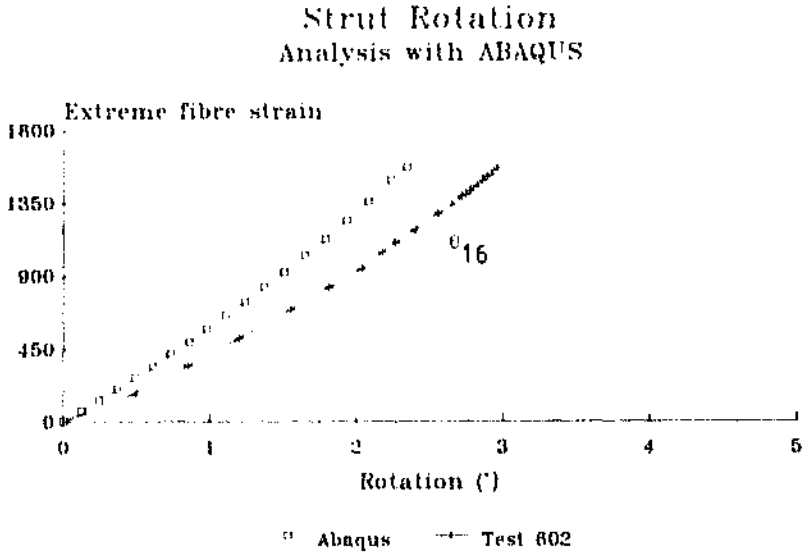

Figure 6.05-b: Strut's rotational response at node 16, see Figure 6.01 Test 602

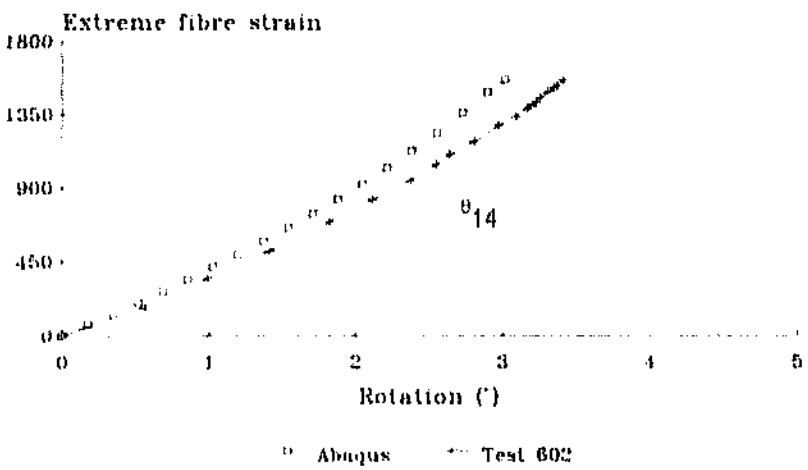

Figure 6.05-c: Main chord's rotational response at node 14, see Figure 6.01 Test 602

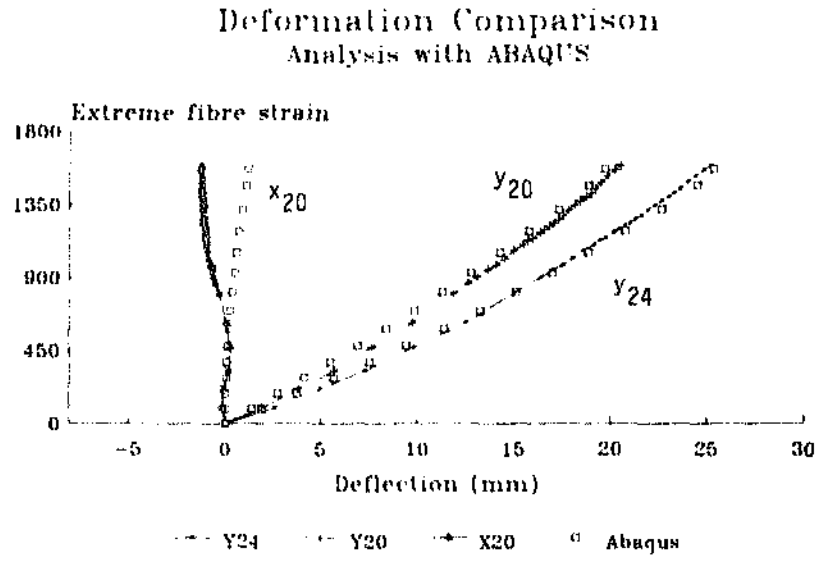

Figure 6.06-a: Vertical and horizontal strut deflections, see Figure 6.01
Test 302

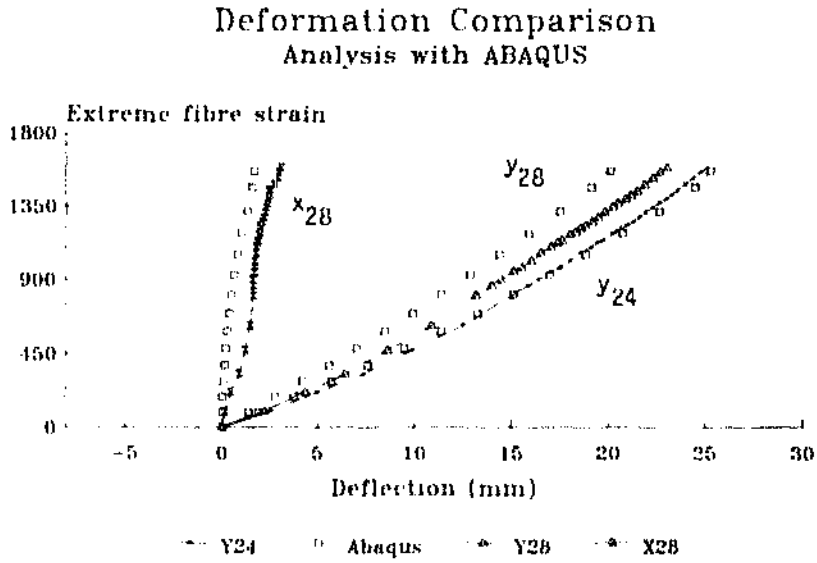

Figure 6.06-b: Vertical and horizontal strut deflections, see Figure 6.01
Test 302

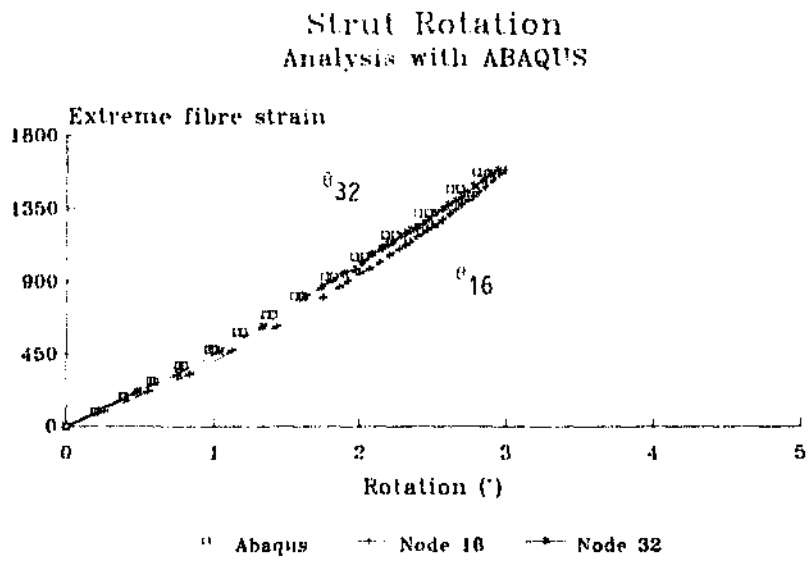

Figure 6.06-c: Strut rotational response at nodes 16 and 32, Figure 6.01 Test 302

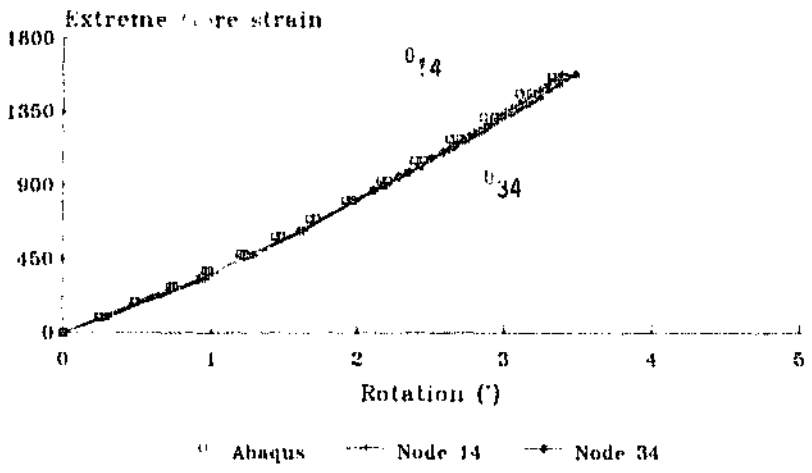

Figure 6.06-d: Main chord's rotational response at nodes 14 and 34, Figure 6.01 Test 302

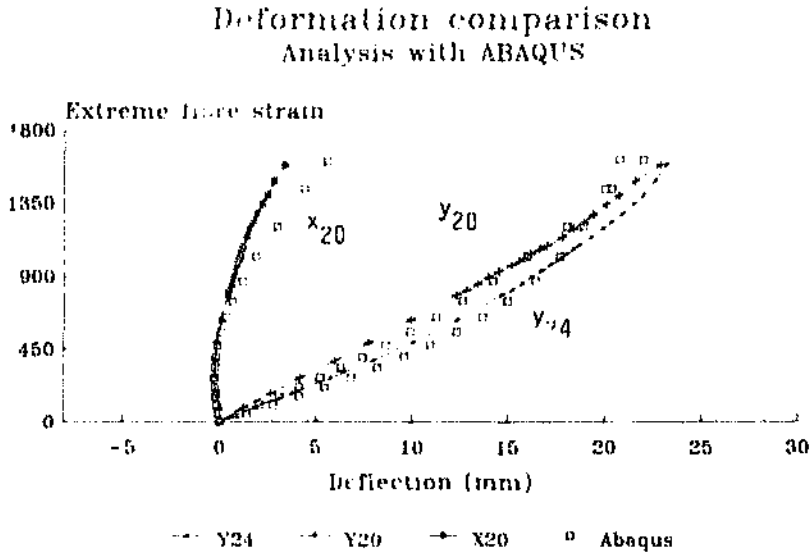

Figure 6.07-a: Vertical and horizontal strut deflections, see Figure 6.01 Test 801

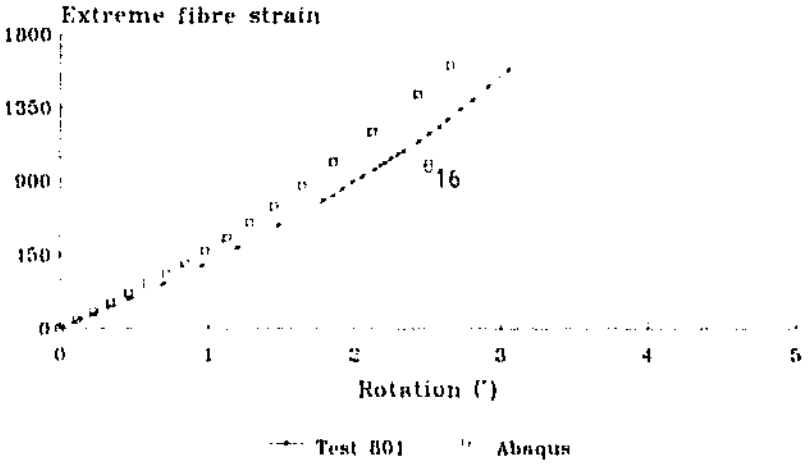

Figure 6.07-b: Strut's rotational response at node 16, see Figure 6.01 Test 801

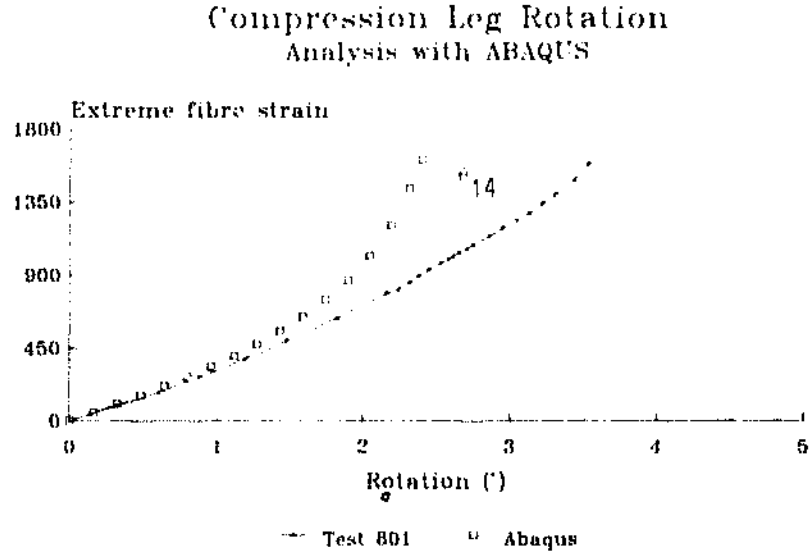

Figure 6.07-c: Main chord's rotational response at node 14, see Figure 6.01
Test 801

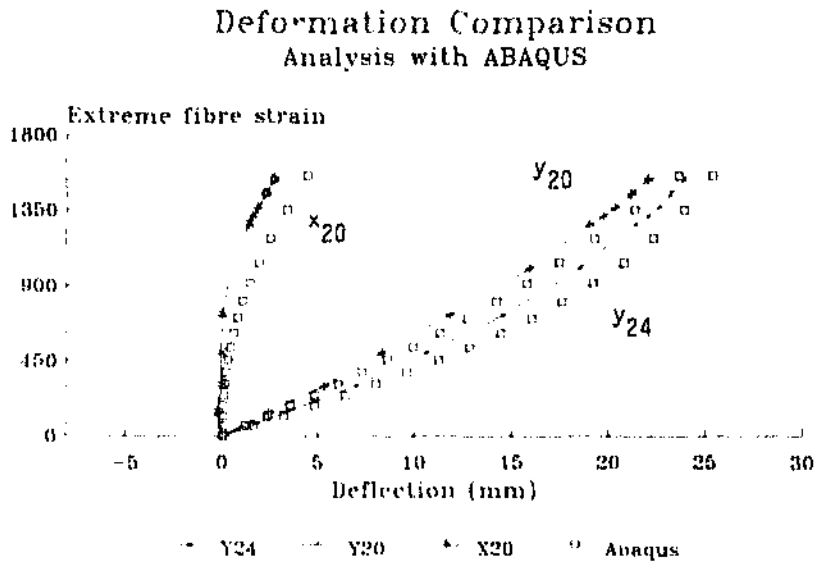

Figure 6.08-a: Vertical and horizontal strut deflections, see Figure 6.01
Test 802

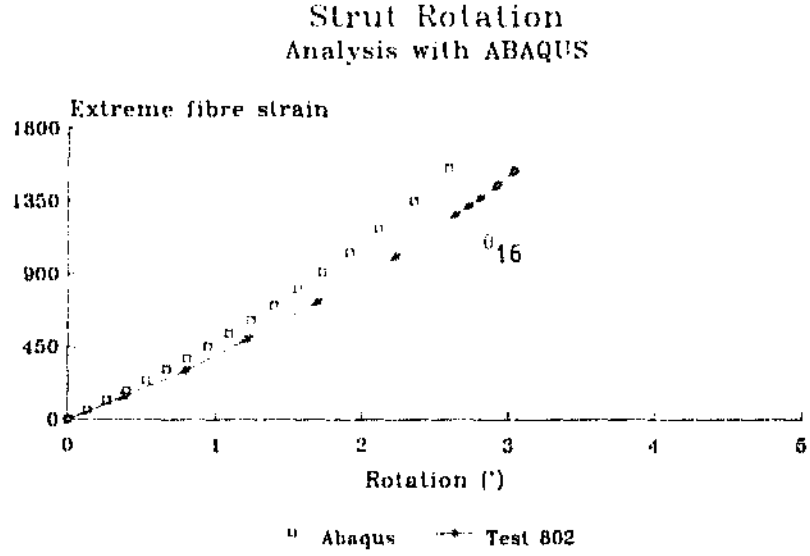

Figure 6.08-b: Strut's rotational response at node 16, see Figure 6.01 Test 802

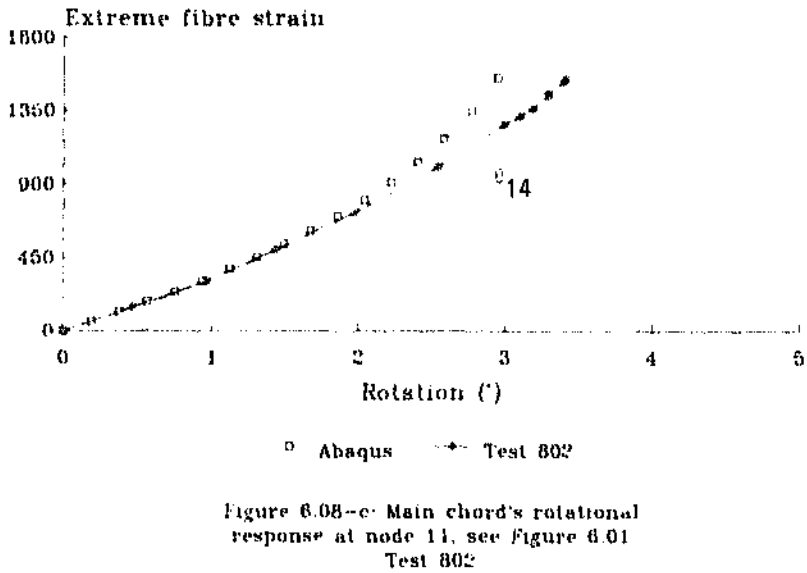

Figure 6.08-c: Main chord's rotational response at node 11, see Figure 6.01 Test 802

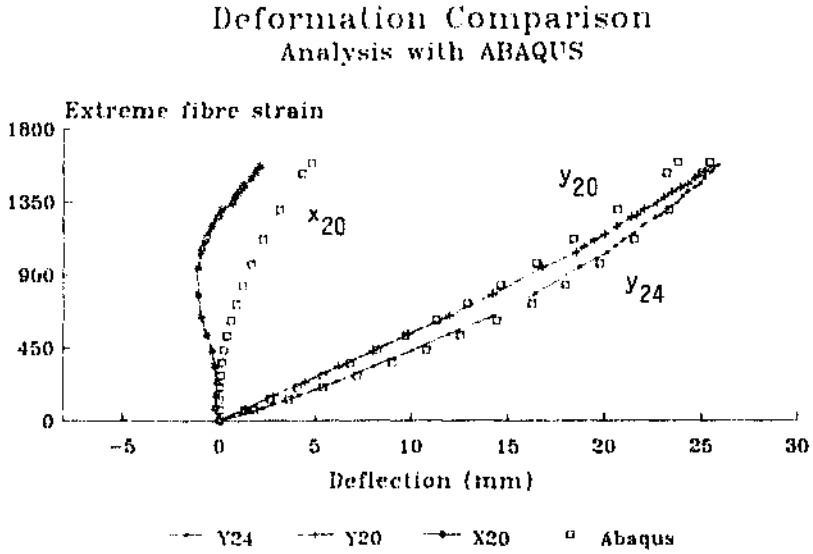

Figure 6.09-a: Vertical and horizontal strut deflections, see Figure 6.01 Test 804

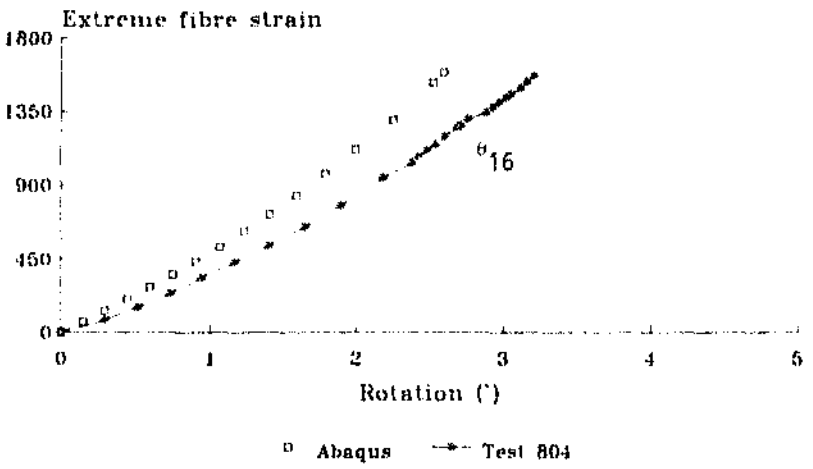

Figure 6.09-b: Strut's rotational response at node 16, see Figure 6.01 Test 804

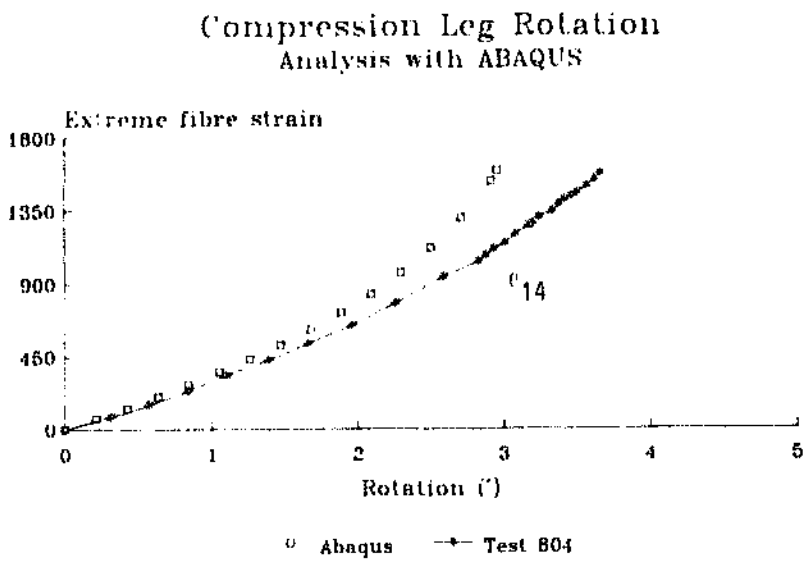

Figure 6.09-c: Main chord's rotational response at node 14, see Figure 6.01 Test 804

experimental frames and the ABAQUS model, allows for the following conclusions to be drawn:

- The calculated failure loads are slightly optimistic at low values of slenderness ratio, and slightly conservative at higher levels of slenderness.

- The mechanism of failure is correct in all cases, including the frame with parallel legs.

- The in- and out-of-plane deflections of the bracing are predicted correctly at all levels of slenderness, and for 1- and 2-bolt connections.

- The strut-end flexural rotations are always smaller that the recorded rotations. Similarly, the leg torsional rotations

are smaller than the experimental records, but the difference increases considerably for frames with 1-bolt connections.

The ABAQUS model was also used to examine some full-scale cross-bracing tests, as described in the next Section.

6.3.2 - CIGRE tests reported by Wood [49,63]

Data on the frames and diagonal specimens for these tests are given in Tables 4.05-a and 4.05-b of Chapter 4, and a typical frame is shown in Figure 2.01 of Chapter 2. Results from the analyses with ABAQUS are given in Table 6.02 below. The parameters I_{xB} and I_{zB} in Columns 2-3 of Table 6.02 are the second moment of area and the polar moment of area respectively, corresponding to the beam elements in the structure simulating the bolts. Column 4 gives the main leg torsional restraint coefficient S_{zL} at the supports, which is considered for these tests as Fixed, as indicated in Figure 2.01. The calculated failure loads are listed in Column 5, which are compared with the test results in Column 6.

It can be seen in Table 6.02 that the predicted failure loads are in almost all cases higher than the recorded values (5% higher as an average, with a c.o.v. of 10%). These approximations are, however, reasonably good. It must be noted in Table 6.02, Column 2-3, that the values of flexural and torsional stiffness for the bolt elements in the ABAQUS model are the same values which were defined for the tests in the present investigation (by calibration against the experimental data), where conditions of the frames were substantially

Experimental results reported by Wood [49] and CIGRE [63]

Table 6.02: ABAQUS - Comparison of results

Test Designation	ABAQUS Tests reported by Wood [49]				Test results
	I_{xB} (mm^4)	I_{zB} (mm^4)	S_{zL}	$\frac{f_{ult}}{f_y}$	$\frac{f_{ult}}{f_y}$
1	2	3	4	5	6
005	1.0E 5	1.0E-2	F	0.300	0.288
006	1.0E 5	1.0E-2	F	0.281	0.273
031	1.0E 5	1.0E-2	F	0.305	0.288
032	1.0E 5	1.0E-2	F	0.304	0.270
014	1.0E 5	1.0E 3	F	0.304	0.325
015	1.0E 5	1.0E 3	F	0.311	0.345
038	1.0E 5	1.0E 3	F	0.293	0.260
039	1.0E 5	1.0E 3	F	0.283	0.270
040	1.0E 5	1.0E 3	F	0.331	0.295
041	1.0E 5	1.0E 3	F	0.328	0.265

different.

Also, the frames in the CIGRE tests had lateral bracings for out-of-plane restraint, as seen in Figure 2.01, which were not reproduced in the computer model. Finally, while the beam at the top of the frame in Figure 2.01 was not rigidly connected to the main legs (as stated in the test reports [49,63]), a fully-fixed connection was assumed in the ABAQUS model in order to simplify the analysis.

These and other unknown conditions and characteristics of the actual tests explain the differences between the experimental and calculated results.

6.4 - Comparison of PANEL and ABAQUS models

Cross-bracing systems have been examined with PANEL, an experimental, flexibility analysis computer model, and ABAQUS, a